Contribution to the Definition of Non Deterministic Robust Optimization in Aeronautics Accounting with Variable Uncertainties

J. Pons
G. Bugeda
F. Zárate

Contribution to the Definition of Non Deterministic Robust Optimization in Aeronautics Accounting with Variable Uncertainties

J. Pons
G. Bugeda
F. Zárate

Summary of contents

Figure Index

Tables Index

CIMNE Monography

Contribution to the definition of Non-deterministic Robust Optimization in Aeronautics accounting with variable uncertainties.

Author: Jordi Pons i Prats

Doctoral Program in Aerospace Science and Technology
Polytechnic University of Catalonia

Supervisors:
Prof. Gabriel Bugeda
Dr. Francisco Zárate

RMEE – Departament de Resistència de Materials i Estructures a l'Enginyeria
UPC – Universitat Politècnica de Catalunya
CIMNE - International Centre for Numerical Methods in Engineering

Abstract

Abstract (English)

Shape optimization is a largely studied problem in aeronautics. It can be applied to many disciplines in this field, namely efficiency improvement of engine blades, noise reduction of engine nozzles, or reduction of the fuel consumption of aircraft. Optimization for general purposes is also of increasing interest in many other fields.

Traditionally, optimization procedures were based on deterministic methodologies as in Hamalainen et al (2000), where the optimum working point was fixed. However, not considering what happens in the vicinity of the defined working conditions can produce problems like loose of efficiency and performance. That is, in many cases, if the real working point differs from the original, even a little distance, efficiency is reduced considerably as pointed out in Huyse and Lewis (2001).

Non deterministic methodologies have been applied to many fields (Papadrakakis, Lagaros and Tsompanakis, 1998; Plevris, Lagaros and Papadrakakis, 2005). One of the most extended non-deterministic methodologies is the stochastic analysis. The time consuming calculations required on Computational Fluid Dynamics (CFD) has prevented an extensive application of the stochastic analysis to shape optimization. Stochastic analysis was firstly developed in structural mechanics, several years ago. Uncertainty quantification and variability studies can help to deal with intrinsic errors of the processes or methods. The result to consider for design optimization is no longer a point, but a range of values that defines the area where, in average, optimal output values are obtained. The optimal value could be worse than other optima, but considering its vicinity, it is clearly the most robust regarding input variability.

Uncertainty quantification is a topic of increasing interest from the last few years. It provides several techniques to evaluate uncertainty input parameters and their effects on the outcomes. This research presents a methodology to integrate evolutionary algorithms and stochastic analysis, in order to deal with uncertainty and to obtain robust solutions.

Resum (Català)

El problema d'optimització de perfils aerodinàmics és un dels més estudiats dins de l'àmbit de l'aeronàutica. Pot ser aplicat en múltiples disciplines, com la millora d'eficiencia en àleps de turbines, reducció de soroll en toveres de motors, o la reducció del consum de fuel de l'avió. L'optimització en general és un camp de creixent interès en molts altres camps.

Tradicionalment, els procediments d'optimització estaven basats en metodologies deterministes com ho fan a Hamalainen et al (2000), de manera que resultaven en un punt òptim de funcionament. De totes maneres, si no es considera què passa al voltant d'aquest punt de treball pot sorgir un problema. Aquest problema pot provocar, en molts casos, que si el punt de treball varia lleugerament de les condicions del punt òptim, encara que sigui una distància mínima, l'eficiència es vegi reduïda en gran mesura com s'indica a Huyse i Lewis (2001).

Els procediments no-deterministes han estat aplicats en molts camps (Papadrakakis, Lagaros and Tsompanakis, 1998; Plevris, Lagaros and Papadrakakis, 2005). Un dels mètodes no-deterministes més estesos és l'anàlisis estocàstic. Però el cost de computació dels anàlisis de fluido-dinàmica (CFD) han evitat fins ara la seva extensa implantació a l'optimització de forma. Inicialment, l'anàlisi estocàstic va ser desenvolupat en el camp de la mecànica estructural. La quantificació de la incertesa i els estudis de variabilitat poden ajudar a tractar amb els errors intrínsecs dels processos i mètodes utilitzats. El resultat deixa de ser un punt per convertir-se en un rang de valors que defineix l'àrea òptima. Aquesta àrea pot contenir valors pitjors que l'òptim determinista, però considerant l'àrea total el resultat és millor i més robust en front de la variabilitat de les entrades.

La quantificació de la incertesa és un tema d'interès des de fa relativament pocs anys. Les tècniques de quantificació de la incertesa permeten avaluar incerteses en els paràmetres d'entrada i els seus efectes en els resultats. Aquest treball d'investigació presenta una metodologia que integra algoritmes evolutius i anàlisis estocàstic per treballar amb incerteses i obtenir solucions robustes.

Resumen (Castellano)

El problema de la optimización de perfiles aerodinámicos es uno de los más estudiados dentro del ámbito aeronáutico. Puede ser aplicado en múltiples disciplinas, como la mejora de eficiencia en álabes de turbinas, la reducción del ruido en toberas de motores, o la reducción del consumo de combustible del avión. La optimización en general es un campo de creciente interés en otras muchas disciplinas.

Tradicionalmente, los procedimientos de optimización estaban basados en metodologías deterministas como las descritas en Hamalainen et al (2000), de manera que resultaban en un punto óptimo de funcionamiento. De todas formas, si no se considera qué pasa entorno de este punto de trabajo puede surgir un problema. Este problema puede provocar, en muchos casos, que si el punto de trabajo varia ligeramente de las condiciones del punto óptimo, aun siendo una distancia mínima, la eficiencia se vea reducida en gran medida como se indica en Huyse and Lewis (2001).

Los procedimientos no-deterministas han sido aplicados en muchos campos (Papadrakakis, Lagaros and Tsompanakis, 1998; Plevris, Lagaros and Papadrakakis, 2005). Uno de los métodos no deterministas más utilizados es el análisis estocástico. Pero el coste computacional de los análisis de fluido-dinámica (CFD) ha evitado hasta la fecha su aplicación extensiva a la optimización de forma. Inicialmente, el análisis estocástico fue desarrollado en el campo de la mecánica estructural. La cuantificación de la incertidumbre y los estudios de variabilidad pueden ayudar a tratar con los errores intrínsecos de los procesos y métodos utilizados. El resultado deja de ser un punto para convertirse en un rango de valores que definen el área óptima. Esta área puede contener valores peores que el óptimo determinista, pero considerando el área total el resultado es mejor y más robusto ante la variabilidad de las entradas.

La cuantificación de la incertidumbre es un tema de interés desde relativamente poco tiempo hacia aquí. Las técnicas de cuantificación de la incertidumbre permiten evaluar incertidumbres en los parámetros de entrada y sus efectos en los resultados. Este trabajo de investigación presenta una metodología que integra algoritmos evolutivos y análisis estocástico para trabajar con incertidumbres y obtener soluciones robustas.

Agraïments

Després d'escriure tota la tesis sembla increïble com m'és de difícil escriure aquestes línies; massa gent en ment que d'una manera o altra m'han ajudat a portar a terme aquesta tasca. No ha estat gens fàcil compaginar feina i tesis, però el suport i l'ajuda rebuda han estat molt importants.

Agrair, doncs, la feina feta per el Prof. Gabriel Bugeda i el Dr. Francisco Zárate, per la seva paciència i suport. Així mateix pel suport incondicional del Prof. Eugenio Oñate i de tota la gent de CIMNE; des dels dos Robertos i l'Enrique fins a la Mercè, la Ma Carmen i l'Anna amb tot el seu equip. Mencionar de manera especial a en Dr. Chris Lee, que des de la seva incorporació a CIMNE fa prop de dos anys ha estat una guia a seguir i de qui aprendre molt. Igualment, mencionar en Dr. Felipe González, investigador de la Universitat de Queensland, Austràlia, que va compartir unes profitoses reflexions a l'inici d'aquesta recerca.

A la colla d'amics de l'ETSEIB: Albert, Anna, Xavier i Sergi, que són parcialment culpables de la meva passió per l'enginyeria, i a la colla Routier: Paco, Joan, Alfonso, Tomàs i la resta, que tants quilòmetres m'ha acompanyat. Als DoCTA: Àngela, Eli, Xevi, i molt especialment a la Mercè, que comparteix amb mi moments molt especials.
A la meva família, en especial a la mare i al pare, que tant m'han donat des de sempre. Al pare per transmetre'm la passió per volar, i la mare per ajudar-me a arribar sempre més lluny.
A tota aquella gent que és plenament conscient del meu agraïment, però que no puc anomenar aquí, gràcies altre cop.

Agraïr la col·laboració del Dr. G.J.A. Loeven, de la Delft University of Technology, per facilitar-me el codi del mètode de col·locació probabilistica. Aquesta col·laboració ha estat emmarcada dins el projecte NODESIM-CFD on CIMNE i la TU Delft participaven conjuntament. Igualment, agrair a l'Enrique Ortega i al Dr Roberto Flores, de CIMNE, els codis de PUMI (CFD) i aero-elàstics basats en PFEM i que he utilitzat extensament en aquest treball de recerca. Al Dr. Roberto López pel seu codi de xarxes neuronals. Hem de mencionar, també, al Prof. Mark Drela, que desenvolupà el codi XFoil i que també hem utilitzat aquí. Finalment, agrair el suport de l'equip de GiD en l'utilització del software de pre i post-procesat, a COMPASSIS per l'utilització de TDYN, i al Dr. Francisco Zárate pel suport en l'utilització de STAC.

Acknowledgements

I should translate the acknowledgement chapter in order to avoid dismissing anyone who helps me during the development of my research.

After writing all this document it is not easy to write few lines to thanks all the people who has helped me during all these years. Too much people are in mind. Sharing the time between working in a company and developing this research has not been easy, but people help me a lot.

I want to thanks to Prof. Gabriel Bugeda and Dr. Francisco Zárate, who have been patient and supervised my research. I have also to thanks Prof Eugenio Oñate due to his continuous support, as well as all the colleagues from CIMNE; the two Roberto, and Enrique, and also Mercè, Ma Carmen, Anna and all her team. Special mention is Dr. Chris Lee, who from his arrival at CIMNE two years ago has guided me, and from who I have learnt a lot. Mention, as well, Dr. Felipe Gonzalez, from Queensland University, Australia, who shared some relevant comments at the beginning of this research.

Thanks to my ETSEIB friends; Albert, Anna, Xavier and Sergi, who are partially responsible of my engineering passion. To my cycling friends, the Routier group, Paco, Joan, Alfonso, Tomàs and all others, with whom I have ridden thousands of kilometres. To DoCTA group, Àngela, Eli, Xevi and specially to Mercè, who shares with me really special moments. To my family, to my parents. To my father, I got his passion to aviation and to fly. To my mother, who always help me to keep progressing. To all these people who know I'm in debt with them but I cannot mention here.

I need to mention the collaboration from Dr. G.J.A. Loeven, de la Delft University of Technology, who provide me the Probabilitic Collocation code in the framework of NODESIM-CFD project. Thanks, also, to Enrique Ortega and Dr. Roberto Flores, from CIMNE, for the PUMI (CFD code) and aero-elastic codes they developed and provided to this research. Thanks to Dr. Roberto López to facilitate the use of his developments in Artificial Neural Networks. To Prof. Mark Drela, who developed XFoil, to facilitate its use. Finally, give my thanks to GiD team, in CIMNE, for the support on the use of the pre and post processor software, to COMPASSIS for the support of TDYN, and to Dr. Francisco Zárate for his support on STAC.

List of Notations

AoA: Angle of attack

$b_{i,n}(t)$: Bezier polynomials

C_d: Coefficient of drag

C_{dp}: Coefficient of pressure drag

C_l: Coefficient of lift

C_m: Coefficient of momentum

$c_i(x)$: Constraint function for optimization

ξ: random variable

ξ_h: Horizontal damping

ξ_θ: Angular damping

$f_i(x)$: Objective function for optimization

$h_{ci}(t)$: Elastic vertical displacement of the profile, dependant on time. This is the displacement component of flutter.

LHS: Latin Hypercube sampling

μ: Statistical mean value

μ_r: Wing mass ratio

M: Mach number

MC: Monte-Carlo

N_t: time steps for the numerical simulation of the flutter phenomena

PCM: Probabilistic Collocation Method

PDF: Probability density function

$\theta_i(t)$: Elastic angular oscillation of the profile, dependant on time. This is the angular component of flutter.

σ: standard deviation

x_cg: x-coordinate of the centre of gravity location

x_ea: x-coordinate of the elastic axis position

$\omega_i(\xi)$: stochastic term

t_{tx}: duration of taxi, fixed to 5 minutes.

ffr: fuel flow reference; minimum fuel flow of each engine (kg/h).

SE: single engine taxi; 0= taxi with only one engine, 1= taxi with two engines

th_{tx}: throttle adjustment (% of full throttle).

v_{to}: take-off speed (kt)

l_r: runway length (m)

h_{to}: altitude of departure airfield (ft)

w_{to}: wind during take-off (kt)

AA: Acceleration altitude (ft)

CR2AA: climb ratio to acceleration altitude (ft/min)

v_{aa}: Mach number at acceleration altitude (% Mach)

CI_{aa}: Cost Index during flight to acceleration altitude

th_{aa}: throttle position during flight at acceleration altitude

CR2C: climb ratio to cruise altitude (ft/min)

CA_1: Cruise altitude 1 (ft)

w_{c1}: wind at cruise level 1 (kt)

v_{c1}: Mach number at cruise level 1

d_{od}: distance from departure to destination airfields (NM)

CI_{c1}: cost index during cruise 1

CRCC: climb ratio to cruise altitude 2 (ft/min)

CA_2: Cruise altitude 2 (ft)

w_{c2}: wind at cruise level 2 (kt)

CI_{c2}: cost index during cruise 2

CRFA: descent ratio to final approach altitude (ft/min)

h_d: altitude of the destination airfield (ft)

1   Introduction

Optimization is becoming a daily task in engineering departments. It is of increasing importance thanks to the recent improvements regarding methods and applications. Optimization methods can be applied to almost all engineering fields, and to most engineering design phases; from conceptual to detailed design. Optimization plays an important role in order to define the optimal solution from the beginning.

Several methods have been defined and used in the context of the optimum design. Usually, each method is oriented to the improvement of one specific type of problem. Brute force methods, gradient methods, simulated annealing methods, stochastic methods, evolutionary algorithms and further developments define the path followed by optimization methods. History shows that calculus of variations is not a recent topic. The research by Johan Bernoulli or by Fermat is a good example of the mathematical development and scientific interest about this topic. Calculus of variations is the seed of the optimization methods used today.

Evolutionary algorithms, on the other hand, have demonstrated their capabilities to deal with any kind of problems. They are efficient and fast, and avoid local minimum thanks to random search techniques (Goldberg, 1988 & 1994). Hundreds of references can be found regarding evolutionary optimization applied to airfoil design, see for example Chafedar, Xuan, Rasheed (2003), Chiba et al (2003), Desideri, Janka (2004), or Marco, Desideri, Lanteri (1999) to mention a short list.

Optimization methods have been used in the scientific and industrial community for solving many applications. Each application requires a specific solver to solve a specific problem. Based on mathematical methodologies, some of them inspired on nature, optimization methods use iterations to converge to the optimum. The solver will provide the evaluation of the objective function for each individual in order to perform the optimization loop. A relevant fact regarding the associated computational cost is that the computer science is growing with huge steps. The efficiency and reliability of computers are improving every day, and the calculation capacity is also increasing while the machine cost is decreasing. Nowadays, the public in general can accede to the

computation equipment that some time ago was restricted only to big companies and research centres of the universities. The combination of the computer advances and new advances in techniques that ensure a fast convergence of the numerical methods leads to an increasing efficiency of the solvers, which helps to increase the interest and attraction to specific applications.

Computational Fluid Dynamics is a good example that confirms the previous statements. Advances in Computational Fluid Dynamics (CFD), with the application of Particle Finite Element Method (PFEM), help to better simulate fluid-structure interaction problems (Oñate et al, 2008), or efficiently deal with potential flow (Ortega, Oñate, Idelsohn, 2007), or with compressible flow (Ortega, Oñate, Idelsohn, 2009). These developments help to develop a parallel field as aerodynamic optimization; from shape optimization, to flow control applications, but also aero-elastic problems.

The extended use of the numerical simulation as a design tool is now enhanced with optimization techniques because it leads to a fast convergence to the best design. Numerical simulation or virtual prototyping is the best alternative to physical prototyping; the cost of physical prototypes is removed, numerical simulations are easy to modify and the cost of those modifications is lower. The use of numerical methods and tools enables to test more designs, obtaining more information and using more parameters, in less time than using physical prototyping.

Many engineering applications require solving optimization problems to define the optimal design. The problem definition is always the same; an objective function is defined on a constrained search space in order to be maximized or minimized. In many cases, the optimization problem includes nonlinear objective functions, and/or nonlinear constraint functions. But, even if the functions are linear, engineering problems can be too complex to be easily solved (like the fluid dynamics case); because they can present local solutions and no analytical function can be calculated. Traditional approaches usually converge to these local optimal solutions as in Bazaraa, Sherali and Shetty (1993), or Nash and Sofer (1996), because their search range is limited to a neighbourhood of the starting point.

If the objective functions were well-known, differentiable and smooth, it would be analytically solved. However, engineering problems are usually unknown, or non-differentiable or smooth. Then, a method that explores all search space is required. The so-called non-deterministic or stochastic methods take advantage of the random generation of each individual in order to ensure searching across all input space. Even though they are called stochastic methods, they are not focused on the analysis of a problem considering the uncertainty of input variables.

Uncertainty is also an important parameter to be taken into consideration. Introduction of uncertainty in the simulation process will produce robust results. Uncertainty can be associated to the method of calculation, but also to the input variables, which represent some nature behaviour, or some manufacturing parameters and tolerances.

Uncertainty can be classified in two categories, as described by Durga et al (2006); the first one is the so called random uncertainty. Behaviour of nature, which has an inherent variability, is the best example. Thanks to empiric observation random uncertainty can be accurately modelled and represented through the use of probabilistic methods. The

second category is the so called epistemic uncertainty, which comes from a lack of knowledge of the behaviour of the system. Usually, it is not well represented or modelled using classical probabilistic approaches and it leads to non-probabilistic methods based on interval specifications.

Error estimation in CFD is also a very important field in development. Numerical errors, mainly related to simplification, approximation of functions, modelling of the flow, or turbulence, are clear examples and several solutions have been defined. But the new trend is the introduction of physical uncertainties coming from a lack of knowledge of the physics phenomena.

Some decades ago, engineers did not consider uncertainty, and statistical behaviour of the variables was not introduced into the calculation process. However, it meant that optimized design produced a single optimal point. Mathematically speaking, a point is a non-dimensional object, so physically speaking it is impossible to determine due to the physical uncertainty of the measures. Error in calibration, tolerances or manufacturing errors should be taken into consideration. It is well-known that a pair of measures of any kind will not be equal between them. In order to define the optimum, it is better to use the point itself but also the probability to lie on this region. The highest the probability, the largest the region will be, and vice versa. It implies more accuracy but also more computational resources and time.

Uncertainty quantification is a very recent topic, see for example Loeven and Bijl (2008), Loeven and Bijl (2009) or Mathelin, Hussaini, Zang (2008) for aerodynamic applications, Plateeuw (2009) for turbulence modelling, Witteveen and Bijl (2008) for diffusion problems or Constantine, Doostan and Iacarrino (2009) for heat transfer problems. The usual treatment of uncertainty is based on multi-point robust design. The uncertainty on parameters is modelled by selecting uniformly distributed values along the range. The multi-point technique does not care about the probabilistic and statistical definition of the input values, but on discrete evaluations. See Huyse and Lewis (2001), Li, Padula (2003), Li, Huyse, Padula (2002), or Lee et al (2008, 2009, 2010) for airfoil design using multi-point methodology.

Taking advantage of the mentioned improvements, the contribution of this research is the development of a methodology that combines the capabilities of evolutionary algorithms and stochastic analysis to define an optimization method, which takes into account uncertainty on the input variables, and its effect on the output values.

This research has focussed its attention on robust design and robust optimization techniques. The main contributions can be listed as follows:

- Implementation of a stochastic procedure based on Monte Carlo techniques
- Implementation of the stochastic procedure for stochastic and robust optimization
- Implementation of a methodology to reduce the computational cost of such procedure based on Artificial Neural networks
- Establishment of a comparison point between standard optimization methodologies, based on deterministic procedures, and a new implementation of the stochastic and robust optimization methodologies.

- Application of the stochastic procedure, as well as the stochastic and the robust optimization procedure to Computational Fluid Dynamics, Fluid-Structure Interaction and mission planning problems as a validation point.

It is worth mentioning that this new procedure is dealing with variables uncertainties, defining them in a stochastic way. One can confuse stochastic optimization methods, like evolutionary algorithms, with stochastic definition of the input variables. The first one does not take into account uncertainty, only random definition of initial values to ensure a good search strategy. In addition, the new procedure will be a stochastic robust methodology. Taking advantage of the stochastic definition of the input variables, the new methodology will be able to deal with robust optimization problems.

A comparison can be established with previous research done by others in order to highlight the differences and the main contribution of this research.

- Stochastic calculus has not been further developed in the CFD field, due to its expensive computational cost.
- The use of surrogate models is spread out from few years ago, when the research in this field enhanced the cost of generating the models, compared to the accuracy it provides.
- All the applications regarding robust design optimization uses a few numbers of points to statistically analyse each individual. It is not a proper way to perform and statistic analysis due to the lack of accuracy.

This document is organized in 5 main chapters. The first one is this introduction. The second one is the study of the state of the art, where evolutionary algorithms, stochastic calculus, and aerodynamics concepts are developed and analysed from the point of the view of what is going on and what is coming in a near future. The third chapter describes the stochastic procedure that helps to introduce the uncertainty into the analysis. It is a first step which leads to the developments on the fourth chapter. The fourth chapter describes the developments on robust optimization using uncertainty quantification techniques. Stochastic and robust procedures have been defined to deal with input uncertainty and to analyse the output variability. The third and fourth chapters include several test cases and examples for a better understanding and comparison among deterministic and both stochastic and robust procedures. Finally, the fifth chapter is where the conclusions are developed.

2 State of the art

2.1 Introduction

Robust optimization methods are quite a brand new topic. Even though optimization and sensitivity analysis have a large trajectory it was quite hard to think on coupling them together. Sensitivity studies were extremely computationally expensive. Reviewing the state of the art, few references are found that consider uncertainties on optimization analysis. Few of them use CFD solvers and those which use them are the most recent ones. One of the first researches dealing with uncertainty and CFD applications is done by Huyse and Lewis (2001), who dealt with shape optimization of 2-D airfoils. More recent researches have already introduced the Uncertainty Quantification concept as a set of methods that propagate the uncertainty within the optimization loop. Loeven and Bijl (2008), and Loeven and Bijl (2009), Eldred and Bunkardt (2009), are some of them.

When dealing with computationally expensive analysis surrogate models are commonly used. In optimization analysis, the use of a surrogate model helps to reduce the required computational effort. Due to the lack of accuracy of the surrogate models, some other methods are emerging. The most remarkable ones are the reduced-order methods (ROM), which are based on very recent developments and should be considered as an emerging technology, rather than a mature one. Cervera, Codina and Galindo (1996) have proposed two strategies to simplify the work when dealing with coupled problems, Badia and Codina (2000) have proposed the use of pressure segregation methods to deal with fluid-structure interaction problems, and they have applied the method to bridge aero-elasticity analysis. Badia and Codina (2009) have developed a simplification based on subscales approximations. Some of these developments are related to extremely expensive analysis, so even though reduced order models decrease computational time, it is still not enough to provide a fast and accurate response for an optimization process. Due to this issue, they are not considered in this research, but should be considered for the near future.

Two are the main topics developed in this chapter; namely optimization methods and uncertainty quantification. All of them are strongly related to this research since optimization methods and uncertainty quantification methods are the core of this research monography.

This chapter is divided in two main sections. The first one is the description and analysis of the state of the art of the optimization methods. And the second section is the description of uncertainty quantification techniques.

As additional information, Appendix I, II and III are devoted to provide a brief introduction of some relevant topics related to the present research. Numerical methods are of great importance regarding the solver definition, but also the surrogate models definition. Appendix I contains a description of numerical methods that are directly related to the present research. It also includes a description of the required tools. STAC, the stochastic manager tool, TDYN and PUMI CFD solvers, GID as the pre and post-processor tool, the Aero-elastic tool, all of them are described in Appendix I. It also includes a description and validation of the Artificial Neural Networks that has been selected as the surrogate model. A general introduction of relevant aerodynamics concepts is provided in Appendix II. It includes a brief introduction to flow theory and non-dimensional coefficients. Finally, Appendix III briefly describes shape parametrization, focusing on Beziers Curves, as one of the main common methods.

2.2 Optimization methods

Optimization methods can be classified using several criteria: the type of problems they can solve, if they deal with linear or non-linear objective functions, or constraints, if they need second or higher order derivative of the objective function, etc.

The most common criteria of classification are:
- The number of control variables (Inputs):
  - Discrete optimization: it defines a limited number of input values.
  - Calculus of variations: it accounts an infinite number of input variables.
- Definition of the control variables:
  - Deterministic: it defines the next individual to be evaluated according the data from the previous loop. A typical example of a deterministic method is the Gradient Method.
  - Random or stochastic: it defines the next individual according the data from previous loop but using some random criteria or method. An example of a stochastic method is the Evolutionary Algorithm
- Treatment of individuals:
  - Non-populated based method: it uses a single individual in each iteration. Examples are Newton's method for the non-populated method.
  - Populated based method: it groups the individuals in population to take advantage of the multi-individual search. Evolutionary Algorithm as a populated-based method.
- Type of equations that defines the objective functions or constraints:
  - Linear: it uses linear functions.
  - Non-linear: it uses non-linear functions.
  - Geometric: it is a particular case of the non-linear because it deals with polynomial functions.
  - Quadratic: it is another particular case of the non-linear programming. It is told to be the best behaved non-linear case.
- Type of constraints:

- Constrained: it includes the constraint definition within the problem formulation.
  - Unconstrained: it does not include any constraint.
- Number of objective functions:
  - Single-objective problem: only one function must be optimized.
  - Multi-objective problem: two or more functions must be optimized at the same time.
  - Some methods have the single, but also the multi-objective definition.
- Type of variables:
  - Binary: it codifies the input variables as binary strings.
  - Integer: it uses some or all the control variables defined as integers
  - Real-valued: it uses some of the control variables defined as a real value.
- Uncertainty:
  - Deterministic: it does no deal with any variability of the control values.
  - Stochastic, non-deterministic and Robust take into account the variability of the control variable.

From this research's point of view, a relevant classification concerns the uncertainty management. Robust design optimization methods can be based on standard methods, which usually do not take into consideration the uncertainty definition of the input variables. Some modifications should be applied to take into account the variability of input and output variables.

The classification using the criteria of the definition of the input variables can lead to a simple confusion. The stochastic or random methods are those which take advantage of random generation of the populations in order to ensure the best searching strategy. Random generation of the individuals to be evaluated is a good strategy not only to spread them across the whole search space, but also to avoid to be trapped in local minima. Although they are also referred as stochastic optimization methods, they do not consider uncertainty quantification. During this research, whenever stochastic is referred, in almost all the cases it will describe uncertainty related issues.

A clear example of this issue is Evolutionary Algorithms. They are described as non-deterministic and also stochastic methods. Evolutionary Algorithms are population-based methods, which take advantage of random definition of the initial population and of pseudo-random methods to generate the new ones. However, they are not intrinsic robust optimization methods, and do not consider uncertainty on the input parameters.

Robust design optimization is a topic under development. Robust means that result values do not suffer from big variations when small variations are present in the input variables. The variations of the input value are directly related to uncertainties. Uncertainty quantification is a major concern in order to reduce the computational cost of the robust design and optimization. A solution to deal with uncertainty is to define a multi-point problem. It defines several evaluation values for each input variable, usually uniformly distributed along the range. It does not consider any probabilistic or statistical definition, and in addition they usually use few evaluation points. Due to the fact that robust optimization takes into consideration the variance of the input and/or output variables, a multi-point criteria could not be enough to define an accurate value of variance.

Some relevant research and first steps on robust design was done by Huyse and Lewis (2001), who focused on the development of an effective strategy based on stochastic optimization; the authors defined a non-deterministic multi-point optimization procedure that achieve the best performance and minimal cost by managing the uncertainty and obtaining the best solution. Other researches have studied the robust optimization method. Nagarathinam et al (2006) have clearly differentiated between non-deterministic and robust optimization methods. They use an evolutionary algorithm, which is improved using the so-called Hierarchical Genetic Algorithm. This algorithm uses a hierarchical topology of the members of the population, which are distributed into three layers. The first one is used by the refined calculations, another one by the course calculations and exploration for new optimal points and the last intermediate layer is used as a "bridge layer" between refinement and exploration layers.

Aeronautical engineers deal with multi-objective and multi-disciplinary problems as their daily work, due to the multi-physics environment and numerous objectives involved on the problems to be solved. CFD solvers are time-consuming, which means optimization problems can be unaffordable, even without considering the multi-objective character. Trade-offs are not an easy task, and optimization methods try to solve this issue.

Lots of methods have been developed. The most popular ones are still under development and improvement. New ones will be developed to fulfil specific requirements of specific problems, and old ones could be refurbished whenever the circumstances or applications facilitate their renaissance.

In the following sections, some of these methods and procedures are reviewed.

2.2.1 Newton method, and Quasi-Newton Method

The Newton method is mainly a method developed to find the roots of a function, but it can be used to locate maximum or minimum values of a continuous and second order derivable function using and iterative process. Dennis and More (1977) compared Newton and Quasi-Newton's methods in order to justify their development and further applications, but Broyden (1967) was the first who described the application of Quasi-Newton's method to minimization problems. Sorensen (1982) improved the convergence of the method to overcome some problems when minimization analysis is faced. Deuflhard (1974) developed an extended method to deal with "singular" Jacobian matrix.

The used iterative scheme is:

$$x_{n+1} = x_n - \frac{f'(x_n)}{f''(x_n)}, \quad n \geq 0. \qquad \text{2-1}$$

In Equation 2-1 x is the location of the optimal value. This scheme is based on the Newton-Raphson method to find the roots of a function, which starts with a first guess of the root, x_0, to iteratively look for the real root, x:

$$
\begin{aligned}
x_1 &= x_0 - \frac{f(x_0)}{f'(x_0)}, \\
x_{n+1} &= x_n - \frac{f(x_n)}{f'(x_n)}, \quad n \geq 0
\end{aligned}
$$

2-2

Extending this scheme to a multi-dimensional problem:

$$
x_{n+1} = x_n - H(f(x_n))^{-1}\nabla f(x_n), \quad n \geq 0.
$$

2-3

From the previous schemes, we know that the evaluated function $f(x)$ must be differentiable, and the Hessian matrix (H) must be invertible. In addition, we should be careful with the Hessian matrix because even if it is invertible, in some cases it can be ill-conditioned and lead to divergence problems.

In order to solve this kind of problem, a B matrix is introduced that facilitates to invert H.

$$
B(f(x_n)) \approx H(f(x_n))
$$

2-4

The Quasi-Newton method needs to compute the first derivative, but it does not need to compute the Hessian matrix because it is approximated using the B matrix, which is updated in each iteration analysing the gradients. Its iterative scheme is:

$$
\begin{aligned}
x_{n+1} &= x_n - \alpha_n B(f(x_n))^{-1}\nabla f(x_n), \quad n \geq 0 \\
B(f(x_n))^{-1} &\approx H(f(x_n))^{-1}, \quad \text{the Hessian matrix.}
\end{aligned}
$$

2-5

The Quasi-Newton method can be a generalization of the Secant method (Press et al, 2002), which is based in a recurrent procedure to calculate the roots of the function based on the approximation of the root from secant lines. Although the similarities they have, the Secant Method and the Gradient Method were initially developed independently.

2.2.2 Linear programming

The Linear programming method is an optimization technique to be applied to linear function with linear constraints. The Simplex method is a representative of linear programming methods.

The linear constraints define the feasible space, and if they are properly defined, they will ensure that an optimum value will be found.

2.2.2.1 The Simplex Algorithms

A *simplex* is defined as a figure of N + 1 vertex in the N-dimensional search space (a tetrahedron in the 3D space, or a polytope). The constraints of the problem define a polytope. A polytope is a convex and unbounded region defined by all the inequalities that define the constraints of the problem. The concept of the method is, following the sides of the polytope,

to find the vertex which is the optimal solution. Convergence of the method for low dimension problem has been demonstrated by Lagarias et al (1998).

The simplex algorithm has been selected as one of the top-ten methods for linear programming.

2.2.3 Non-Linear programming

Non-linear programming is the name given to the set of techniques to solve an optimization problem over a non-linear objective function and/or a set of non-linear constraints. In some non-linear cases, convex optimization techniques can be used by splitting the problem into different linear functions that will lead to the use of convex techniques of linear programming.

2.2.3.1 Downhill Simplex Method

The Downhill Simplex Method deals with non-linear problems, using the same concept of *Simplex* as in the Simplex Algorithms. Each simplex defines a solution in the search space. The simplex can be expanded, contracted, and reflected. Rogalsky et al (2000) compared several methods when dealing with shape optimization problem. Downhill simplex is compared with Evolutionary algorithms, which provide the best performance for this kind of problems.

If x_0 is defined as the centre of gravity of the simplex, which is defined by the vector $x= \{x_1, x_2, ..., x_n\}$.

A contraction is:

$$x = x_0 - \lambda$$	2-6

An expansion is

$$x = x_0 + \lambda$$	2-7

A reflection is

$$x = -x_0$$	2-8

If the reflected vertex, is equal to the one used as reference for the reflection, then

$$x = x_0$$	2-9
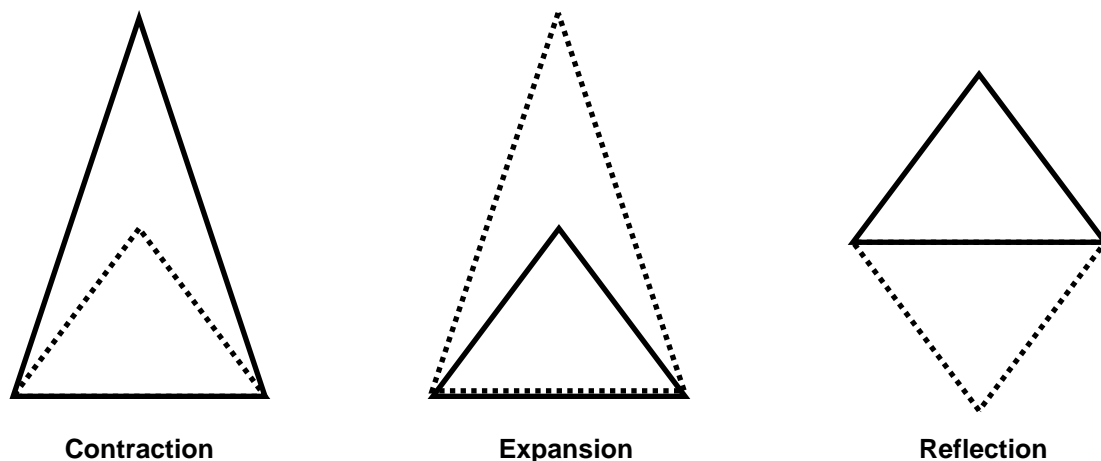
Figure 2-1. Contraction, Expansion and Reflection examples in a 2D Simplex, a triangle.

There are, of course, several combinations of the above modifications. The Downhill Simplex Method takes a series of random steps as follows. First, it finds the point where the objective function is the highest (high point) and the lowest (low point). Then it reflects the simplex around the high point. If the solution is better, it tries an expansion in that direction; else, if the solution is worse than the second-highest point, it tries an intermediate point. If no improvement is found after a number of steps, the simplex is contracted, and started again (Nelder and Mead, 1965).

An appropriate sequence of such steps will always lead to a minimum. Better results are obtained when a large number of steps are tried.

2.2.4 Stochastic programming

The stochastic methods take advantage of the random definition of the input variables, even in the intermediate iterations of an optimization process, in order to ensure the best spread out of the evaluations across the search space.

Some of the stochastic methods are based on natural phenomena, like Simulated Annealing and Genetic Algorithms. Find further details in Section 2.2.4.1 and 2.2.4.2. Both of them use information from the previous iteration to "randomly" generate the next one, in order to combine the best search in all the feasible space but taking into consideration the fittest values previously obtained.

Genetic Algorithms (GA) provide the capability to search in a large design space, combined with the capability to manage a large amount of input parameters. Simulated Annealing shows its best in low number of design variables problems, providing more accurate solutions and spending less time than GA. Mengistu and Whaly (2000) defined an optimization procedure that uses the best of both; Genetic Algorithms and Simulated Annealing.

2.2.4.1   Simulated Annealing

The starting point of this technique has an analogy with the thermodynamics of equilibrium. Condensed matter consists of a very large number of molecules, whose energy is described by the Boltzmann probability distribution:

$$P(E) = e^{-\left(E/kT\right)}$$

	2-10

Where E is the energy of the configuration, T is the temperature and k is the Boltzmann constant. The system is characterized by thermal fluctuations about the average energy, which is the most probable configuration of the system in a thermal equilibrium. The Boltzmann equation states that all the energy levels are in principle allowed, although high and low energies can be equally unlikely. At a macromolecular scale, the individual energies give rise to the equilibrium temperature. Systems that are slowly cooled reach a minimum state of energy, because the molecules are given enough time to rearrange in ordered crystals. On the contrary, if a system is rapidly quenched from high temperatures, it assumes a polycrystalline state that is meta-stable. The slow cooling (*annealing*) is essential to drive the system into a minimum state of energy.

Simulated Annealing and Numerical Optimization

Metropolis, Rosenbluth and Rosenbluth (1953) first applied this idea to simulate a system at thermal equilibrium. In such a simulation, given a small random movement, corresponding to a fluctuation *dE*, the new configuration is accepted if *dE < 0*; if *dE > 0* it is treated probabilistically, e.g. it is accepted with a probability *P(dE) = exp(-dE/kT)*. This model is known as the Metropolis algorithm. Kirkpatrick, Gelatt and Vecchi (1983) take the idea of the Metropolis algorithm and apply it to combinatorial (and other) optimization problems. From the physical process, the numerical elements are applied as shown in Table 2-1.

Thermodynamic Simulation	Combinatorial Optimization
System States	Feasible Solutions
Energy	Cost
Change of State	Neighbouring Solutions
Temperature	Control Parameter
Frozen State	Heuristic Solution

Table 2-1. Thermodynamic simulation and combinatorial optimization equivalence

For an optimization problem the objective function *f* is used instead of the energy *E* and the system is defined by its parameters *x*. This algorithm requires some additional tuning, because the result is strongly dependent on the annealing schedule, the number of trials at a given temperature and the starting temperature. The random search used by this method avoids to be trapped on local minima.

Regarding performance of the method, Simulated Annealing cannot be applied to all problems. It is known that some functions do not accept annealing due to their shape; mainly because the lack of smoothness. It means that annealing will be trapped on local minima without the capability to reach high-temperature states that will lead to better low-temperature

states (global minimum). Rutenber (1989) described this situation in his general description and overview of the state-of-the-art about Simulated Annealing.

Even though this described issue, Wang and Damodaran (2001) apply Simulated Annealing to an aerodynamic shape optimization problem. Due to the time-consuming codes to solve the Euler and Navier-Stokes equations, they implement a parallel computing platform to improve calculation time.

2.2.4.2   *Genetic Algorithms*

Genetic algorithms belong to a more general set of techniques named Evolutionary Strategies or Evolutionary Algorithms. The two most common strategies are Genetic algorithms, based mainly on three operators; cross-over, selection, and mutation, and Evolution strategies. Evolution strategies differ from Genetic Algorithms because of the use of mutation over recombination. As explained by Papadrakakis, Lagaros and Tsompanakis, (1998) and by Whitley (2001), the new developments are mainly used to machine learning, and Evolution Strategies are used to optimization, whereas Genetic Algorithms are viewed as a multi-purpose technique that can be successfully applied to optimization, too.

The Genetic Algorithms are population-based techniques. They are devoted to the improvement of the individuals of a population in an iterative optimization loop. The Genetic algorithms techniques are based on evolution-like mechanisms, which provide the ability to learn from the environment having no control on it. Basically, evolution is a consequence of random modifications that are based on hereditary information. These modifications could be recombination of the chromosome strings, mutation, and crossover of genetic information between parents. Considering that all living species are well adapted to their environment, the same techniques can be applied to look for the optimum value in an optimization problem.

In a numerical optimization problem, the Genetic Algorithm technique provides a methodology applicable to any kind of problems. Such a method does not need to have a complete knowledge of the problem itself, but it will find the optimum value anyway.

Using the natural genetic process, crossover is the basic recombination mechanism that allows beneficial genes to be represented in the new children DNA. The DNA information is swapped. Several processes are developed, and new ones are in development in order to optimize the crossover efficiency, and the convergence speed of the overall GA technique.

Mutation is a refinement that keeps the health of the new populations, avoiding a too fast convergence to a non optimum value. Generally speaking, this process corresponds to selecting at random a few members of the population, determining at random a location in the strings and switching the bit at that location.

Numerically, such a process can be easily programmed. Inputs can be converted to their binary representations, if binary representation is selected. However, Genetic Algorithms can only use a real-coded input string. The input string, which will contain the input values, can be shorter using real coded representations, but not all the problems accept this kind of codification. The user should select between binary or real codification according to the input parameters.

Selection is the technique that gets to the fittest individuals the chance to be reproduced. As it can be guess, Selection determines the best individuals over the whole population.

Recombination is the creation of a new individual taking information of two parents. Half of the individual comes from one parent and the other half from the second parent.

Further description of these strategies is going to be presented in next sections, because of the interest of this method.

A fitness function is defined, and each individual is associated to its objective function value (its fit value). Therefore, the fittest individuals will have bigger probability to be chosen; they will become parents of a new generation. To generate each new individual of a new population, the crossover, mutation and selection operator can be applied to the parents. Each operator can be assigned a probability to operate on a given parent.

A genetic algorithm can use binary-coded or real-coded variables. Binary-coded variables need to be coded and decoded during the input and output phases of the optimization. To code the variables the number of genes or chromosomes must be previously defined, so the binary string must contain the binary representation of the number. Those variables that use discrete values can also be binary coded.

There are several developments, even considering only Genetic Algorithms and avoiding the most general category of Evolutionary Strategies. Sasaki et al (2001) used Adaptative Range Multi-Objective Genetic Algorithms (ARMOGA) for the optimization of an aerodynamic wing, minimizing transonic and supersonic drag and structural moments in the wing. Deb and colleagues in (Deb, 2003; Deb, Anand and Joshi, 2002; Deb et al, 2000; Deb et al, 2000; Deb and Goel, 2000; Deb, Pratap and Moitra, 2000) extensively studied Genetic algorithms and created the Non-dominated Sorting Genetic Algorithms, the so called NSGA, and its evolution NSGA-II, while developing new applications with real coding genetic algorithms.

2.2.4.2.1 Crossover

The crossover operation is based on the need to reproduce the best members of each population to generate the next one, so the optimization can evolve to the optimum value. Crossover is a recombination of the chromosomes from the best individuals. The simplest crossover technique is done with binary-coded, but real-coded cross-over is also feasible (Deb, Anand and Joshi, 2002). There are several methods to produce this recombination; the main ones are the single point crossover, the two-point crossover and the last one, the crossover on a straight line (or uniform crossover):
   a) One-point crossover: from two parents it is possible to generate two new offspring dividing the parents into two parts (head and tail of the binary string), and then, interchanging the tails to create two new individuals to be evaluated.
   b) Two-point crossover: a generalization of the one-point crossover is the two-points, and even the multi-point crossover. Dividing the binary string in two different points (or more than two in the multi-point case), it consists on the recombination of the portions into new offspring.
   c) Multi-point crossover: this type of crossover is based on the definition of the new offspring gene by gene to define the new chromosomes. The information can be taken from one or two parents, which randomly provide the value of each gene of the new

individual. No values are predefined to the chromosomes and are randomly selected from the information provided by the parents.

2.2.4.2.2 Mutation

The mutation operator creates new offspring from changing the value of a selected gene. Mutation is generally presented as a secondary operator used mainly to avoid being trapped in local minimum. Mutation should introduce new information to the genetic chain, refreshing the individual information. It is important to take into consideration that increasing the mutation probability, the convergence to a non-global minima can be increased, but also it can produce the opposite effect reducing or completely enabling the convergence.

The crossover operator is commonly the most important because, compared with mutation, it is faster, so the whole search space can be quickly analysed. Although this generally accepted, mutation can be used instead of crossover in many cases, obtaining similar results.

There are mainly two types of mutation. The first one consists on mutating all the genes, according to the mutation probability. The second type is the so-called creep mutation which applies a tiny variation to the values, or what is the same, it changes only one bit. Figure 2-2 shows an example of the creep mutation.

Mutation Point

Offspring 1 0 1 0 0 1 0 0 1 0

Mutated Offspring 1 0 1 0 1 1 0 0 1 0
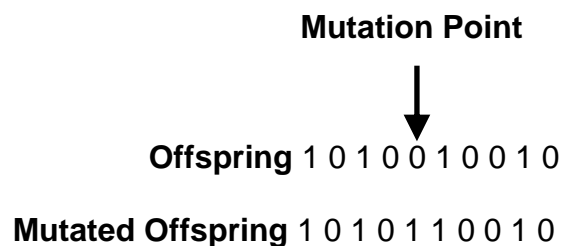
Figure 2-2. Creep Mutation example

2.2.4.2.3 Selection

The selection operator is used to define which individual will be chosen to generate the new offspring. The selection operator defines the probability of an individual to be selected according to its fitness value, the value coming from the evaluation of the fitness function. There are several ways to define the selection probability, and the definition of the best one is mainly a problem related issue. Some selections techniques can be Fitness proportionality, Roulette wheel, Stochastic Universal Sampling, Tournament selection, or Ranking.

A brief introduction of each of them is provided:
   a) Fitness proportional selection: In this case, the selection probability of the individuals is calculated by dividing their fitness value by the sum of all the other fitness of the individuals.
   b) Roulette wheel selection: An individual is selected by spinning the wheel, which is divided according to the selection probability. The selection probability is calculated according the values of the fitness function. The bigger the probability selection, the

larger the wheel section assigned to each individual. At the end it is based on the probability of each individual.

c) Stochastic Universal sampling: It is an improvement of the Roulette wheel. It avoids bias and it minimizes spread because it uses a constant selection step along the wheel.

d) Tournament selection operates by choosing some individuals randomly from a population, creating the so-called mating pool, and selecting the best from this group to survive in the next generation. Its simplest form is binary selection, where a random pair of individuals is selected from the population and the pair with higher fitness is copied to the mating pool or population.

e) Ranking: individuals are ranked by their fitness values. The best individual receives rank 1; the second receives rank 2 and so on. A selection probability is reassigned in accordance with the ranking order.

Selection is needed to gain diversity and avoid premature convergence. The selection level has to be defined in the appropriate value to ensure evolution.

2.2.5 Robust Design and Optimization

Robust optimization techniques are a set of methodologies that take into account the uncertainty in the input variables of an optimization problem. They are based on the known or estimated probabilistic information of the input variables.

Robust optimization deals with feasibility and robustness concepts. Both of them manage uncertainty information in order to keep the best design regarding reliability or robustness. These two concepts are quite similar, but they present some basic differences; as explained in Crespo and Kenny (2005) in a reliability-based formulation, the probability of violating the prescribed design requirements by inequality constraints is minimized. In a robustness-based formulation, a metric that measures the tendency of a random variable/process to cluster close to a target scalar/function is minimized. Crespo and Kenny (2005) studied both reliability and robustness-based formulations to be applied in a multi-objective optimization procedure.

Robust optimization techniques can be based on deterministic optimization methods. They use a non-intrusive uncertainty quantification method, combined with the optimizer to create a non-deterministic analysis. Intrusive uncertainty quantification methods are expensive, mainly in the implementation. They require the modification of the numerical solver. Non-intrusive methods use the solver as a black box, so uncertainty is defined in a parallel box that feeds the solver with the values to be evaluated. Later on, all the results are treated to obtain their mean and variance deviation.

2.2.6 Deterministic and non-deterministic design optimization

Both deterministic and non-deterministic optimization are applied in many fields, but, due to the complexity and the required long calculation time of the solver, non-deterministic optimization has not extensively been applied to too many engineering fields so far.

The so-called deterministic optimization does not use any information about the nature of the input variables and only the range and the search space are considered. Mathematically speaking, it means that all values are considered with the same probability. However,

engineering problems do not have such behaviour and some variables can follow a normal density probability function, for example.

To take this behaviour into consideration with a non-intrusive technique requires more calculation time due to the generation of more individuals and populations, which means more cases to be evaluated. Although it is applied in other fields, CFD requires a long time for each evaluation, so the computational total time is rapidly increased. This is the main reason why non-deterministic optimization has not been extensively applied to CFD so far, and the reason why one hardly can find literature about the topic.

The deterministic optimization can provide us a very high precision optimum value, but it will be completely isolated from reality; as mentioned by Beyer and Sendhoff (2007) robust optimization takes into consideration some important points from the real world:
1) Almost all optimization procedures are based on approximation models, so it means an intrinsic error exists in the optimization procedure and in its result.
2) Manufacturing tolerances are not included in the calculations. They can affect the performance of the system during its life-cycle.
3) Life cycle of the system; including parameters fluctuation, materials wear down, parts replacement due to maintenance, and some other factors that change the initial state of the systems also affect the performance, and they produce a variability around the nominal working point.
4) Maintenance issues, and environmental considerations, for example, limit the ability to reach the optimum design and they must be taken into account during the design process. They are the constraints of an optimization analysis.

All this factors introduce variability on the system conditions, uncertainties during design, manufacturing and use of the system, and all of them should be considered during the optimization process.

Non-deterministic or Robust optimization, establishes its roots in the researches developed by Taguchi in 1940's developed as quality improvement methods (Taguchi and Chowdhury, 2000). Taguchi's method or Robust design is mainly oriented to the process design rather than to the product design. It can be understood as a design of experiments methodology. Taguchi's method is an unconstrained method. Taguchi's method has been largely used in engineering applications, see for example Clarich et al (2004), or Pediroda and Clarich (2004). As stated on the robust design by Park et al. (2006) and references therein, and in the robust optimization review by Beyer and Sendhoff (2007), and also references therein, it introduces the concept of robustness using the function

$$L(f) = k(f - m)^2.$$
<div align="right">2-11</div>

A quadratic loss function L where k is the constant to define the loss and m is the target value.

The expected value of loss is then defined as

$$Q = E(L(f)) = k\left(\sigma^2 + (\mu - m)^2\right),$$
<div align="right">2-12</div>

Where μ is the mean value of f and σ is the standard deviation. Then the robust design is aimed to minimize the average loss. From this starting point, Taguchi's method defines a

scale factor *s*, as the ratio between m and *μ*. Applying this scale factor on equation 2-12 the next equation 2-13 is obtained

$$\eta = 10\log_{10}\left(\mu^2 \big/ \sigma^2\right).$$

2-13

That is called the signal to noise *(S/N)* ratio, or signal noise.

The research on Taguchi's method by Park et al (2006) defines the transfer function to ensure effectiveness of S/N ratio, and identifies if robust design will be obtained depending on the S/N ratio before solving the problem. Some other developments over the Taguchi's method uses meta-models to approximate the analysis in order reduce the calculation time required. The point is that the accuracy of the method strongly depends on the accuracy of the meta-model.

Several attempts have been made in order to solve multi-objective problems with Taguchi's method. As Park et al. (2006) describe in their research, some solutions based on weight factors. They apply the Fuzzy theory to determine the weight factors and to avoid the strong dependency on the designer intuition. Some other researches improve Taguchi's method by including constraints as explained in reference therein Park et al (2006).

Several references can be found for optimization methods, deterministic methodologies are the most extensively applied, see for example Monge and Tobio, (1988), Hua et al, (2003), other ones use the so called probabilistic methods or stochastic methods, like Evolutionary Algorithms, which are population-based methods, or simulated annealing (Obayashi, Sasaki and Takeguchi, 1998; Wang and Damodaran, 2001; Dietz, Vob and De Breuker, 2004; Sasaki et al, 2001; Deb, 2003).

Stochastic-probabilistic methods are the next step to the so-called robust optimization, taking into account uncertainties like it has been developed by Thamotheram et al (2002), Bugeda et al (2003) and Balsa-canto et al (2003).

Although there are some methods and techniques for uncertainty quantification in the optimization procedure, almost all methodologies consider few points into the range of uncertain variables. Li and Padula (2003), for example, define five values within the range of uncertainty for the Mach number when dealing with airfoil shape optimization. Lee et al (2008, 2009, 2010) use the same technique to evaluate the mean and the standard deviation of the results due to the uncertainty given by the Mach number and the angle of attack.

2.2.7 Multi-objective optimization

All engineering problems are multi-objective problems. The problem can be simplified by only analysing one of the objective functions. But the entire real-world problems will always involve two or more objective functions.

Engineers have the responsibility to analyse all the set of solutions and to choose the most appropriate one. The best one no longer exists, because the combination of multiple best solutions for each objective will provide us a set of optimal solutions. Analysing two or more objective functions leads to the need of selecting the best possible combination, and

sometimes it depends on external factors not included on the optimization procedure. Then the usual situation in multi-objective optimization is that improving one of the objectives can mean the second objective to get worse. The concept of Pareto Optimality is the most convenient way to select the best solutions.

2.2.7.1 *Pareto Optimality*

The Pareto Optimality concept was established by Vilfredo Pareto in 1906 in his "*Manual of Political Economy*". The Pareto Optimality defines the optimal points of a multi-objective optimization as the points that improve one of the objectives without getting worse one of the others. It means that all objective functions improve their values to an optimum or it cannot be considered an optimal point.

Firstly described in economics, it has been easily transferred to engineering and other fields. The Pareto Optimality has become a powerful tool to define the set of optimal solutions, so the designer can choose the preferred ones according to several design criteria (Beyer and Deb, 2000; Golberg, 1988; Deb, 2003).

2.2.7.2 *Pareto Frontier*

The representation of the optimum set of values is the so called Pareto Frontier or Pareto Set. The mathematical definition of Pareto frontier is as follows:

Being an optimization process which seeks the minimum point,
$$f : \Re^n \to \Re^m$$
is the function that gives a design space point *x* of *n* dimensions, a judgement criteria *y=f(x)* of *m* dimensions.

X is the feasible subset of $\Re^n$ and *Y=f(X)*.

The Pareto frontier is the subset of *Y* compounded by the non-dominated points. A point *a* is called to dominate *b* if $x_i \leq y_i$ for each *i*, and $x_i < y_i$ for some *i*. It is represented as $x \succ y$, and it is said that *x* strictly dominates *y*. Figure 2-3 is an example of the Pareto front. The black set of points is the Pareto frontier, while the red set is the whole set of feasible solutions.
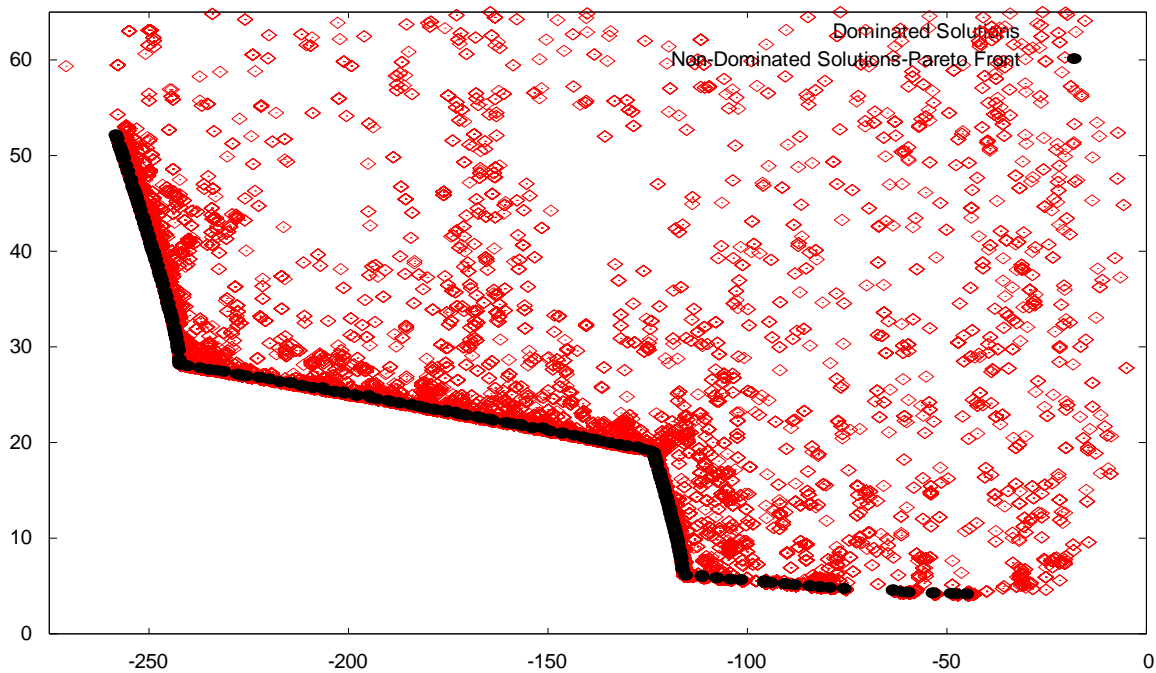
Figure 2-3. Non-Dominated solutions

2.2.7.3   *Upgrading Genetic Algorithms*

Genetic algorithms, as the more general description of evolutionary algorithms, are considered one of the best methods to deal with multi-objective problems. However, they are always under development, with new methodologies which improve mutation, or cross-over, input treatment, or procedures to better fulfil each problem requirement.

Schaffer (1985) defined the first multi-objective application for genetic algorithms with his Vector Evaluated Genetic Algorithm (VEGA). The Multi-objective formulation of Genetic Algorithms was reviewed in Fonseca and Fleming (1993) or a more recent one in Toshev and Korsenov (2007). Both of them present several developments regarding multi-objective genetic algorithms and conclude that, although performance criteria can be defined, each problem has specific requirements and the algorithms developed can fit better to the specific problems.

As already mentioned, Sasaki et al (2001) developed an Adaptative Range Multi-Objective Genetic Algorithm (ARMOGA), which provides better performance dealing with transonic wing shape optimization. Regarding noisy solutions, Strength Pareto Evolutionary Algorithms (SPEA) developed by Ziztler and Thiele (1999) uses dominance criterion for fitness assignment and selection of solutions to avoid misleading optimum solutions due to noise on the solution. SPEA2 and SPEA2+ developed by Ziztler in 2001, introduce improvements on the searching techniques (crossover and selection). They reinforce the searching capabilities of these methods while ensuring the best performance and also while ensuring the maintenance of diversity on the solutions that will lead to optimum values. A comparison between well-known NSGA-II by K.Deb and SPEA, SPEA2 and SPEA2+ by Ziztler has been evaluated by Hiroyasu, Nakayama and Miki (2005).

2.3 Uncertainty quantification

Although uncertainty is usually identified with error, it can also be associated with lack of knowledge. Error is the difference between the real value and the measured/calculated one, but this is not the magnitude of interest in our case. Uncertainty refers to how this lack of knowledge is modelled, and how it can be introduced into analysis.

Several methods have been developed to deal with uncertainty quantification. The first one is the Monte Carlo method, which provides an easy way to model random probabilistic values in a non-intrusive way. In addition, it enables the analysis of full statistics of the variables; namely the four main statistical moments. It is well-known that one of the major drawbacks of Monte Carlo methods is the associated huge computational effort.

Non-intrusive methods can be coupled with the numerical solver without modifying it, or at least without major changes.

Another proposed technique is the so-called perturbation method, which basically involves expanding the variables around their mean values, using Taylor series. This technique is limited to Gaussian or quasi –Gaussian processes due to the fact of a difficult incorporation of terms of order higher than two. In addition, it only provides low order statistics, due to its low order approximations.

Other methods that are under development are Probabilistic collocation methods. They provide the capability to capture statistical behaviour with few samples. Each sample is weighted according the probability density function of the variable. The main drawback of the Probabilistic Collocation methods is that the higher the number of variables is, the higher the complexity of implementation is.

2.3.1 Monte Carlo Techniques

Monte Carlo method defines a set of non-intrusive sampling techniques. Monte Carlo sampling, Latin Hypercube sampling, and Orthogonal sampling are briefly introduced in Sections 2.3.1.1, 2.3.1.2, 2.3.1.3.

All this sections contain concepts that are used by STAC. STAC is a stochastic calculus manager which provides the capability to perform stochastic analysis in a non-intrusive way. It takes advantage of Monte Carlo techniques (see Appendix I).

2.3.1.1   Monte Carlo sampling

The Monte Carlo method provides a flexible procedure to statistically analyse a problem using probabilistic information of the input variables. It is very useful to compute full statistics; it is considered an exact method to account with uncertainty in the sense it does not require any assumptions or approximations.

Monte Carlo method uses the input variables and their probability density function to generate a set of samples of the input variables. Each sample is a combination of a randomly generated value of each input variable, and it is used to perform the simulations (an evaluation or a shot,

in Monte Carlo terminology) instead of using directly the probability density function of each input variable. The method works inverting the probability density function, which will be introduced later.
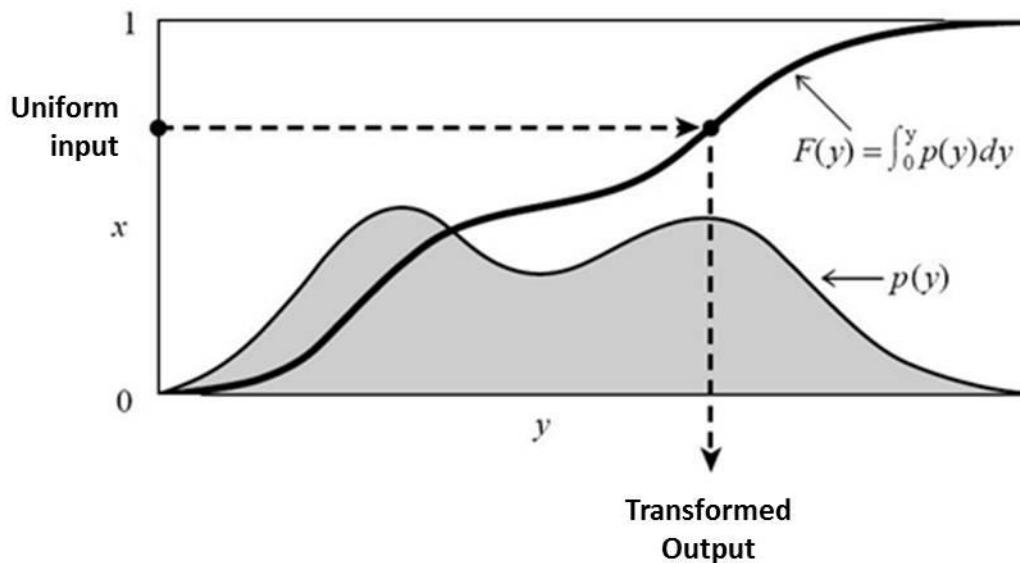
Figure 2-4. Inversion of the probability density function

The method uses the relation $y(x) = F^{-1}(x)$. Geometrically, $F(y)$ is the area under the $p(y)$ curve (the probability density function of y). Therefore, the relation described above is the same as saying that: choose a uniform random x, then find the value y that has that fraction x of probability area to its left. As shown in Figure 2-4, the probability density function provides the capability to transform a value, which is uniformly distributed or has a uniform probability to be selected within a range [0,1], to a transformed one which follows a Gaussian distribution within a pre-defined range.

The amount of shots (samples) calculated must ensure the convergence from a statistical point of view. The confidence intervals (+/- 5%) of the mean are used for such purpose. The mean μ_e is estimated dividing the sum of the values by the total number of values.

Statistics show that

$$M = \frac{\mu_e - \mu}{\sigma_x \sqrt{\dfrac{1}{N}}}$$

μ_e : mean estimation

μ : true mean

N : number of values

σ_x : std deviation

2-14

The random variable M is normally distributed with mean μ_M equal to zero, and standard deviation σ_M equal to 1. Then the probability that M lies within the range [a, b] is

| | 2-15 |

Where $\Phi(x)$ is the standard normal variable, a widely tabulated variable.

The normalized statistical moments have their application on the comparison between probability density function which have been defined using different values of mean and standard deviation. During the present research the normalised values have been used.

Using the notation of the so called Significance Level, α, where

$$[\alpha] = \left[-k_{\alpha/2}, k_{\alpha/2}\right] \quad \text{and} \quad \Phi(k_{\alpha/2}) = 1 - \frac{\alpha}{2}$$

, it can be written that the probability that the true mean lies within the range $[\alpha] = \left[-k_{\alpha/2}, k_{\alpha/2}\right]$ is

| $$P\left[\bar{x} - \frac{k_{\alpha/2}}{\sqrt{N}} \le \mu \le \bar{x} + \frac{k_{\alpha/2}}{\sqrt{N}}\right]$$ | 2-16 |

As previously mentioned, the application of Monte Carlo's method uses common values of α within the range [0,03; 0,05], depending on how restrictive one needs to be.

Cumulative Frequency

If a random variable Y can take a real number $a \le Y \le b$, and if the upper limit b is a deterministic real value x, then the probability that Y is less or equal to x, $F(x)$, becomes a function of x. This probability is shown by the hatched region in the Figure 2-5, and mathematically written as follows:

| $$F(x) = P[a \le Y \le x]$$ | 2-17 |
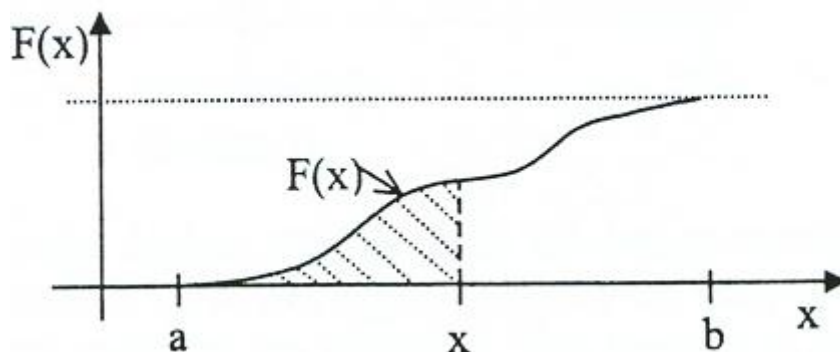
Figure 2-5. Cumulative Frequency

Probability density function

The probability density function describes the expected concentration and spread of the random variable *Y* within a range [*a, b*]. This is done by considering the probability that *Y* assumes a value in the range [*x, x+Δx*].

$$p(x) = \lim_{\Delta x \to 0} \frac{F(x + \Delta x) - F(x)}{\Delta x} = \frac{dF(x)}{dx}$$	2-18

If Δ*x* approaches to zero, *p(x)* approaches $\dfrac{dF(x)}{dx}$, the first derivative of the cumulative distribution function and it is called the probability density function, hereafter referred to as PDF. The cumulative distribution frequency is related with the probability density function as:

$$F(x) = \int_a^x p(x) \, dx$$	2-19

Both Cumulative Frequency and Probability density function have been used for the calculation of *x* value according its probability.

Generation of a Random Number

The equation $X_{i+1} = a \cdot X_i \cdot \text{mod } m$ is the expression of the linear congruential method, which is used to generate random numbers in the range [0, 1]. *"mod"* is a function that removes the value of *m* from the value of *a·Xᵢ* until the residual is less or equal to *m*. The values of *a* and *m* are defined by the user. STAC code, which has been extensively used during our research, uses the values: a=2³¹-1, and m=890706376 (Hurtado and Barbat, 1998; Hurtado, 2004). See Appendix I for further details about STAC.

Uncertainty quantification based on Monte Carlo method provides the capability to obtain the full statistics. Based on the variance rule for samples of *N* elements, it can be the main advantages are that its convergence rate does not depend on the number of independent random variables, and that its application is straightforward (Mathelin, Hussaini and Zang, 2005).

Some techniques that improve its convergence rate are Latin Hypercube, or importance sampling.

2.3.1.2 *Latin hypercube sampling*

The statistical method of Latin hypercube sampling (LHS) was developed to generate a distribution of plausible collections of parameter values from a multidimensional distribution. It can be considered an improvement method over Descriptive Sampling and it is often applied in uncertainty analysis. Latin Hypercube sampling improves the convergence rate of Monte Carlo sampling (Mathelin, 2008).

McKay, Conover and Beckman (1979) describe firstly this technique. Ronald, Iman, Helton and Campbell (1981) further elaborate it in 1981.

In the context of statistical sampling, a square grid containing sample positions is a Latin square if (and only if) there is only one sample in each row and each column, as shown in figure 2-6. A Latin hypercube is the generalisation of this concept to an arbitrary number of dimensions, whereby each sample is the only one in each axis-aligned hyper-plane containing it.
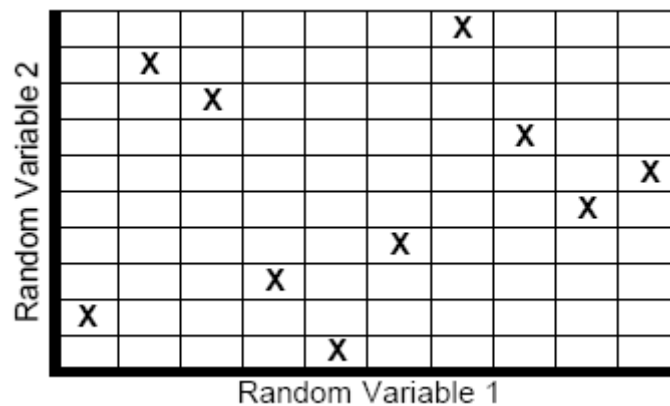
Figure 2-6. Latin Square

When sampling a function of N variables, the range of each variable is divided into M equally probable intervals. M sample points are then placed to satisfy the Latin hypercube requirements; note that this forces the number of divisions, M, to be equal for each variable. Also note that this sampling scheme does not require more samples for more dimensions (variables); this independence is one of the main advantages of this sampling scheme. Another advantage is that random samples can be taken one at a time, remembering which samples were taken so far.

2.3.1.3 Orthogonal sampling

Orthogonal sampling adds the requirement that the entire sample space must be sampled evenly. Although more efficient, orthogonal sampling strategy is more difficult to implement since all random samples must be generated simultaneously.

Figure 2-7 is a representation on how the probabilistic definition of the variable affects the way the samples are spread across the sampling space.
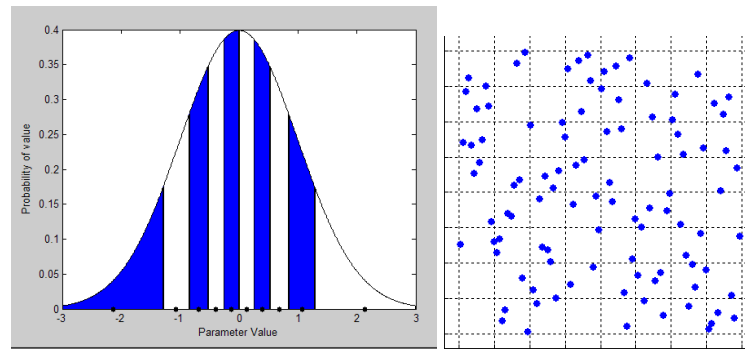
Figure 2-7. Latin Hypercube samples spread out

In two dimensions the difference between random sampling, Latin Hypercube sampling and orthogonal sampling can be explained as follows:

In random sampling, new sample points are generated without taking into account the previously generated ones. Thus one does not necessarily need to know beforehand how many sample points are needed.

In Latin Hypercube Sampling one must first decide how many sample points to use and for each sample point remember the row and column the sample point is located.

In Orthogonal Sampling, the sample space is divided into equally probable subspaces. All sample points are then chosen simultaneously making sure that the total ensemble of sample points are a Latin Hypercube sample and that each subspace is sampled with the same density.

Thus, orthogonal sampling ensures that the ensemble of random numbers is a very good representation of the real variability; Latin Hypercube Sampling ensures that the ensemble of random numbers is representative of the real variability whereas traditional random sampling (sometimes called brute force) is just an ensemble of random numbers without any guarantees.

2.3.2 Probabilistic collocation method

Several methods have been developed to deal with uncertain input parameters and to propagate this uncertainty to the solution.

Both the Monte Carlo method and its evolution, the Latin Hypercube sampling have been already discussed. They are based on the computation of samples from the probability density function of the input variables, which are used to compute deterministic calculation of the solver. From this set of deterministic solutions mean and standard deviation values can be calculated.

The Monte Carlo method is usually seen as an expensive method to deal with uncertainties. Some cases need to deal with a large amount of samples in order to catch the mean and deviation of the input and output values.

Other methods do not use the concept of random sample, but use the concept of collocation. It means that the uncertain space is represented by a set of weighted values that provide a good

understanding of the behaviour of the uncertain parameter. Points, or the so called collocation points, and weights are calculated based on a Gauss-quadrature of the uncertainty space. The required quantity of solver evaluations quickly increases with the number of uncertain parameters to deal with. But it also increases due to the degree of the spectral expansion representing the uncertain parameters. However, the number of shots is less than other uncertainty quantification methods.

The Probabilistic Collocation method uses quadrature techniques to obtain the points where the solver will be evaluated, and they use fixed values for same probability density functions using the same mean and the standard deviation. Figure 2-9 to 2-14 show the quadrature points obtained for different degrees of the polynomial, which defines the quadrature collocation, when a non-truncated or a truncated probability density functions are defined. The truncated case uses a truncation interval defined by the mean plus 3 times the standard deviation, which means the 99,7% of the probability. Non-truncated PDF spreads collocation points across a wide range when the polynomial order of the collocation method is increased, while truncated PDF fixes a limited range of values where the collocations points are located, even the polynomial order is increased. Figure 2-8 illustrates the truncated or non-truncated PDF concepts.
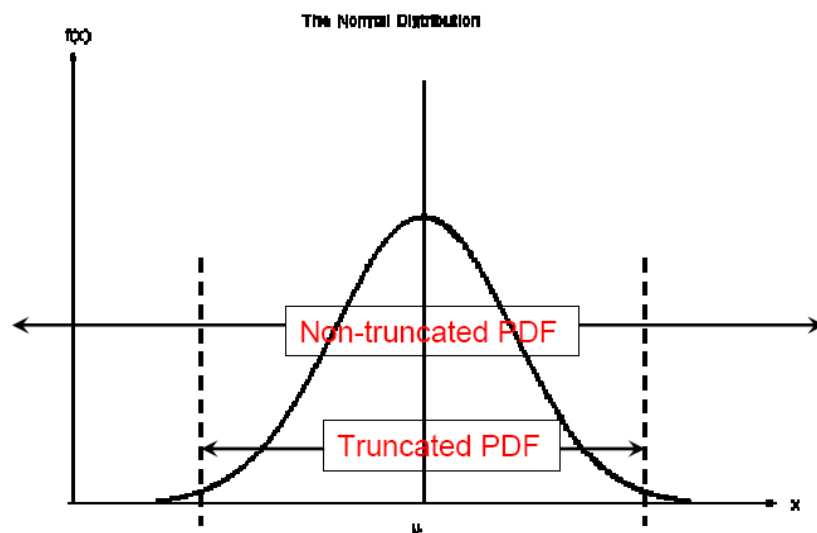
Figure 2-8. Truncated and non-truncated PDF

Figure 2-9 compares the set of quadrature points obtained for the polynomial of degree equal to 5 for a non-truncated and a truncated PDF. Figure 2-10 compares the points for degree equal to 10. Both truncated and non-truncated cases are plotted.

Figure 2-11 compares the points for the non-truncated cases of degree 5, 10, and 15. Figure 2-12 the weight of each collocation point from Figure 2-11. And Figure 2-13 compares the points for the truncated cases. Figure 2-14 shows the weight of each collocation point from Figure 2-13. The figures show the points where the solver is evaluated. These are the collocation points extracted from the probability density function.

Comparing Figure 2-12 and 2-14, the reader can observe how the truncated PDF limits the range of the collocation points. The Gaussian bell defined in the non-truncated case, Figure

2-12, is thinner than that in Figure 2-14 due to the larger range of values of the collocation points.
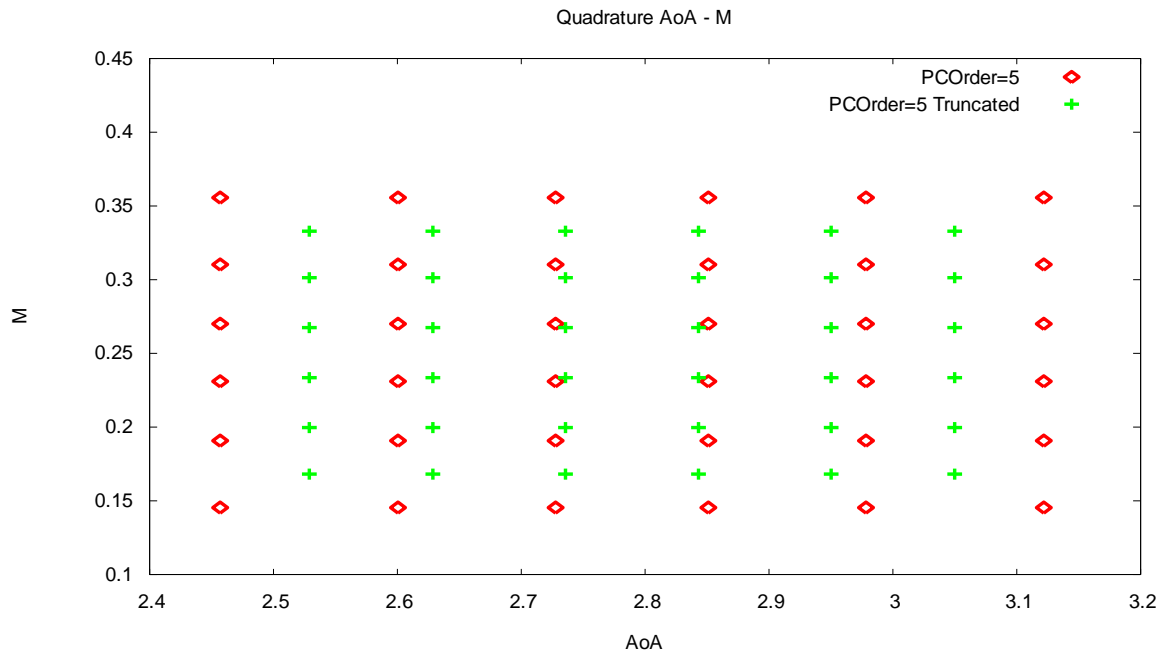
Figure 2-9. Quadrature points for order 5, truncated and non-truncated PDF
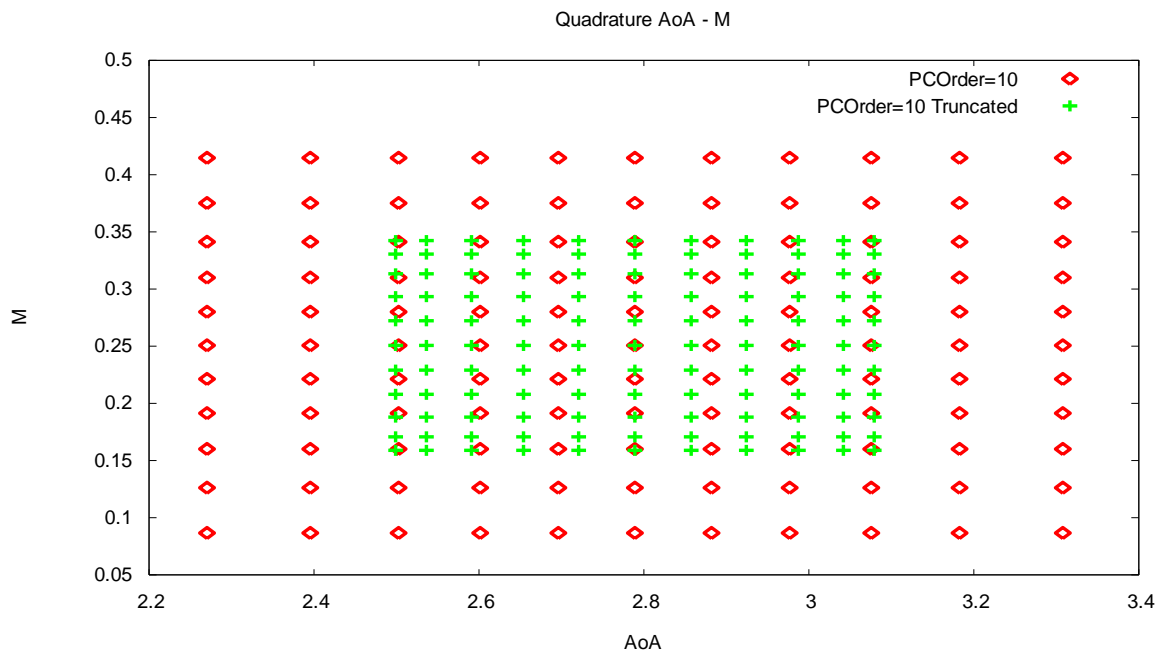
Figure 2-10. Quadrature points; PC order 10, truncated and non-truncated PDF
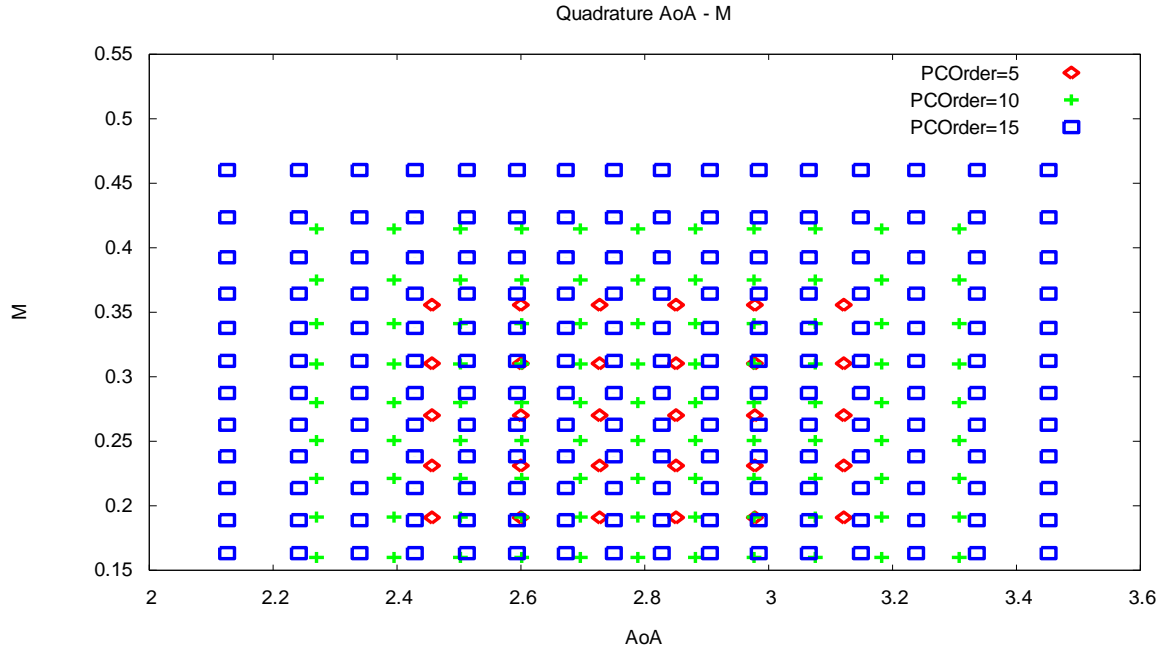
Figure 2-11. Quandrature points PC order 5, 10 and 15, non-truncated PDF
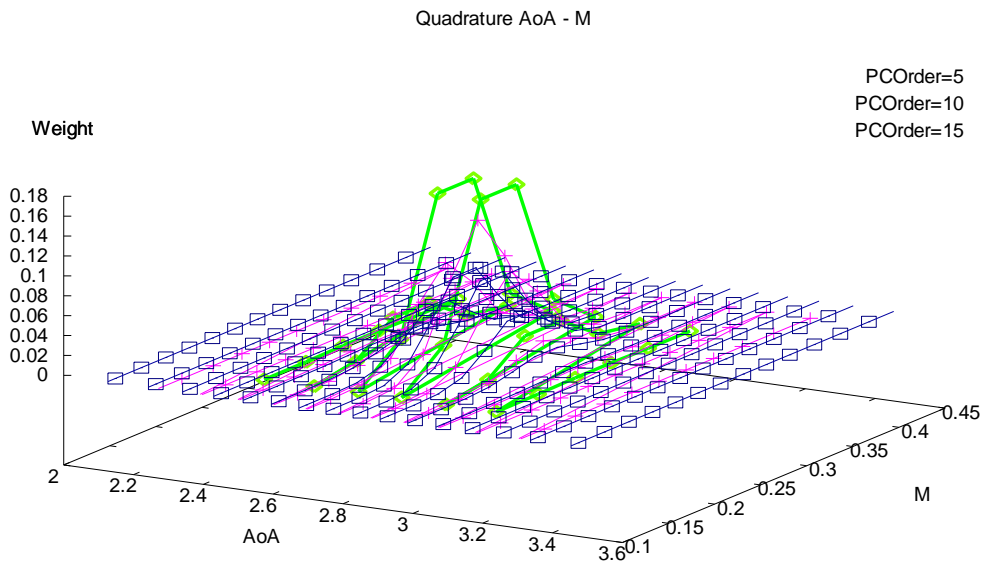
Figure 2-12. Weights of PC order 5, 10 and 15, non-truncated PDF
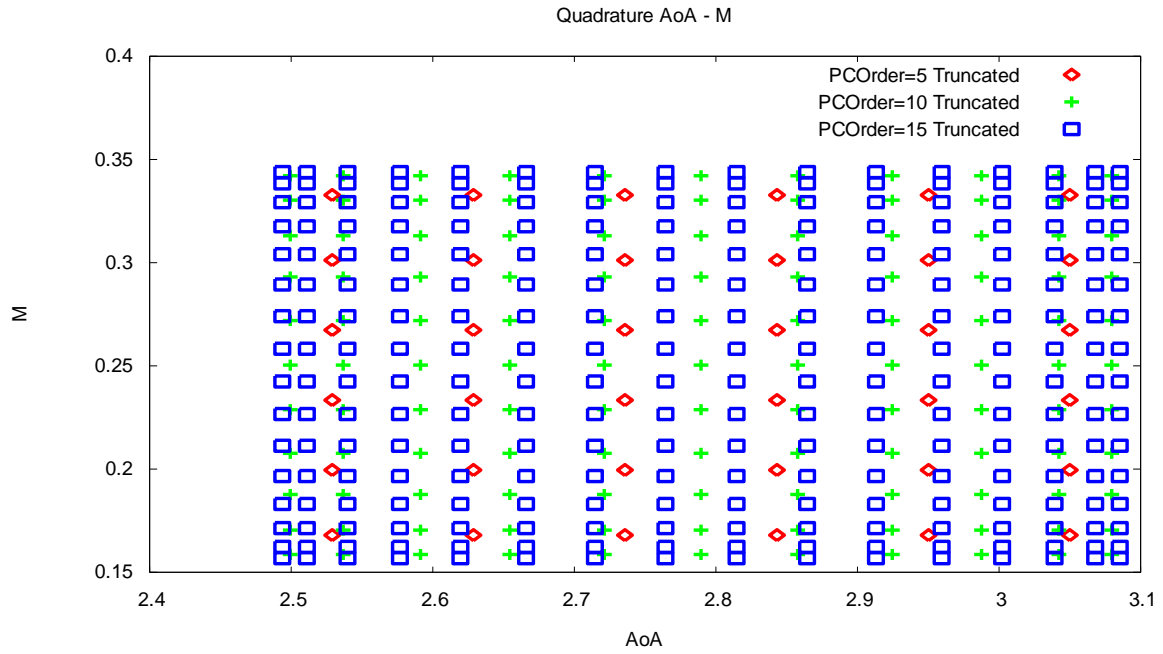
Figure 2-13. Quadrature points PC order 5,10 and 15, truncated PDF
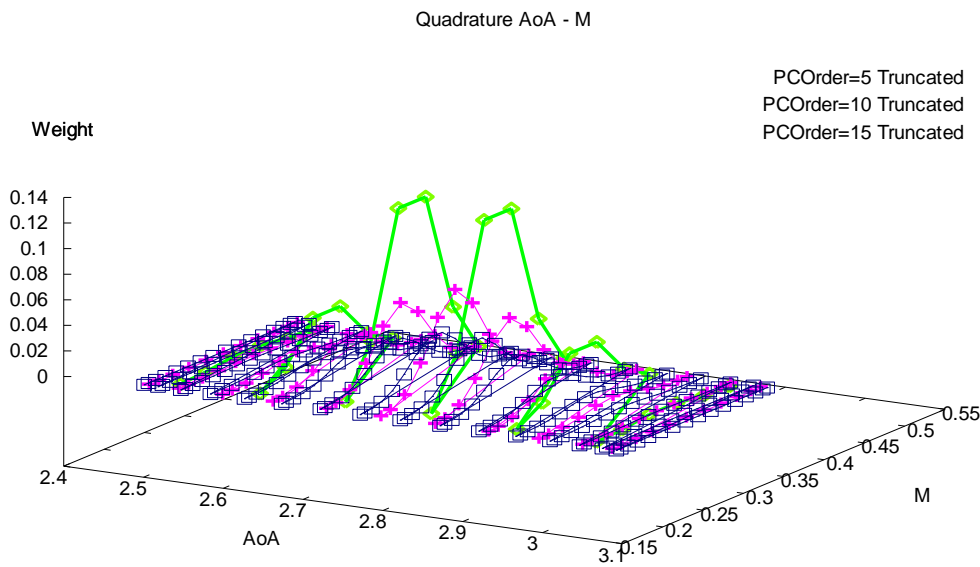
Figure 2-14. Weights of PC order 5,10 and 15, truncated PDF

It is clear that truncated probability density function (PDF) limits the range of the collocation points. However, the selection of a truncated or a non-truncated PDF does not affect the mean and the standard deviation and both of them represent the same population. As already mentioned, the mean and the standard deviation remain to the defined values, whichever the degree of the polynomial is, or the selected PDF is.

The quadrature technique has defined the collocation points and their weights. Figure 2-15 and 2-16 illustrate how the mean and 3σ range of the input variables remain constant when the degree of the polynomial increases.

Due to the fact that the Probabilistic Collocation method does not use the concept of samples as Monte Carlo or Latin Hypercube do. It has no sense to analyse the variability of the set of samples, because all of them will be the same set of values; exactly the same values.
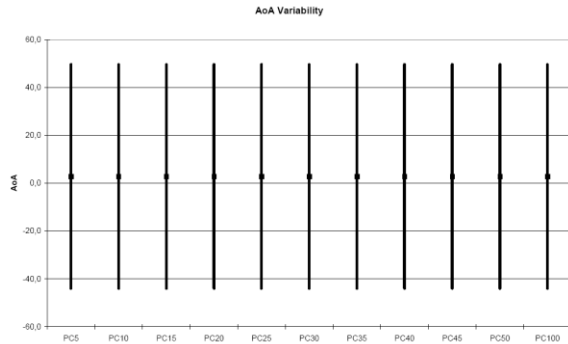
Figure 2-15. AoA variability
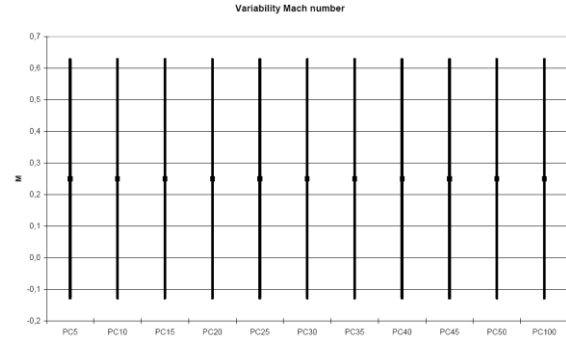
Figure 2-16. M variability

As it can be seen in Figure 2-15 and 2-16, increasing the degree of the polynomial does not lead to a better representation of the input values, but it leads to a larger number of collocation points to be evaluated, so it is computationally expensive. It is clear that increasing the degree the only difference in the output is an increasing amount of collocation points.

Non-intrusive methods uses the solver as a black box, and do not need to modify it, but intrusive methods are completely coupled with the solver. For complex applications, a non-intrusive approach has the advantage of using an existing solver without modifications.

As mentioned above, the need to find faster methods facilitates the development of the method described below.

Polynomial chaos expansions represent stochastic quantities as spectral expansions of orthogonal polynomials. Stochastic Galerkin method takes advantage of this representation of the uncertainty space to represent the input and outputs. It is a good method to deal with steep and non-linear solutions, but its intrusive characteristic make it difficult to implement and it requires an efficient and robust solver to deal with a system of coupled equations.

The stochastic collocation is a non-intrusive method developed to address the limitations of the Stochastic Galerkin method. It uses deterministic evaluations of carefully selected samples in order to quantify uncertainty through the analysis.

Further developments and applications of Probabilistic Collocation method (PCM) have been developed by Webster, Tatang and McRae (1996), where the PCM is used to deal with uncertainties in a complex model as global climate change. They also compare it with the Monte Carlo method and conclude that the PCM enables a significant reduction of model evaluations. Foo, Wan and Karniadakis (2008) present a generalized form of the PCM, the so-called Multi-element PCM (ME-PCM), which prescribes the discretization for each variable. Other developments, such as in Blatman and Sudret (2008), or Nobile, Temprone and Webster (2007) define new structured collocation methods which enable a faster convergence and a lower computational costs. Several applications and further details on the development can also be found in Parussini and Pediroda (2007 and 2008), who deal with geometric

uncertainties, Xiu and Karniadakis (2002 and 2003), who apply Polynomial Chaos to fluid simulation, and Xiu et al (2002), who apply generalized polynomial chaos to stochastic modelling.

2.3.2.1 Polynomial Chaos Expansion

Considering the problem from Equation 2-20, defined in a d-dimensional bounded domain

$$D \in \Re^d, d = 1,2,3$$
$$L(x,t,\omega, p(\omega); u(\omega)) = f(x,t,\omega, p(\omega)) \quad for\, all\, x \in D$$

2-20

Where $u(\omega)$ is the solution, and $p(\omega)$ are the input data. Input data is represented by parameters or stochastic processes, ω. In order to find the solution and numerically solve the equation, the working space of stochastic processes, ω, is reduced from the infinite-dimensional space into a finite space. A truncated spectral expansion of the stochastic process characterizes the random inputs, by setting N random variables, $\xi(\omega)$. Thanks to the Boob-Dynkin Lemma, the solution can be written as $u(x,t,\omega)=u(x,t,\xi)$.

Polynomial chaos expansions is a second order stochastic process as

$$X(x,t,\omega) = \sum_{i=0}^{\infty} \chi_i(x,t)\Phi_i(\xi(\omega))$$

2-21

$\{\Phi_i(\xi)\}$ is an orthogonal basis, that means

$$\langle \Phi_i, \Phi_j \rangle = \langle \Phi_i^2 \rangle \delta_{ij}$$

2-22

Where δ_{ij} is the Kroneker delta, $\langle *,* \rangle$ is the inner product

$$\langle f(\xi), g(\xi) \rangle = \int_\Gamma f(\xi)g(\xi)\rho(\xi)d\xi$$

2-23

where $\rho(\xi)$ denotes the weight function that depends on the type of each defined random variable.

Table 2-2, from Eldred (2009) and Mathelin (2008), defines the relationship between the probability distribution and its optimal polynomial basis.

Distribution	Polynomial	Weight function	Support range
Normal	Hermite, Hen(x)	e-x2/2	$[-\infty,\infty]$
Uniform	Legendre, Pn(x)	1	[-1,1]
Beta	Jacobi, Pn(α,β)(x)	(1-x)α (1+x)β	[-1,1]
Exponential	Laguerre, Ln(x)	e-x	$[0,\infty]$
Gamma	Generalized Laguerre, Ln(α)(x)	xα e-x	$[0,\infty]$

Table 2-2. Summary of subsonic regime results

In other words, the basic idea is to project the variables of the problem onto a stochastic space, which is defined by a set of orthogonal polynomials $\Phi_i(\xi(\omega))$, where $\xi(\omega)$ are the random variable and ω the random event. Then, is clear that the convergence rate and the required number of terms N_{pc} in Equation 2-24 to obtain a desired accuracy level depend on the random process to be approximated, but also the random variables used, as is pointed by Mathelin and Hussaini (2003) and Mathelin (2008).

$$X(x,t,\omega) = \sum_{i=0}^{N_{pc}} \chi_i(x,t) \Phi_i(\xi(\omega)) \qquad \text{2-24}$$

$$N_{pc} + 1 = \frac{(n_{pc} + p_{pc})!}{n_{pc}! \, p_{pc}!} \qquad \text{2-25}$$

Where n_{pc} is the dimensionality, p_{pc} is the order of expansion.

Blatman and Sudret (2008) have developed an adaptive algorithm which takes the significant polynomial coefficient, and they have defined as a Sparce Polynomial Chaos expansion.

The so-called Generalized Polynomial Chaos (gPC), also known as Wiener-Askey polynomial chaos takes the orthogonal basis Φ so that the weighting function takes the same form as the probability density function of the random variable ξ.

This approach estimates the coefficients of the polynomial basis based on a set of solution evaluations. To calculate the sampling, linear regression, tensor-product quadrature or Smolyak sparse grid approaches can be used. The linear regression approach uses a single linear least squares solution to find the coefficients which best match the known outputs. Eldred (2009) has also used spectral projection as an alternative method. In that case, responses are projected against each polynomial basis, using inner products, and it extracts polynomial coefficients using orthogonality properties. In any case, Polynomial chaos uses approximation values for polynomial coefficients, which could not provide the required accuracy.

This approach is developed by Jakeman and Roberts (2009), Eldred (2009) and Witteveen (2008), for example. Witteveen deals with multiple uncertainties defining boundary conditions. He defines new strategies and compares them in order to keep the best one.

As explained, in Polynomial Chaos method a random variable z can be expressed as

$$z = \sum_{i=0}^{\infty} z_i \Phi_i(\xi(\omega)) \qquad \text{2-26}$$

So the product of two random variables z and y

$$zy = \sum_{i=0}^{\infty} \sum_{j=0}^{\infty} z_i y_j \Phi_i(\xi(\omega)) \Phi_j(\xi(\omega)) \qquad \text{2-27}$$

That considering the Galerkin truncation

$$zy_k = \sum_{i=0}^{N_{pc}} \sum_{j=0}^{N_{pc}} z_i y_j < \Phi_i(\xi(\omega)) \Phi_j(\xi(\omega)) \Phi_k(\xi(\omega)) > \quad \forall k \in [0; N_{pc}] \qquad \text{2-28}$$

If $N_{pc}+1$ coefficients of $z \cdot y$ product are computed, the number of operations are of order $O(N_{pc}^3)$. It is easy to understand that increasing the random variable leads to a fast increase of its complexity. To manage several random variables in the same problem, Stochastic Collocation methods have been developed.

2.3.2.2 *Stochastic Galerkin method*

The Stochastic Galerkin method is a further development of the Polynomial Chaos method. In this case, a Galerkin projection is used to project the random variables expansion, generally based on Karhunen-Loeve expansion method, to the polynomial basis. A Galerkin projection minimizes the error in the Polynomial Chaos expansion.

When using Stochastic Galerkin method, it should be taken into consideration the requirement of smoothness for solution function, in order to ensure fast convergence (Jakeman and Roberts, 2009). But in addition, an advantage of Galerkin methods is pointed out by Witteveen (2008); the computational effort of collocation approaches usually increases faster than the required one in Galerkin approaches.

Constantine, Doostan and Iaccarino (2009) present a hybrid scheme that mixes collocation and Galerkin methods in order to reduce the computational cost. They conclude that this hybrid scheme provides accurate and converged statistics, reducing the number of the required deterministic evaluations.

2.3.2.3 *Stochastic Collocation method*

The Stochastic Collocation Expansion method is based on the Stochastic Galerkin method. It combines the Stochastic Galerkin method concept with non-intrusive sampling, which means it only requires the solution of decoupled equations and it can be used in combination with "external" solver. The Stochastic Collocation method enables applications to Spectral Discontinuous Galerkin methods, and reduces the cost of Polynomial Chaos methods.

In the Stochastic Collocation method one uses the Probability Density Function of the random variable as the basis of the transformation between its random space to its artificial stochastic space. It simplifies the quadrature approximation of both variables and product truncation in Equation 2-28.

2.4 Conclusions

Several optimization methods have been introduced. Evolutionary algorithms are general purpose methods. They have been selected in the present research because of the lack of knowledge about the fitness functions. The combination of several input variables and the discontinuities, as those appearing during the analysis of a transonic flow with shock wave,

leads to an unpredicted behaviour of the problem. Evolutionary algorithms, and especially genetic algorithm, can reach a good converged optimal solution in such conditions.

Several Uncertainty Quantification methods have also been presented. Each of them has its advantages and drawbacks. The intrusive techniques have been dismissed due to their complexity and the need of modifying the solver.

The non-intrusive techniques can be compared, as done in Table 2-3.

	Multi-point	Monte Carlo	Latin Hypercube	Probabilistic Collocation
Evaluation Points	Fixed	Samples	Samples	Fixed and Weighted
Full Statistics (μ, σ, Skew, Kurt)	μ, σ with Low accuracy	All	All	μ, σ
Number of Uncertainties	Unlimited	Unlimited	Unlimited	Restricted due to computational cost
Calculation time	Depends on # of uncertainties	Expensive but constant	Expensive but constant	It exponentially increases with # uncertainties
Statistical Sampling	No	Yes	Yes	Yes

Table 2-3. Comparison of main UQ techniques

Due to the statistical definition of the Monte Carlo and Latin Hypercube sampling techniques, they have been selected as the main uncertainty quantification techniques. The fact that other techniques use fixed evaluation points has been understood as a relevant drawback. Anyway, Probabilistic Collocation method has been applied in order to compare the results and methodologies. The selection of Monte Carlo and Collocation techniques has been done according the statistical definition of the evaluation points.

Taking into account the uncertainties, one can deal with uncertain input data, with uncertain objective function or with uncertain restrictions. A clear differentiation can be done between stochastic and robust methods, although both of them deal with uncertainties.

As shown in Table 2-4, if the problem is defined in a deterministic way it means all the values have been defined to a single fixed value and the results are also a single fixed value. In the other hand, if only the input values are defined as variable the analysis is stochastic. And if input values, and/or objective function, and/or restrictions are defined as variables, a robust method is in use.

Type of method	Input Data	Objective Function	Restrictions	Output / Fitness function
Deterministic	Fixed	Fixed	Fixed	Fixed
Stochastic	Variable	Fixed	Fixed	Variable
Robust	Fixed	Variable	Fixed	Variable
Robust	Fixed	Fixed	Variable	Variable
Robust	Variable	Variable	Variable	Variable

Table 2-4. Definition of Deterministic, Stochastic and Robust methods

In this research, stochastic and robust methods have been described and applied to the solution of several test cases.

2.5 Summary

This chapter provides a general overview of the main topics which are related to the research work of this research.

Optimization methods and uncertainty quantification methods are the two main topics which have been analysed. They are the main core of the present research. Regarding optimization methods a brief introduction of the main available methods is provided. But the focus is on the evolutionary algorithms and the genetic algorithms.

Uncertainty quantification methods have been also introduced. Probabilistic based methods, Monte-Carlo methods and Probabilistic collocation techniques are described to get a better understanding which is the new trend when dealing with uncertainties and probabilistic definition on the variables.

3 Stochastic procedure

3.1 Introduction

During design phase, uncertainty on the physical phenomena should be taken into consideration. The lack of knowledge, tolerances in manufacturing processes or measuring errors lead to a lack of accuracy on the numerical models which generates uncertainty on the results. Design engineers should take uncertainty into account in order to obtain a robust design solution. Variability on the input parameters or on the boundary conditions is transferred to output whatever the source of uncertainty is.

When the design engineer deals with variability without knowing about it, he can arrive to completely wrong conclusions. It is really important to ensure the best understanding of the phenomena under study, but also the associated uncertainties and the associated variability of the parameters.

The present chapter comprises a set of numerical variability analysis on the problem parameters; namely CFD, FSI or Mission planning problems. Several parameters with uncertainty have been considered, single CFD discipline or multi aero-elastic discipline analyses have been used in order to detect the most relevant parameters in terms of their influence in the results. In both CFD and FSI problems, lift and drag coefficients have been selected as the main output parameters. Different input parameters have been selected depending on each test case.

Following tests are mainly intended to check if the stochastic procedure leads to meaningful results that can be used in further development of a stochastic and robust optimization method. In this research, the stochastic procedure will use a non-intrusive method to spread uncertainties through the analysis. It is based on Monte Carlo and Latin Hypercube sampling techniques. In order to have a comparison reference, Probabilistic collocation method has also been used. Physical meaning of the results has been evaluated as a validation check.

As mentioned, Monte Carlo and Latin Hypercube sampling techniques are quite similar. Both are based on the same concepts, although Latin Hypercube is said to improve the variance convergence. Section 3.3 is devoted to the analysis and comparison of both.

3.2 Methodology

The methodology of the analysis in chapter 3 is based on the statistical definition of the input variables and the statistical analysis of the output values. In order to better understand how the stochastic analysis is performed, and how the procedure to be followed is, the flowcharts in Figure 3-2 and 3-3 are shown below. Figure 3-1 shows the representation of a classical deterministic flow chart in order to be compared with the stochastic ones. It shows a procedure as simple as a solver evaluation.
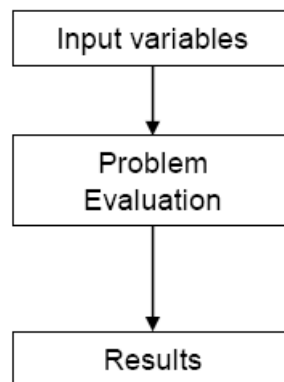
Figure 3-1. Flowchart of a deterministic analysis

Figure 3-2 identifies the main steps of a stochastic analysis using Monte Carlo or Latin Hypercube sampling. Both of them use the same procedure. First step is the selection of the stochastic variables. They are chosen from the whole set of input variables of the problem. For a CFD analysis, as shown in sections 3.5 and 3.5.2, different flow parameters can be selected; namely airflow speed, angle of attack, angle of incidence, etc. For an aero-elastic problem, devoted to the analysis of the flutter phenomena, as done in section 3.6, both flow and structural parameters can be selected.

The statistical definition of the variables is the next step. It uses the definition of a probability density function (PDF). After selecting the PDF (Gaussian, uniform, t-student …), the main probabilistic parameters should be selected. The mean and standard deviation are, usually, the main ones, but it depends on the type of selected distribution. For instance, in the case of a uniform PDF the lower and upper bounds of the variables must be defined.

From the PDF, STAC (see Appendix I for details about this tool) generates a set of random values, which will be applied to the problem in order to define the evaluation sampling points. One evaluation with the solver at each point is required to get the set of output values as a result. Later on all these results will be statistically analysed to obtain the mean and variance values.
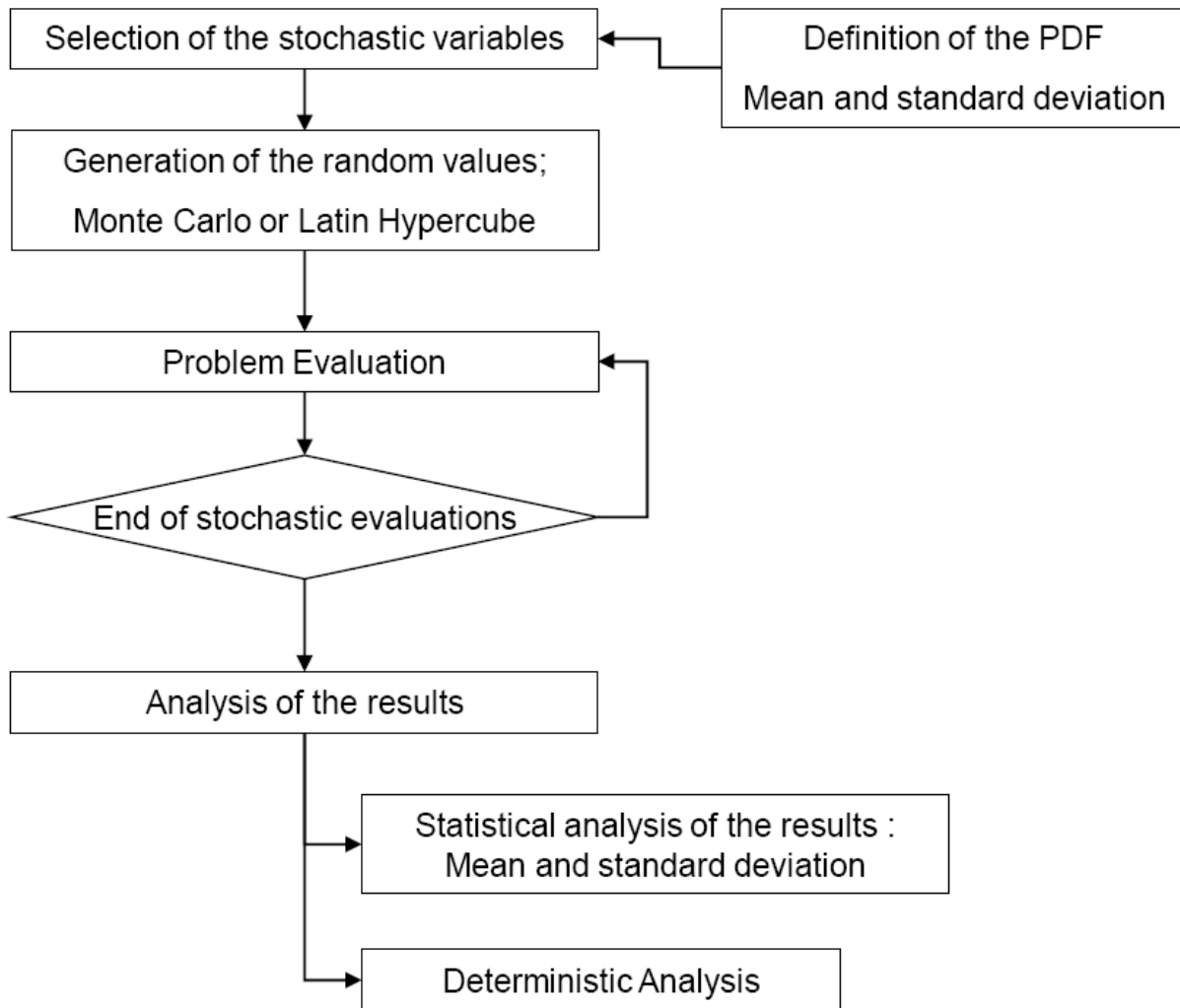
Figure 3-2. Flowchart of the Monte Carlo and Latin Hypercube analysis

The evaluation of all the stochastic samples is the step with the larger computational cost. Compared with a deterministic analysis with a single solver evaluation, the stochastic analysis will multiply this cost by the number of stochastic evaluations.

The statistical analysis of the results will provide their statistical moments; mean, standard deviation, skewness and kurtosis. They represent the trend of the set of results (Mean), the dispersion in its distribution (standard deviation), how centred the distribution is (skewness), and finally how sharp the peak of the distribution is (kurtosis). Additional information can be taken from each individual analyses, which are single deterministic evaluations.

The flowchart in Figure 3-3 has some common points with Figure 3-2. The main difference is how the evaluation points are generated and managed. Probabilistic Collocation method (PCM) is a powerful stochastic tool. It generates evaluation points from the statistical information of the input parameters, but this generation is not random, it is always univocal. Taking a PDF with the same mean and the same standard deviation, PCM will always generate the same evaluation points with the same weights. It will lead to the calculation of the same outputs, and then the same output mean and standard deviation will be obtained. PCM only enables the possibility of the calculation of the two primary statistical moments; mean and standard deviation. Both of them are calculated using mathematical equations.
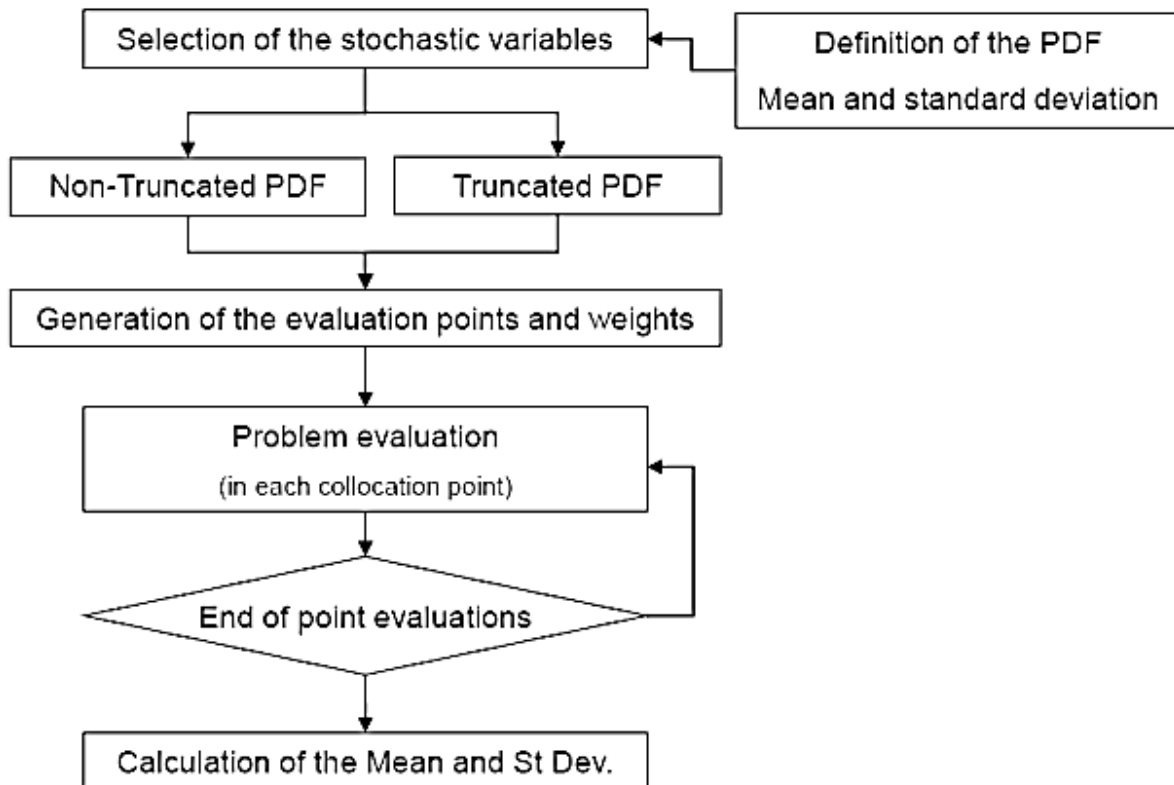
Figure 3-3. Flowchart of the Probabilistic Collocation Method

Section 2.3.2 discuss about PCM and provide additional details on this methodology. As explained, PCM only evaluate few points. This is one of the main key differences between PCM and Monte Carlo or Latin Hypercube. The amount of points is defined depending on the degree of the polynomial defining the collocation method.

3.3 Latin Hypercube Sampling vs. Monte Carlo sampling

This section is mainly focussed on the study of Monte Carlo and Latin Hypercube as uncertainty quantification methods (Helton and Davis, 2003; Durga et al, 2006). Latin Hypercube Sampling (LHS), is generally described as an improved Monte Carlo sampling technique. LHS divides the search space into portions, which can be selected according the probability density function that defines the variable, in order to ensure a better representation of the whole space. LHS uses fewer samples to obtain the same level of accuracy when modelling the search space (see McKay, 1979).

In order to compare both sampling techniques, and mainly to evaluate the reduction of required shots when using LHS, the following analysis is established. Several analyses have been performed for each sampling technique with 5 to 250 stochastic samples. All of them have been compared with. The CFD analysis of this profile is executed using the Monte Carlo and Latin Hypercube set of samples, and the lift and drag coefficients are statistically analysed as results.

The conditions of the flow have been defined as:
- Mach number: $\mu = 0,23$, $\sigma = 0,02$, normal probability distribution.

- Angle of attack: µ = 2,79º, σ = 0,279, normal probability distribution.

The magnitudes used for the comparison are the mean (µ) and the standard deviation (σ) of the ratio C_L/C_D, defined by Equations 3-1 and 3-2.

$$\mu\left(\frac{C_l}{C_d}\right) = \frac{\sum_{i=0}^{n_s} \frac{C_{li}}{C_{di}} \cdot}{n_s} \qquad i = 0,1,2,...n_s \tag{3-1}$$

$$\sigma^2\left(\frac{C_l}{C_d}\right) = \frac{\sum_{i=0}^{n_s}\left(\frac{C_{li}}{C_{di}} - \mu\left(\frac{C_l}{C_d}\right)\right)^2 \cdot}{n_s - 1} \qquad i = 0,1,2,...n_s \tag{3-2}$$

Latin Hypercube should require a lower amount of required evaluations (the so-called shots) in order to obtain the same or quite the same mean and standard deviation values. It is expected to obtain a significant reduction of the amount of shots, providing a tool to reduce the computation time.

Table 3-1 shows the results obtained, and the relative difference between each LHS analysis and the Monte Carlo's reference. Figure 3-4 shows the behaviour of the set of values. Section 3.5.2 shows an additional comparison between both sampling methods.

Sampling Method	Shot Qty	Cl/Cd values		Deviation wrt MC250	
		Mean	Std Dev	Mean	Std Dev
LHS	5	81,750	0,445	0,27%	171,66%
LHS	10	81,156	0,743	-0,46%	353,91%
LHS	50	81,358	0,314	-0,21%	92,13%
LHS	100	81,454	0,140	-0,09%	-14,30%
LHS	150	81,475	0,211	-0,06%	29,04%
LHS	250	81,608	0,161	0,10%	-1,51%
MC	5	81,758	1,378	0,28%	741,92%
MC	10	80,886	0,338	-0,79%	106,71%
MC	50	81,588	0,346	0,07%	111,42%
MC	100	81,614	0,131	0,11%	-19,85%
MC	150	81,455	0,103	-0,09%	-37,06%
MC	250	81,528	0,164	0,00%	0,00%

Table 3-1. LHS and MC comparison

Table 3-1 and Figure 3-4 show how Latin Hypercube converges to the real mean and standard deviation values quicker than Monte Carlo sampling method.

Comparison of the Mean Value (Mc vs LHS)
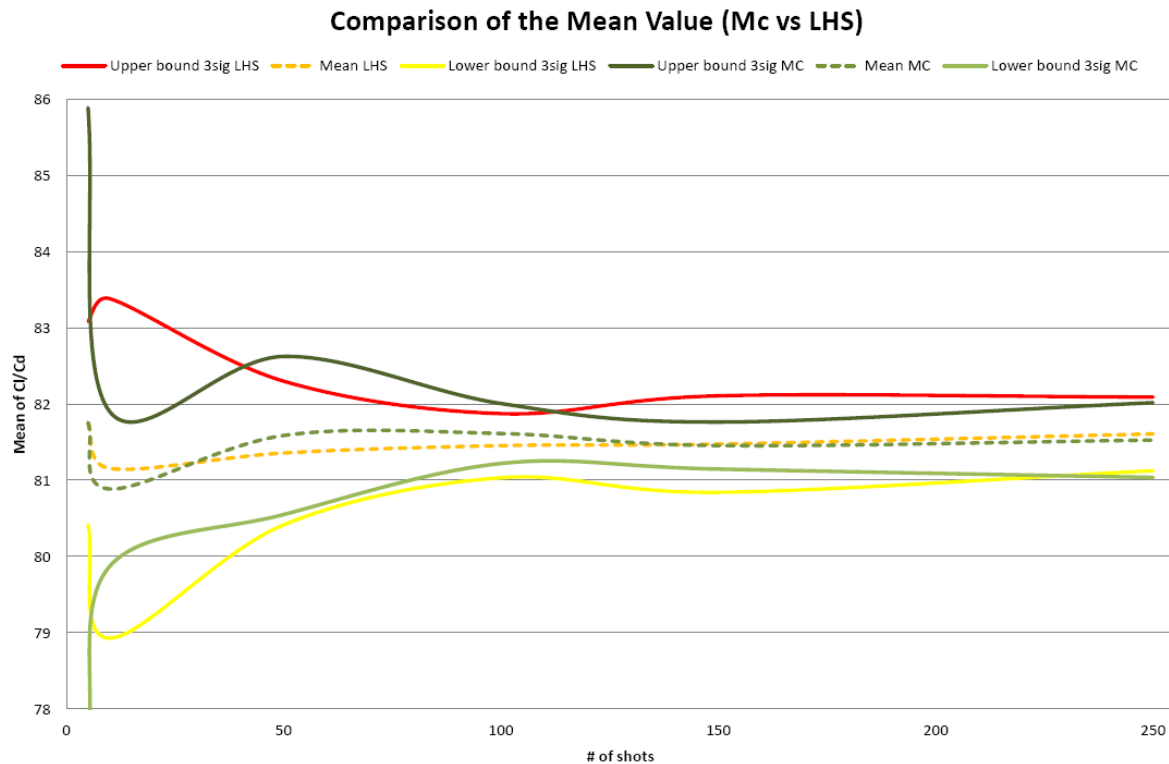
Figure 3-4. Comparison of the mean value between Monte Carlo and Latin Hypercube sampling techniques

3.4 Stochastic analysis applied to the study of the influence of the mesh size variation in the CFD results

3.4.1 Introduction

It is well-known that mesh sizes have a direct effect on the accuracy of the finite element analysis. Due to this reason, the analysis of the influence of the mesh size variability in the results has been selected as the first test of the stochastic procedure. Using a fixed geometry, mesh sizes are randomly defined and applied to a CFD analysis in order to capture the changes in the output induced by the mesh variability. Monte Carlo method has been selected to define the random values of sizes.

Because the fluid has been treated in a laminar flow, with low Mach number and moderate angle of attack, results should confirm the expected behaviour that changes in mesh sizes applied to the vicinity of the profile boundary will have larger effect on the variability of the output than mesh sizes applied in the rest of the domain.

The main aim of the present Section 3.4 is to present the coupling between PUMI, the CFD solver, and STAC, the stochastic manager, and to show an illustrative example about the mesh variability and its effects. Details about STAC and PUMI can be found on Appendix I.

3.4.2 Procedure

Mesh sizes applied to each one of the elements of the geometry are defined according to a probabilistic definition; Gaussian and Uniform probability distributions have been combined in the definition of a set of stochastic analyses, mainly intended to analyse output variability of the lift and drag coefficients of a 2D RAE2822 profile. Additional information about airfoil profiles can be extracted from UIUC database and PDAS website.

Based on the defined geometry, see Figure 3-5 and 3-6, two control areas have been defined around the profile. The inner one is mainly intended to capture the behaviour of the airfoil, and the outer one is intended to expand the control area in order to ensure a correct definition of the value of pressure of the free flow. Additional information about the RAE2822 is available in Appendix IV.

The dimensions of the defined geometry are:
- Chord Length of the profile: 1 m
- Diameter of the inner mesh: 6 m
- Diameter of the outer mesh: 30 m
- Distance from Leading edge to the limit of the inner mesh: 3m

The boundary conditions have been defined as:
- Free velocity applied to the point of the trailing edge
- Infinity boundary Roe applied to the external limit of the outer mesh
- Slip wall enforced condition applied to the profile lines

The conditions of the flow have been defined as:
- Mach number: 0,734
- Angle of attack: 2,79º

The SI units have been used through all this research.
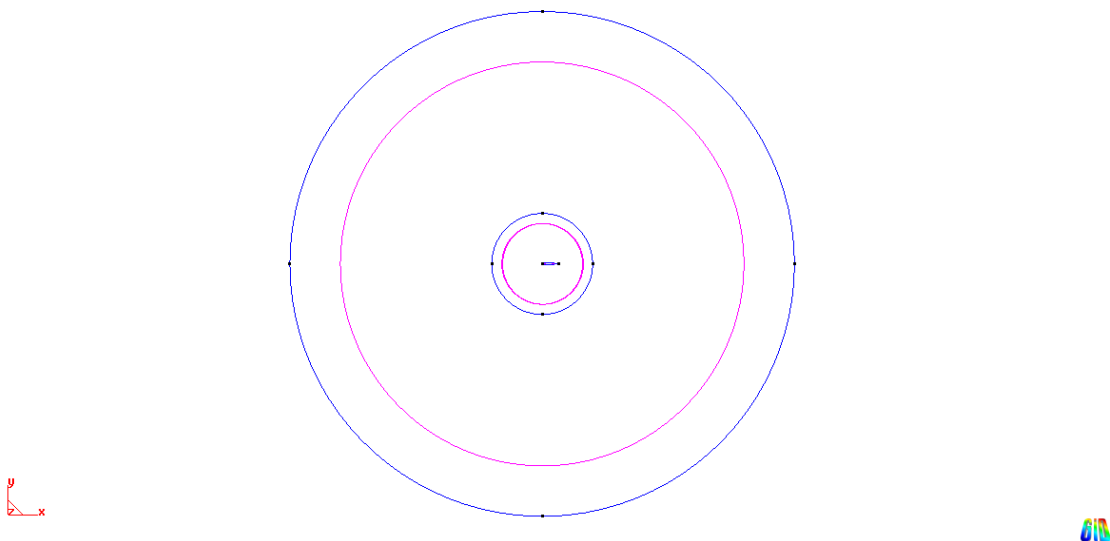
Figure 3-5. General view of the outer and inner control areas
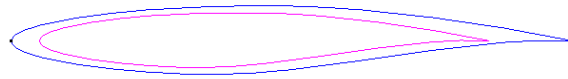
Figure 3-6. Detail of the RAE2822 airfoil profile

The mesh size distribution is defined through three different sizes, which are applied to profile lines, inner control area surface and outer control area surface. Figure 3-8 is an example of one of the obtained meshes.

The names of each value are:
- SL: size applied to profile lines.
- SS: size applied to inner surface.
- SG: size applied to outer surface.

STAC, the stochastic management tool, and PUMI, the Fluid Dynamics (CFD) solver, which have been used in this analysis, are described in Appendix I. Both of them have been coupled in the way described in Figure 3-7. STAC is managing the input and output information; namely the selection of the input parameters and their statistical definition when assigning a probability density function, as well as it is providing the statistical numerical and graphical analysis. The CFD solver is invoqued by STAC at each evaluation.
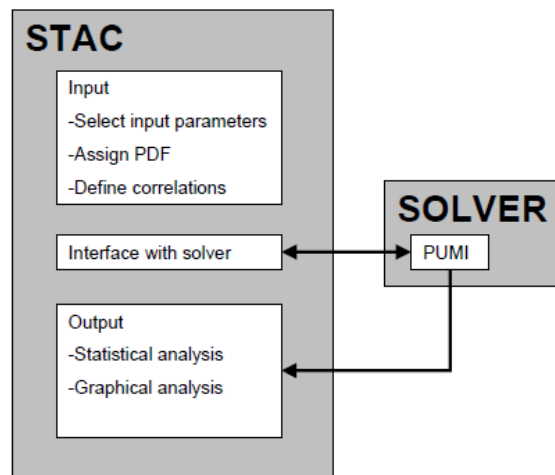
Figure 3-7. STAC and CFD solver coupling.

Normal and uniform probability density functions (PDF) have been used to define the mesh size values. Normal PDF focuses the attention of the analysis on the mean value of the mesh sizes. It is expected that output values follow a Gaussian distribution when the same statistical distribution is applied to the input values. To compare the statistical distributions of the input and the output values the mean and the standard deviation have been used as reference on the comparison. On the other hand, uniform PDF, which is defined by the lower and upper bound of the variables, has been used as a second comparison point. Roughly speaking, the selected range of values which define the statistical samples from Gaussian and uniform PDF have been defined as similar as possible, in order to easily establish the comparison.
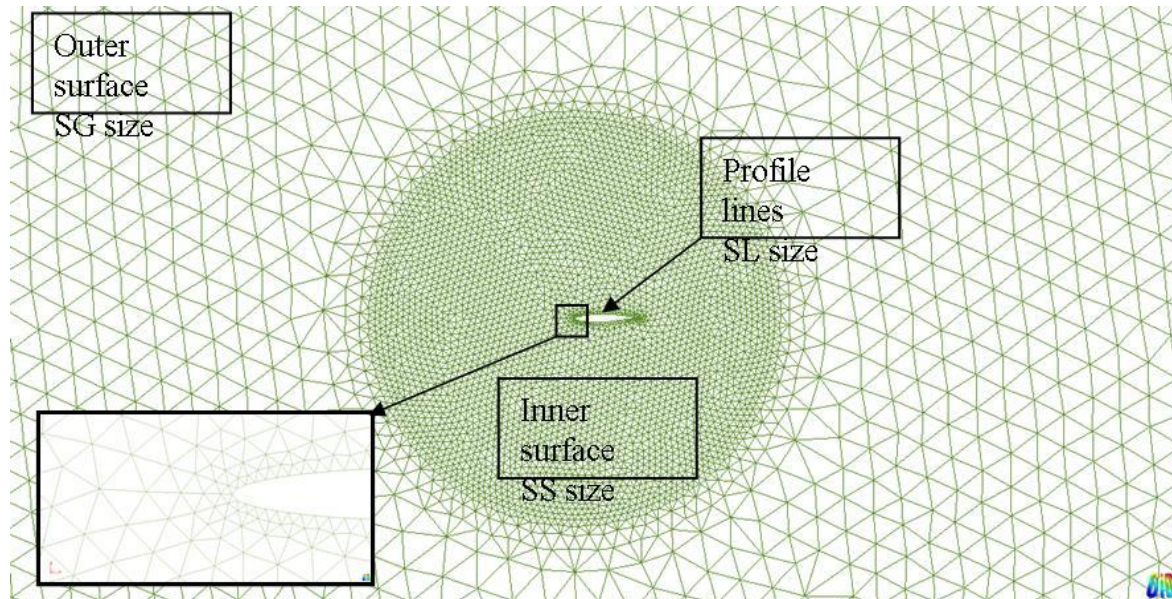
Figure 3-8. General view of the mesh.

Nine different test cases have been analysed. The first eight apply normal PDF to mesh sizes. In the first case the inner surface size, SS, and the outer surface size, SG, remain constant while the profile size, SL, is defined with a mean value of 0,05 and a standard deviation equal to 0,005. In the second case, SL and SG remain constant, and SS is defined with μ=0,5 and σ=0,05. SL and SS remain constant, and SG with μ=1,1 and σ=0,11 in case 3. In case 4 only SG remains constant, μ_{SL}=0,05 and σ_{SL}=0,005, μ_{SS}=0,5 and σ_{SS}=0,05. SL remains constant in case 6 while μ_{SS}=0,5 and σ_{SS}=0,05, μ_{SG}=1,1 and σ_{SG}=0,11. In cases 5, 7, and 8 none of the parameters remain constant, they define one of the three σ as a multiple of their previous values. Finally, in case 9 uniform density functions are applied to all the parameters. Table 3-2 summarizes the definition of all the cases.

The analysed cases are:

Mesh Size	Lines; SL		Inner Surface; SS		Outer Surface; SG	
	Mean	Std Deviation	Mean	Std Deviation	Mean	Std Deviation
Case 1: Normal PDF	0,05	0,005	0,5	--	1,1	--
Case 2: Normal PDF	0,05	--	0,5	0,05	1,1	--
Case 3: Normal PDF	0,05	--	0,5	--	1,1	0,11
Case 4: Normal PDF	0,05	0,005	0,5	0,05	1,1	--
Case 5: Normal PDF	0,05	0,005	0,5	--	1,1	0,11
Case 6: Normal PDF	0,05	--	0,5	0,05	1,1	0,11
Case 7: Normal PDF	0,05	0,005	0,5	0,05	1,1	0,11
Case 8: Normal PDF	0,05	0,010	0,5	0,10	1,1	0,22
	Lower bound	Upper bound	Lower bound	Upper bound	Lower bound	Upper bound
Case 9: Uniform PDF	0,035	0,065	0,35	0,65	0,77	1,43

Table 3-2: Definition of cases

As shown in Table 3-2, different combinations of the parameters have been defined for each analysed case. Some of the combinations use random and/or constant definitions, in order to identify which variable is the most significant one.

3.4.3 Results

The mean and the standard deviation of C_l (lift) and C_{dp} (pressure drag) coefficients are the output for all the analyses. Pressure drag coefficient has been selected, instead of drag coefficient, because the PUMI solver is based on Euler equations without accounting for boundary layer effects. It means that no viscous drag calculation is performed, and only at transonic regime, when shock occurs, drag is calculated. At subsonic regime the value of drag is zero (except numerical noise). Table 3-3 is the brief description of the results obtained. The table lists the maximum, the minimum, the standard deviation and the mean values of the input variables; mesh sizes, and the output variables; C_l and C_{dp} coefficients.

Expected values should point to a larger influence of the mesh size applied to the profile lines (SL size) and to the inner surface (SS size), mainly for the first one, in both C_l and C_{dp} cases. Previous to the analysis, the results for those cases which combine more than one mesh size could not be easily predicted. But, generally speaking, the expected trend should be that the higher variability is introduced by the mesh size applied to profile, whichever the combination of parameters is.

If the ranges of +/- 3σ of C_l and C_{dp} are plotted for each case, and comparing both plots, the output variability can be easily checked. The larger effect, as expected, is produced by line size variation (SL). In all the analyses where SL value is stochastically defined, the variability of the results is larger. Figure 3-9 and 3-10 show the mentioned ranges of σ. The central point is the mean value, and the larger the bar is, the larger the variability is.
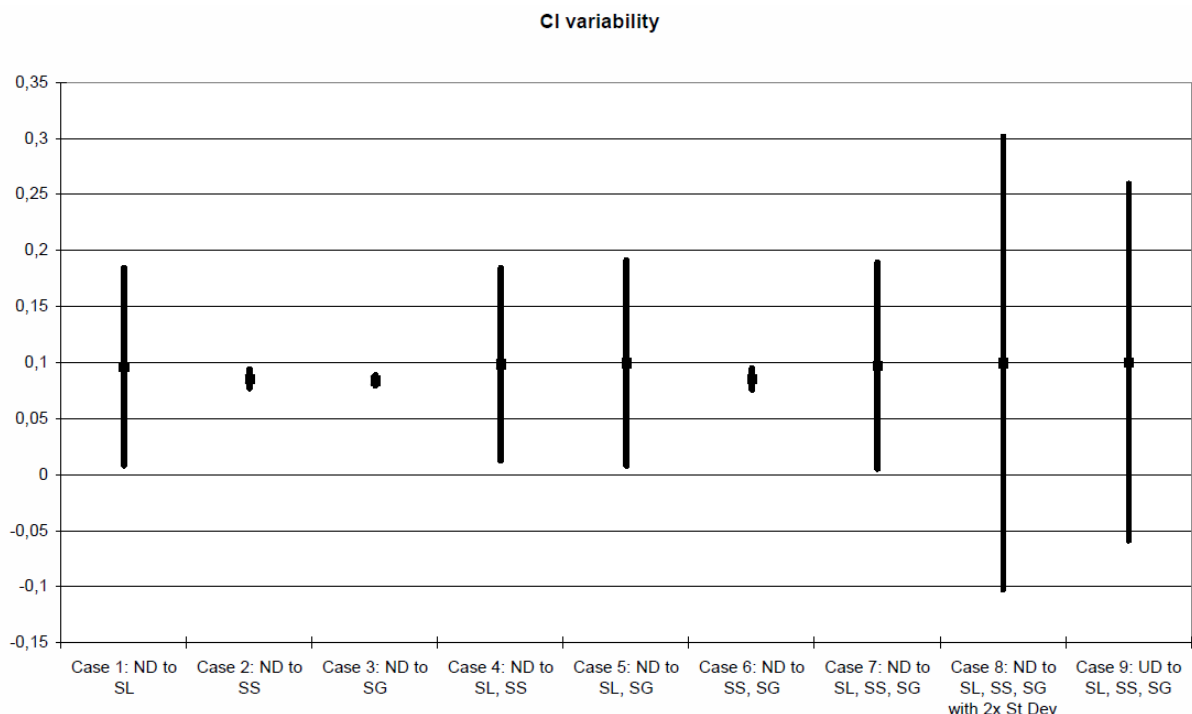
Figure 3-9. C_l variability.

	SL	SS	SG	C_l	C_{dp}	C_l/C_{dp}
Case 1: Normal PDF						
Min	0,034	--	--	0,003	0,009	0,316
Max	0,063	--	--	0,194	0,019	13,246
Std Dev	0,005	--	--	0,029	0,003	1,934
Mean	0,051	--	--	0,096	0,014	6,937
Case 2: Normal PDF						
Min	--	0,349	--	0,080	0,011	7,291
Max	--	0,631	--	0,090	0,011	8,120
Std Dev	--	0,051	--	0,003	0,000	0,297
Mean	--	0,500	--	0,085	0,011	7,656
Case 3: Normal PDF						
Min	--	--	0,717	0,080	0,011	7,284
Max	--	--	1,424	0,090	0,011	8,107
Std Dev	--	--	0,119	0,002	0,000	0,172
Mean	--	--	1,100	0,084	0,011	7,413
Case 4: Normal PDF						
Min	0,034	0,364	--	0,002	0,008	0,282
Max	0,065	0,620	--	0,197	0,019	13,808
Std Dev	0,005	0,051	--	0,029	0,004	1,928
Mean	0,050	0,498	--	0,098	0,014	7,042
Case 5: Normal PDF						
Min	0,035	--	0,851	0,003	0,009	0,297
Max	0,064	--	1,349	0,187	0,019	13,163
Std Dev	0,005	--	0,107	0,031	0,003	2,065
Mean	0,050	--	1,092	0,099	0,014	7,090
Case 6: Normal PDF						
Min	--	0,353	0,734	0,078	0,011	7,093
Max	--	0,637	1,369	0,090	0,011	8,248
Std Dev	--	0,050	0,112	0,003	0,000	0,312
Mean	--	0,499	1,091	0,085	0,011	7,650
Case 7: Normal PDF						
Min	0,031	0,317	0,767	0,002	0,009	0,210
Max	0,064	0,614	1,319	0,223	0,019	14,019
Std Dev	0,005	0,052	0,111	0,031	0,003	2,113
Mean	0,050	0,496	1,086	0,097	0,014	7,040
Case 8: Normal PDF						
Min	0,019	0,274	0,585	-0,020	0,007	-2,485
Max	0,076	0,787	1,701	0,313	0,020	16,050
Std Dev	0,010	0,099	0,221	0,067	0,004	4,358
Mean	0,049	0,504	1,084	0,100	0,013	6,808
Case 9: Uniform PDF						
Min	0,035	0,351	0,773	0,002	0,008	0,194
Max	0,065	0,647	1,429	0,191	0,019	13,594
Std Dev	0,008	0,087	0,183	0,053	0,003	3,752
Mean	0,049	0,502	1,096	0,100	0,013	7,366

Table 3-3. Obtained numerical result values

The variability of each case is directly related to those values defining the input parameters. The first three cases identify the effect from single parameters, but other cases combine more than one variability effect. The last case, that is defined using uniform distribution, uses similar value ranges as case number 7. The obtained results significantly differ when compared C_l, but are almost the same for C_{dp} results.
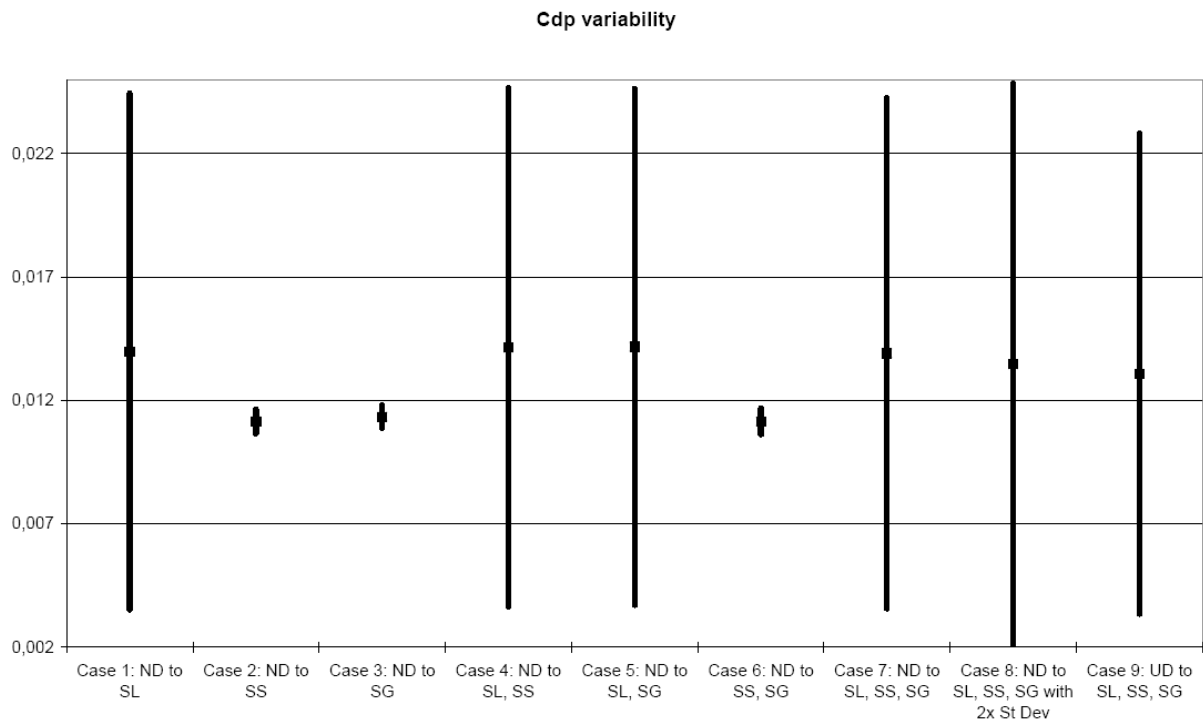
Cdp variability

Figure 3-10. C_{dp} variability.

Both C_l and C_{dp} variations do not have the same order of magnitude, so the comparison of the coefficient of variation can help to compare the variability of C_l and C_{dp}. The coefficient of variation is the ratio between the standard deviation and the mean values. It normalizes the variance, so it can be used to compare different probability density functions. In all the analyses, C_{dp} has smaller coefficients, which means lower variation. Table 3-4 summarizes the values of the coefficient of variation.

Mesh Size	Coefficient of Variation				
	SL	SS	SG	C_l	C_{dp}
Case 1: Normal PDF	0,100	0,000	0,000	0,306	0,249
Case 2: Normal PDF	0,000	0,100	0,000	0,034	0,015
Case 3: Normal PDF	0,000	0,000	0,100	0,018	0,013
Case 4: Normal PDF	0,100	0,100	0,000	0,292	0,248
Case 5: Normal PDF	0,100	0,000	0,100	0,307	0,246
Case 6: Normal PDF	0,000	0,100	0,100	0,038	0,015
Case 7: Normal PDF	0,100	0,100	0,100	0,317	0,248
Case 8: Normal PDF	0,200	0,200	0,200	0,676	0,281
Case 9: Uniform PDF	0,025	0,250	0,055	0,529	0,248

Table 3-4. Coefficient of Variation for C_l and C_{dp} distributions

As mentioned, expected values are confirmed after this analysis. The most affecting mesh size, SL, is that applied to the profile boundary. It contributes to capture the drag, which could be considered as the most sensitive output value. The second most affecting mesh size is the one applied to the inner surface. Inner surface is defined to capture lift, accurately capturing the flow behaviour around the profile, so it is easily understandable that it has a greater effect on the results variability.

3.4.4 Conclusions

First stochastic analysis helps to define the stochastic procedure. The stochastic management tool, STAC, and the CFD solver, PUMI, are correctly coupled. This enables to control whatever variables the user needs to work with; from mesh sizes to boundary or flow conditions.

The general procedure has been established as defined in section 3.2. The procedure described in the flowchart in Figure 3-2 has been applied to the variability analysis and it is ready to be applied to solve CFD and aero-elastic problems.

3.5 Uncertainty applied to a stochastic CFD analysis

3.5.1 Variability of the flow variables

3.5.1.1 Introduction

The developed integration of the stochastic analysis management tool and the CFD solver is now used to determine the effects of the variability of results with respect to the flow parameters. The chosen flow parameters are the angle of attack and the velocity of the airflow (Mach number). The outputs will be C_l and C_{dp}, as defined in the previous test case. The same procedure as in Section 3.4 has been used. It is described in Section 3.5.1.2.

In addition, the results obtained from the stochastic analysis are compared with the deterministic ones in order to justify the present approach.

3.5.1.2 Procedure

Based on the same geometry of a RAE2822 profile, as in Section 3.4.2, see Figure 3-11 and 3-12, the defined mesh is shown in Figure 3-13. The main values that define the problem are as follow:

The dimensions of the defined geometry are:
- Chord Length of the profile: 1 m
- Diameter of the inner mesh: 6 m (fine mesh)
- Diameter of the outer mesh: 30 m (Course mesh)
- Distance from Leading edge to the limit of the inner mesh: 3m

The boundary conditions have been defined as:
- Free velocity applied to the point of the trailing edge
- Infinity boundary Roe condition applied to the external limit of the outer mesh
- Slip wall enforced condition applied to the profile lines

The conditions of the flow have been defined as:
- Mach number: see Table 3-5 for details.
- Angle of attack: see Table 3-5 for details.

The SI units have been used through all this research.
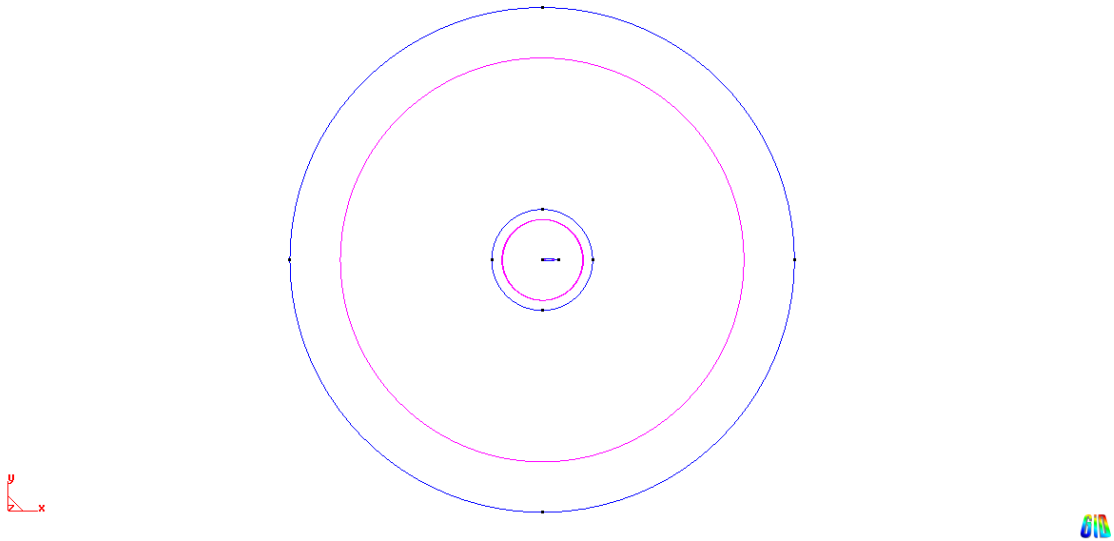
Figure 3-11. General view of the outer and inner control areas
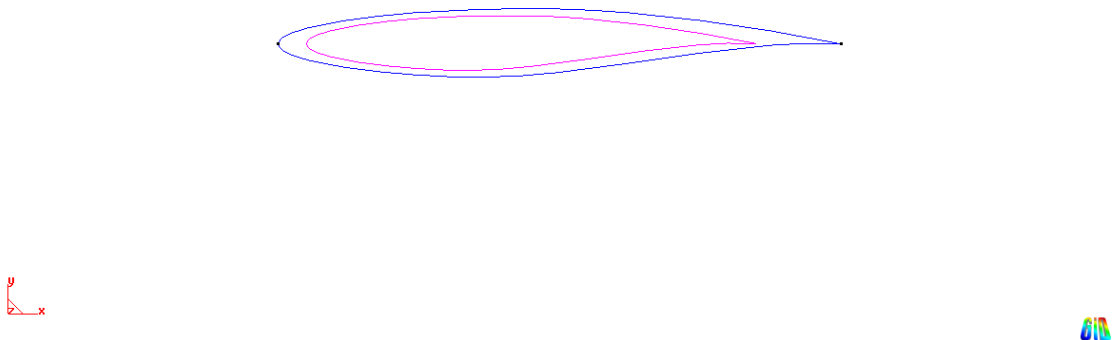
Figure 3-12. Detail of the RAE2822 airfoil profile

Figure 3-13 shows the used finite element mesh. It has been selected taking care of a trade-off between accuracy of the results and the time calculation. The applied mesh sizes are:
- Size to the leading and trailing edge points: 0,02
- Size to the profile lines: 0,05
- Size to the inner surface: 0,1
- Size to the outer surface: 0,75
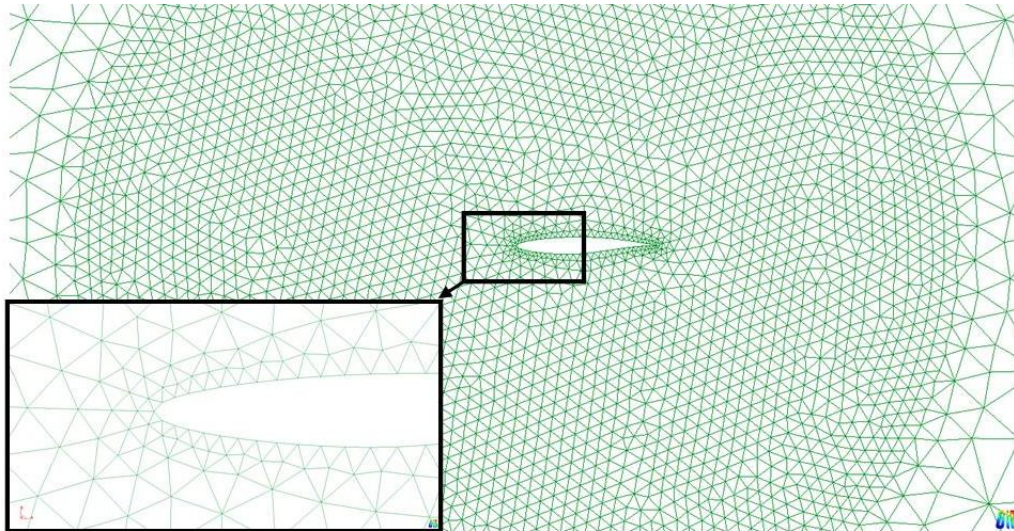
Figure 3-13. General view of the mesh.

As done in the mesh size test case, normal and uniform probability density functions have been defined for each selected parameters. Several combinations of them enable the analysis of the influence of each one on the variability of the output.

The angle of attack (AoA) and Mach number (M) have been selected as input parameters with uncertainties. Several probabilistic definitions have been applied to both of them, in order to analyse the behaviour of the output data C_l and C_{dp} with respect to the variability of the input data.

Similarly of what was done in the mesh test case, 8 cases have been defined. The first and the second one define the values for the angle of attack or the Mach number as constant. From cases 3 to 7 several mean and standard deviation values have been applied to both angle of attack (AoA) and Mach number (M); using case 3 as reference case 4 doubles the standard deviation value of angle of attack, and case 5 multiply by 3 this value, maintaining other values as in case 3. Compared with case 3, case 6 divides by two the deviation value of M, and case 7 multiplies it by 1,5. The last case applies uniform distributions to angle of attack and Mach number.

The definition of the input parameters for each analysis has been described in Table 3-5:

Flow Conditions	*Angle of Attack; AoA*		*Mach number; M*	
	Mean	*Std Deviation*	*Mean*	*Std Deviation*
Case 1: Normal PDF	4	--	0,7	0,08
Case 2: Normal PDF	4	0,5	0,7	--
Case 3: Normal PDF	4	0,5	0,7	0,08
Case 4: Normal PDF	4	1,0	0,7	0,08
Case 5: Normal PDF	4	1,5	0,7	0,08
Case 6: Normal PDF	4	0,5	0,7	0,04
Case 7: Normal PDF	4	0,5	0,7	0,12
	Lower bound	**Upper bound**	**Lower bound**	**Upper bound**
Case 8: Uniform PDF	2,5	4,5	0,45	0,95

Table 3-5: Definition of test cases

STAC is the stochastic manager that generates the set of probabilistic samples. A new set of samples are generated whenever is required. The PUMI input file is fed with the samples to evaluate all of them and to get the resulting cloud of points. Finally, the statistical analysis of the resulting cloud of points lead to the mean and standard deviation used to compare among cases.

3.5.1.3   *Results on the variability of the flow parameters*

Table 3-6 shows the list of the maximum, minimum, standard deviation and mean values of the input variables; AoA and M, and the output variables; C_l and C_{dp} coefficients. The results of the deterministic case are also added for comparison.

The analysis of all these values is intended to confirm the known relationship between lift (C_l), drag (C_{dp}), angle of attack (AoA) and Mach number (M). The well-known relationship is the result to be obtained in order to validate the procedure.

The ranges of +/- 3σ of C_l and C_{dp} have been plotted in Figure 3-14 and 3-15 for each case described in Table 3-5. Comparing both plots, it can be observed that C_l presents lower variability than C_{dp}, but each case produces similar effects on C_l and C_{dp}. If normal distribution is applied to AoA while M remains constant, lower variability on C_l and C_{dp} values is obtained than if a normal distribution is applied to M and AoA, for instance.

The use of a solver based on the Euler equations, combined with the random definition of the angle of attack and Mach number and the fact that the solver does not impose any restriction on the produced value for C_{dp}, cause that in some cases the obtained shock drag value has no physical meaning. The Euler solver is not taking into account the boundary layer effect, so if the Mach number is clearly subsonic the drag value provided comes only from numerical noise and not from a real drag value. The values are shown to maintain the integrity of the range of values of the results, although it is well-known that for an accurate analysis, the jordiskype
shock drag must be zero for the subsonic cases.

Figure 3-14 and 3-15 show the ranges of the variance in each analysed case. The variability of lift and pressure drag coefficients has been analysed and plotted.

In order to compare, the coefficient of variation can be used. It measures the variance of the obtained distribution. It is easy to observe that C_{dp} distribution is more sensitive to input data variation than C_l. If the first two cases are taken (normal distribution to M or to AoA), for instance, it can be seen that coefficient of variation of C_l distribution is lower than C_{dp} one, and lower than 1 (the limit between lower variation and larger variation distributions).

Coefficient of variance can be compared when M or AoA are constant. M produces larger influence than AoA, which in both C_l and C_{dp} distributions presents lower coefficients of variation. Table 3-7 summarizes the coefficient of variations of each analysis.

	AoA	M	C_l	C_{dp}
Case 1: Normal PDF				
Min	--	0,469	0,197	0,001
Max	--	0,951	0,802	0,116
Std Dev	--	0,080	0,113	0,023
Mean	4,000	0,694	0,575	0,015
Case 2: Normal PDF				
Min	3,021	--	0,477	0,000
Max	5,242	--	0,678	0,004
Std Dev	0,471	--	0,043	0,001
Mean	4,042	0,70	0,566	0,002
Case 3: Normal PDF				
Min	2,573	0,490	0,217	0,000
Max	5,282	0,982	0,888	0,125
Std Dev	0,478	0,082	0,127	0,027
Mean	3,991	0,707	0,582	0,018
Case 4: Normal PDF				
Min	0,829	0,462	0,249	0,000
Max	6,793	0,864	1,031	0,103
Std Dev	1,026	0,079	0,151	0,021
Mean	3,924	0,694	0,578	0,014
Case 5: Normal PDF				
Min	-0,225	0,505	0,153	0,000
Max	8,241	0,941	1,050	0,137
Std Dev	1,502	0,081	0,166	0,027
Mean	4,008	0,701	0,572	0,017
Case 6: Normal PDF				
Min	2,764	0,595	0,402	0,000
Max	5,348	0,796	0,862	0,054
Std Dev	0,474	0,041	0,085	0,008
Mean	3,964	0,695	0,562	0,006
Case 7: Normal PDF				
Min	2,714	0,334	0,156	0,001
Max	5,203	1,095	0,872	0,124
Std Dev	0,473	0,119	0,147	0,031
Mean	4,039	0,689	0,559	0,021
Case 8: Uniform PDF				
Min	2,505	0,450	0,126	0,001
Max	4,498	0,949	0,845	0,124
Std Dev	0,586	0,147	0,165	0,044
Mean	3,504	0,698	0,465	0,034
Deterministic case				
	4,000	0,700	0,56205	0,00084

Table 3-6. Numerical Result values
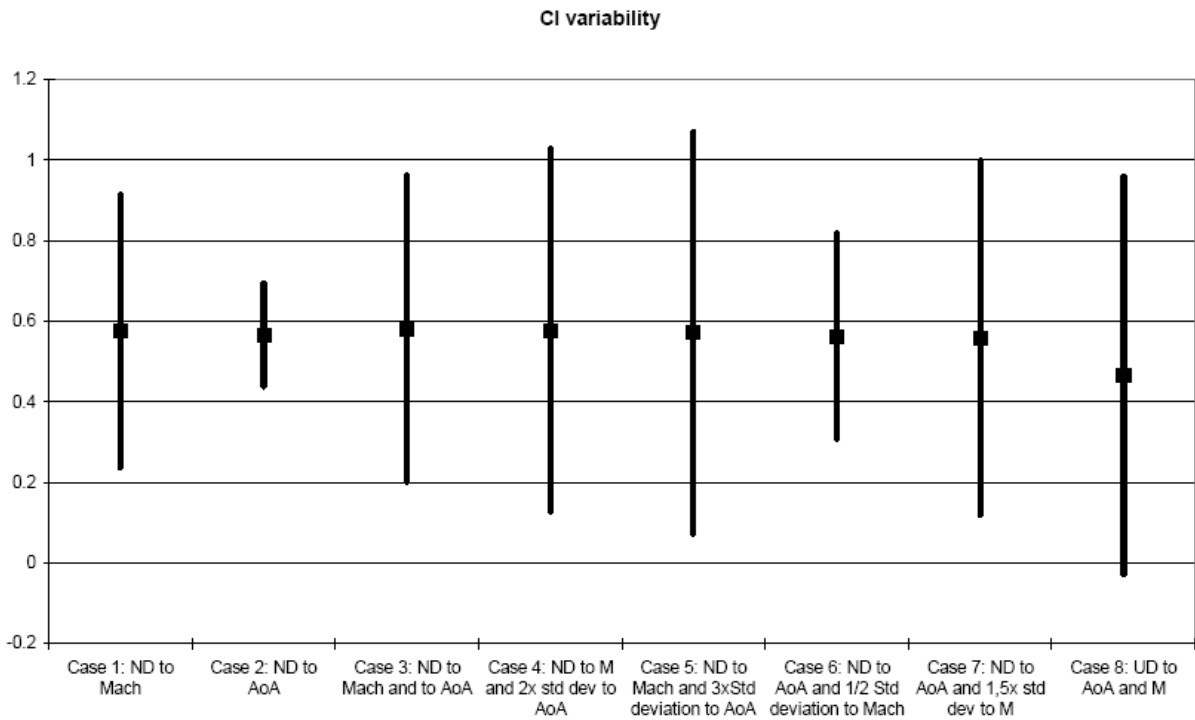
Figure 3-14. C_l ranges
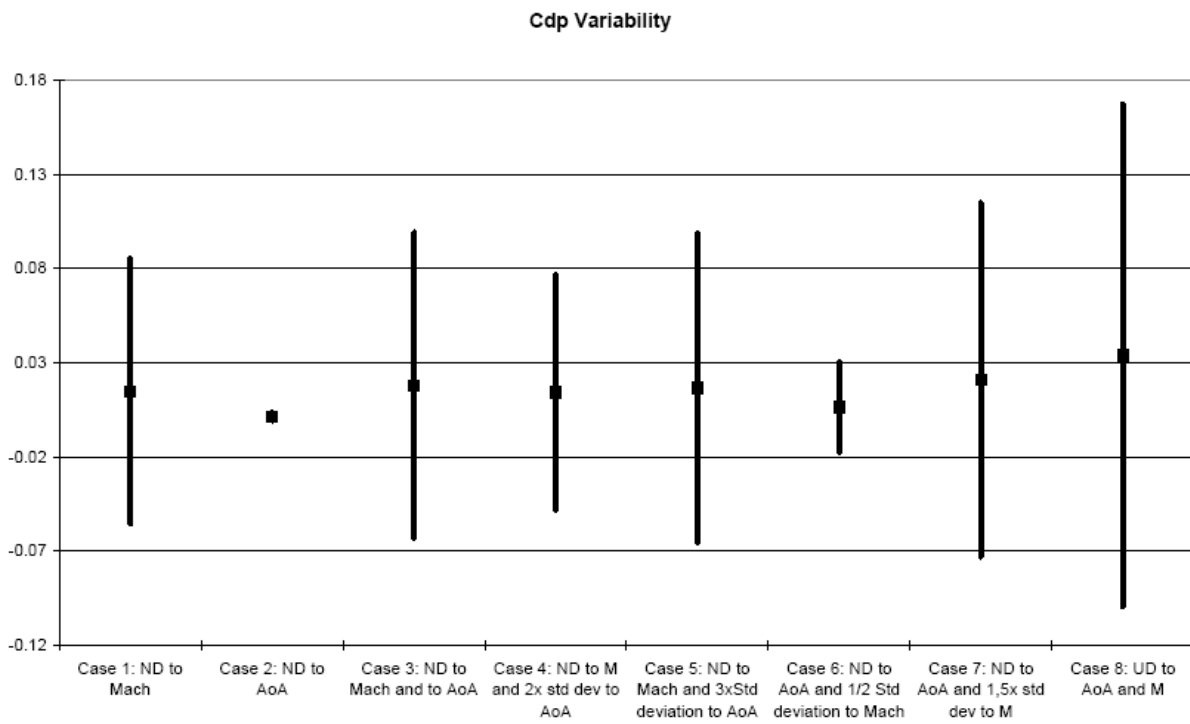
Figure 3-15. C_{dp} ranges

Environmental variables	Coefficient of Variation			
	AoA	M	C_l	C_d
Case 1: Normal PDF	0	0,114	0,196	1,579
Case 2: Normal PDF	0,125	0	0,076	0,483
Case 3: Normal PDF	0,125	0,114	0,218	1,516
Case 4: Normal PDF	0,25	0,114	0,260	1,455
Case 5: Normal PDF	0,375	0,114	0,291	1,643
Case 6: Normal PDF	0,125	0,057	0,151	1,253
Case 7: Normal PDF	0,125	0,171	0,263	1,493
Case 8: Uniform PDF	0,048	0,060	0,354	1,310

Table 3-7. Coefficient of Variation for Cl and Cd distributions

Figure 3-16 to Figure **3-22** provide a plot of graphical analysis showing the variability of the output variables C_l or C_{dp} versus any of the input parameters, while the other one remains constant.

Figure 3-16 shows how C_l increases with M, up to a limit, where shock waves can appear. It follows the typical shape of a polar curve. It can be seen how the values are concentrated around the point corresponding to the near value of M.
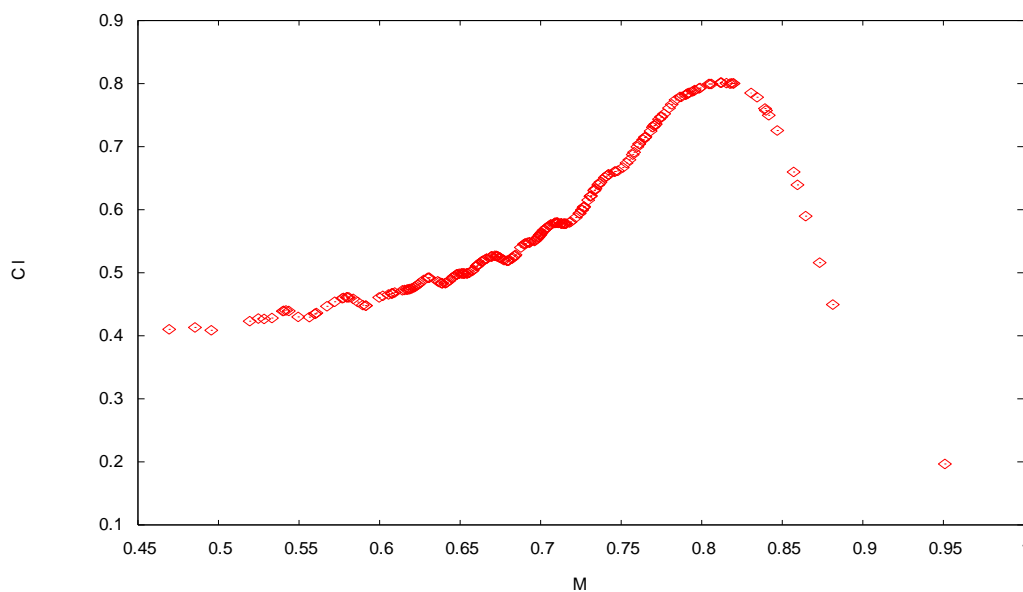
Figure 3-16. Case 1; Cl vs M, AoA constant

Figure 3-17 shows how C_{dp} follows a quite constant behaviour until transonic values of M begins to increase. The CFD used solver, PUMI, only provides C_{dp} values because it is based on Euler equations, without calculating boundary layer effects. Then, the provided value is negligible up to transonic values, when shock pressure appears and C_{dp} can be calculated.
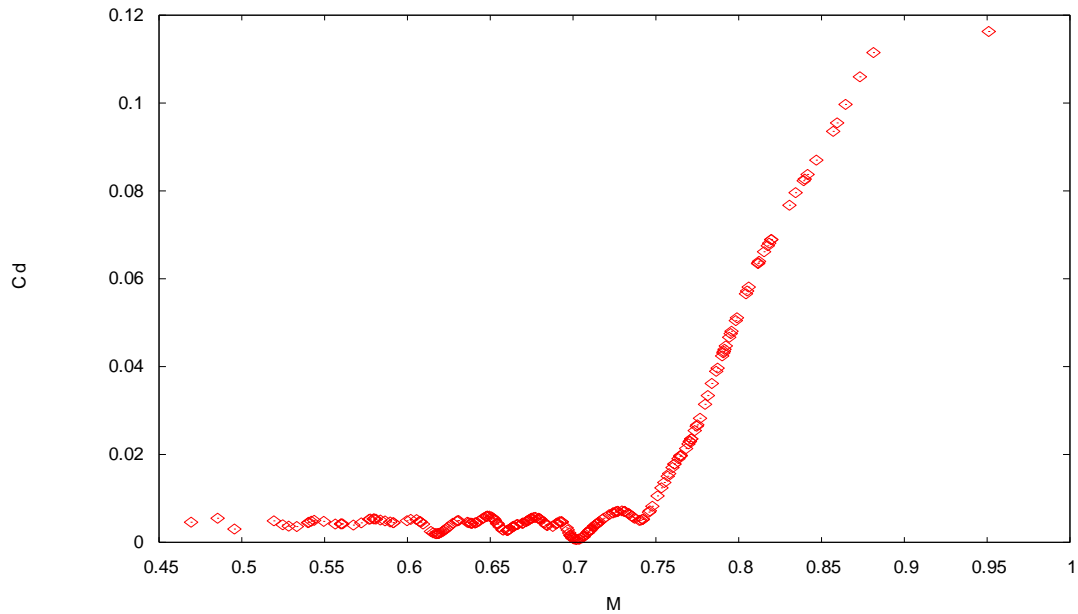
Figure 3-17. Case 1: C_{dp} vs M, AoA constant

Figure 3-18 shows a straight line portion of the polar curve. Notice that the range of values is small enough to ensure values lower than 15°, where the polar curve begins to decrease.
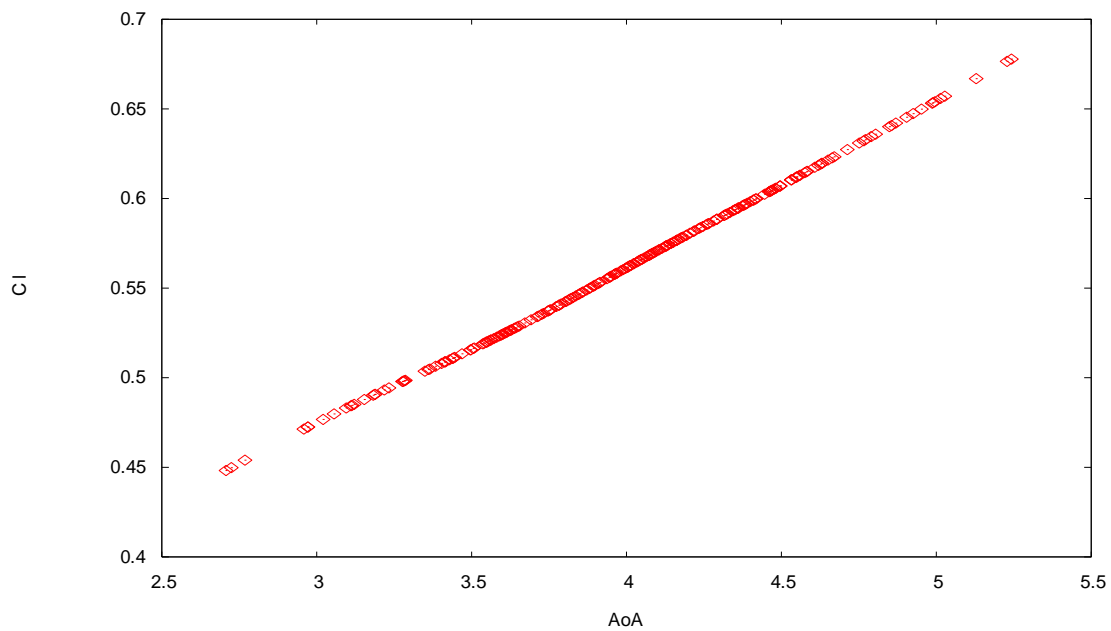
Figure 3-18. Case 2: C_l vs AoA, M constant

A similar situation can be noticed in Figure 3-19, where C_{dp} is plotted versus AoA. RAE22822 airfoil is not symmetric, then pressure drag C_{dp} has a local minimum value around its optimal position for the prescribed Mach number, while it generally increases with AoA.

Cdp Variability
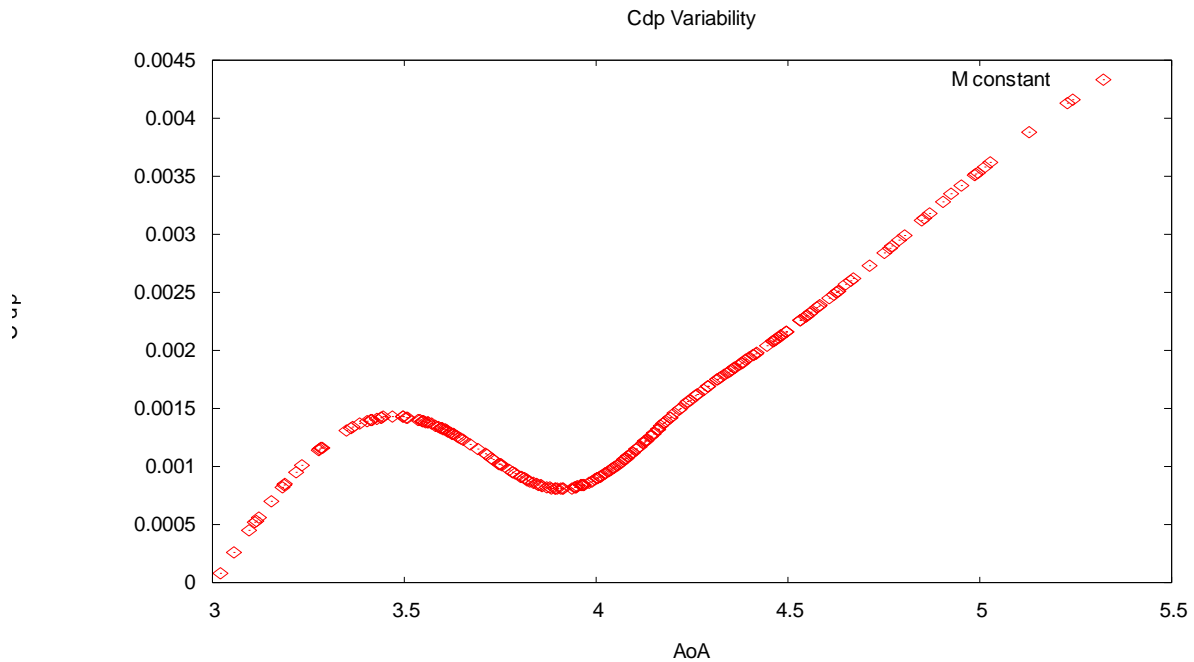
Figure 3-19. Case 2: C_{dp} vs AoA. M constant

In all the above figures the effect of the normal distribution applied to the Mach number or the angle of attack can be also observed, as pointed out previously.

Figure 3-20 to 3-24 show how the previous plots are modified when AoA or M are probabilistically defined.

The original line, which means a constant AoA, increases its width when standard deviation applied to AoA also increases.

Figure 3-20 shows a clear dependency between C_l and AoA; on one hand, in subsonic and low transonic regimes, M<0,8, the plot presents a great variability of C_l while increasing the standard deviation of AoA, even considering the effect of doubling and multiplying by 3 this value, or considering a uniform distribution. On the other hand, in high transonic regime, the variability of C_l is lower, and the plot is a thinner line of points.
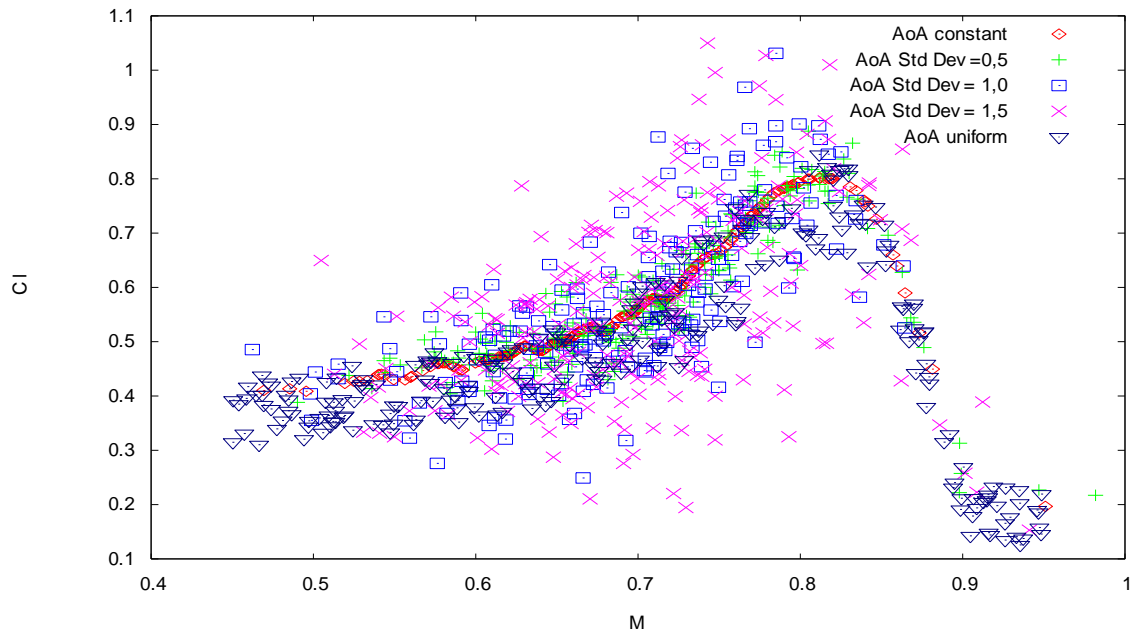
Figure 3-20. Case 1, 2,4,5 and 8: Cl vs M; AoA several distributions

Figure 3-21, where C_{dp} is plotted as done with C_l, shows a lower variability of C_{dp} due to AoA. In opposite to what happens with C_l, C_{dp} variability increases in transonic regime, due to the presence of shock waves. Variability in subsonic regime is associated to numerical noise of the solver, instead of being associated to C_{dp} variance.
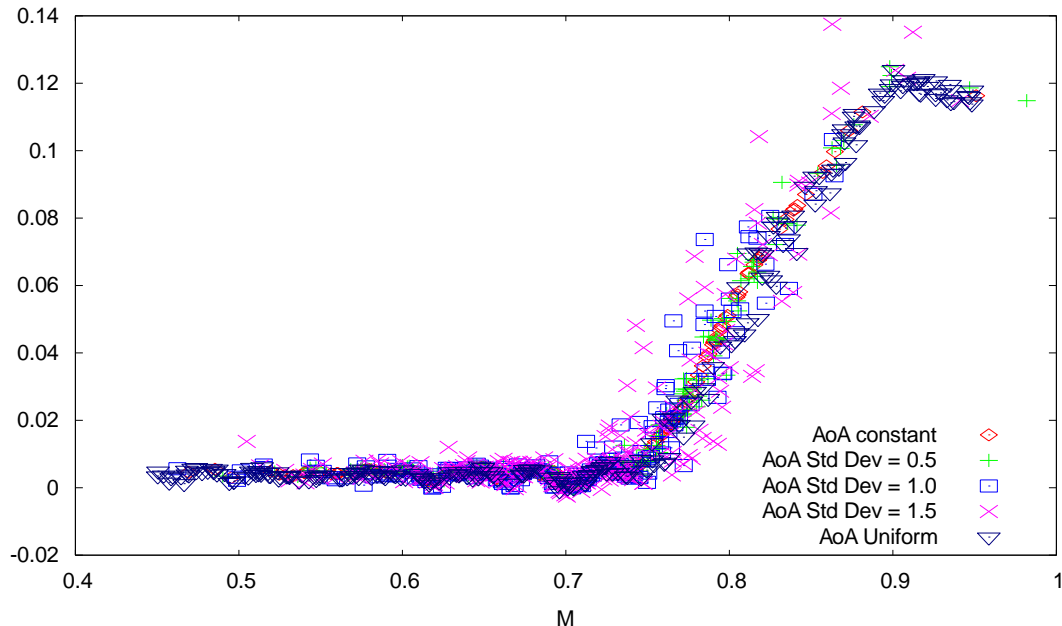
Figure 3-21. Case 1, 2,4,5 and 8: C_{dp} vs M; AoA several distributions

Figure 3-22 shows a linear relationship between AoA and C_l, as it has to be due to the range of values of AoA. The variability induced by M is regularly spread along the curve. It can also be observed the effect of shocks in transonic regime. This phenomenon produces a reduction of the C_l values that can be easily identified on the plot.
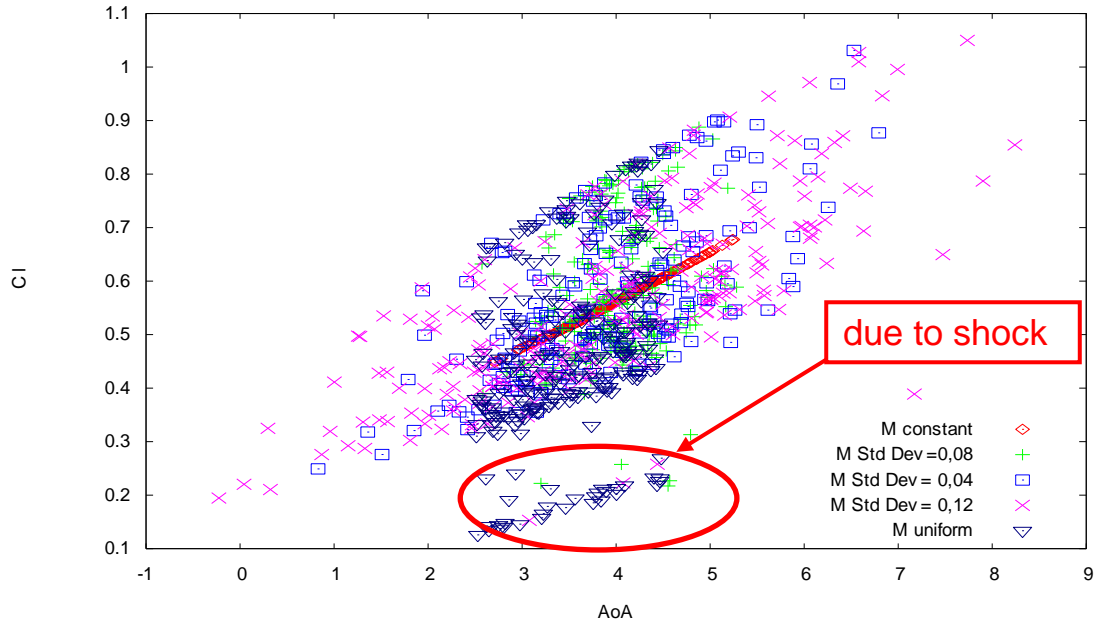
Figure 3-22. Case 2, 3, 6, 7 and 8: C_l vs AoA; M several distributions

Figure 3-23 and 3-24 are the 3D representation of the previous plots. C_l and C_{dp} coefficients have been plotted against AoA and M.
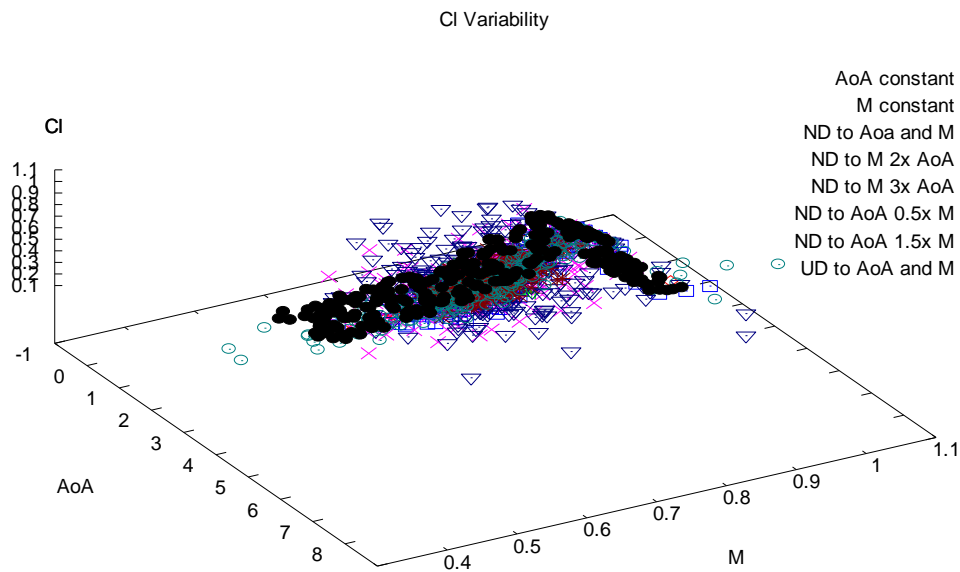
Figure 3-23. All Cases: C_l vs AoA and M

Figure 3-20 to 3-22 show the 2D projection of those Figure 3-23 and 3-24, which can help to understand how AoA and M values are spread around the range. They can only help to understand the induced variability to aerodynamic coefficients.
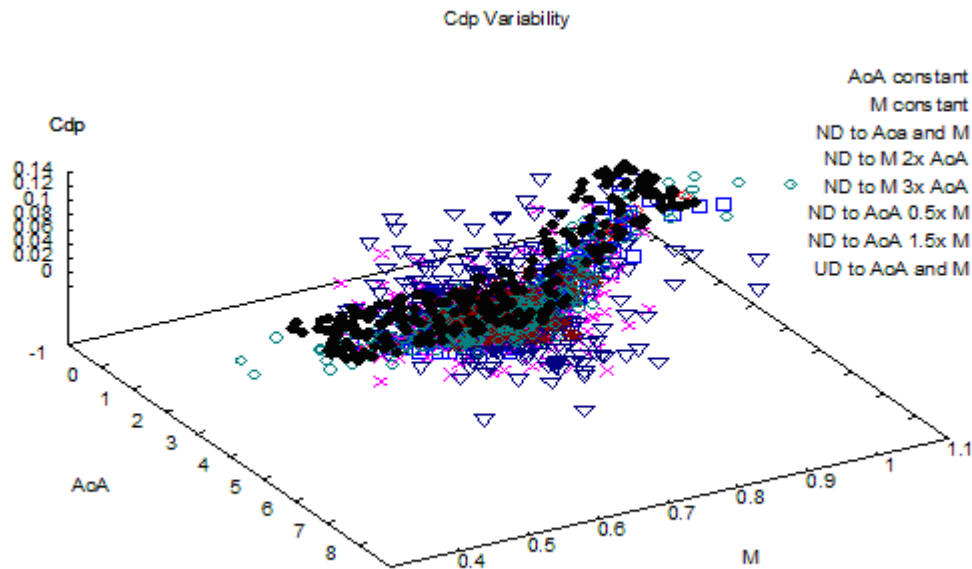
Figure 3-24. All Cases: C_{dp} vs AoA and M

3.5.1.4 Preliminary conclusions on the variability of the flow parameters

The previous plots has a strong relationship with the polar curve of the profile. Similarities can be detected between the deterministic polar curve, and the stochastic representations. The main difference is the fact the stochastic analysis can detect effect that a single deterministic analysis cannot detect, like shocks.

It is very important to emphasize that the stochastic analysis provide information about the behaviour of the profile when the input parameters are slightly modified. This information includes the possible presence of shock waves. This is not provided by the classical deterministic analysis.

3.5.2 Comparison of Monte Carlo and Latin Hypercube sampling methods

3.5.2.1 Introduction

Due to the high computational cost involved in stochastic analysis a comparison between Monte Carlo and Latin Hypercube sampling methods has been established in order to guess which of them requires a smaller number of sampling points for the same level of accuracy. From the results of section 3.3 it can be concluded that LHS should improve efficiency while reducing the amount of evaluations required, so reducing the cost.

The first aim is to establish if there is any difference between MC and LHS, as expected from previous conclusions. A secondary aim is to analyse how the variability on the input values is transferred to the output values; if the variability induced by the sampling is relevant enough to be taken into account and if the main source of the variability is from the statistical

sampling or from the variability of the input values. All these questions should be answered to better face further developments regarding optimization problems.

The variability study is performed on the aerodynamic analysis of a 2D profile, namely a RAE2822 profile, applying a stochastic definition on the angle of attack and the Mach number.

3.5.2.1.1 Sampling variability

From the statistical point of view, samples are a representation of the population. Samples converge to the whole population when their amount is increased. Mathematically speaking, the mean of the set of samples tend to be the mean of the whole population. The standard deviation of the set of samples is

$$S = \frac{\sigma}{\sqrt{n}}.$$	3-3

where S is the standard deviation of the set of samples, n is the number of samples in the set, and σ is the standard deviation of the whole population.

Due to the relationship expressed in equation 3-3, the standard deviation of different sets of samples can differ between them from even if both sets belong to the same population. The following example has been used to study the effect of the different sampling procedures.

3.5.2.2 Procedure

The sampling effects have been analysed using the same problem definition for different cases as a basic reference. The RAE2822 2D profile is analysed to evaluate the variability induced on C_l and C_{dp} coefficients by the variability defined for the angle of attack and the Mach number.

In order to evaluate sampling variability the analysis is mainly focused on the comparison of the results obtained when applying different sets of samples. Sets with 5, 10, 50, 100, 150 and 250 samples have been used with both sampling algorithms (MC and LHS). For each amount of sampling points, 5 different sets have been generated and compared. A comparison among the sets with the same amount of samples, and also with those sets with different amount of samples has been established.

All this procedure is performed using Monte Carlo and Latin Hypercube samples, so different factors are considered when analysing the results. STAC stochastic analysis software and PUMI and XFoil CFD solvers have been used as the main tools for the stochastic analysis; the first one for transonic regime and the second one for subsonic regime.

A relevant task is to compare the Monte Carlo and the Latin Hypercube sampling techniques, since previous results seem to show that LHS has a better efficiency. The fact that Latin Hypercube sampling technique is said to better represent the sampled space leads to think it could generate improved results compared with other sampling techniques, such as Monte Carlo.

Details of the procedure are:
- Sets with different number of samples have been randomly defined, i.e., no correlation between different sets has been defined. No information from previous sets has been used to generate a new one. Each set is applied to the same stochastic analysis in order to evaluate the variability introduced by the sampling.
- For a given number of samples, the analysis is repeated 5 times. All five times the mean and the standard deviation of input values have been kept constant.
- The sets, those containing 5, 10, 50, 100, 150 or 250 samples, also represent the same probability density function, with same mean and same standard deviation. The only difference is the amount of generated samples.

At the end of the complete process a total of 30 stochastic analyses have been performed using Monte Carlo sampling technique, and 30 using the Latin Hypercube sampling technique.

This process have been applied first to a subsonic stochastic analysis and second to a transonic one.

3.5.2.2.1 Details on the subsonic analysis

The subsonic case is solved using XFoil CFD solver. The main used parameters are as follow:
- Number of panels: 160 (used by Xfoil to define a discrete geometry)
- Reynolds number: $6,5 \cdot 10^6$
- Mach number: defined as stochastic value
- Angle of attack: defined as stochastic value

No mesh is required to work with XFoil, only the profile has to be inputted. Figure 3-25 shows the points that define the profile, as well as the profile line. The transition is set as free. For details about RAE2822 profile refer to Appendix IV.
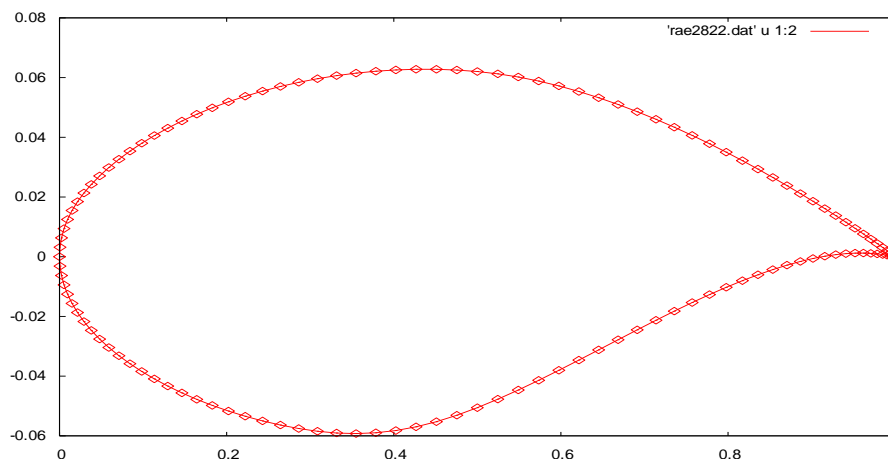
Figure 3-25. Definition of the RAE2822 profile for XFoil CFD solver

3.5.2.2.2 Details on the transonic analysis

The analysis is based on the geometry of a RAE2822 profile, as described in Section 3.5.2.1. The CFD solver used is PUMI. The main values that define the problem are as follow:

The dimensions of the defined geometry are (Figure 3-11):
  - Chord Length of the profile: 1 m
  - Diameter of the inner mesh: 6 m (fine mesh)
  - Diameter of the outer mesh: 30 m (Coarse mesh)
  - Distance from Leading edge to the limit of the inner mesh: 3m

The boundary conditions have been defined as (Figure 3-12):
  - Free velocity applied to the point of the trailing edge
  - Infinity boundary Roe condition applied to the external limit of the outer mesh
  - Slip wall enforced condition applied to the profile lines

The conditions of the flow have been defined as:
  - Mach number: see Table 3-5 for details.
  - Angle of attack: see Table 3-5 for details.
  - Reynolds Number: $6,5 \cdot 10^6$

Figure 3-13 shows the defined mesh. It has been selected taking care of a trade-off between accuracy of the results and the time calculation. The applied mesh sizes are:
  - Size to the leading and trailing edge points: 0,02
  - Size to the profile lines: 0,05
  - Size to the inner surface: 0,1
  - Size to the outer surface: 0,75

3.5.2.3   *Result of the Monte Carlo and Latin Hypercube comparison*

The results are presented in a tabulated and in a graphical way. The mean and the standard deviation presented in the tables have been calculated using the mean values of each 5 repetitions, so the trend to the real mean has been compared between the 6 different analyzed cases.

The fact that the results of the transonic case include the effect of the shock waves on the profile have leaded to perform the same analysis but in subsonic regime. Shock wave in transonic regime produces additional variability that makes more difficult to take clear conclusions. The main aim is to separate the shock wave effect on the lift and drag from the variability induced by the input values and set of samples variability.

First of all, tabulated results are presented in Table 3-8 (subsonic case) and in Table 3-13 (transonic case). Each table shows a comparison of the results produced by MC and LHS sampling techniques for the same numbers of sampling points (5, 10, 50, 100, 150, 250 samples). Listed results include minimum and maximum values, and mean and standard deviation of the 5 generated repetitions of samples.

In a second step, the angle of attack (AoA) and the Mach number (M) evolution when increasing the amount of samples have been compared. Figure 3-26 and 3-27 are the mean and the standard deviation of the angle of attack. Figure 3-28 and 3-29 are the mean and the standard deviation of the Mach number.

Figure 3-26 to 3-29 show the comparison between MC and LHS results. The evolution of the mean and the standard deviation of both the angle of attack and the Mach number are plotted and compared with three reference values. These reference values are the real ones (both

mean and standard deviation, taken from the PDF definition), and also the mean and standard deviation of such cases using 500 and 9000 samples. These two last test cases have been used as reference due to the fact that the real values of the standard deviation of C_l and C_d are unknown. The obtained values using 500 or 9000 samples are good approximations to the real standard deviation, while the deterministic test case value can be used as the reference for the mean value. Table 3-9 shows the obtained results in a deterministic analysis.

LHS 5 samples	AoA	M	C_l	C_d	MC 5 samples	AoA	M	C_l	C_d
Minimum	2,214	0,2060	0,459	0,0062	Minimum	2,791	0,1783	0,522	0,0066
Maximum	3,411	0,2832	0,598	0,0070	Maximum	3,338	0,2533	0,590	0,0070
Std Deviation	0,435	0,0291	0,050	0,00030	Std Deviation	0,236	0,0302	0,030	0,00015
Mean	2,845	0,2421	0,533	0,0067	Mean	3,138	0,2214	0,564	0,0069
LHS 10 samples	**AoA**	**M**	**C_l**	**C_d**	**MC 10 samples**	**AoA**	**M**	**C_l**	**C_d**
Minimum	2,214	0,2060	0,459	0,0062	Minimum	2,369	0,1894	0,483	0,0064
Maximum	3,411	0,2832	0,598	0,0070	Maximum	3,224	0,2688	0,570	0,0069
Std Deviation	0,370	0,0226	0,043	0,00025	Std Deviation	0,251	0,0259	0,026	0,00014
Mean	2,810	0,2349	0,528	0,0067	Mean	2,815	0,2278	0,528	0,0067
LHS 50 samples	**AoA**	**M**	**C_l**	**C_d**	**MC 50 samples**	**AoA**	**M**	**C_l**	**C_d**
Minimum	2,169	0,1737	0,452	0,0062	Minimum	2,120	0,1716	0,455	0,0062
Maximum	3,470	0,2647	0,603	0,0071	Maximum	3,398	0,2844	0,599	0,0070
Std Deviation	0,280	0,0242	0,032	0,00018	Std Deviation	0,273	0,0238	0,031	0,00017
Mean	2,776	0,2263	0,523	0,0066	Mean	2,814	0,2297	0,528	0,0067
LHS 100 samples	**AoA**	**M**	**C_l**	**C_d**	**MC 100 samples**	**AoA**	**M**	**C_l**	**C_d**
Minimum	2,093	0,1830	0,449	0,0061	Minimum	2,140	0,1620	0,453	0,0062
Maximum	3,638	0,2765	0,615	0,0071	Maximum	3,368	0,2795	0,586	0,0070
Std Deviation	0,322	0,0226	0,036	0,00021	Std Deviation	0,267	0,0227	0,030	0,00017
Mean	2,780	0,2306	0,524	0,0066	Mean	2,773	0,2284	0,523	0,0066
LHS 150 samples	**AoA**	**M**	**C_l**	**C_d**	**MC 150 samples**	**AoA**	**M**	**C_l**	**C_d**
Minimum	2,134	0,1518	0,452	0,0062	Minimum	2,217	0,1842	0,464	0,0063
Maximum	3,443	0,2939	0,598	0,0070	Maximum	3,744	0,2889	0,633	0,0072
Std Deviation	0,281	0,0232	0,031	0,00018	Std Deviation	0,282	0,0221	0,032	0,00018
Mean	2,788	0,2295	0,525	0,0066	Mean	2,814	0,2304	0,528	0,0067
LHS 250 samples	**AoA**	**M**	**C_l**	**C_d**	**MC 250 samples**	**AoA**	**M**	**C_l**	**C_d**
Minimum	1,617	0,1709	0,399	0,0056	Minimum	1,915	0,1561	0,429	0,0059
Maximum	3,684	0,2880	0,629	0,0072	Maximum	3,608	0,2923	0,615	0,0071
Std Deviation	0,298	0,0236	0,033	0,00020	Std Deviation	0,280	0,0244	0,031	0,00018
Mean	2,792	0,2303	0,525	0,0066	Mean	2,795	0,2303	0,526	0,0066

Table 3-8. Summary of subsonic regime results for Latin hypercube and Monte Carlo sampling using different number of samples

Deterministic results	AoA	M	C_l	C_d
Mean	2,79	0,23	0,5246	0,00666

Table 3-9. Deterministic values

Table 3-10 and Table **3-11** show the four statistical moments of the Angle of attack and the Mach number. The mean, which defines the trend of the samples, the standard deviation, which measures the dispersion of the population, the skewness value, a measure of the symmetry of the probability distribution and the kurtosis value, which measures how tall is the peak described by the distribution are listed and compared. Considering the defined mean and standard deviation (AoA, μ=2,79 and σ=0,279; M, μ=0,23 and σ=0,023), the reader can observe that the larger the number of samples is, the better the accuracy is. On the other hand, the differences between Latin Hypercube and Monte Carlo are not significant.

Angle of attack Latin Hypercube	Samples	Mean	Std Dev	Skewness	Kurtosis
	5	2,845	0,435	-0,3235	1,1095
	10	2,810	0,370	-0,0838	-0,6315
	50	2,788	0,292	-0,0937	0,0463
	100	2,783	0,282	0,0719	0,1680
	150	2,802	0,276	-0,0126	-0,0300
	200	2,798	0,287	-0,0830	-0,0928
	250	2,789	0,281	-0,0299	0,1443
Angle of attack Monte Carlo	Samples	Mean	Std Dev	Skewness	Kurtosis
	5	2,823	0,242	-0,0514	-1,3324
	10	2,751	0,278	0,6102	0,4909
	50	2,790	0,287	-0,0240	0,1864
	100	2,776	0,276	0,0534	-0,2311
	150	2,808	0,283	-0,0163	-0,0523
	200	2,796	0,274	0,0511	0,0200
	250	2,794	0,271	-0,0524	0,1104

Table 3-10. Statistical moments of Angle of Attack for subsonic case

Mach number Latin Hypercube	Samples	Mean	Std Dev	Skewness	Kurtosis
	5	0,242	0,029	0,2922	0,0846
	10	0,235	0,023	0,9475	1,1375
	50	0,229	0,022	0,0254	-0,2103
	100	0,230	0,023	-0,0017	-0,2670
	150	0,230	0,022	0,0607	-0,0395
	200	0,230	0,022	-0,0120	0,0257
	250	0,029	0,003	-0,3837	0,4303
Mach number Monte Carlo	Samples	Mean	Std Dev	Skewness	Kurtosis
	5	0,229	0,025	0,0067	-0,4863
	10	0,231	0,019	-0,1497	-0,1079
	50	0,229	0,023	-0,0699	0,0851
	100	0,229	0,023	0,0962	0,1314
	150	0,229	0,023	-0,0794	-0,1372
	200	0,230	0,023	0,0842	-0,0400
	250	0,231	0,023	-0,0390	0,1024

Table 3-11. Statistical moments for M for subsonic case
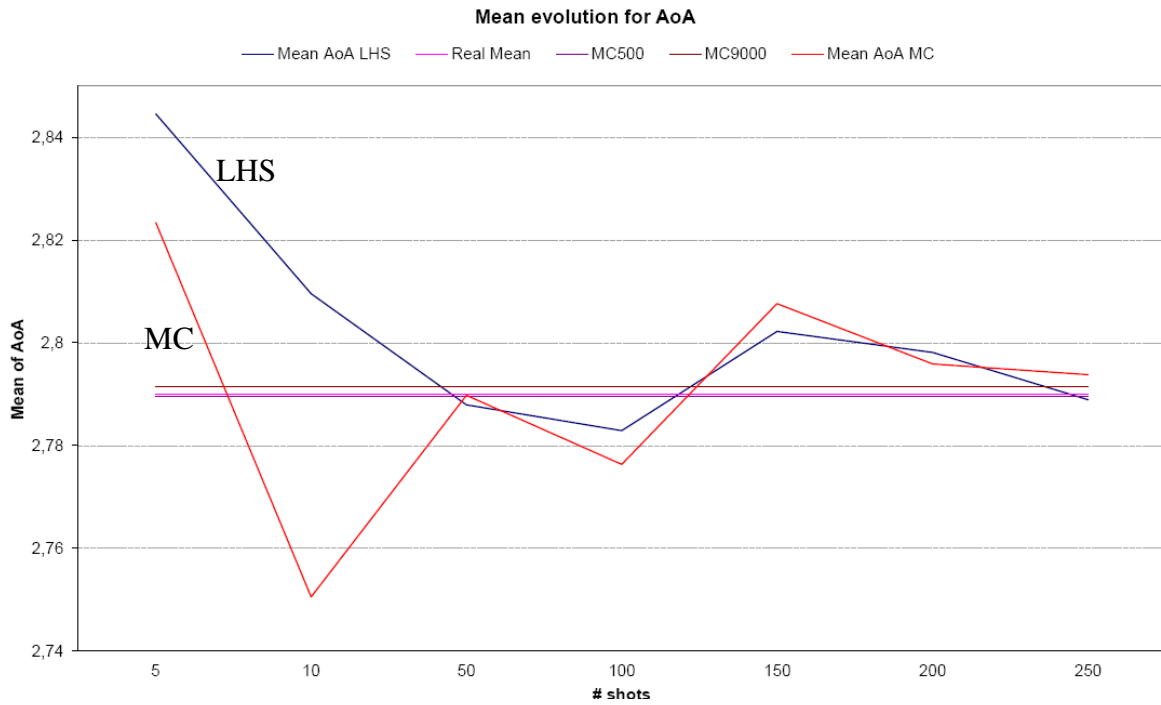
Figure 3-26. Evolution of AoA mean when increasing the amount of samples (Subsonic)
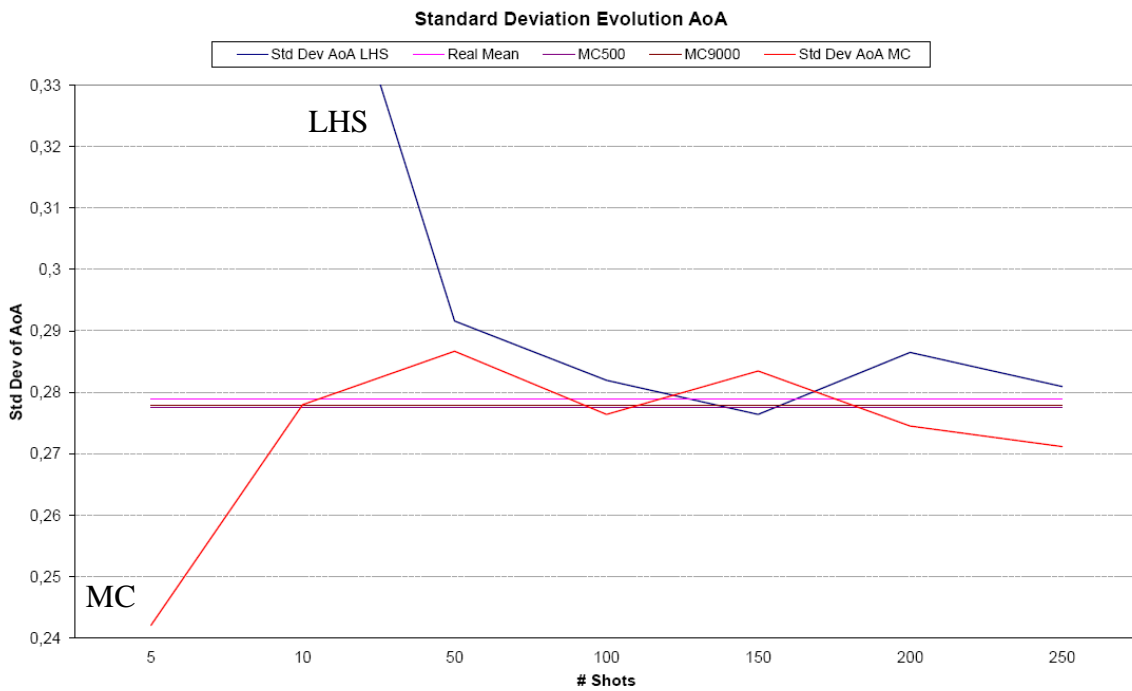
Figure 3-27. Evolution of AoA St Deviation when increasing the amount of samples (Subsonic)
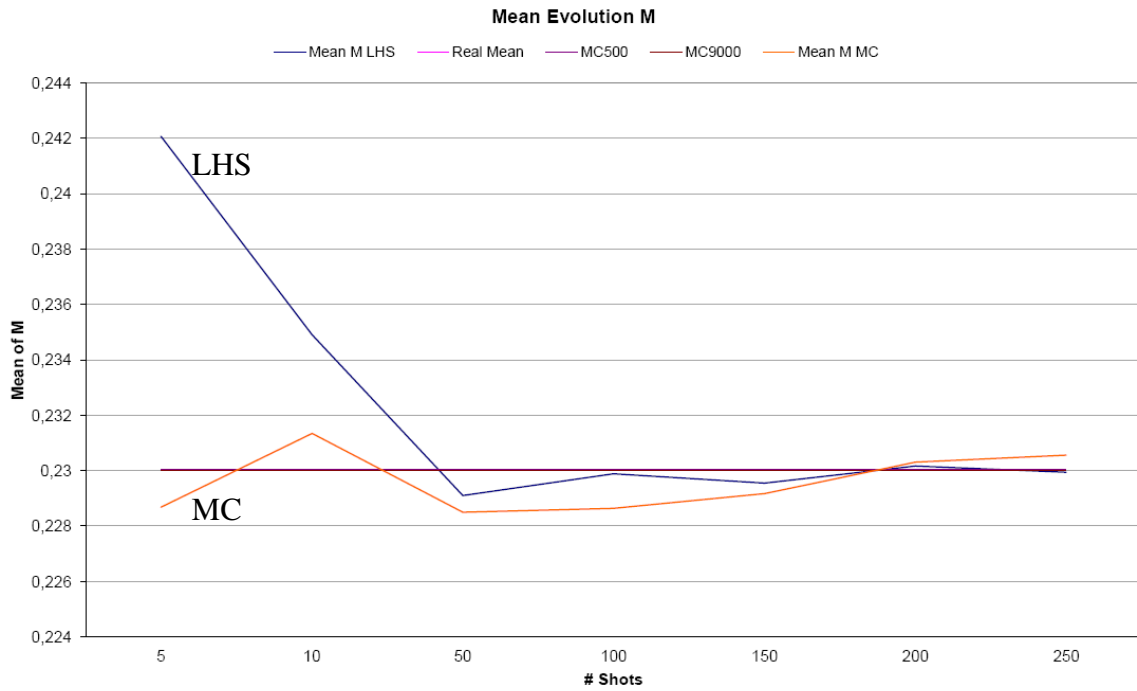
Figure 3-28. Evolution of M mean when increasing the amount of samples (Subsonic)
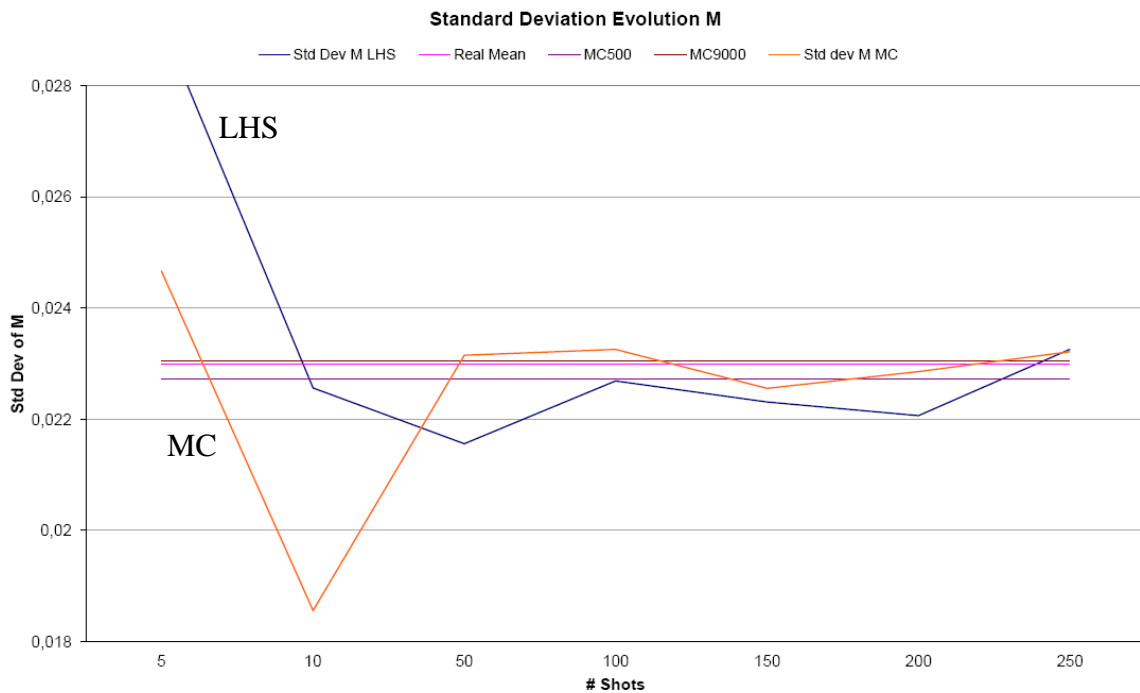
Figure 3-29. Evolution of M St Deviation when increasing the amount of samples (Subsonic)

Histograms in Figure 3-30 and 3-31 provide additional information to compare Monte Carlo and Latin Hypercube samplings. Two representative cases of 250 samples of Angle of attack, and Mach number have been selected. One of them plots the Latin Hypercube samples (Figure 3-30, and 3-32), and the other plots the Monte Carlo samples (Figure 3-31 and 3-33), it can be observed they are pretty similar. The reader can observe that the differences between

Monte Carlo and Latin Hypercube cannot be easily detected from the obtained results. In conclusion, it can be assumed that the capture of the variability is almost the same when using MC or LHS sampling techniques. On the other hand, the variability between the set of 5 samples and the set of 250 samples is relevant. It agrees with the statistical theory that the larger the number of samples is, the better accuracy is obtained.

Histogram AoA LHS 250 shots
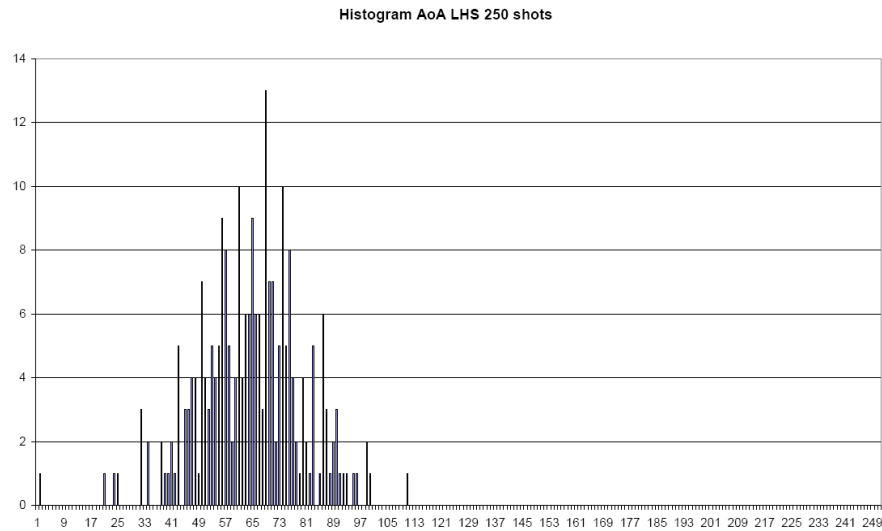
Figure 3-30. Histogram of AoA for 250 LHS samples case (Subsonic)

Histogram AoA MC 250 shots
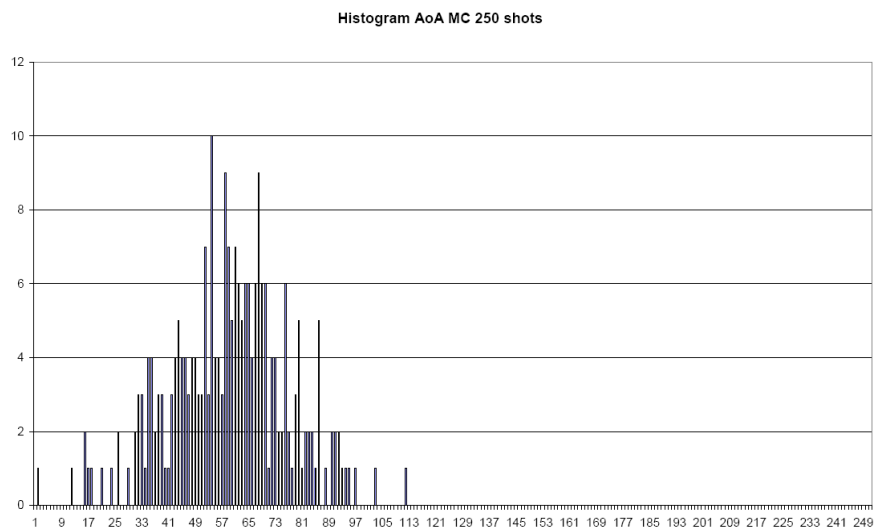
Figure 3-31. Histogram of AoA for 250 MC samples case (Subsonic)
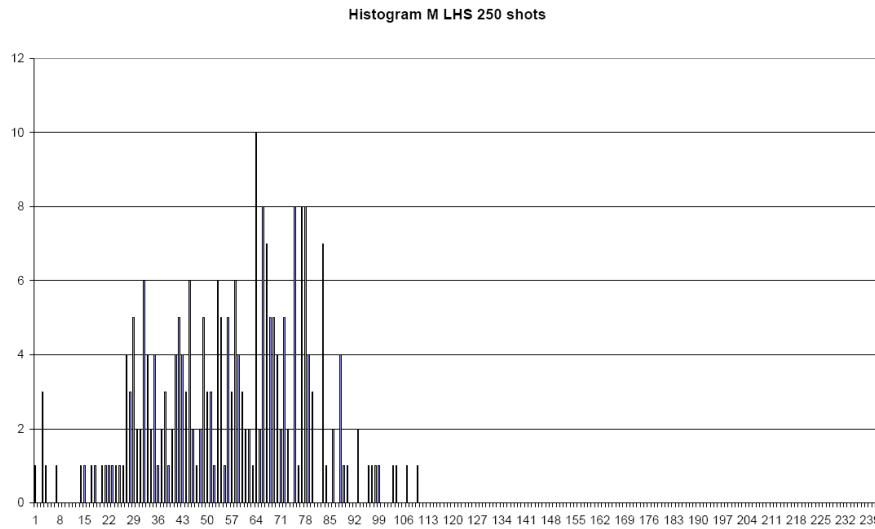
Figure 3-32. Histogram of M for 250 LHS samples case (Subsonic)
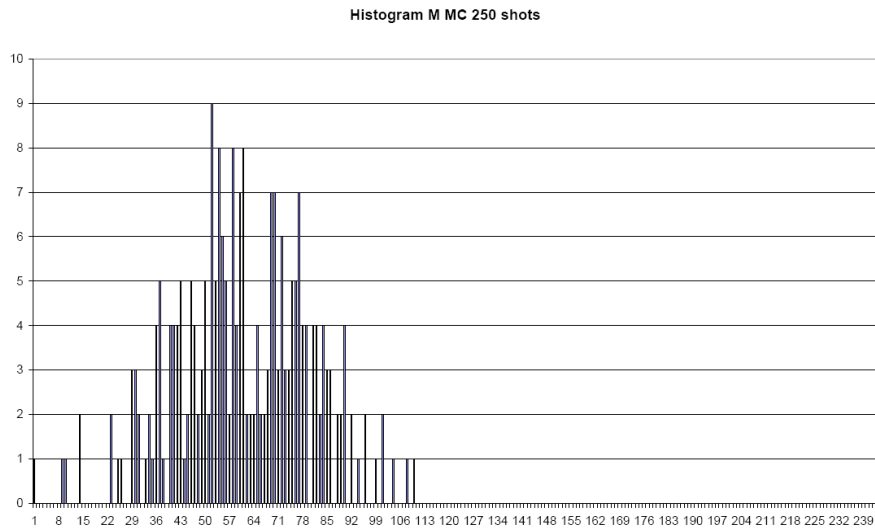
Figure 3-33. Histogram of M for 250 MC samples case (Subsonic)

The transonic test cases have been analysed in a similar way the subsonic test cases have done. Table 3-12 shows the obtained results of a deterministic analysis.

Deterministic results	AoA	M	C_l	C_{dp}
Mean	2,79	0,734	0,7094	0,0262

Table 3-12. Deterministic values for the transonic analysis

LHS 5 samples	AoA	M	Cl	Cd	MC 5 samples	AoA	M	Cl	Cd
Minimum	2,316	0,606	0,283	0,0139	Minimum	2,074	0,568	0,310	0,0138
Maximum	3,407	0,888	0,640	0,1154	Maximum	3,121	0,881	0,612	0,1098
Std Deviation	0,085	0,013	0,030	0,0179	Std Deviation	0,075	0,029	0,022	0,0134
Mean	2,799	0,722	0,430	0,0243	Mean	2,692	0,743	0,452	0,0300

LHS 10 samples	AoA	M	Cl	Cd	MC 10 samples	AoA	M	Cl	Cd
Minimum	1,952	0,600	0,325	0,0137	Minimum	2,082	0,587	0,092	0,0139
Maximum	3,277	0,876	0,652	0,1082	Maximum	3,602	0,922	0,668	0,1228
Std Deviation	0,056	0,021	0,019	0,0113	Std Deviation	0,093	0,030	0,048	0,0128
Mean	2,723	0,742	0,450	0,0282	Mean	2,744	0,762	0,448	0,0406

LHS 50 samples	AoA	M	Cl	Cd	MC 50 samples	AoA	M	Cl	Cd
Minimum	2,188	0,461	0,123	0,0138	Minimum	2,098	0,529	0,111	0,0137
Maximum	3,703	0,902	0,689	0,1253	Maximum	3,688	0,933	0,671	0,1258
Std Deviation	0,049	0,008	0,005	0,0021	Std Deviation	0,034	0,011	0,008	0,0053
Mean	2,787	0,733	0,451	0,0283	Mean	2,823	0,732	0,441	0,0301

LHS 100 samples	AoA	M	Cl	Cd	MC 100 samples	AoA	M	Cl	Cd
Minimum	1,998	0,539	0,120	0,0136	Minimum	1,814	0,488	0,111	0,0135
Maximum	3,860	1,069	0,669	0,1239	Maximum	3,659	0,925	0,665	0,1252
Std Deviation	0,017	0,007	0,005	0,0022	Std Deviation	0,015	0,004	0,008	0,0024
Mean	2,804	0,734	0,445	0,0282	Mean	2,790	0,735	0,445	0,0301

LHS 150 samples	AoA	M	Cl	Cd	MC 150 samples	AoA	M	Cl	Cd
Minimum	1,903	0,499	0,105	0,0136	Minimum	1,749	0,528	0,107	0,0131
Maximum	3,598	0,989	0,664	0,1247	Maximum	3,727	0,931	0,681	0,1249
Std Deviation	0,019	0,004	0,007	0,0026	Std Deviation	0,016	0,006	0,007	0,0043
Mean	2,791	0,734	0,445	0,0289	Mean	2,788	0,735	0,446	0,0295

LHS 250 samples	AoA	M	Cl	Cd	MC 250 samples	AoA	M	Cl	Cd
Minimum	1,788	0,489	0,109	0,0134	Minimum	2,008	0,509	0,106	0,0136
Maximum	3,637	0,960	0,679	0,1255	Maximum	3,786	0,969	0,666	0,1255
Std Deviation	0,018	0,004	0,004	0,0018	Std Deviation	0,019	0,002	0,003	0,0006
Mean	2,805	0,736	0,446	0,0298	Mean	2,800	0,733	0,447	0,0285

Table 3-13.Summary of transonic regime results for Latin hypercube and Monte Carlo sampling using different number of samples

Table 3-14 and 3-15 summarize the four statistical moments of the performed analysis for the transonic test cases. Table 3-14 presents the values of angle of attack, and Table 3-15 the values of Mach number. Considering the defined mean and standard deviation (AoA, $\mu=2{,}79$ and $\sigma=0{,}279$; M, $\mu=0{,}734$ and $\sigma=0{,}0734$), the reader can again observe that the larger the number of samples is, the better the accuracy is. On the other hand, the differences between

Latin Hypercube and Monte Carlo are not significant. This conclusion confirms that obtained with the subsonic analysis.

Angle of attack	Samples	Mean	Std Dev	Skewness	Kurtosis
Latin Hypercube	5	2,730	0,327	-0,330	-1,904
	10	2,674	0,372	-0,606	-0,303
	50	2,749	0,305	0,668	0,330
	100	2,783	0,278	0,110	-0,340
	150	2,808	0,285	0,055	-0,237
	200	2,817	0,293	0,087	-0,364
	250	2,730	0,327	-0,330	-1,904
Angle of attack	Samples	Mean	Std Dev	Skewness	Kurtosis
Monte Carlo	5	2,765	0,269	0,098	-0,436
	10	2,727	0,410	0,740	1,773
	50	2,853	0,267	-0,410	-0,173
	100	2,807	0,270	0,152	0,373
	150	2,799	0,255	-0,138	-0,077
	200	2,819	0,292	0,216	0,485
	250	2,765	0,269	0,098	-0,436

Table 3-14. Statistical moments of Angle of Attack for transonic case

Mach number	Samples	Mean	Std Dev	Skewness	Kurtosis
Latin Hypercube	5	0,724	0,088	0,522	-3,201
	10	0,746	0,046	0,726	0,356
	50	0,735	0,079	-0,713	1,865
	100	0,731	0,067	0,106	0,027
	150	0,735	0,077	-0,037	-0,110
	200	0,731	0,072	-0,029	0,613
	250	0,724	0,088	0,522	-3,201
Mach number	Samples	Mean	Std Dev	Skewness	Kurtosis
Monte Carlo	5	0,750	0,056	0,989	0,167
	10	0,799	0,082	0,048	-0,857
	50	0,731	0,072	-0,078	-0,248
	100	0,724	0,074	-0,033	-0,310
	150	0,728	0,075	-0,387	-0,228
	200	0,734	0,071	-0,189	0,100
	250	0,750	0,056	0,989	0,167

Table 3-15. Statistical moments for M for transonic case

Similar conclusions can be extracted from the transonic values. Figure 3-34 to 3-37 show the comparison between the mean and the standard deviation of the angle of attack and the Mach number. Figure 3-34 shows the evolution of the mean of the angle of attack while the amount of samples increases. Figure 3-35 shows the evolution of the standard deviation. Figure 3-36 and 3-37 show the evolution of the transonic Mach number.

Mean Evolution for AoA
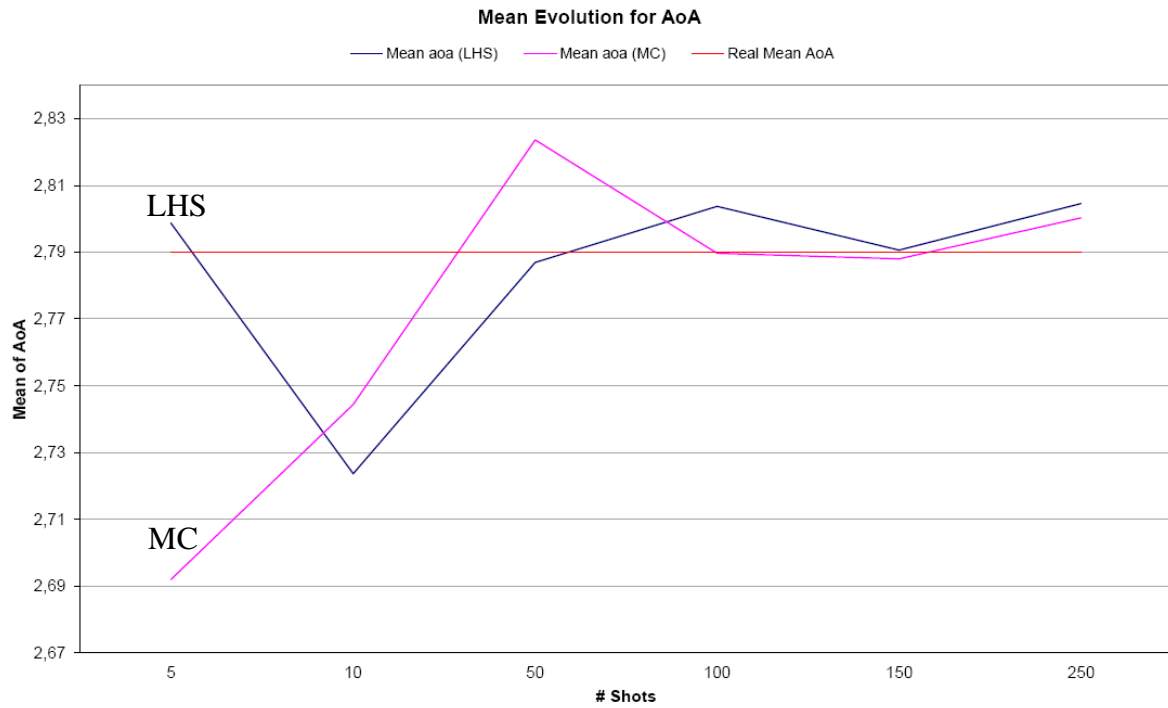
Figure 3-34. Evolution of AoA mean when increasing the amount of samples (Transonic)

Std Dev Evolution for AoA
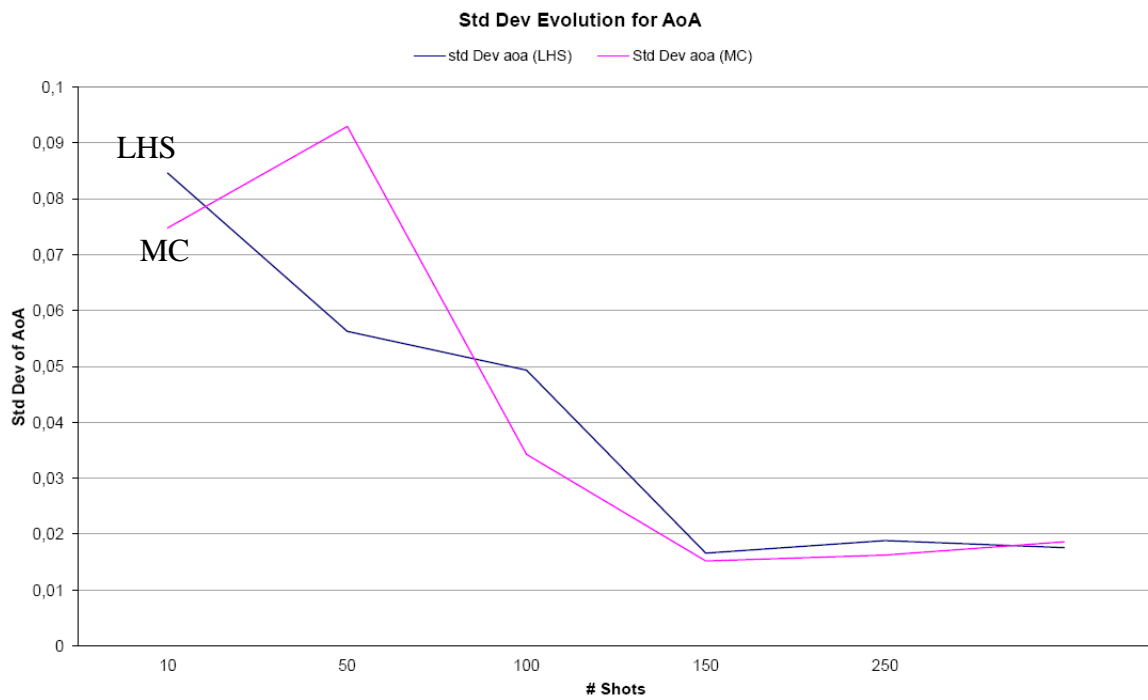
Figure 3-35. Evolution of AoA std deviation when increasing the amount of samples (Transonic)

Mean Evolution for Mach Number
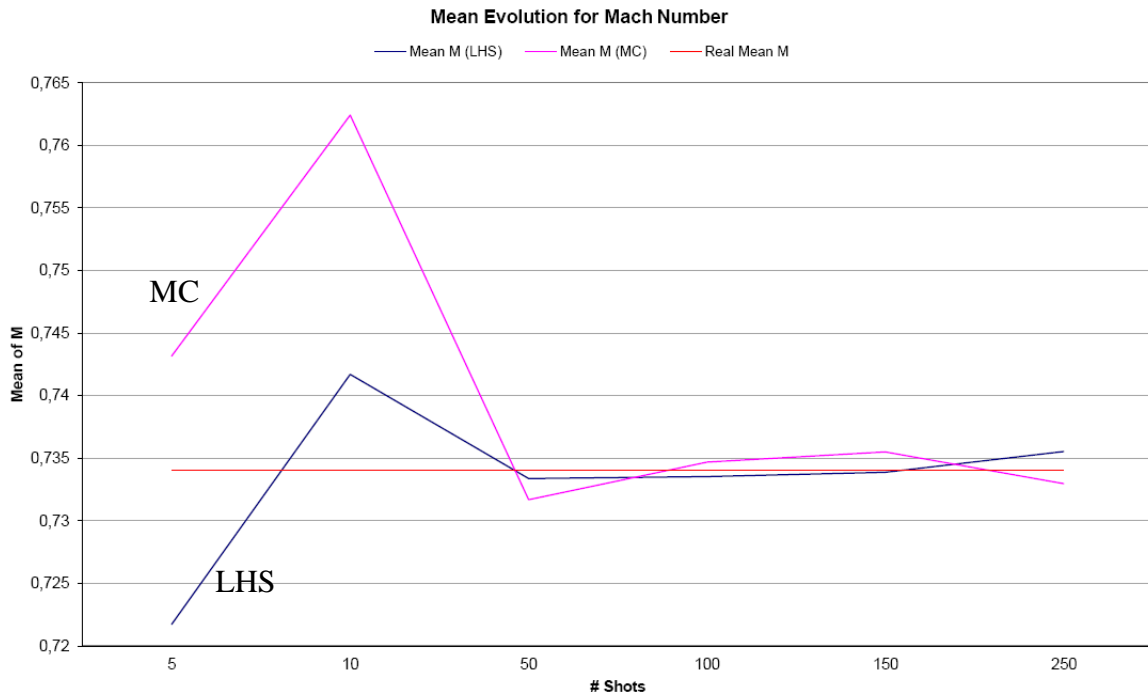
Figure 3-36. Evolution of M mean when increasing the amount of samples (Transonic)

Std Dev Evolution for Mach Number
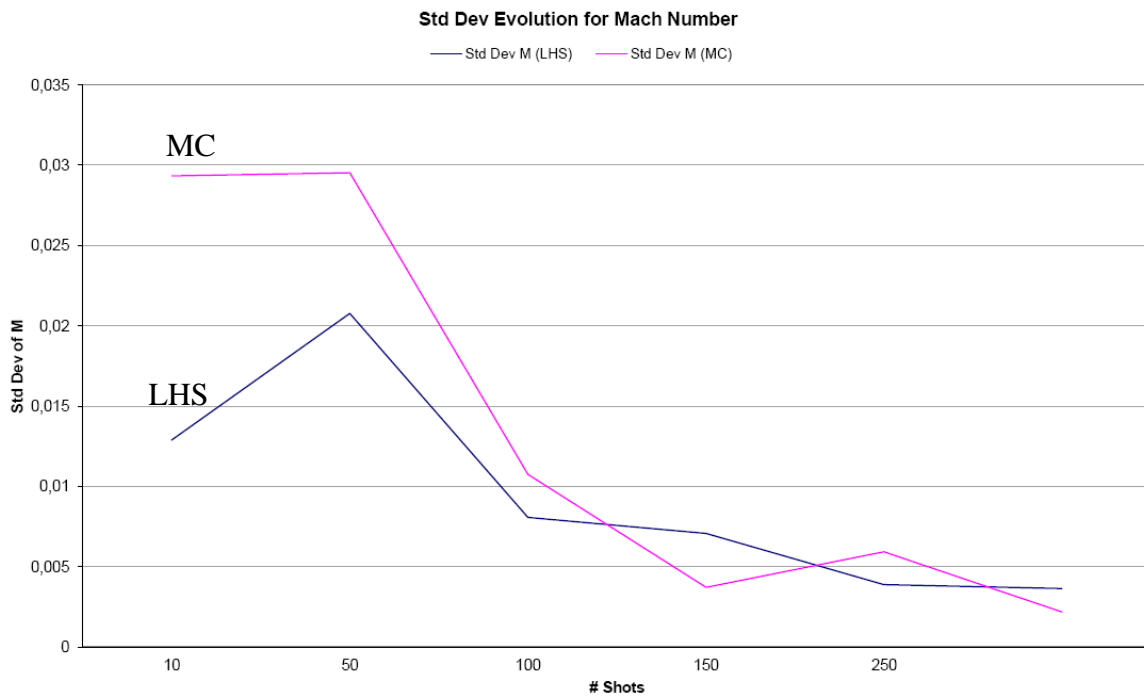
Figure 3-37. Evolution of M St deviation when increasing the amount of samples (Transonic)

The input variables are not directly affected by the flying regime. But both subsonic and transonic cases have been presented. As expected, and due to statistical reasons, the shown values are slightly different, but both of them show the same trend. In both cases, the mean value of the Angle of attack and the Mach number converge to the real mean when increasing the number of samples.

Although, both Monte Carlo and Latin Hypercube (blue and magenta lines respectively in the Figure 3-34 to 3-37) catch the real values and converge to it, a slight difference can be detected in the case of Latin Hypercube. Latin Hypercube sampling shows a closest value to the converged mean when number of samples is low. But the standard deviation is the parameter which presents a most significant difference. The standard deviation of the Latin Hypercube case presents a quicker trend to the real value with a low number of samples. Latin Hypercube Sampling technique improves Monte Carlo sampling technique regarding variance convergence. The results showing a faster convergence of the standard deviation when defining samples with LHS confirm the fact that Latin Hypercube Sampling technique better represents the working space with its selected samples.

The main point when analysing the output values is to detect if this slight difference between Monte Carlo and Latin Hypercube Sampling is transferred to outputs.

The first thing the reader can observe is that standard deviation in the subsonic case is lower than in the transonic case. It clearly confirms that the shock wave is inducing additional variability.

Another point is that the variability in the input values is transferred in a special way to the output. It means that the angle of attack and the Mach number values produce specific effect on lift and drag coefficient due to the relationship between parameters. If the formula that relates angle of attack and Mach number with lift and drag is analysed it can be observed that the velocity is quadratic and the angle is a plain value. It can be easy to expect a different behaviour of lift and drag.

The lift and the drag coefficients also show a convergence when increasing the amount of samples. The standard deviation of the repetitions of the analysis also tends to converge. In addition, the standard deviation of the Latin Hypercube Sampling cases shows slight more stable values. Although they converge to the final value, the difference between the set of 5 samples and the set of 250 samples are lower than those observed on Monte Carlo cases. Figure 3-38 to 3-45 clearly show this behaviour.

Figure 3-38 to 3-45 are a comparison of the behaviour of the mean and the standard deviation of C_l and C_d (subsonic case) or C_{dp} (transonic case) coefficients when input parameters are defined using Latin Hypercube or Monte Carlo sampling. All of them compare the convergence while increasing the amount of samples. To facilitate the comparison some reference values, plot as horizontal lines, are used. The selected reference values are obtained from the same problem definition with a set of 500 or 9000 Monte Carlo samples (referred as MC500 and MC9000 in Figure 3-38 to 3-41). In Figure 3-38 the mean value of the population is also used as reference. It is mentioned as "Real mean", and it is the mean value applied to the PDF in order to obtain the samples.

In all the cases, increasing the amount of samples leads to closer values compared with the reference ones. Both sampling cases, namely Monte Carlo and Latin Hypercube sampling,

have a similar convergence rate. Both of them are affected by sampling variability, and the trend curve is not so smooth.

Comparing the relative errors it can be confirmed that these conclusions are the right ones.
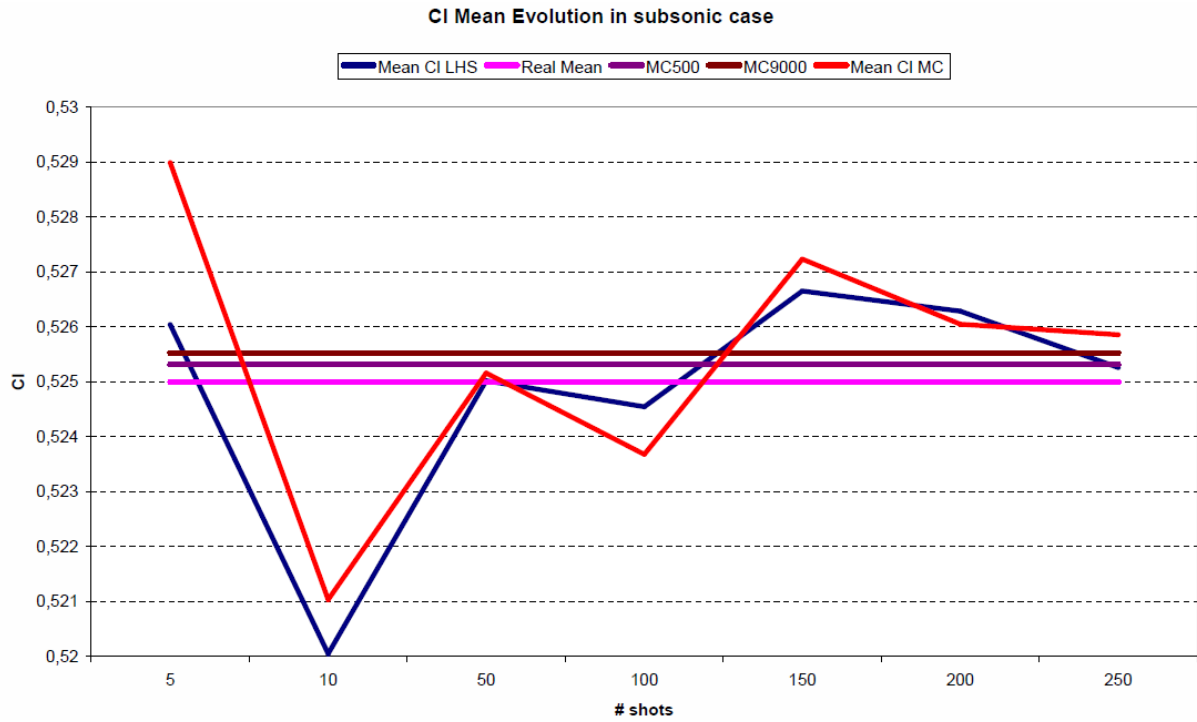
Figure 3-38. C_l mean evolution (Subsonic)

Figure 3-39. C_l St Deviation evolution (Subsonic)

Mean Cd Evolution in subsonic case
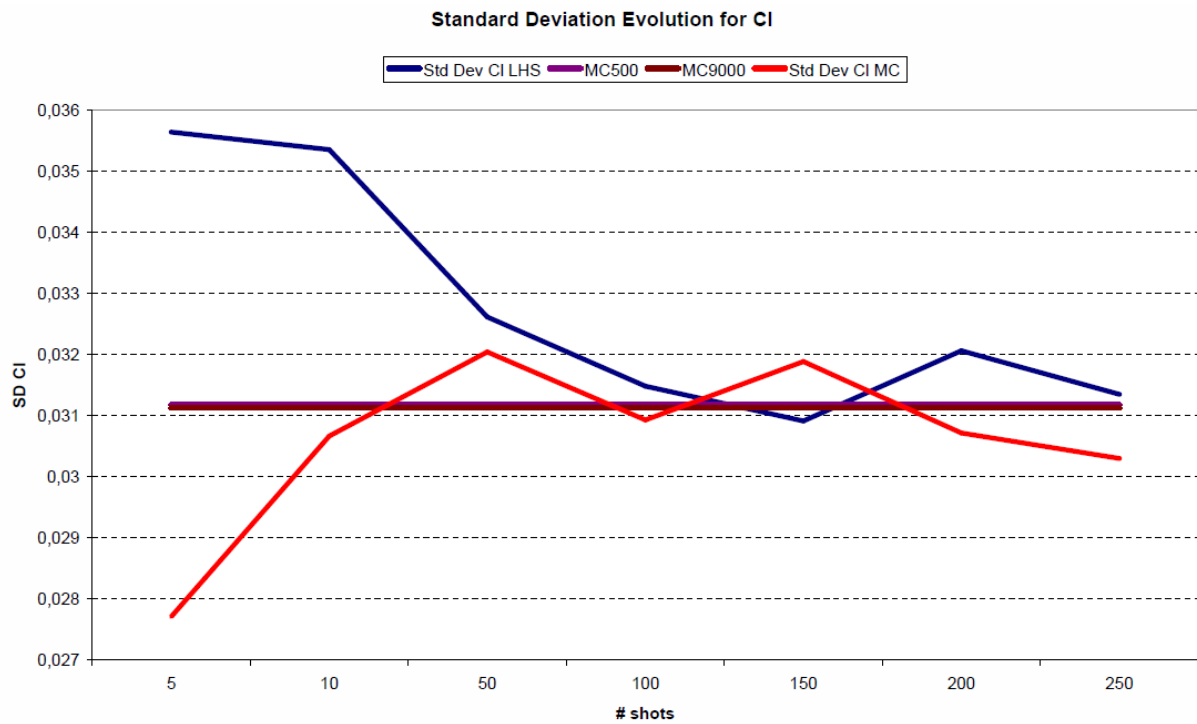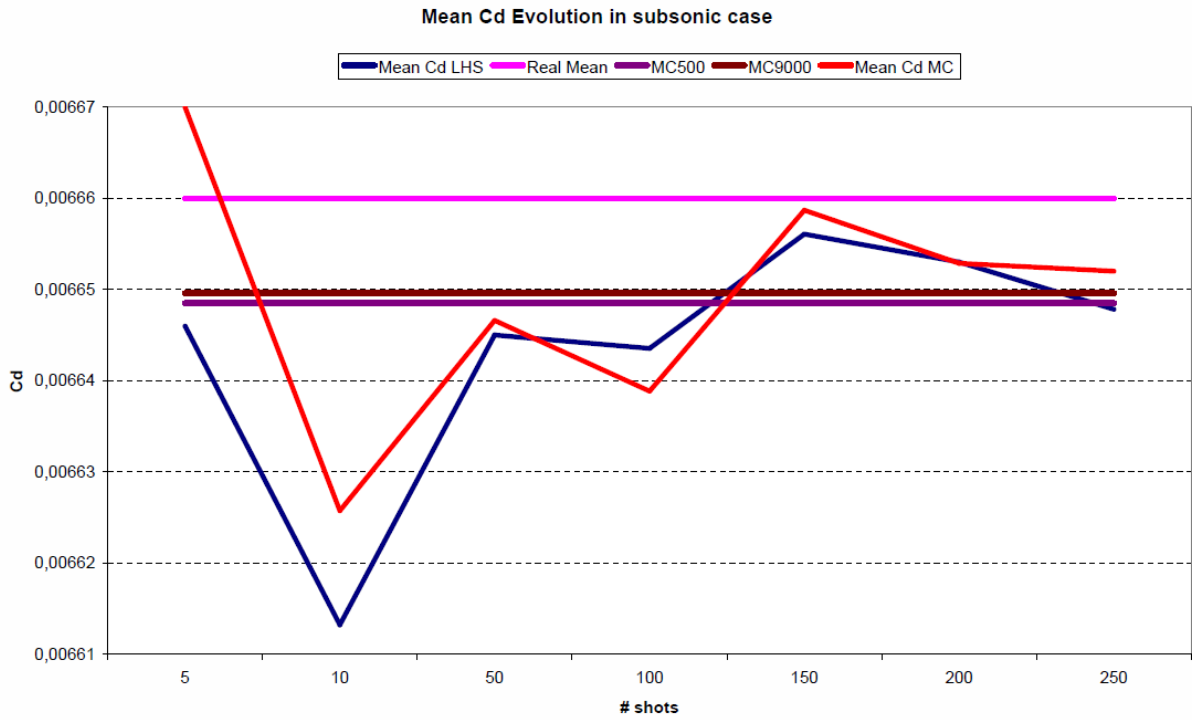
Figure 3-40. C_{dp} mean evolution (Transonic)

Standard Deviation Evolution Cd
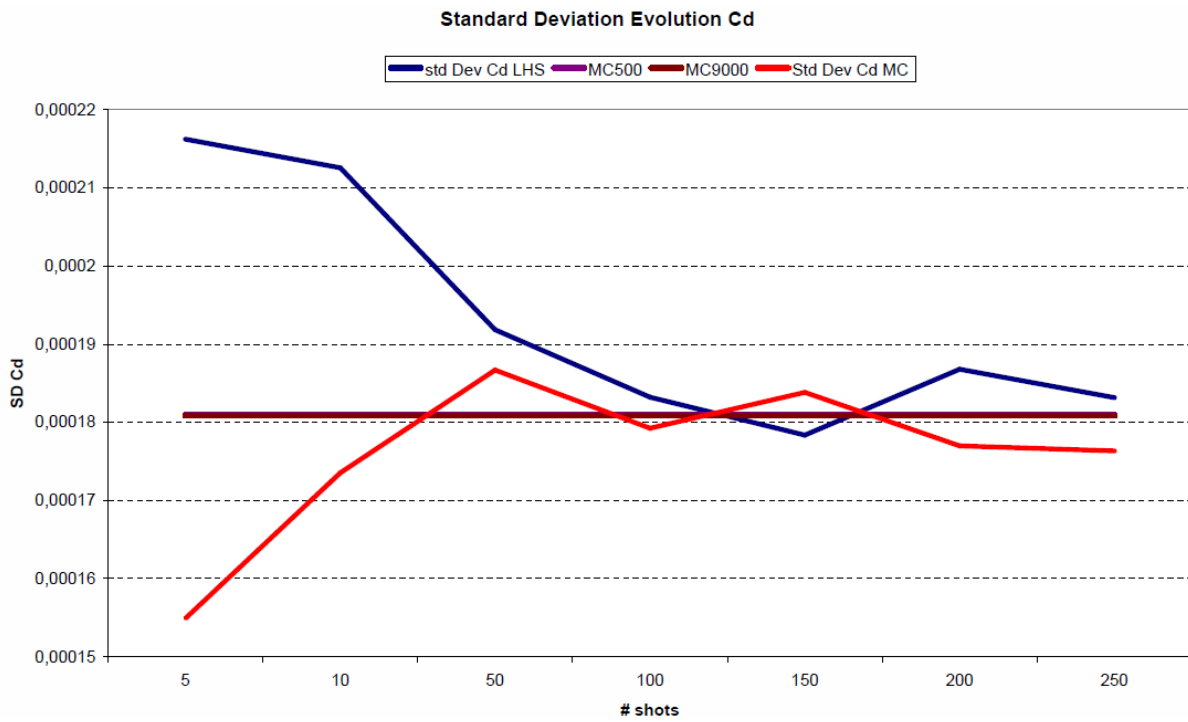
Figure 3-41. C_d St Deviation evolution (Subsonic)
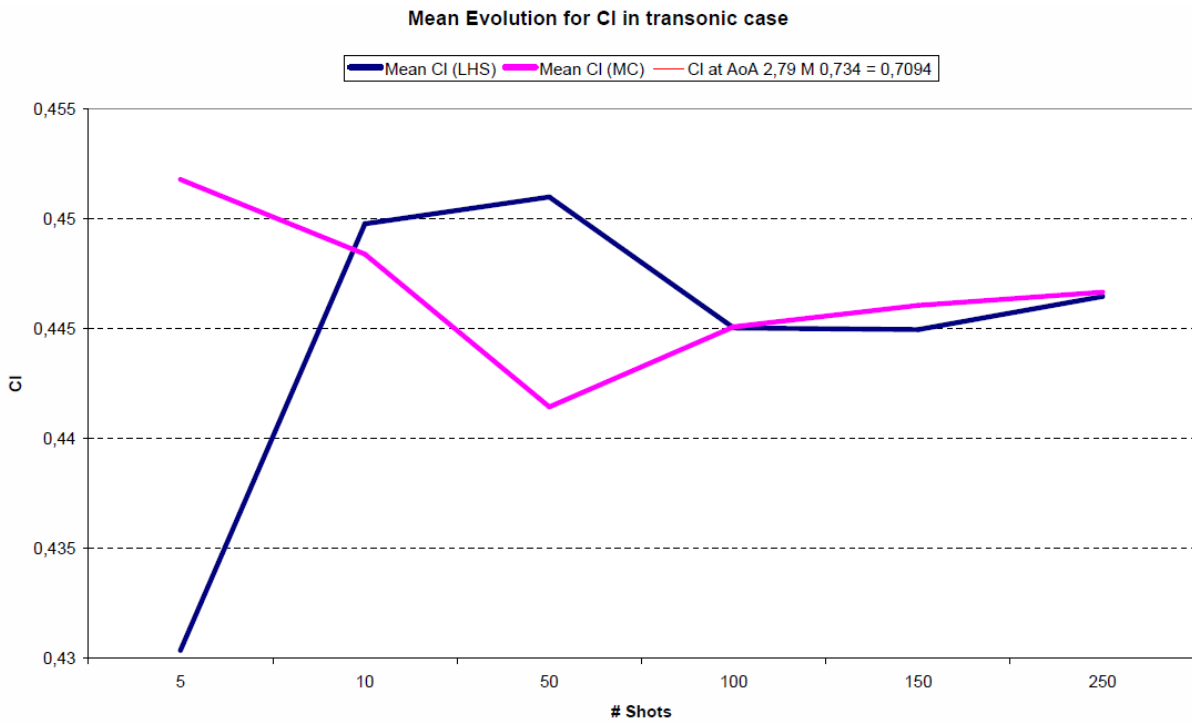
Figure 3-42. C_l mean evolution (Transonic)
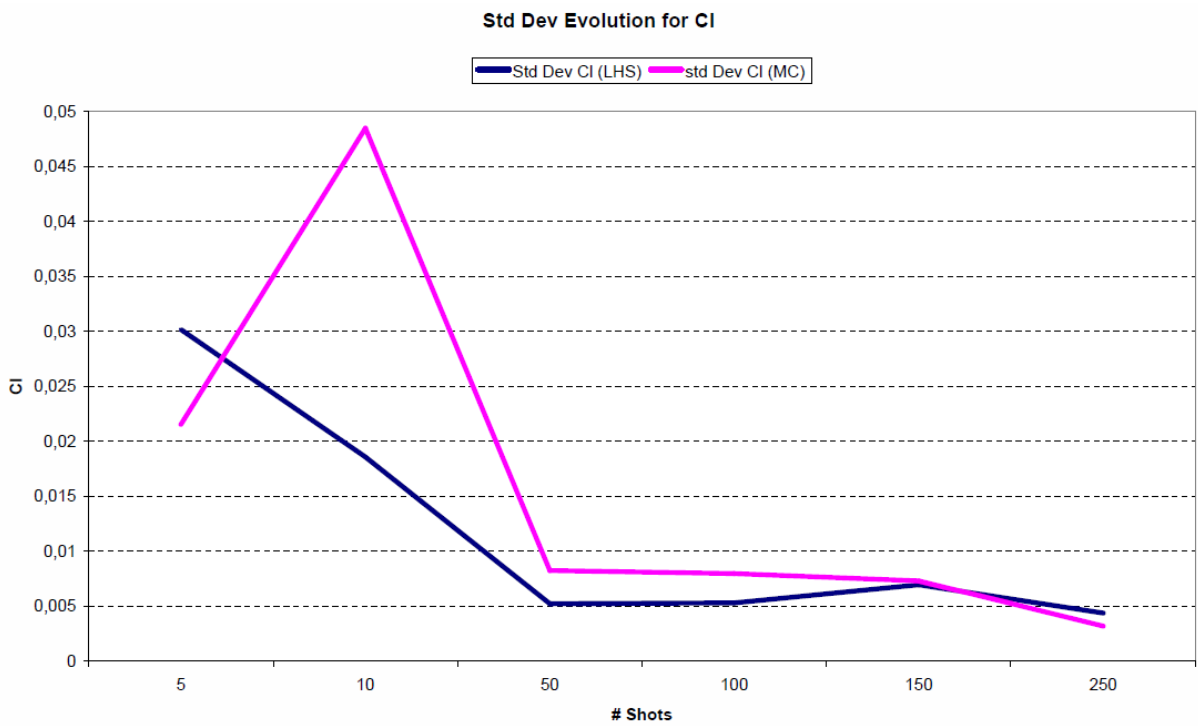
Figure 3-43. C_l St Deviation evolution (Transonic)

Mean Cdp Evolution in transonic case
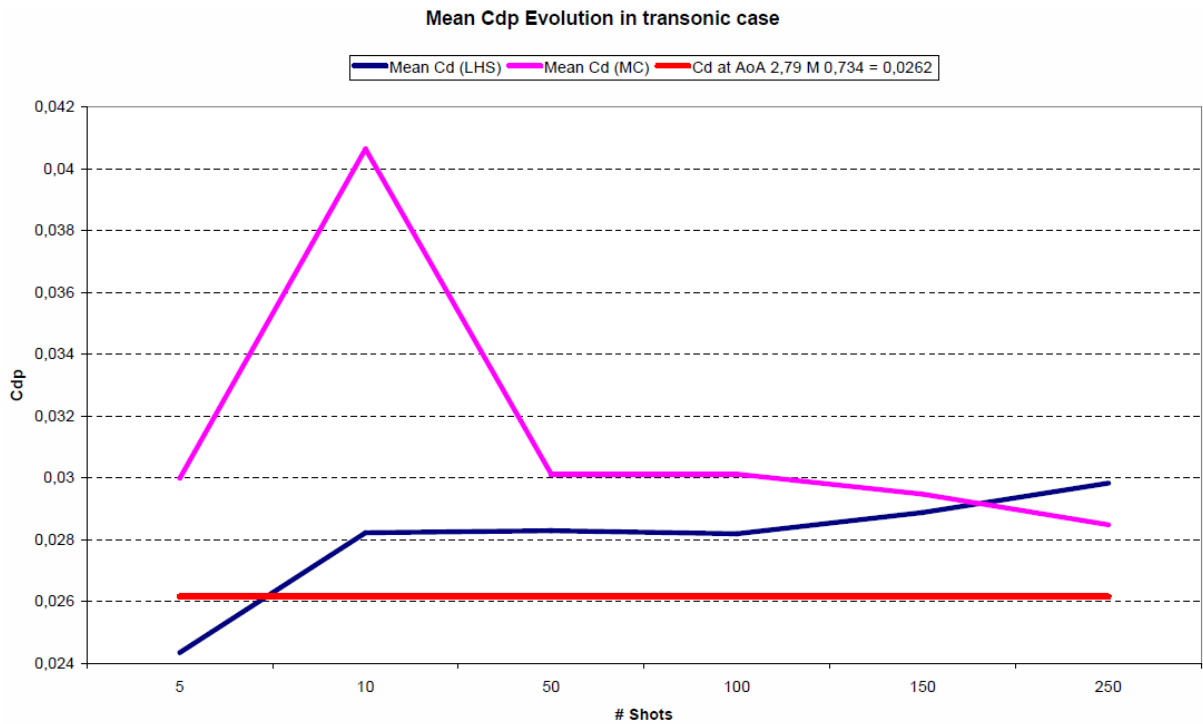
Figure 3-44. C_{dp} mean evolution (Transonic)

Standard Deviation Cdp in transonic case
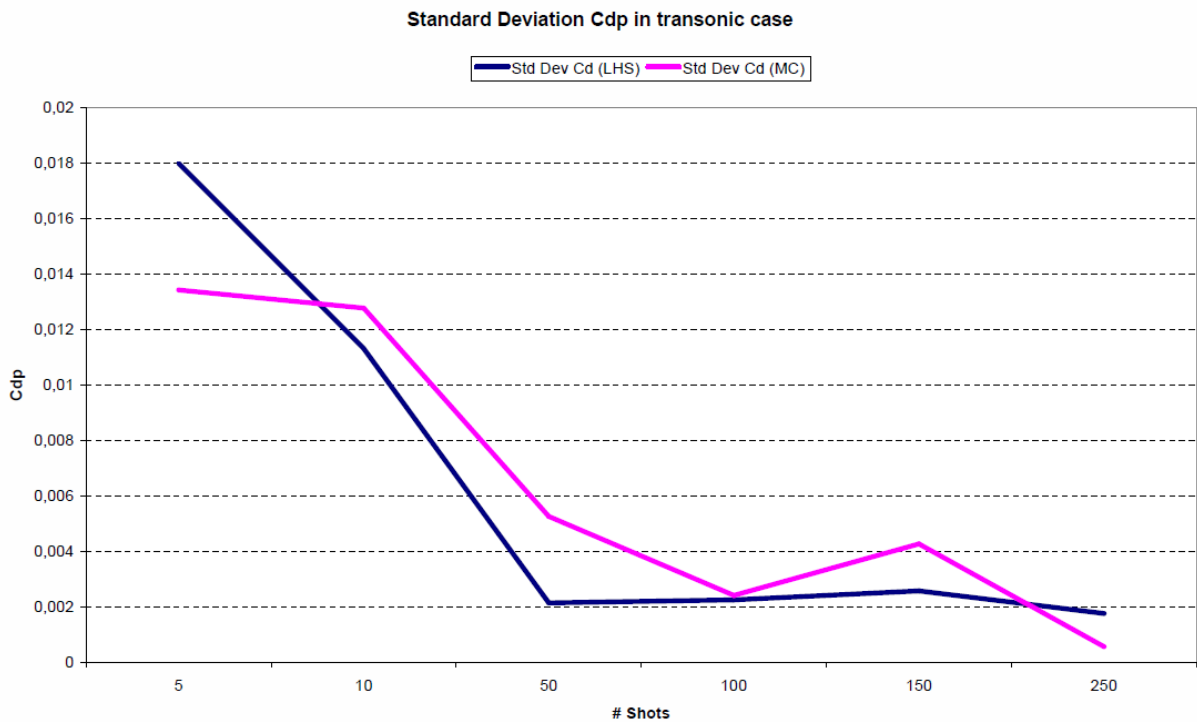
Figure 3-45. C_{dp} Std Deviation (Transonic)

In order to carefully take some conclusions, some measurements of the error have been used. Two calculated values have been used as references. In Figure 3-46, the deterministic value has been used as reference, and the error of the different amount of analysis samples has been plotted for the lift, and the drag coefficients, when using a Monte Carlo or a Latin Hypercube

sampling techniques. For additional information the errors of a 500 and 9000 Monte Carlo analysis samples are added to the plot.
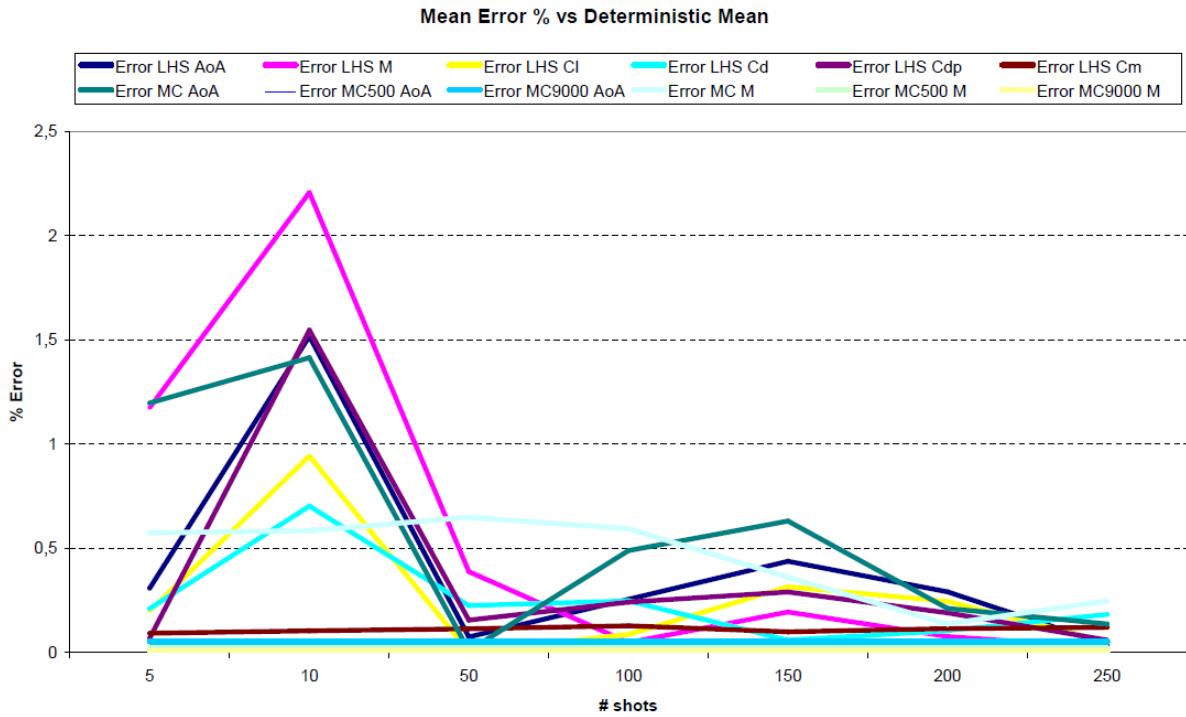
Figure 3-46. Error MC/LHS vs Deterministic (subsonic)
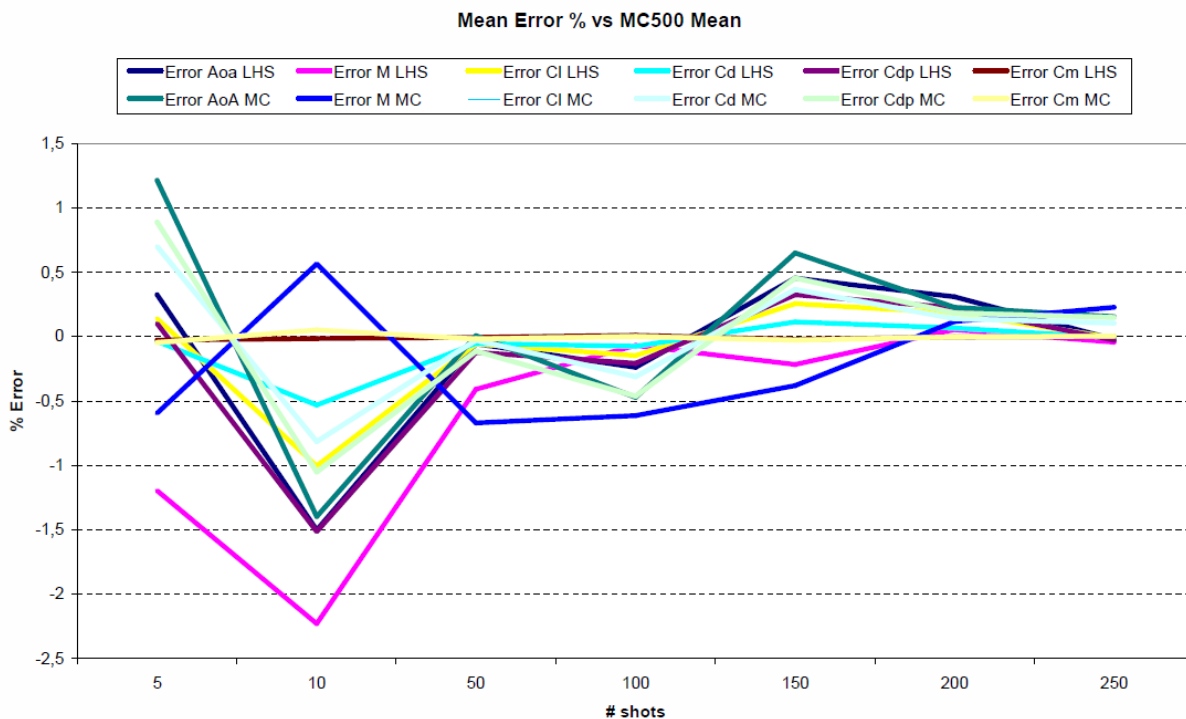
Figure 3-47. Error MC/LHS vs Monte Carlo 500 shots (subsonic)

Figure 3-47 compares the same values with a 500 samples Monte Carlo analysis, in order to evaluate the availability to reduce the amount of samples without decreasing the accuracy.

In both cases, error values remain below 2.5%. Errors are the addition of all the errors involved on the analysis; definition of the geometry, CFD numerical analysis, and sample induced error or variability.

3.5.2.4 Preliminary conclusions of the Monte Carlo and Latin Hypercube comparison

It has been verified that the Latin Hypercube sampling technique is able to better capture the input variability compared with the Monte Carlo sampling technique. What was expected and it has not been clarified is the fact that this better representation of the input variability is translated to a better capture of the output variability. It has been expected that Latin Hypercube would provide a better representation of the output variability compared with Monte Carlo, but the results show slight differences between them. It leads to the conclusion that Monte Carlo and Latin Hypercube are equivalent from the output variability point of view.

3.5.3 Variability analysis using the Probabilistic Collocation method

3.5.3.1 Introduction

Several methods have been developed to deal with uncertainty quantification (UQ). Stochastic methods are considered computationally very expensive, although they provide full statistics of the outputs. Stochastic methods are based on statistical random sampling instead of on defining a multi-point analysis, which selects a fixed set of points through all the analysis to check the random space.

The Probabilistic Collocation method is one of the most successful developments in UQ. It has been applied in several disciplines as thermal analysis or CFD analysis. The main advantage of PCM compared with stochastic analysis is the lower computational cost to obtain the mean and standard deviation of the output variables. On the other hand, its major drawback is that it uses a multi-point strategy because given a PDF, with a defined mean and standard deviation, the evaluation points are always the same. The reader can refer to section 2.3.2 and references Loeven and Bijl (2008, 2009) and Leoven et al (2007) for additional details about the method.

The objective of this section is to compare stochastic sampling methods, Monte Carlo and Latin Hypercube, with the Probabilistic Collocation method; understand how PCM works and evaluate their pros and cons.

3.5.3.2 Procedure

Input parameters have been defined with a normal probability density function. The statistical values are μ_{AoA}=2,79 , σ_{AoA}=0,01 , and μ_M=0,25 , σ_M=0,001.

To calculate the mean and the standard deviation of the output, when dealing with two uncorrelated stochastic variables, the following expressions can be used:

$$\mu_u = \sum_i^{N_p} \sum_j^{N_p} u_{ij}(a,m) \cdot w_{a_i} \cdot w_{m_j}$$

3-4

$$\sigma_u^2 = \sum_i^{N_p} \sum_j^{N_p} u_{ij}(a,m)^2 \cdot w_{a_i} \cdot w_{m_j} - \left(\sum_i^{N_p} \sum_j^{N_p} u_{ij}(a,m) \cdot w_{a_i} \cdot w_{m_{ji}} \right)^2$$

3-5

Where $u_{ij}(a,m)$ is the function evaluation in the *(ij)-th* collocation point. The weight for each uncorrelated stochastic variable is w_{ai} and w_{mj}. And N_p is the total amount of collocation points defined.

3.5.3.3 *Results applying the variability using Probabilistic Collocation Method*

The collocation method defines evaluation points and weights using a quadrature method as described in section 2.3.2, This is directly translated to the output values. Figure 3-48 shows how the output behaviour is also almost constant in lift and momentum coefficient (C_m). Drag coefficient is not plotted because the resultant figure has no sense since Euler solver does not consider boundary layer effects.
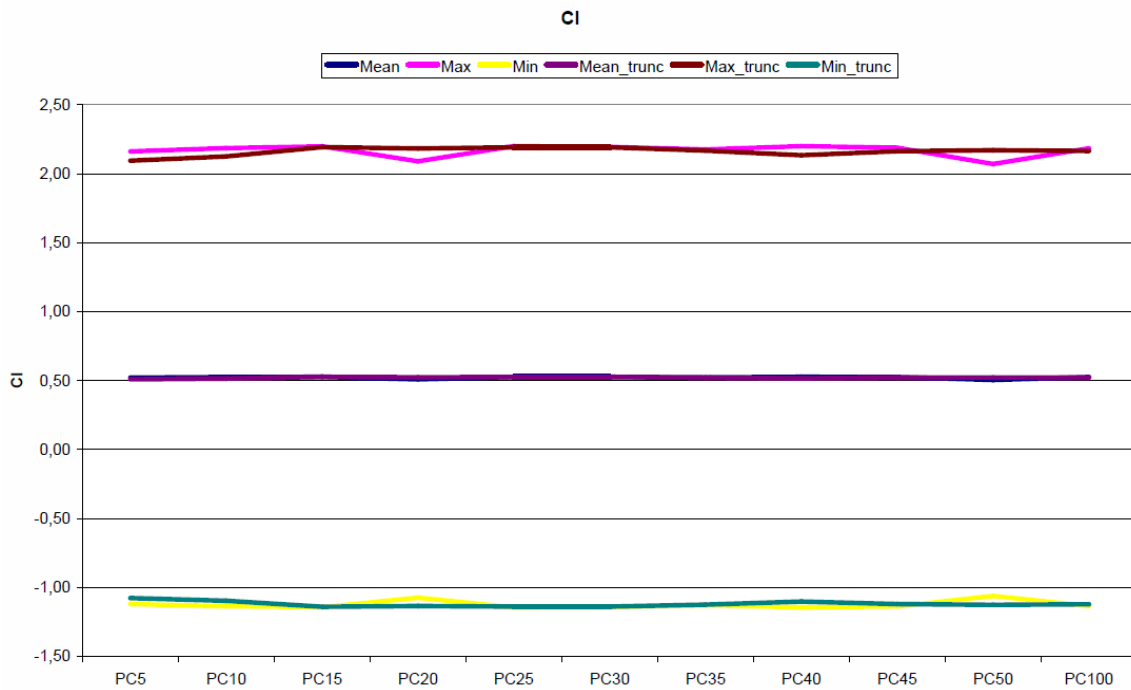
Figure 3-48. Cl comparative for truncated and non-truncated PDF (+/-3std dev ranges and mean)
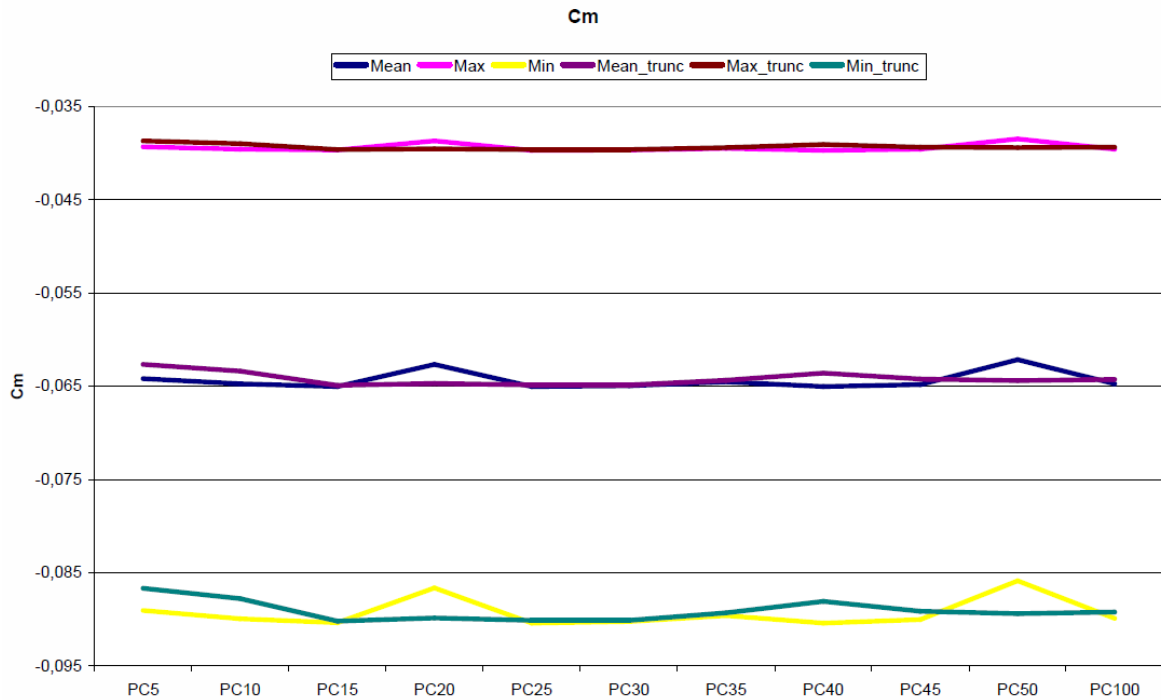
Figure 3-49. Cm comparative for truncated and non-truncated PDF (+/-3std dev ranges and mean)

Figure 3-50 presents the plot of error of the results compared with the mean value of the deterministic case. All of them remain under 4.5%, but a large sensitivity to the numerical analysis can be detected. The plot shows a peak for the point defining polynomial degree equal to 35 that is associated to numerical noise.
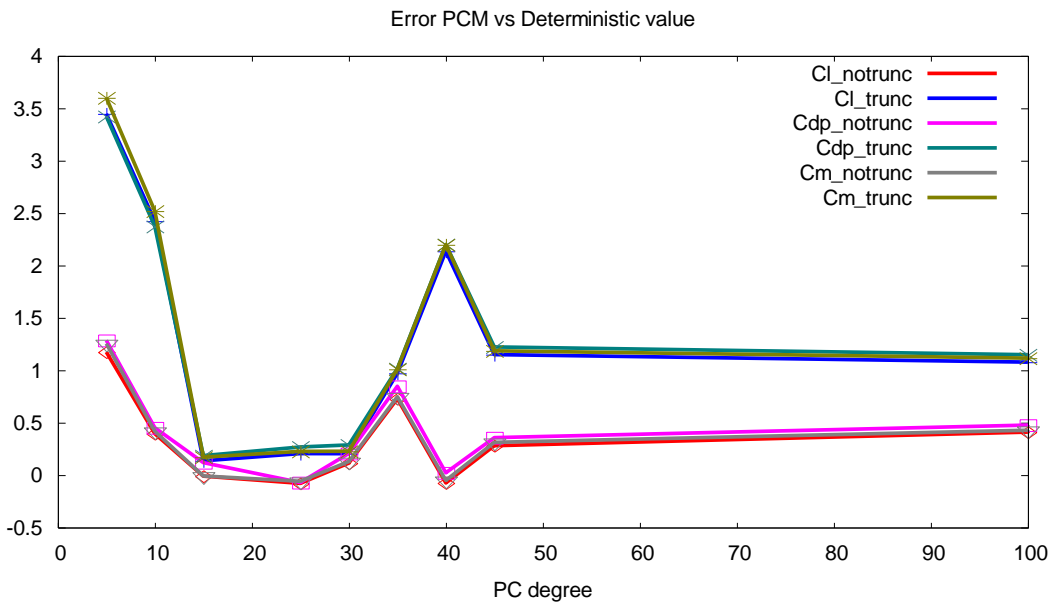
Figure 3-50. Errors PCM vs Deterministic values

Lift, and momentum coefficients have been analysed when truncated and non-truncated probability density functions have been defined. Errors obtained for the truncated cases follow the same behaviour, as happens on the non-truncated cases.

3.5.3.4 Preliminary conclusionsw when using Probabilistic Collocation Method

Probabilistic Collocation Method is a powerful method for Uncertainty Quantification. It reduces the computational cost, providing the two main statistical moments of the results. The results show how the PCM approximation leads to a narrow error which provide a good accuracy on the results.

A comparison can be establish between stochastic techniques and PCM, both have their advantages and their drawbacks, both leads to accurate results and both are able to capture the variability induced by input uncertainty. The user should select between them considering the requirements from the problem and the available computational resources.

3.5.4 Conclusions from the different stochastic analysis of a CFD problem

When analysing variability against flow conditions, and considering the range of values applied to the input values, it is easy to identify the correlation between the input and output variables. The polar curve can be identified in those plots where one of the variables has been defined as constant. The polar curve shape can also be identified when variability effects appear on the plot without considering constant values, as happens in Figure 3-17 and 3-21, for instance.

The comparison with the deterministic analysis shows that the stochastic analysis provides a better understanding of the global phenomena around the nominal point. In the transonic test case the deterministic values do not identify the point when the shock wave appears. The stochastic analysis is able to identify it while analysing the nominal point.

Regarding the mesh size test case, the mesh size is strongly related with the geometry of the profile and the control area. It was expected that the mesh size applied to profile lines produced larger effect on the results, but it was not easy to anticipate the effect of the sizes applied to the inner control area or the outer area.

The fact that PUMI CFD solver is based on Euler equations must be taken into consideration, so the calculation of drag is an approximation that can affect the final behaviour of the results of the transonic test case. The used solver only provides the pressure or shock drag and it is not computing the boundary layer effect. This fact demonstrates the need of knowing the solver and understands its use. If not conclusions can easily be wrong.

This chapter has also been aimed to clarify the differences between the Monte Carlo and the Latin Hypercube sampling techniques regarding its efficiency to capture the real value of the mean and standard deviation. It can lead to a significant reduction of the required evaluations and a reduction on the computational cost. But it is also devoted to verify if different sets of samples, coming from the same population, produce same effects on the results and if the sampling variability is transferred to the output values in the same way in both the Monte Carlo and the Latin Hypercube techniques. Although Latin Hypercube better captures the input data behaviour than Monte Carlo, the output data behaviour is captured as good as with both Monte Carlo and Latin Hypercube techniques.

Robust optimization procedures will take advantage of the definition of computing samples to increase the robustness of the solution. Instead of defining a multi-point procedure, a probabilistic robust procedure will be defined. The variability due to the sampling points has to be under control. In addition, the comparison between MC and LHS to check if LHS enables the reduction of the amount of samples has been investigated.

Analysing both aims, it can be concluded that the differences between the results obtained with Monte Carlo and Latin Hypercube sampling techniques are small. Latin Hypercube does not improve the output variability results and leads to no-reduction of the amount of samples used to characterize the probability distribution. On the other hand, it has been verified that samples are not introducing additional variability. All the statistical set of samples are a well representation of the whole population.

The Probabilistic Collocation method (PCM) is a powerful method to deal with uncertainties. It provides an easy method to evaluate the mean and the standard deviation, defining a predefined and limited amount of evaluations. As stated on the state of the art section, PCM and other collocation methods increase their complexity when increasing the number of uncertain parameters to deal with.

Table 3-16 shows Pros and cons of this method against stochastic method, as a brief summary of Table 2-3:

	Stochastic	PCM
Full Statistics	Yes	No
# Uncertainties	No limitation	Increase complexity and calculation time
Calculation time	Big number of evaluations	Small number of evaluations
Statistical Sampling	Yes	No
Fixed Multi-point	No	Yes

Table 3-16. Comparison between stochastic techniques and PCM

The PCM provides the capability to obtain a fast output, but the fact that stochastic analysis uses statistical sampling helps to ensure robustness during and optimization problem. During optimization, stochastic methods can provide different set of samples for each population, or even for each individual. A study of when it is convenient to generate different sets of sampling points will be presented in chapter 4.

Anyway, the PCM is a method to take into account for further developments or specific cases where robustness is not so important compared to a faster solution.

From the point of view of the applicability of the method to a CFD problem, no relevant issues have been raised. Mesh size, geometry parameters, and flow conditions have been defined as stochastic parameters. Then any kind of problem can be solved. The requirement is that the user should know the probability distribution of the variables in advance. The selection of the amount of the stochastic samples to be generated will define the accuracy; the larger the amount of samples is, the more accurate the stochastic representation will be.

3.6 Variability on an aero-elastic problem

3.6.1 Introduction

This section describes the analysis of the variability of output values against flow and structural parameters of an aero-elastic problem defined for a RAE2822 airfoil.

The analysis is mainly focussed on the study of the behaviour of the output data when a stochastic definition is used for several input parameters to study the flutter phenomena. These input parameters are the Angle of Attack, the Mach number of the free stream, the x-coordinate of the elastic axis, and the damping coefficients for vertical and angular movements. Applying random values for these parameters the behaviour of the angular movement (Theta, θ), vertical movement (h_c), lift, drag and momentum coefficients and their minimum and maximum values is analysed.

The aims of the analysis are to describe the effects on the time evolution of aero-elastic values (lift, drag, vertical movement and angular spin, for example) when flow is defined with uncertainties. This analysis provides a better understanding of the response of an aero-elastic system under input variability. Figure 3-51 is a graphical description of the test case.
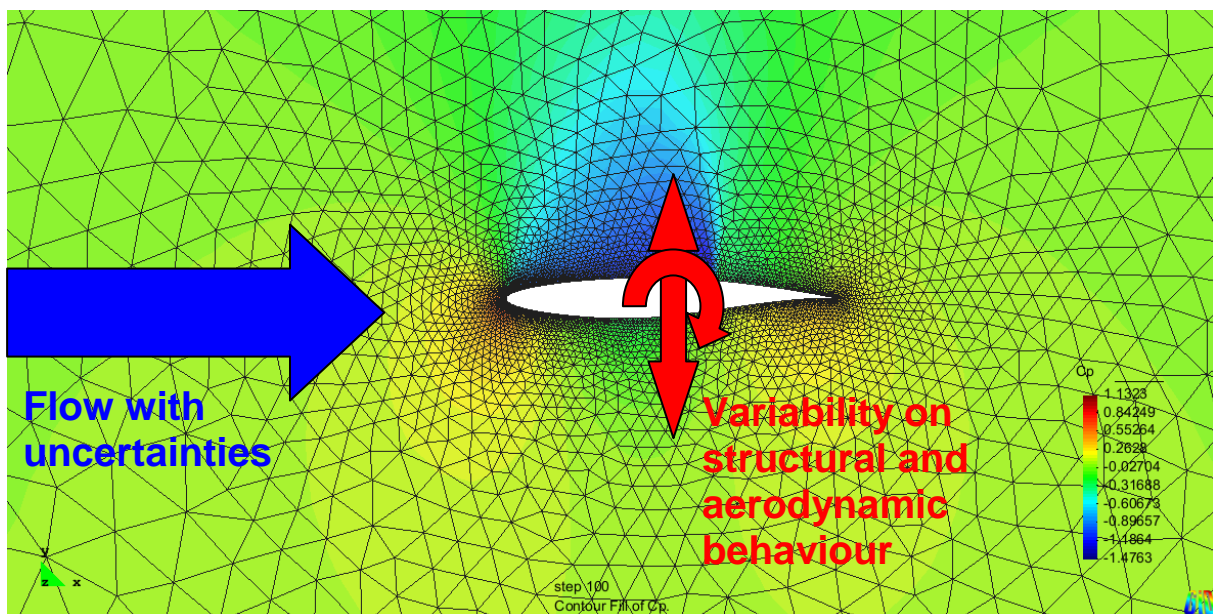
Figure 3-51. Representation of the aero-elastic problem under uncertainties

3.6.2 Used Tools

The software tools used for this stochastic analysis are: STAC, which is used as stochastic calculus manager, and an Aero-elastic solver, based on a compressible flow solver developed by E. Ortega et al. (2007)(2009), which provides the numerical analysis for each stochastic shot (run) of STAC.

The used aero-elastic solver is a recent development. It couples a 2D Finite Point method CFD solver with a simplified structural solver for the analysis of the elastic response of a wing profile. It considers the infinite profile assumption, and reduces the structural study to a spring-damp system. This system enables the study of two degree of freedom; vertical

movement and angular movement around elastic axis. The aero-elastic solver is further described in the Appendix I.

3.6.3 Procedure

Input parameters are the angle of attack (AoA) and the Mach number (M), as the flow field parameters, the elastic axis x-coordinate (x-EA), the vertical movement (z-dp) and the angular movement damping (a-dp), as the structural parameters. A normal probabilistic distribution has been applied. For all them the main values applied are described in Table 3-17:

	Mean	Standard deviation
Angle of attack	2,79	0,279
Mach number	0,734	0,01
x-EA	0,4	0,04
z-dp	0,25	0,025
a-dp	0,25	0,025

Table 3-17. Probabilistic Values

A first test case has been defined where all the parameters are defined statistically. It acts as the fully non-deterministic reference case. A fully deterministic case, which uses the mean value of each parameter, has also been calculated to compare as the second reference case.

To generate the mesh, the following mesh sizes have been applied:
- Leading and trailing edge points: 0,002
- Profile boundary: 0,001
- Control area default size: 0,1

3.6.4 Results

3.6.4.1 Fully deterministic analysis results

An initial deterministic analysis has been performed in order to be used as reference for the stochastic calculation. The values of the different parameters used for the deterministic analysis are equal to the mean values used later for the next stochastic analysis (see Table 3-17).

Table 3-18 shows the evolution of output parameters at different time steps for the deterministic analysis.

step	time	Theta, θ (º)	h_c	C_{dp}	C_l	C_m
50	25	-0,63750E-02	0,21673	0,2019E-01	0,8567	-0,7136E-03
100	50	-0,24378E-01	0,22571	0,1945E-01	0,8438	-0,1516E-02
150	75	-0,22342E-01	0,22422	0,1945E-01	0,8435	-0,1419E-02
200	100	-0,21217E-01	0,22384	0,1947E-01	0,8438	-0,1359E-02

Table 3-18. Deterministic Values at different time steps

Table 3-19 is the compilation of minimum and maximum values.

	Theta, θ (º)	h_c	C_{dp}	C_l	C_m
Max	0,00859	0,25622	0,02029	0,8577	0,00009
Min	-0,42774	0	0,01185	0,6335	-0,02476

Table 3-19. Deterministic Max/min Values

Figure 3-52 to 3-56 show the evolution of output parameters versus time. The damping coefficients are high enough to ensure a fast convergence. Theta, θ, and h_c evolutions start at zero because they refer to incremental values (angle and height). Other parameters start from the value obtained by a stationary analysis.

Theta evolution presents an initial spin, clockwise and lower than 0,5º, that initiates a small oscillation before convergence to a close to zero value.
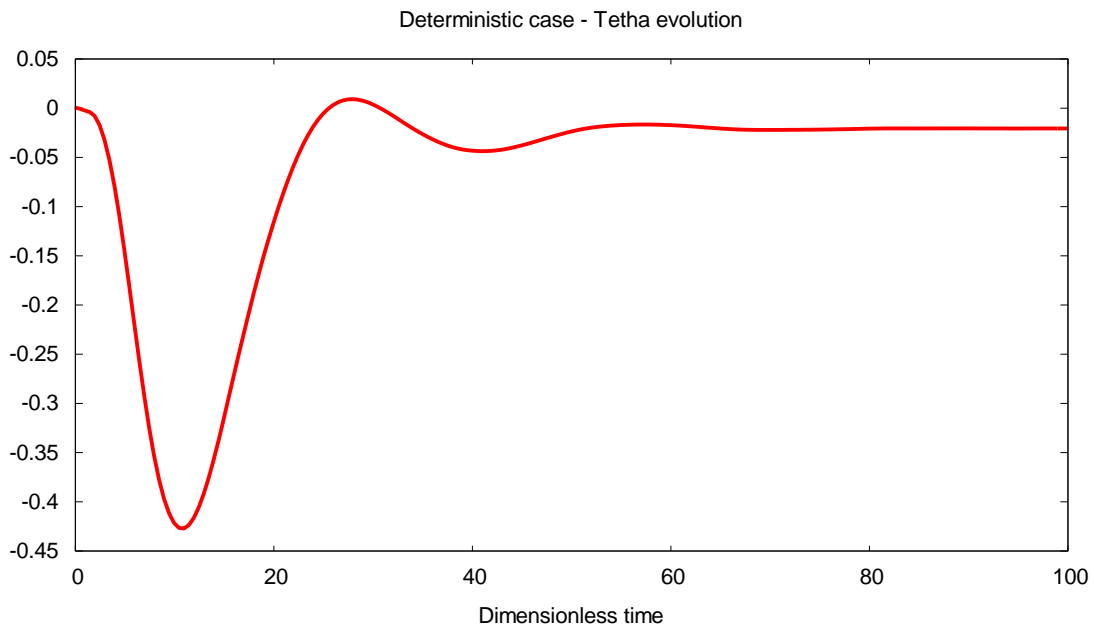
Figure 3-52. Theta vs time. Deterministic case

Similarly, h_c or height value behaves with an initial oscillation which leads to a convergence value around 0,22.

Deformation of a real wing during a real flight can confirm that the aero-elastic effect is larger on deformation than in angular spin. The deformation of the wing is easily detected, while angular deformation is not so much apparent.

Deterministic case - h/c evolution
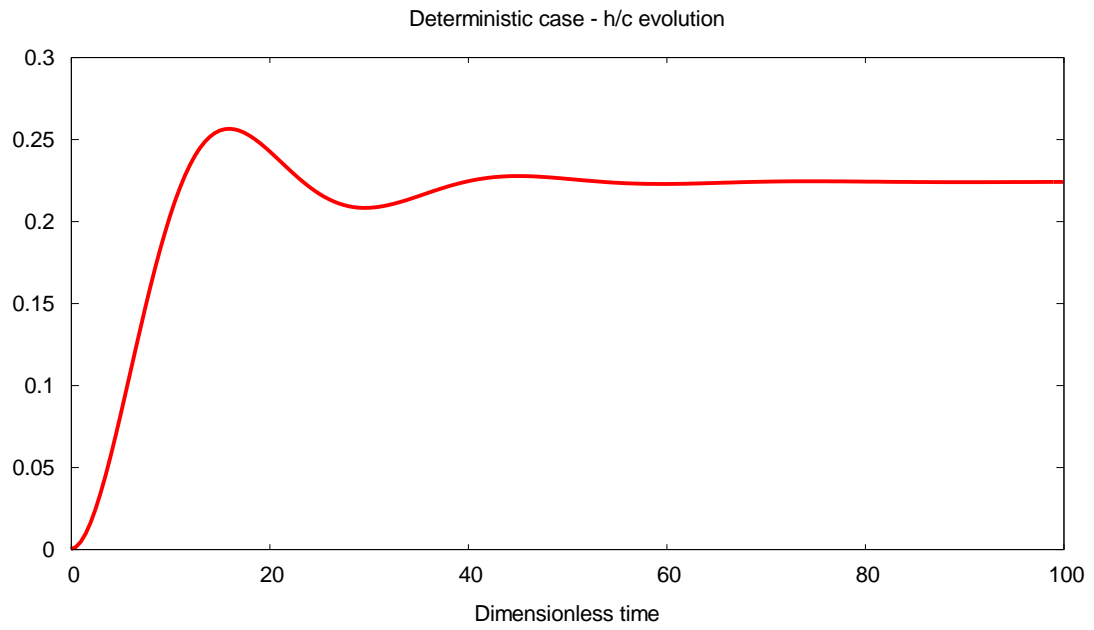
Figure 3-53. h_c vs time. Deterministic case

Deterministic case - Cdp evolution
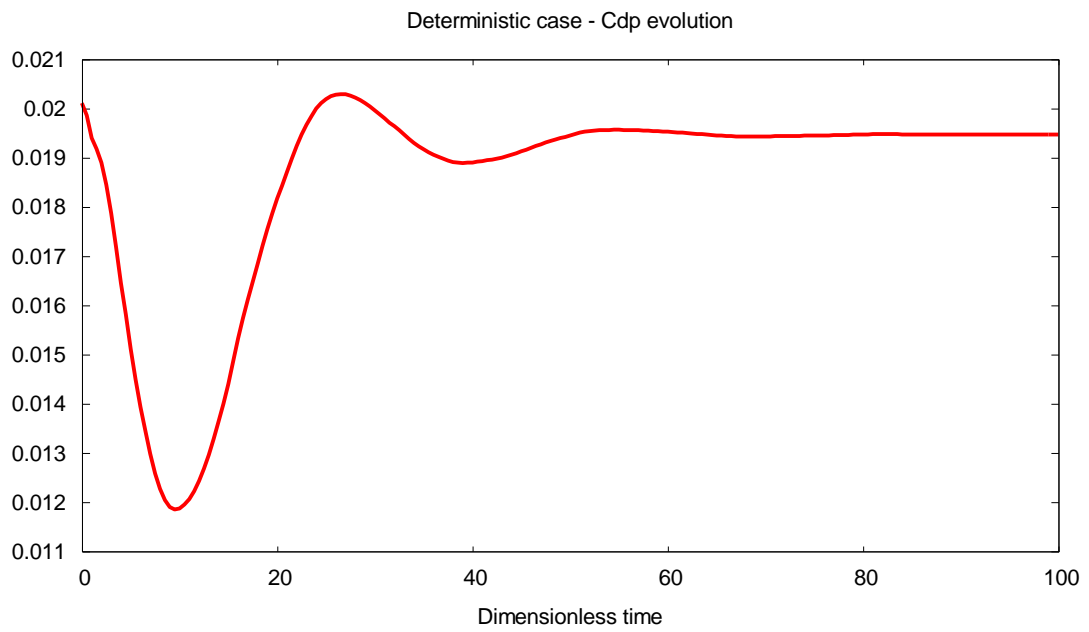
Figure 3-54. C_{dp} vs time. Deterministic case

Deterministic case - Cl evolution
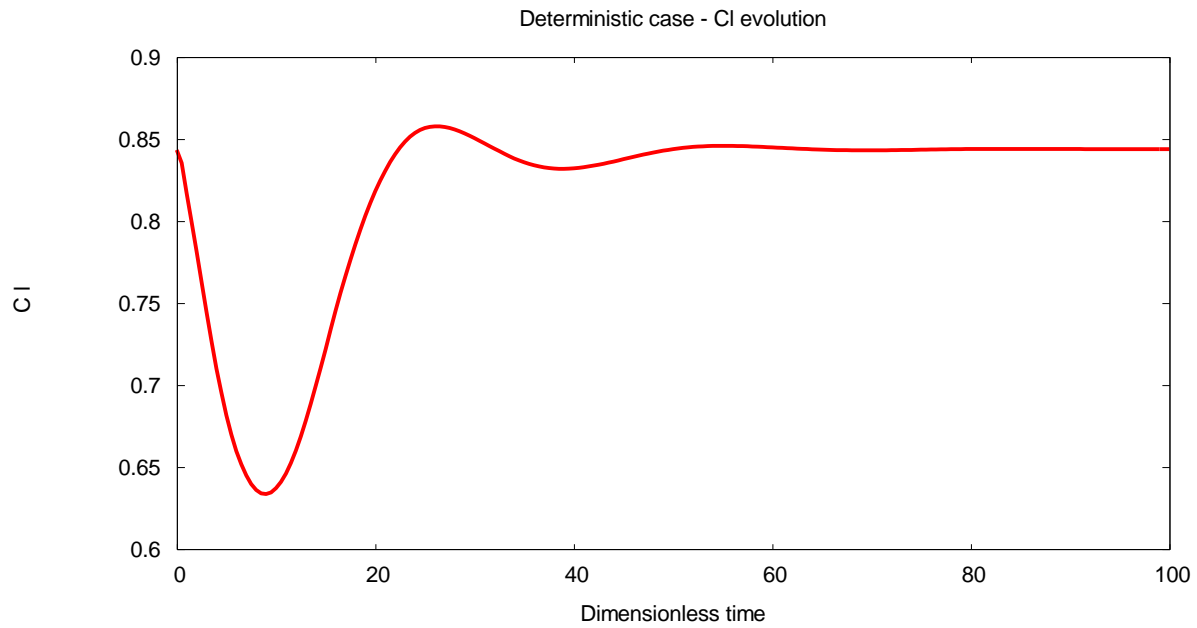
Figure 3-55. C_l vs time. Deterministic case

Deterministic case - Cm evolution
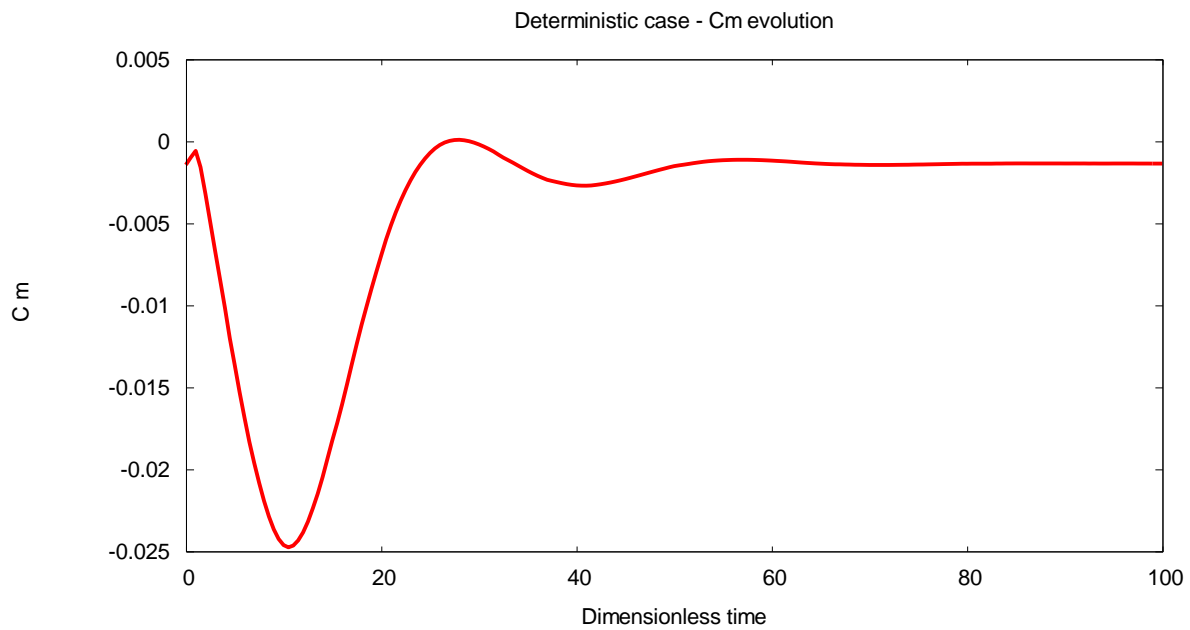
Figure 3-56. C_m vs time. Deterministic case

The behaviour of the lift, pressure drag and momentum coefficients is plotted in Figure 3-54, 3-55 and 3-56. All of them follow a similar behaviour with a fast convergence due to the defined input values.

3.6.4.2 *Results of the stochastic analysis*

Once stochastic values, as described in Table 3-20, are applied to the problem, theta, h_c, C_l, and C_m can be statistically analysed. Six test cases have been defined, which use a stochastic

definition of the input variables. Some of these test cases define some of the input variables as constant, and some of them combine constant definitions with stochastic definitions.

	AoA		M		x-EA		a-dp		z-dp	
	μ	σ	μ	σ	μ	σ	μ	σ	μ	σ
Case 1	2,79	0,279	0,734	0,01	0,4	0,04	0,25	0,025	0,25	0,025
Case 2	2,79	0,279	0,734	--	0,4	--	0,25	--	0,25	--
Case 3	2,79	--	0,734	0,01	0,4	--	0,25	--	0,25	--
Case 4	2,79	--	0,734	--	0,4	0,04	0,25	--	0,25	--
Case 5	2,79	--	0,734	--	0,4	--	0,25	0,025	0,25	--
Case 6	2,79	--	0,734	--	0,4	--	0,25	--	0,25	0,025

Table 3-20. Cases for stochastic analysis

The comparison of the results is done through the use of the coefficient of variation. Table 3-21 lists the coefficients of the input and the output parameters. Each case is numbered associated to the description in Table 3-20.

	AoA	M	x-EA	z-dp	a-dp	θ (min)	h_c (max)	C_{dp}(max)	C_l (min)	C_m (min)
Case 1	0,0927	0,0133	0,0980	0,0960	0,0930	-0,6952	0,1332	0,9685	10,2331	-0,6719
Case 2	0,0972	0,0	0,0	0,0	0,0	-0,0487	0,0502	0,1293	0,0602	-0,0376
Case 3	0,0	0,0130	0,0	0,0	0,0	-0,6854	0,0120	1,0182	7,0153	-0,6480
Case 4	0,0	0,0	0,1084	0,0	0,0	-0,3362	0,1583	1,0021	0,1032	-0,3340
Case 5	0,0	0,0	0,0	0,1069	0,0	-0,0077	0,0223	0,0	0,0094	-0,0061
Case 6	0,0	0,0	0,0	0,0	0,0981	-0,0018	0,0026	0,0	0,0041	-0,0038

Table 3-21. Coefficient of variation

The low effect that damping coefficients, both vertical and angular movement damping, have on all the output values compared to other input parameters can be observed. Standard deviations of almost all input variables have been defined as the 10% of its mean value. Then, damping coefficients have a coefficient of variation around 0,10, but the obtained coefficient of variation of outputs are significantly lower than this reference value. Also Figure 3-83 to 3-90 clearly show that variability induced by damping coefficients are lower than those by other input parameters.

Table 3-22 to 3-27 show the mean, standard deviation, minimum and maximum values for all the output values. The maximum and minimum values of the time evolution are analysed. It has been considered that both of them are a better representation of the range of values the evolution takes than the use of a single value equal to the mean due to its non-statistical behaviour.

Normal PDF: AoA, M, xEA, Zdp, Adp								
	Max θ	Min θ	Max h_c	Min h_c	Max C_{dp}	Max C_l	Min C_l	Max C_m	Min C_m
Minimum	0,0000	-4,1061	0,1100	-0,2940	0,0052	0,5232	-1,1970	0,0000	-0,2547
Maximum	1,3318	-0,4789	0,2264	0,0000	0,0896	0,8533	0,4137	0,0852	-0,0096
Std Dev	0,1835	1,0398	0,0189	0,0901	0,0169	0,0566	0,5724	0,0117	0,0574
Mean	0,0452	-1,4958	0,1418	-0,0423	0,0174	0,5452	0,0559	0,0029	-0,0854

Table 3-22. Max/min Values for all-stochastic parameters

Normal PDF: AoA								
	Max θ	Min θ	Max h_c	Min h_c	Max C_{dp}	Max C_l	Min C_l	Max C_m	Min C_m
Minimum	0,0000	-1,1146	0,1219	0,0000	0,0058	0,5236	0,2810	0,0000	-0,0682
Maximum	0,0000	-0,8798	0,1561	0,0000	0,0115	0,5531	0,3806	0,0000	-0,0567
Std Dev	0,0000	0,0477	0,0070	0,0000	0,0012	0,0050	0,0205	0,0000	0,0023
Mean	0,0000	-0,9805	0,1402	0,0000	0,0089	0,5248	0,3410	0,0000	-0,0617

Table 3-23. Max/min Values for stochastic AoA

Normal PDF: M								
	Max θ	Min θ	Max h_c	Min h_c	Max C_{dp}	Max C_l	Min C_l	Max C_m	Min C_m
Minimum	0,0000	-3,7819	0,1329	-0,275	0,0088	0,5235	-1,083	0,0000	-0,2161
Maximum	0,0000	-0,9678	0,1420	0,0000	0,0576	0,5237	0,3410	0,0000	-0,0580
Std Dev	0,0000	1,0181	0,0017	0,0954	0,0171	2,4227E-05	0,5424	0,0000	0,0582
Mean	0,0000	-1,4854	0,1391	-0,0426	0,0168	0,5236	0,0773	0,0000	-0,0898

Table 3-24. Max/min Values for stochastic M

Normal PDF:xEA

	Max θ	Min θ	Max h_c	Min h_c	Max C_{dp}	Max C_l	Min C_l	Max C_m	Min C_m
Minimum	0,0000	-2,0488	0,1123	0,0000	0,0088	0,5231	0,2253	0,0000	-0,1032
Maximum	3,5621	-0,3949	0,3128	0,0000	0,1409	1,1690	0,4268	0,2260	0,0315
Std Dev	0,3470	0,3388	0,0230	0,0000	0,0107	0,0772	0,0350	0,0221	0,0197
Mean	0,0848	-1,0077	0,1451	0,0000	0,0107	0,5537	0,3388	0,0054	-0,0589

Table 3-25. Max/min Values for stochastic xEA

Normal PDF: Zdp

	Max θ	Min θ	Max h_c	Min h_c	Max C_{dp}	Max C_l	Min C_l	Max C_m	Min C_m
Minimum	0,0000	-1,004	0,1323	0,0000	0,0088	0,5236	0,3316	0,0000	-0,0629
Maximum	0,0000	-0,9652	0,1483	0,0000	0,0088	0,5236	0,3481	0,0000	-0,0610
Std Dev	0,0000	0,0075	0,0031	0,0000	5,905E-10	0,0000	0,0032	0,0000	0,0004
Mean	0,0000	-0,9833	0,1396	0,0000	0,0088	0,5236	0,3404	0,0000	-0,0619

Table 3-26. Max/min Values for stochastic z-dp

Normal PDF: Adp

	Max θ	Min θ	Max h_c	Min h_c	Max C_{dp}	Max C_l	Min C_l	Max C_m	Min C_m
Minimum	0,0000	-0,9850	0,1387	0,0000	0,0088	0,5236	0,3368	0,0000	-0,0625
Maximum	0,0000	-0,9757	0,1404	0,0000	0,0088	0,5236	0,3435	0,0000	-0,0614
Std Dev	0,0000	0,0018	0,0004	0,0000	5,905E-10	0,0000	0,0014	0,0000	0,0002
Mean	0,0000	-0,9831	0,1396	0,0000	0,0088	0,5236	0,3406	0,0000	-0,0618

Table 3-27. Max/min Values for stochastic a-dp

Figure 3-57 to 3-62 are a comparison of the confidence interval of +/-3σ, for each of the analysed cases: namely all stochastic, stochastic angle of attack, stochastic mach number, or x-coordinate of the elastic axis, or both damping coefficients. The first bar on all plots represents the variability induced by all the stochastic parameters together, which means that all the effects are combined. Other bars represent each stochastic parameter separately.

The reader can observe the greater effect on theta from Mach number, the greater one on h_c is coming from x-coordinate of elastic axis. The C_l and C_{dp} variability is mostly affected by Mach or by x-EA in the case of maximum value. C_m is mostly affected by Mach number, but slightly combined with x-EA effect.

In Table 3-22 to Table **3-27**, maximum or minimum values of theta, h_c, and C_m have not been considered because they are close to zero. Then, they have been neglected in order to reduce the amount of information.

Anyway, C_l has non-zero values for max and min, and it is a remarkable issue that the maximum or the minimum values of the same output parameter are affected differently by several input values. This effect can only be understood considering the elasticity of the wing and its relationship with lift and drag coefficients. The vertical displacement and the angular movement produce a new configuration of the airfoil that leads to equilibrium of the forces acting on the wing. Due to the use of a solver based on Euler equations, with boundary layer effects, the minimum value of C_{dp} is zero. Only the maximum value is considered in this analysis of the results.

Figure 3-57 to 3-62 take the mean value of the stochastic results of time step equal to 100.

	Normal PDF: AoA, M, xEA, Zdp, Adp	Normal PDF: AoA	Normal PDF: M	Normal PDF:xEA	Normal PDF: Zdp	Normal PDF: Adp
Max	1,6236611	-0,837290386	1,569006362	0,008544579	-0,960752175	-0,977743412
Min	-4,6153301	-1,123723614	-4,539815362	-2,023982579	-1,005943825	-0,988549588
■Mean	-1,4958345	-0,980507	-1,4854045	-1,007719	-0,983348	-0,9831465

Figure 3-57. Theta ranges

h/c mean and range [-3s, 3s] evolution

	Normal PDF: AoA, M, xEA, Zdp, Adp	Normal PDF: AoA	Normal PDF: M	Normal PDF:xEA	Normal PDF: Zdp	Normal PDF: Adp
Max	0,198440313	0,161371163	0,144087758	0,214004979	0,148888429	0,140696623
Min	0,085149687	0,119111837	0,134104242	0,076209021	0,130236571	0,138511377
■Mean	0,141795	0,1402415	0,139096	0,145107	0,1395625	0,139604

Figure 3-58. h_c ranges

Cdp (max) mean and range [-3s, 3s] evolution

	Normal PDF: AoA, M, xEA, Zdp, Adp	Normal PDF: AoA	Normal PDF: M	Normal PDF:xEA	Normal PDF: Zdp	Normal PDF: Adp
Max	0,067973793	0,012399769	0,067996408	0,042744252	0,0088	0,0088
Min	-0,033163793	0,005468231	-0,034456408	-0,021405252	0,0088	0,0088
■Mean	0,017405	0,008934	0,01677	0,0106695	0,0088	0,0088

Figure 3-59. C_{dp} ranges

Cl (max) mean and range [-3s, 3s] evolution

	Normal PDF: AoA, M, xEA, Zdp, Adp	Normal PDF: AoA	Normal PDF: M	Normal PDF:xEA	Normal PDF: Zdp	Normal PDF: Adp
Max	0,715095754	0,5398723	0,52367668	0,785459215	0,5236	0,5236
Min	0,375233246	0,5097817	0,52353132	0,321981785	0,5236	0,5236
■ Mean	0,5451645	0,524827	0,523604	0,5537205	0,5236	0,5236

Figure 3-60. C_l (max) ranges

Cl (min) mean and range [-3s, 3s] evolution

	Normal PDF: AoA, M, xEA, Zdp, Adp	Normal PDF: AoA	Normal PDF: M	Normal PDF:xEA	Normal PDF: Zdp	Normal PDF: Adp
Max	1,77321124	0,402612292	1,704569463	0,443773864	0,349989959	0,344792683
Min	-1,66133424	0,279452708	-1,549931463	0,233889136	0,330847041	0,336359317
■ Mean	0,0559385	0,3410325	0,077319	0,3388315	0,3404185	0,340576

Figure 3-61. C_l (min) ranges

Cm mean and range [-3s, 3s] evolution

	Normal PDF: AoA, M, xEA, Zdp, Adp	Normal PDF: AoA	Normal PDF: M	Normal PDF:xEA	Normal PDF: Zdp	Normal PDF: Adp
Max	0,08670048	-0,054763979	0,084745152	0,000117164	-0,060766698	-0,061151473
Min	-0,25740648	-0,068708021	-0,264271152	-0,117975164	-0,063022302	-0,062580527
■Mean	-0,085353	-0,061736	-0,089763	-0,058929	-0,0618945	-0,061866

Figure 3-62. C_m ranges

Above comments can be confirmed checking the Figure 3-63 to 3-90. They represent the complete evolution of output parameters versus time, when stochastic parameters are introduced as input values. All same cases are considered as commented; all input parameters as stochastic ones (figures from 3-63 to 3-67), only angle of attack (from Figure 3-68 to 3-72), only Mach number (from Figure 3-73 to 3-77), x-EA (from Figure 3-78 to 3-82), z-dp (from Figure 3-83 to 3-86) and a-dp (from Figure 3-87 to 3-90).

Tetha evolution - All Parameters
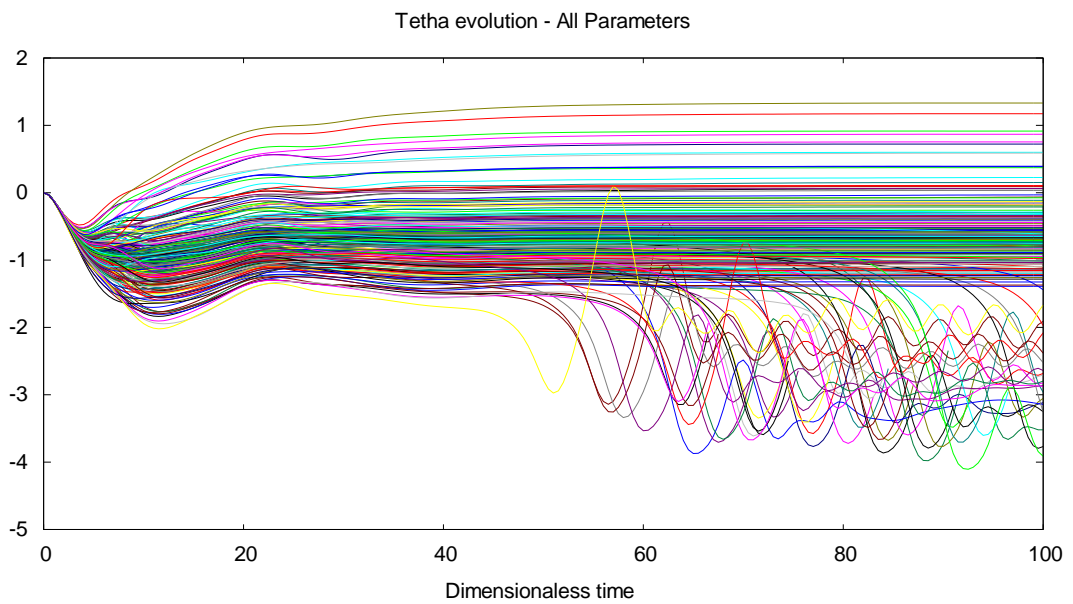
Figure 3-63. Theta evolution (all stochastic parameters)

h/c evolution - All Parameters
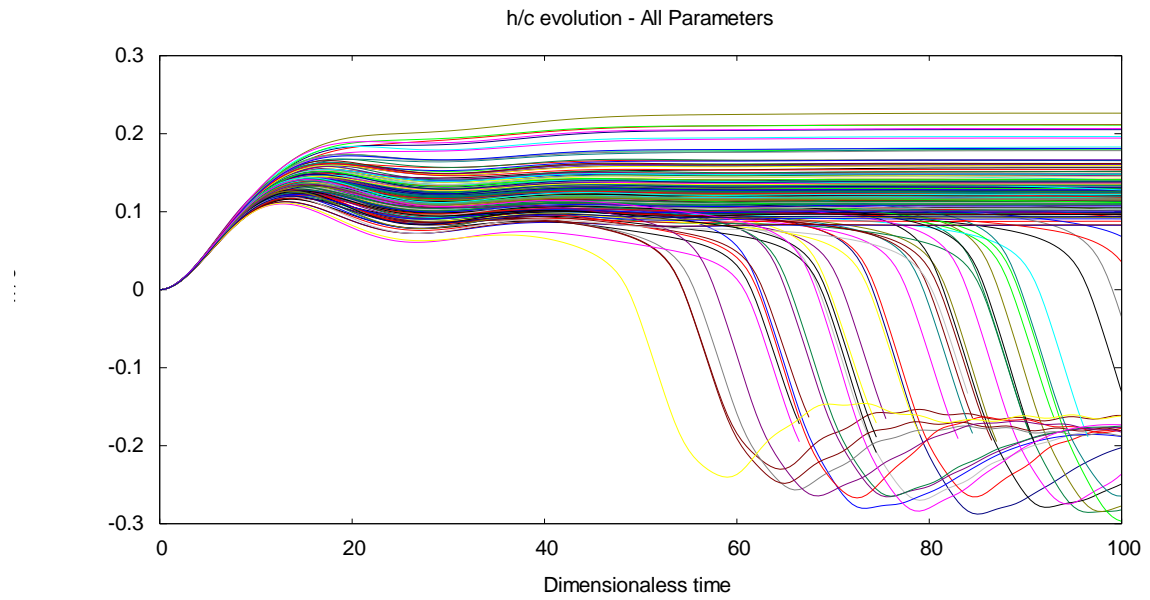
Figure 3-64. h_c evolution (all stochastic parameters)

Cdp evolution - Variation of the all parameters
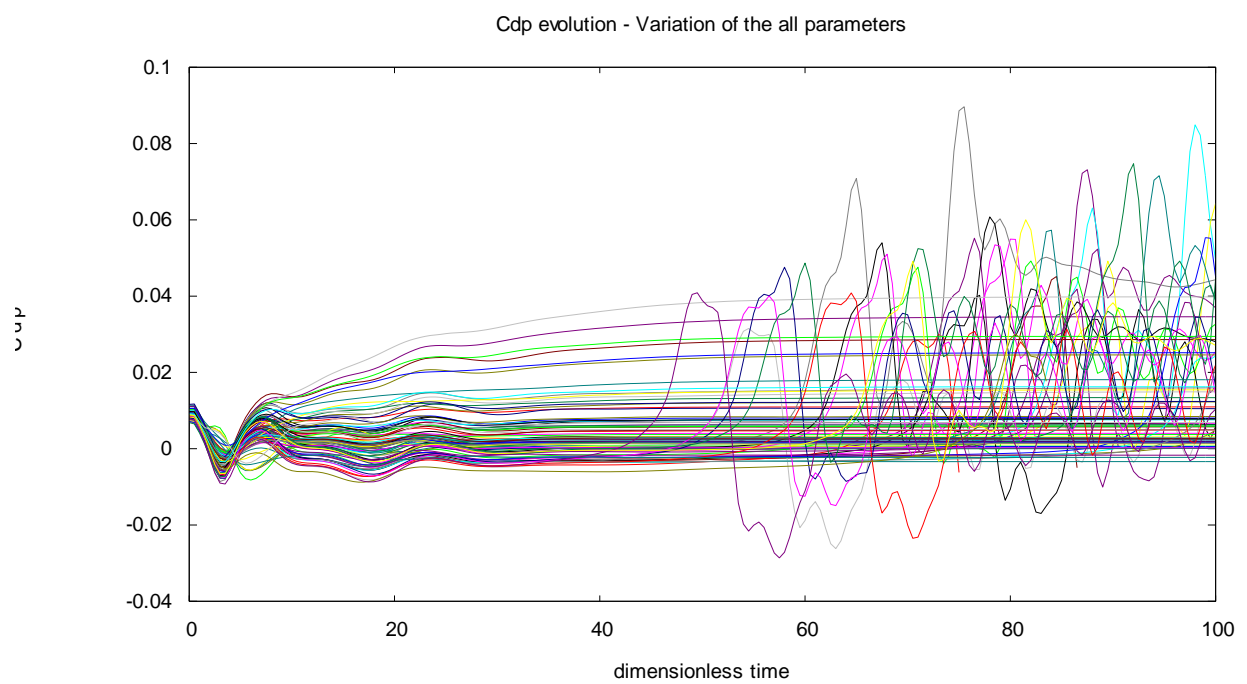
Figure 3-65. C_{dp} evolution (all stochastic parameters)

Cl evolution - All Parameters
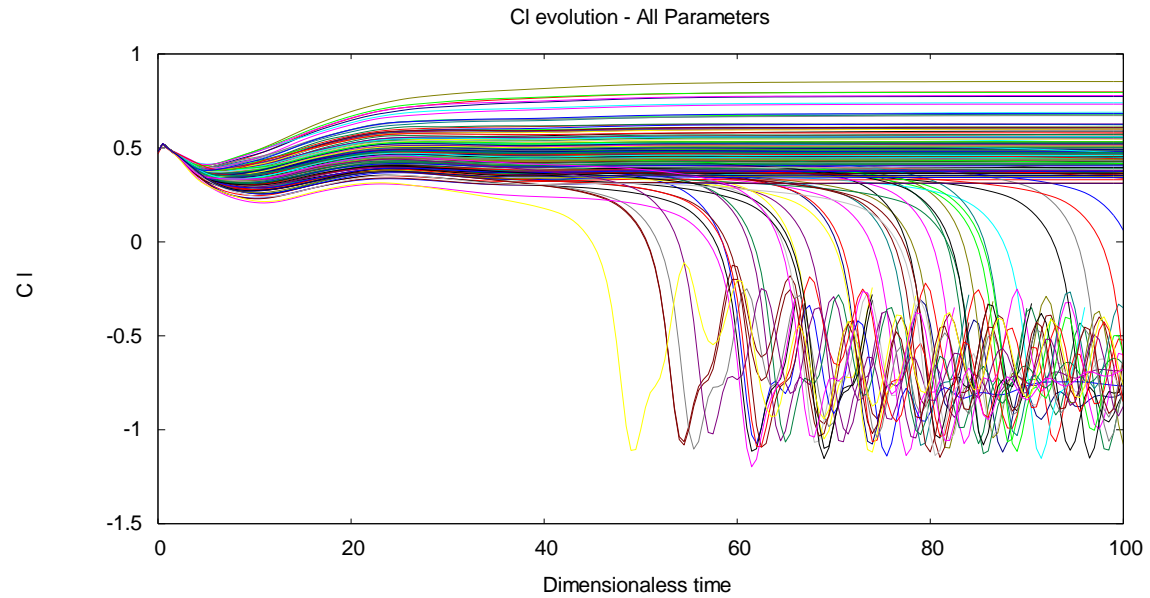
Figure 3-66. C_l evolution (all stochastic parameters)

Cm evolution - All Parameters
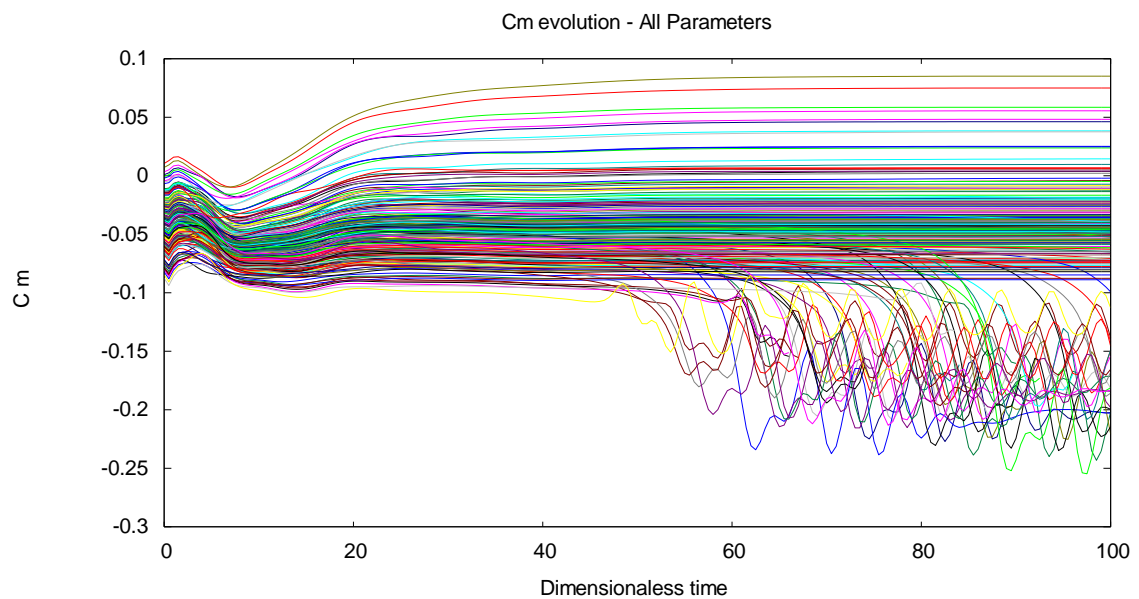
Figure 3-67. C_m evolution (all stochastic parameters)

Applying all stochastic parameters at once, several cases lead to a non-convergence of the results. Most of the results show a "parallel" and converged behaviour, and all plots are similar. The non-convergence effect is produced by one of the stochastic parameters, which defines values that produce aero-elastic instability of the profile. This parameter can be detected analysing the individual effects. In order to calculate the mean and the standard deviation all values have been taken into account.
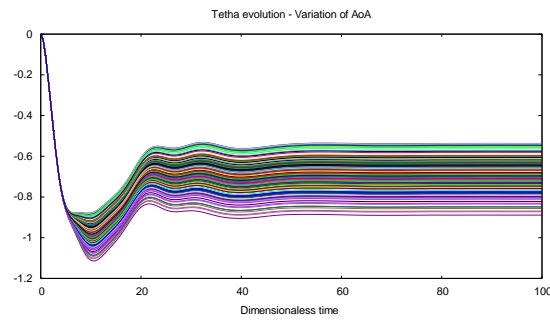
Figure 3-68. Theta evolution (stochastic parameter: AoA)
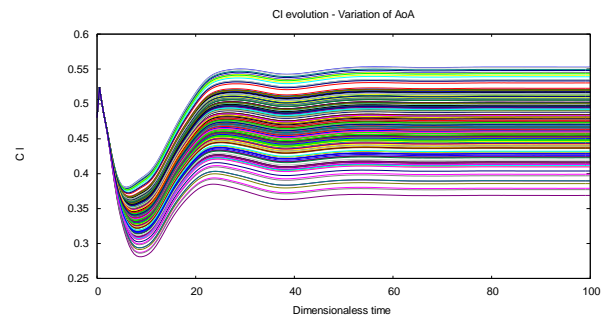
Figure 3-71. C_l evolution (stochastic parameter: AoA)
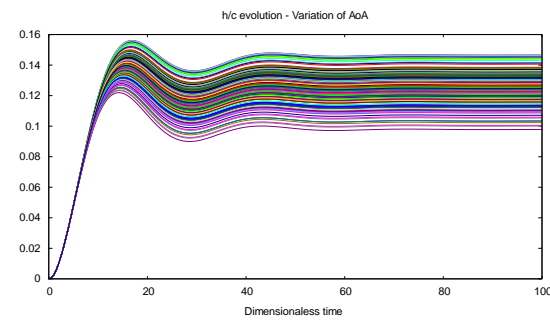
Figure 3-69. h_c evolution (stochastic parameter: AoA)
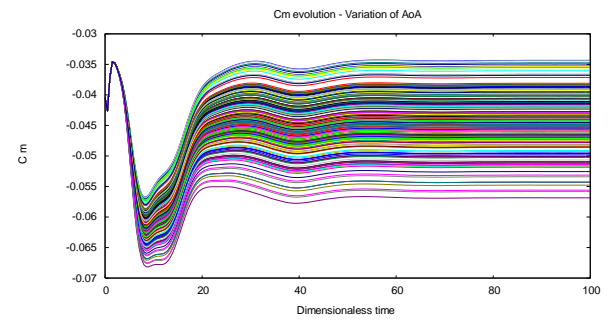
Figure 3-72. C_m evolution (stochastic parameter: AoA)
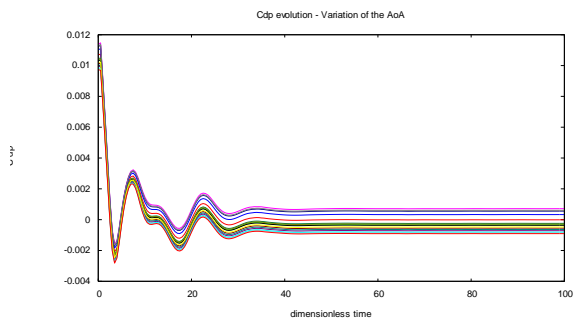
Figure 3-70. C_{dp} evolution (stochastic parameter: AoA)

Analysing the results for the case where only Angle of attack is defined as stochastic value, the reader can observe how all the results converge. After a first step of oscillation, all the output parameters stabilize. Then it is easy to understand that the angle of attack is not the one producing the flutter detected in the previous plots.

Briefly, if only one parameter is defined as stochastic, the convergence can be assured except for the Mach number case. It is clear, then, that the parameter which introduces the non-convergence effect is the Mach number. All other parameters reach convergence on all output values.
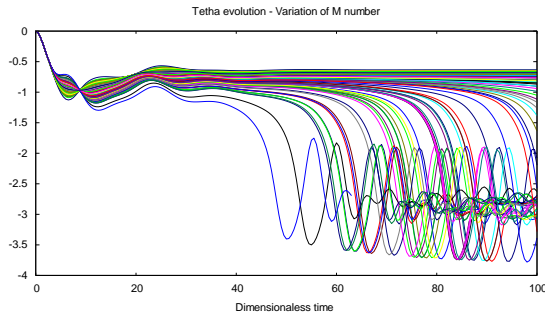
Figure 3-73. Theta evolution (Mach stochastic)
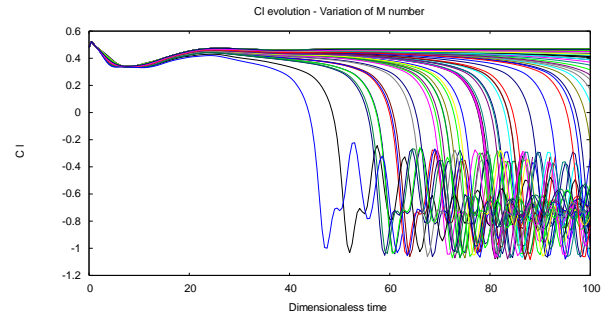
Figure 3-76. C_l evolution (Mach stochastic)
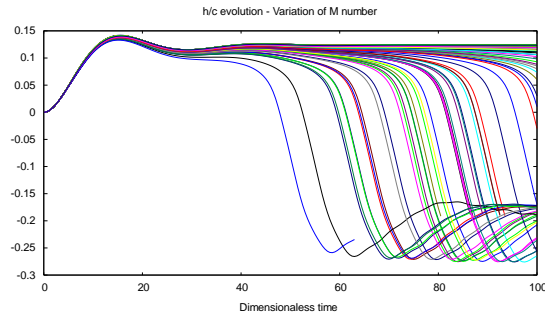
Figure 3-74. h_c evolution (Mach stochastic)
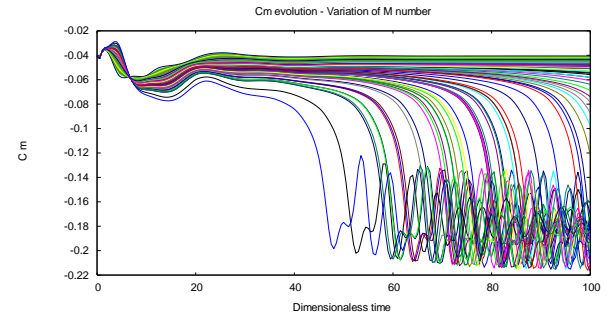
Figure 3-77. C_m evolution (Mach stochastic)
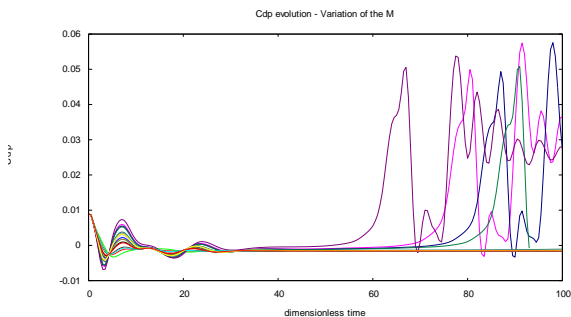
Figure 3-75. C_{dp} evolution (Mach stochastic)

The stochastic definition of the X-coordinate of the elastic axis also leads to converged results. It can be observed that the distribution of the plots is not as regular as in the angle of attack case. It means that some of the axis location produces larger effects on the final values of the output parameters. It is directly related to the centre of gravity location, which, combined with the elastic axis location, can affect the airfoil stability. It will lead to larger stability of theta, θ (spin rotation) and h_c (vertical movement) of the airfoil, which are directly related to C_l, and C_m values.
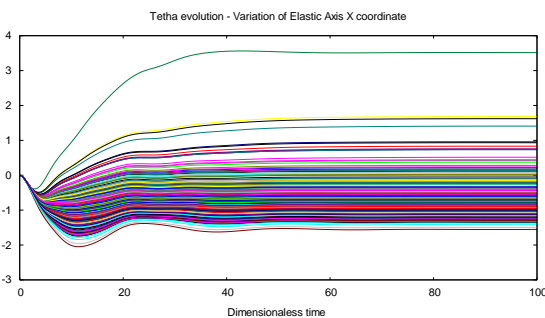
Figure 3-78. Theta evolution with stochastic x-EA
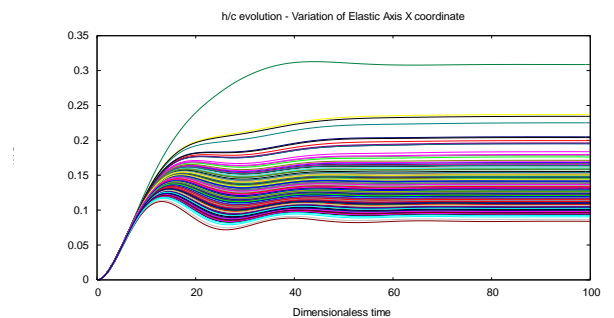
Figure 3-79. h_c evolution with stochastic x-EA
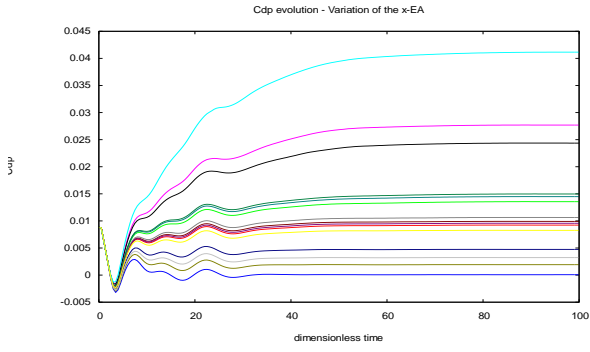
Figure 3-80. C_{dp} evolution with stochastic x-EA
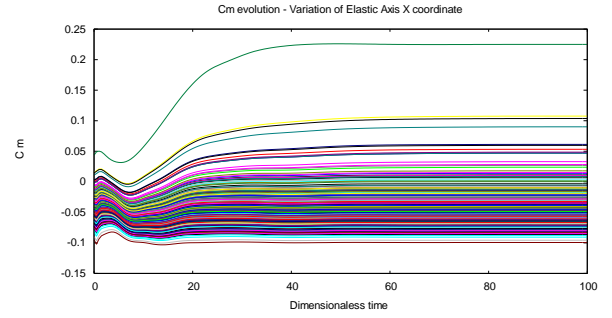
Figure 3-82. C_m evolution with stochastic x-EA
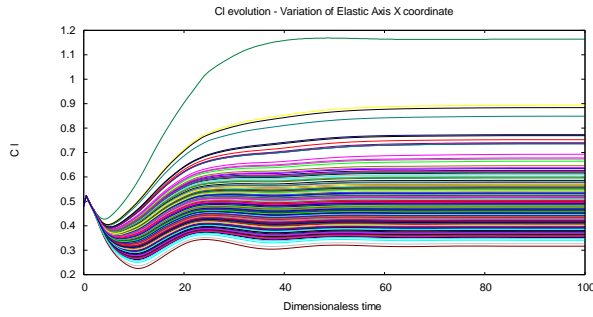
Figure 3-81. C_l evolution with stochastic x-EA
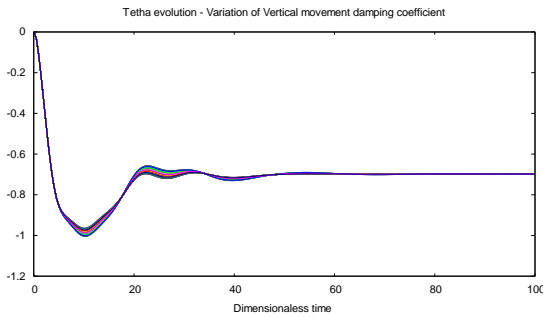
Figure 3-83. Theta evolution with z-dp as stochastic variable
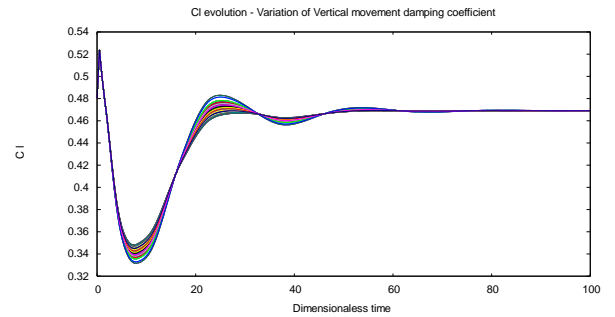
Figure 3-85. C_l evolution with z-dp as stochastic variable
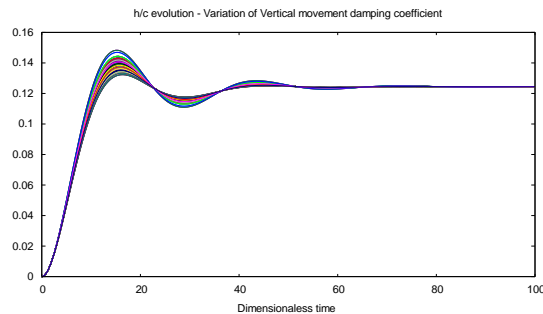
Figure 3-84. h_c evolution with z-dp as stochastic variable
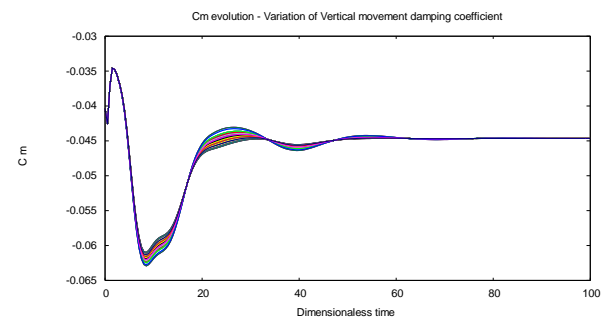
Figure 3-86. C_m evolution with z-dp as stochastic variable

The confidence interval plots suggest that vertical and angular damping have a slight effect on all output parameters, at least on the defined range of study. Figures from 3-87 to 3-90 can confirm this guess. The variation between evolution plots is within a narrow range compared with other plots.

It can be suggested that damping coefficients are not interesting parameters in a variability or uncertainty analysis, due to their small effect on the selected outputs.
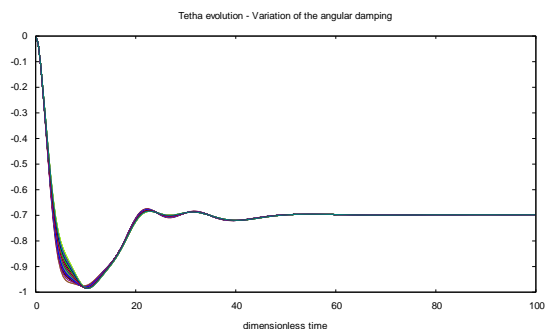
Figure 3-87. Theta evolution with a-dp as stochastic variable
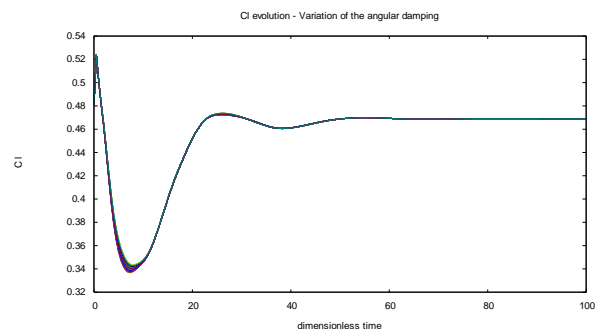
Figure 3-89. C_l evolution with a-dp as stochastic variable
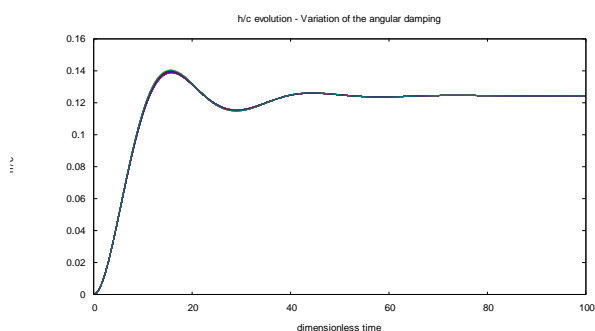
Figure 3-88. h_c evolution with a-dp as stochastic variable
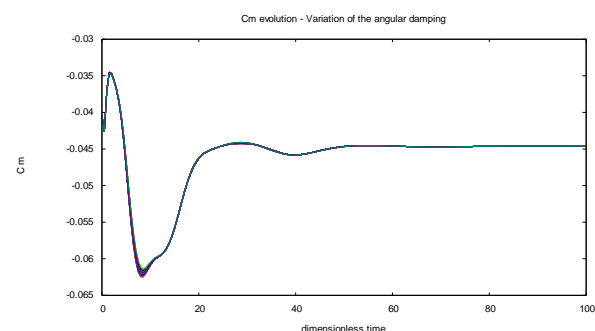
Figure 3-90. C_m evolution with a-dp as stochastic variable

3.6.4.2.1 Uncertainty effects

Figure 3-91 to 3-99 are the representation of the most significant output parameters against the input parameter with uncertainty. The maximum and the minimum values of the time evolution of the outputs have been used to enable a clear identification of the correlation between input and output variables. Physical phenomena can be detected analysing the following plots.

These plots provide additional information to understand the particular behaviour of each output parameter related to the uncertainty input. This is the case of the uncertainty on the Mach number. The values where shock waves begin to appear and produce the shown instability can be clearly identified. Plot of theta angle, θ, or C_l, or C_m versus Mach can easily help to identify the point where shock wave appears; Figure 3-96, 3-98, and 3-99 show a clear discontinuity. Figure 3-91, 3-92, 3-94 and 3-95, like theta or h_c versus angle of attack show a linear relationship between them.

In order to take into account all the time evolution of the parameters, minimum and maximum values have been plotted. The use of a mean value at a certain time step has been considered as being no representative of the time oscillation.
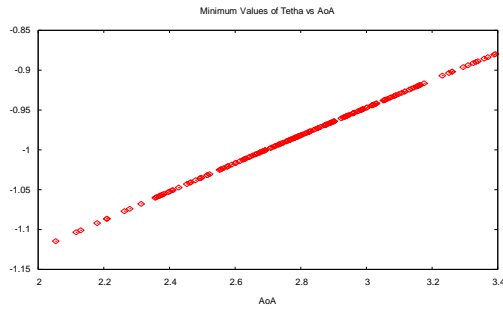
Figure 3-91. Mins of Theta vs AoA
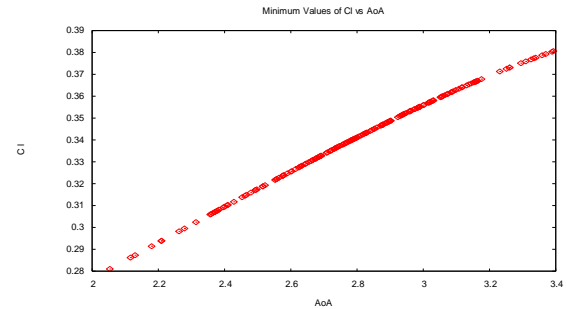
Figure 3-94. Mins of C_l vs AoA
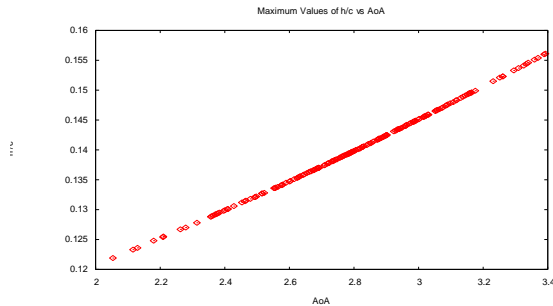
Figure 3-92. Maxs of h_c vs AoA
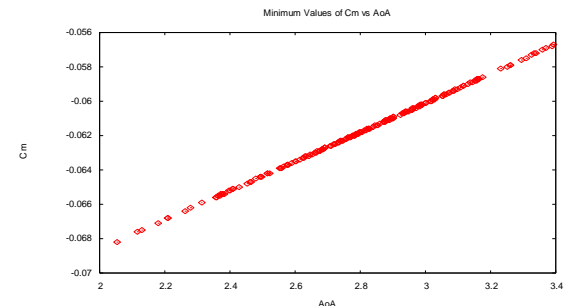
Figure 3-95. Mins of C_m vs AoA
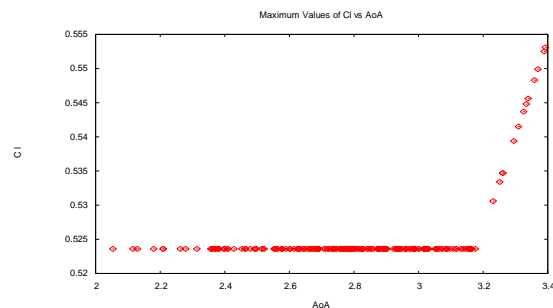
Figure 3-93. Maxs of C_l vs AoA

Figure 3-91 to 3-94 show the relationship between several output values when angle of attack is stochastically defined. The range of values is too small and values are low, so the result is mainly a straight line. But Figure 3-93, where maximum values of lift coefficient are plotted versus angle, shows a completely different behaviour. Maximum values, reached during profile oscillation, remain constant until a point around 3.2º. From this point, lift starts to increase. This effect is due to the combination of two factors; namely the value of Mach number, and the high value of angle. Both induce flow separation.

Analysing the results which are related to Mach number, it can be easily observed how different behaviours are produced. For theta, lift and momentum it is quite similar; when shock waves appear the value falls down abruptly. Of course, pressure drag shows the opposite behaviour, increasingly with shock waves. The maximum oscillation value decreases with the increment of Mach number, which is an expected result.
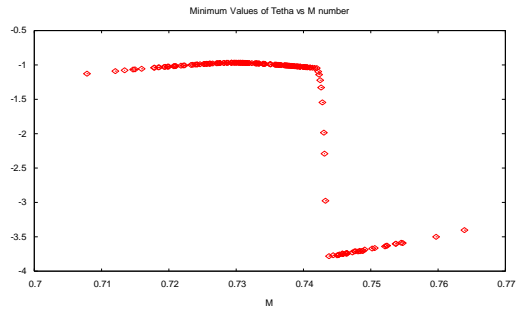
Figure 3-96. Mins of Theta vs M
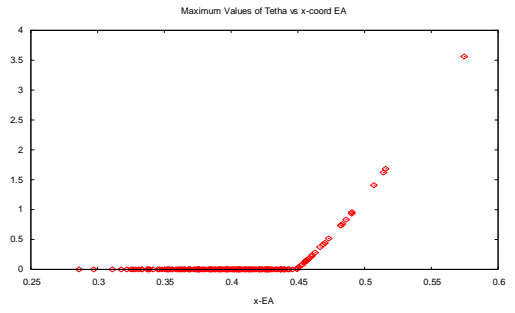
Figure 3-100. Maxs of theta vs x-EA
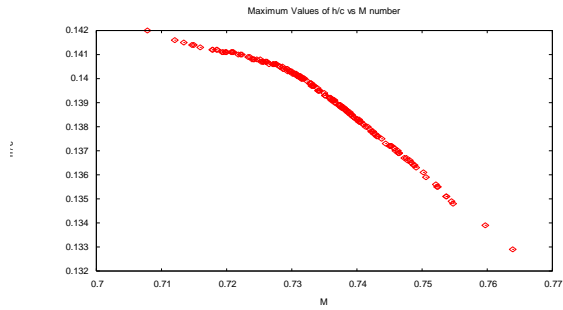
Figure 3-97. Maxs of h_c vs M
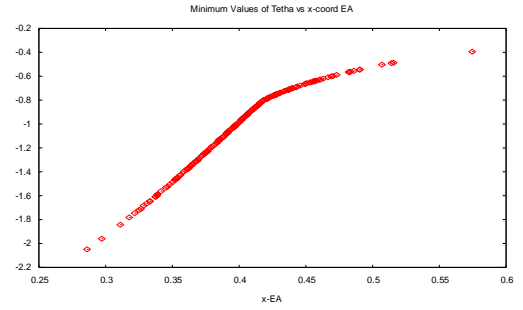
Figure 3-101. Mins of Theta vs x-EA
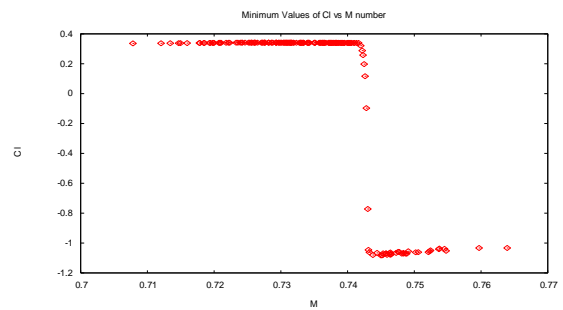
Figure 3-98. Mins of C_l vs M
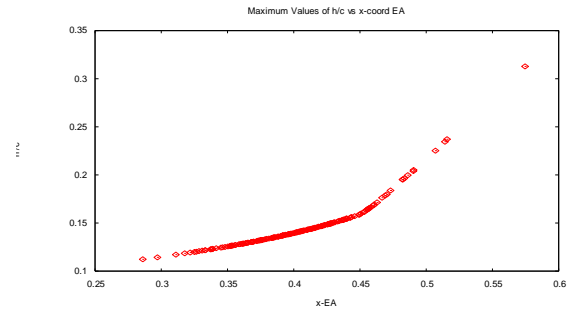
Figure 3-102. Mins of h_c vs x-EA
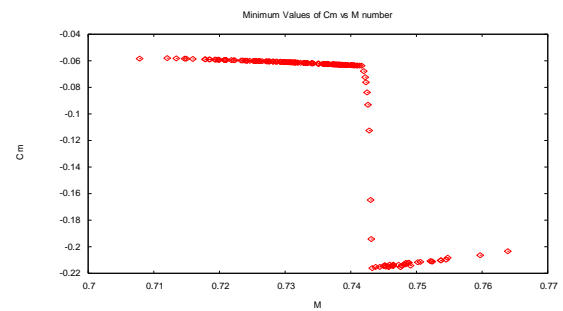
Figure 3-99. Mins of C_m vs M
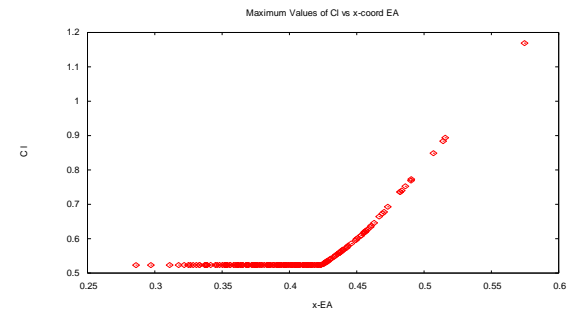
Figure 3-103. Maxs of C_l vs x-EA
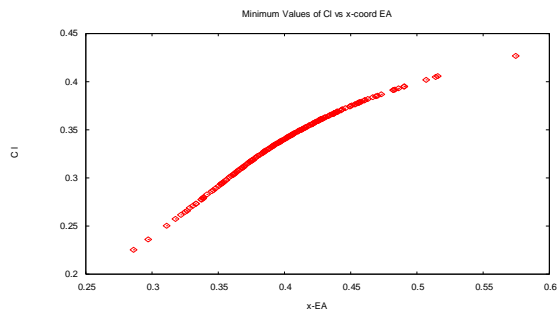
Figure 3-104. Mins of C_l vs x-EA
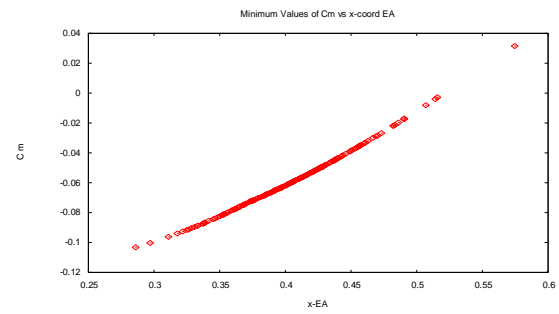
Figure 3-106. Mins of C_m vs x-EA
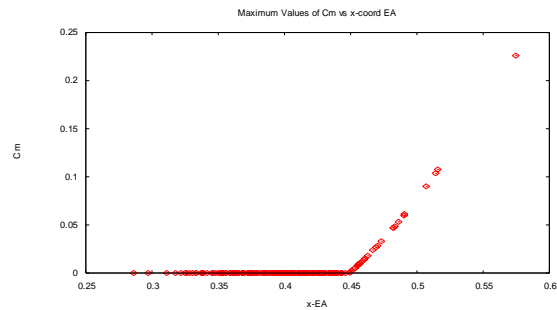
Figure 3-105. Maxs of C_m vs x-EA

The most relevant effect of the position of X-coordinate of elastic axis is on lift and momentum. Both of them gradually increase when axis moves to backward positions. Up to a values of 46% of the chord, elastic axis position produce null or slight effects to other variables.

3.6.5 Conclusions for the aero-elastic test case

Another step has been done in the stochastic procedure definition. An aero-elastic analysis tool has been used successfully, enabling the control of fluid and structural parameters at the same time. As expected from the previous CFD stochastic analysis, the method enables the generation of stochastic values for any kind of variables.

The aero-elastic analysis tool is a more expensive solver, compared with single CFD tool due to the coupling of the two involved disciplines. It is of major importance to enable a good efficiency when dealing with this kind of problems in order to reduce the computational cost. The use of surrogate models can be one of the solutions; once trained they will provide faster outputs for the candidate evaluations. Parallelization of the solver, but also of STAC is also a solution. STAC already includes parallelization capabilities. It requires running on a computer network. Further steps to be done are to be able to use GPU or multi-core computers for parallelization.

Regarding the parallelization issue, it is important that parallelized solver matchs the requirements of the parallelized STAC. If not execution problems can arise, and it could unable to take advantage of these capabilities.

3.7 General Conclusions on stochastic analysis

Stochastic analyses have provided the tools for the study of the output variability for the RAE2822 test case, as well as the aero-elastic problem dealing with flutter effects. Two analyses have been performed regarding flow parameters (angle of attack and Mach number), one has dealt with mesh sizes, and one with the aero-elastic parameters.

Regarding the results on the mesh variability, the obtained results follow the expected trends. The most affecting size is that applied to profile lines. And the most affecting flow parameter has been the Mach number in both the analysis of the 2D profile, and in the aero-elastic analysis.

The application of uncertainty definition to the input variables is transfered to the behaviour of the output values. Applying a normal distribution to input values the results also show a Gaussian behaviour. Then, to accurately perform the analysis it is important to know about the best stochastic representation of the input variables in its working environment.

The convenience of performing stochastic analysis in front of just the deterministic one has been demonstrated by the better understanding of the global phenomena, without missing the focal point on the nominal values. Both CFD and FSI test cases has demonstrated that the deterministic analysis is not able to identify neither the shock wave effects nor the flutter phenomena, while the stochastic analysis clearly identify those effects.

The stochastic procedure has been performed well with all the complexity levels shown in the cases analysed. In all the analysed cases, the use of the coefficient of variation is demonstrated as mandatory to be able to compare the results. A clear example is the analysis of the 2D profile; their analyses produce lift and drag coefficient values as results, mean and standard deviation values have been then calculated, but both values are not comparable. Lift values are at least one order of magnitude larger than drag values. The simplest way to compare the obtained Gaussian distributions is to normalize standard deviation values through the use of the coefficient of variation.

This research has been devoted to two main goals; namely to study the variability induced by the samples, and to study and compare in detail two sampling techniques: Monte Carlo and Latin Hypercube. Considering that samples are generated using the same probability density function, these two goals have been translated into expected conclusions. They should help to clarify how large the effect of the intrinsic variability of the set of samples is. In addition, the level of improvement when using Latin Hypercube sampling, compared with Monte Carlo samples, should be shown. It has been expected that Latin Hypercube sampling would help to increase the convergence of the samples to their real values. A greater convergence rate will help to reduce the amount of samples.

Considering these two goals, and after analyzing the presented results it can be concluded that:
- Latin Hypercube Sampling provides a better representation of the sampled space when the amount of samples is low.
- The best representation of the sampled space when using Latin Hypercube Sampling technique is transferred to output values affecting the standard deviation values.
- This effect will greatly depend on the correlation between input and output values; if it is linear, quadratic or if there are additional parameters that introduce variability.
- In conclusion, it points out the fact that Latin Hypercube Sampling technique will provide a slight improvement compared to Monte Carlo method, due to the dependency on input

output correlation. But it hardly improve the computational cost with a significant reduction of the stochastic samples evaluated. In this sense, Monte Carlo and Latin Hypercube techniques are equivalent.

Finally, Monte Carlo method, Latin Hypercube sampling and Probabilistic collocation method have been compared. A significant influence of the solver has been identified on the final numerical results, in particular its accuracy. Its accuracy, when dealing with uncertainty quantification, is of great importance. But neglecting this effect, it can be concluded that:
- Monte Carlo and Latin Hypercube manage the uncertainty as samples, so variability is better evaluated due to the different set of samples selected for each analysis.
- Probabilistic collocation fixes the evaluated points, so it could be considered as a multi-point evaluation of the function.
- The calculated collocation points and weights remain constant while the probability definition remains the same.
- Probabilistic collocation method can use fewer evaluation points, but this amount of points strongly depends on the number of uncertainties to deal with.
- All three methods have similar error compared to the deterministic case.
- No significant differences in the results are detected using one of these three methods.

As a brief summary of the comparison between Monte Carlo methods and Probabilistic Collocation method, Table 3-28 describes the main issues.

	Monte-Carlo Stochastics	Probability Collocation Method
Uncertainty propagation	Yes	Yes
Full statistics	Yes	No
Computational cost	High	Depending on the # of variables
Multi-point method	No	Yes
Robustness by sampling	Yes	No
Enables use of surrogates	Yes	Yes

Table 3-28 Comparison between Monte Carlo methods and Probabilistic Collocation

The variability effect on an aero-elastic problem has also been analysed. The selected input parameters include not only flow field parameters, but also structural ones. Output parameters also include structural outputs and forces on the wing.

After this analysis some conclusions can be taken:
- Some of the selected parameters have no significance on the study; although it was not an easy conclusion in advance.
- The vertical and the angular coefficients have the smaller effect on the output values.
- Mach number is one of the most relevant parameters to analyse. Its variability introduces greater variability on the output values, and in addition it can lead to a non-convergence result.
- Structural parameters like damping ratios hardly affect lift and drag coefficients.

The aero-elastic study is a clear confirmation that the use of the coefficients of variation is a powerful tool to compare statistical behaviour of the data. They enable to compare results of different order of magnitude, as in the aero-elastic case.

A summary of the test cases in this chapter is provided in the following Table 3-29.

Stochastic Procedure								
Name	**Variables**	**Objectives**	**Uncertainty Quant. Techniques (UQ)**			**Flow Regime**		**Chapter**
			MC	**LHS**	**PCM**	**Subsonic**	**Transonic**	
Mesh variability	Mesh sizes	Analyse sensibility to mesh sizes	Yes	No	No	no	Yes	3.4
Flow conditions	Initial conditions of flow	Analyse sensibility to flow conditions	Yes	No	No	Yes	Yes	3.5
Flow past a 2D profile	Flow and boundary conditions	Analyse sensibility to flow conditions. Compare UQ tech.	Yes	Yes	Yes	Yes	Yes	3.5
Aeroelasticity analysis	Structural parameters	Apply procedure to aeroelasticity problem. Analyse sensibility to structural parameters	Yes	No	No	No	Yes	3.6

Table 3-29. Summary of analysed cases

The next step leads to the use of this information to perform stochastic optimization where the stochastic variables are defined with Latin Hypercube Sampling or Monte Carlo method. In order to decrease the computational time the number of samples defining the stochastic variables has to be reduced. Both Monte Carlo and Latin Hypercube Sampling perfectly describe the population if the number of samples is not dramatically reduced.

3.8 Summary

Chapter 3 describes a compilation of test cases dealing with stochastic analysis. A comparison between Monte-Carlo and Latin Hypercube sampling techniques is also provided. The main aim of this chapter is to establish the best basis for a further robust design optimization, which can take advantage of a good understanding of stochastic methods.

As described in the previous sub-chapter, and summarized in table 3-24, the selected test cases have been those dealing with mesh variability, flow around wing, and an aero-elastic analysis. The used techniques have been Monte-Carlo, and Latin Hypercube sampling, as well as Probabilistic Collocation method.

Probabilistic Collocation method is a new development which combines probabilistic definition with collocation strategies, and it helps to establish a comparison point to evaluate the pros and cons of the pure probabilistic methods, as Monte-Carlo and Latin Hypercube.

Regarding the application of the stochastic procedure to perform uncertainty analysis, it is already remarked that:

- It can deal with any kind of variables and problems.
- The definition of the PDF should be according the real behaviour of the parameter in its working environment.
- The use of the coefficients of variation is useful to better compare and understand the variability of the results.
- Latin Hypercube and Monte Carlo are offering the same efficiency on variability analysis. Latin Hypercube better represents the stochastic behaviour of the variables but is not able to significantly reduce the amount of samples to evaluate.
- Probabilistic collocation method is a useful tool to easily evaluate uncertainty quantification, but it is not dealing with random and probabilistic values to evaluate the stochastic results.

The computational cost of a stochastic analysis is higher than the cost of a deterministic analysis. As a first approximation if the deterministic case takes some time, the stochastic analysis could take this amount multiplied by the number of stochastic samples. Usually it takes even more time.

Table 3-30 shows a comparison of the approximate calculation cost for each problem, defining the computational resources used, as well.

Case	Computer	Deterministic	Stochastic (250 shots)
Mesh variability	Pentium IV @ 1GHz RAM 512Mb	30min	150h
Flow conditions	Intel Core 2 Quad CPU Q9300 @ 2,5GHz RAM 3,48Gb	3min	15h
Flow past a 2D profile	Intel Xeon 16 CPU @ 3,2GHz RAM 15,2Gb	2min	8h
Aeroelasticity analysis	Intel Xeon 16 CPU @ 3,2GHz RAM 15,2Gb	15min	96h

Table 3-30. Approximate calculation cost

4 Stochastic Robust optimization

4.1 Introduction

In this research, the methods dealing with uncertainties are named non-deterministic methods. Deterministic methods are those which, in opposition with the previous definition, do not consider variability of the input parameters. However, some existing deterministic methods are described as non-deterministic due to their random definition of the initial populations, or the random or pseudo-random generation of new members and generations.

The main aim of this research study is to deal with uncertain parameters within the optimization processes. A new definition is also introduced within the non-deterministic methodologies, namely the stochastic and robust procedures. Both of them take into account the uncertainties on the input parameters, but robust procedures also take into account the variability on the output values through the use of the variance or standard deviation values.

In many cases, the deterministic methods are the starting point for the development of non-deterministic methods, and it is important to know about their characteristics, configurations and procedures.

The main objective of this research is to evaluate the capabilities of stochastic and robust optimization procedures. These new procedures have been defined to be integrated in, not only evolutionary algorithms, but also in other optimization methods. This research has been mainly based on evolutionary algorithms and, specifically, on genetic algorithms, which have been analysed on Appendix I: Numerical Methods and Tools.

Regarding the required tools to be used, they are introduced in Appendix I. The reader is referred to the descriptions on the Appendix I to know more details about STAC, the stochastic management tool, which enables the generation of random values according with a prescribed probability density function.

In a first step, a deterministic evolutionary algorithm optimization method is analysed in order to move a step forward to a non-deterministic method. Additional tests devoted to the validation of the evolutionary algorithm can be found in Appendix I.

This section also focuses its attention on stochastic related methodologies applied to the optimization procedure. The use of an analysis tool, or a surrogate model, is maybe one of the most important points to take into account. The definition of random values using Monte Carlo or Latin Hypercube techniques, and their comparison, in a similar way that has been done in Chapter 3, is also considered to validate the selection of a sampling technique. Another interesting point is the use of a fixed set of values or a random set to be applied to each population or individual. A comparison has been established in order to better understand the effect of applying the same samples along the whole analysis or update them with the evaluation of each population or the evaluation of each individual.

Taking advantage of the procedure developed in the previous chapter, the focus of chapter 4 is on the evaluation of the feasibility of its application to a robust design optimization procedure. Using a stochastic definition of the input variables, the objective functions will be stochastically evaluated. Output variables are no longer defined by a single point, but they are defined by their probability density function (PDF), namely mean and standard deviation, or the statistic moments to define the appropriate PDF.

The chapter scheme is as follows: there are two main sections describing the deterministic and stochastic solutions, respectively, of several types of optimization problems. Each main section describes the specific procedures of each problem.

The Chapter 4 presents several test cases. Two main descriptions of each test case is analysed; the first one is the deterministic analysis, which is used as a reference. The second one is the stochastic and robust analyses, which are the core of the chapter and which consider the uncertainty as part of the variable definition and results analysis.

4.2 Methodology

To better understand how the different methods are applied, the following flowcharts not only highlight the main differences but also the similarities among the three of them.

Figure 4-1 shows the flowchart of a deterministic optimization based on evolutionary algorithms. An initial population is randomly generated and evaluated to obtain the initial fitness function values. The evaluation can be done using a solver, but it could also be done by using a surrogate model, which provides a faster evaluation and reduces the computational cost of the whole process. The stop criterion is checked; it can be a stop criteria based on the fitness function, or depending on the number of evaluations or the computational time, or a combination of all of them. If the criterion is fulfilled the optimal population is reached, if not the actual population members are selected, mutated, and combined to get new offspring which define the next generation. The iterative process is done until the criterion is fulfilled.

The basic scheme of a stochastic or a robust optimization is pretty similar to the one from a deterministic case. The main difference is the stochastic evaluation of the individuals of each population, which leads to an increment of the total amount of evaluations, and directly increase the total computational cost.
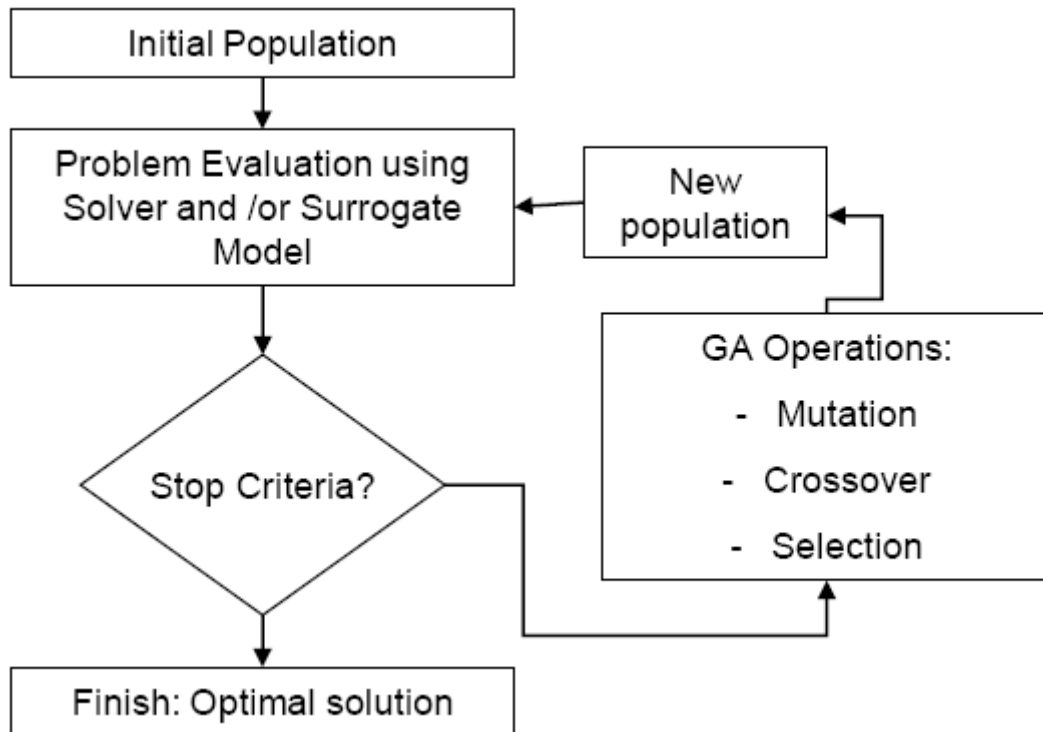
Figure 4-1. Flowchart of a deterministic optimization

As it is shown in Figure 4-2 the flowchart is defining similar steps for both types of processes; the deterministic and the stochastic. An initial population is randomly generated. Its evaluation starts an iterative process that checks if the stop criterion is fulfilled. If it is not fulfilled, new offspring are generated to create a new population and the loop starts again. This is the same as in the deterministic case, but in the stochastic and robust cases it is also necessary to generate the stochastic values for some of the parameters. These parameters are not the control variables but they are directly related to the problem. Applying the stochastic set of values, several evaluations are required and a cloud of results are obtained. To deal with this amount of information, the fitness function will be defined as the mean and/or the standard deviation of the individual evaluations. After the evaluations, a statistical calculation is required in order to obtain the statistical moments. The stochastic procedure calculates the mean value, and the robust procedure calculates the mean and the standard deviation values.

Due to the fact that the computational cost tends to quickly increase with the number of evaluations, the use of a surrogate model can be mandatory.

From the point of view of the evolutionary algorithm nothing has changed. The evolution strategy is applied as it was done in the deterministic case. The individuals are generated in the same way. It only needs to deal with a set of conditions while only one condition was analysed in the deterministic case.
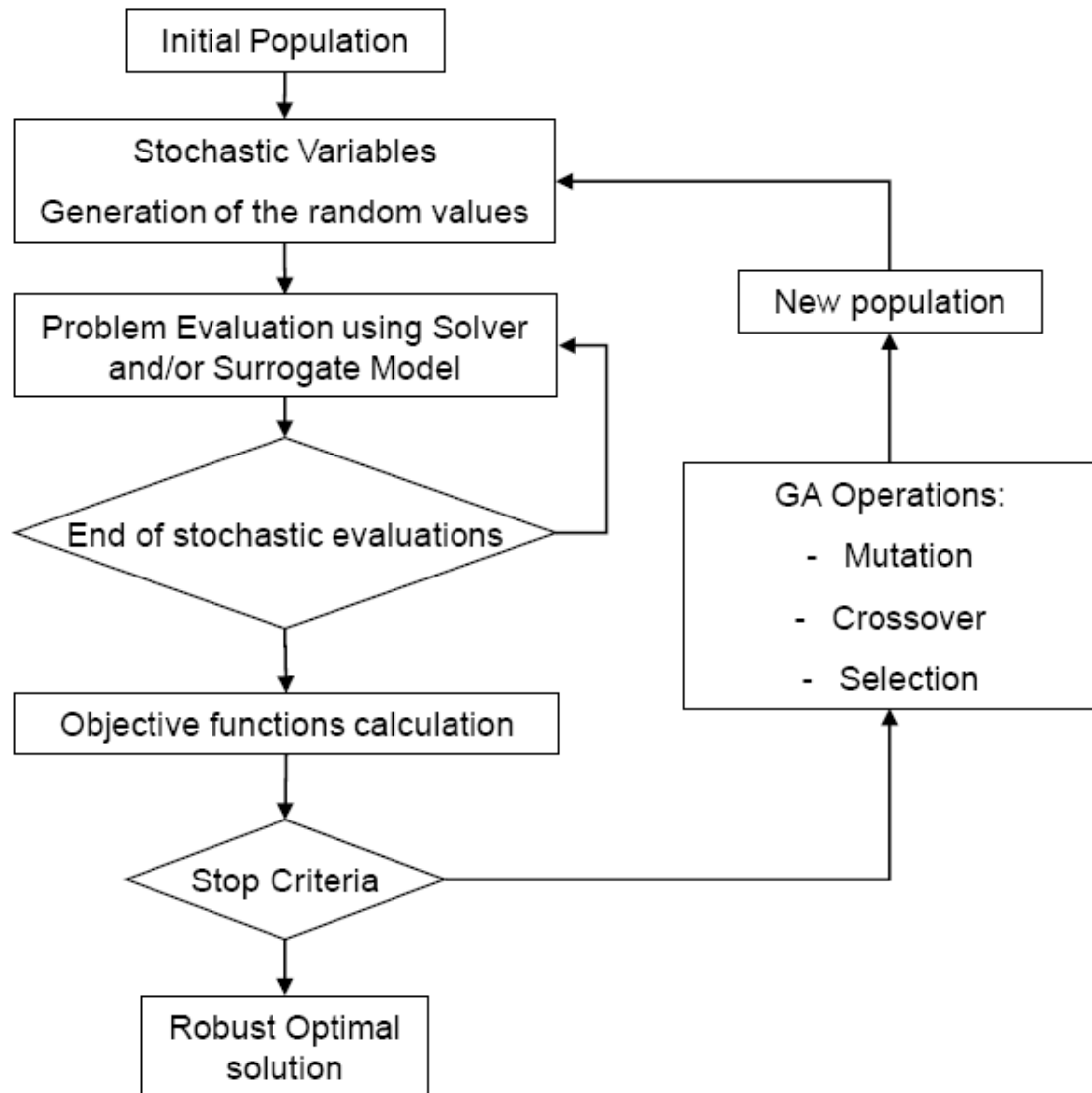
Figure 4-2. Flowchart of a stochastic/robust optimization

4.3 Mathematical test cases

4.3.1 Introduction

In this section, some mathematical test cases have been analysed. They have been defined to test the optimizer when facing constrained problems, and they are considered as validation tests for the optimization algorithms.

The mathematical test cases have been analysed to validate the proposed approach, which includes the stochastic data management. The obtained results will define a comparison between the deterministic and the stochastic one.

The CTP7 and the OSY mathematical test cases (Chafekar et al, 2003, Deb et al, 2000, Deb and Goel, 2000) have been selected among those defined by Prof. Deb. Both test cases have been taken and have been modified to add a stochastic component. Several definitions of the stochastic component are tried out and the results are compared with

those obtained for the deterministic analyses. CTP7 presents a constrain near the optimal Pareto front, and OSY a set of six constrains, four of them being linear.

The differences between the selected deterministic version of the test cases and their stochastic robust definitions ensure a wide study of the effects coming from uncertainty; namely how the problem changes (definition of the fitness function), but also how the results change regarding the Pareto Front shape. The aim of this section is to provide a validation point of the stochastic and robust procedures. First of all, the deterministic solution is obtained and compared with the literature references. Next, the stochastic definition is applied and the results are compared with the deterministic ones.

4.3.1.1 Mathematical Test Cases: CTP7 and OSY

The NSGA-II (Deb et al, 2000; 2002; 2003) algorithm has been selected as the optimizer for the deterministic case. NSGA-II is a multi-use optimizer based on evolutionary techniques, which is able to deal with any kind of problems, as it has been demonstrated through the multiple applications that have been developed (Deb, 2005; Deb et al, 2000; Hiroyasu et al, 2005). The algorithm has been extended by applying uncertainty management strategies.

4.3.1.2 CTP7 Test Case; Deterministic definition

First, a deterministic (or classical) version of the CTP7 test case has been solved. Te corresponding results will be compared with those obtained with the stochastic version of the same test case.

The following parameters have been used to set-up the NSGA-II optimizer in all the CPT7 test cases:
  - Crossover probability: 0,9
  - Mutation probability: 0,16667
  - Maximum amount of populations: 1000
  - Population size: 200

CPT7 is a constrained problem that presents discontinuities in the solution. Dealing with these discontinuities is the main challenge to solve the problem.CTP7 problem is described as (Deb et al, 2000):

Minimize		
$$f_1(x) = x_1$$ $$f_2(x) = g(x)\left(1 - \frac{f_1(x)}{g(x)}\right)$$		4-1
Subject to		
$$c(x) \equiv \cos(\theta)(f_2(x) - e) - \sin(\theta)f_1(x) \geq a\left|\sin\left(b\pi(\sin(\theta)(f_2(x) - e) + \cos(\theta)f_1(x))^h\right)\right|^d$$		4-2

The parameters and constant values used in equations 4-1 and 4-2 are:

$x = \{x_{11},..., x_n\}$

$x_1 \in [0,1]$

$\theta = -0,05\pi$

$a = 40$

$b = 5$

$h = 1$

$d = 6$

$e = 0$

$g(x) = 1 - x_1$
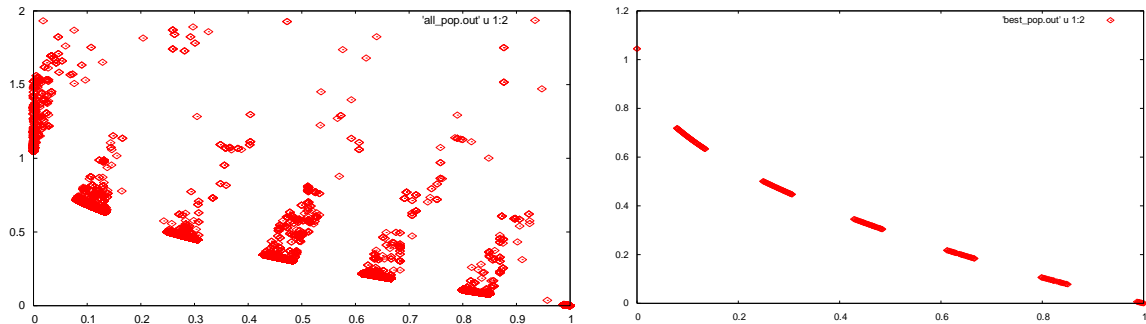
Figure 4-3.- CTP7 constrained test problem: whole populations and Pareto Front

Figure 4-3 shows the representation of the whole population and the Pareto front obtained for the CPT7 mathematical problem. As defined in Deb et al (2000), the constrained feasible space of the solution is represented by the striped area in the right figure, which leads to a dashed Pareto front.

4.3.1.3 CTP7 Test Case; Stochastic definition

Two stochastic definitions have been applied to modify the CTP7 test case. One stochastically modifies the fitness functions, $f'_1(x)$ and $f'_2(x)$, and the second one modifies two parameters of the constraint $c(x)$. In both cases, the fitness functions have been calculated as the mean value of the whole set of evaluations, which have been defined by the stochastic term.

- CTP7 Test Case with stochastic fitness function

CTP7 problem is described by equations 4-3 and 4-4:

Minimize	$f'_1(x) = \mu(x_1 + \omega_1(\xi))$	
Minimize	$f'_2(x) = \mu\left(g(x)\left(1 - \frac{f_1(x)}{g(x)}\right) + \omega_2(\xi)\right)$	4-3

Each of the fitness functions, $f'_1(x)$ and $f'_2(x)$, include a stochastic term, $\omega_1(\xi)$ and $\omega_2(\xi)$, respectively. Both of them are calculated as the mean value of the set of evaluations coming from the introduction of the stochastic term.

Subject to $$c(x) \equiv \cos(\theta)(f_2(x) - e) - \sin(\theta)f_1(x) \geq a\left\|\sin\left(b\pi(\sin(\theta)(f_2(x) - e) + \cos(\theta)f_1(x))^h\right)\right\|^d$$	4-4

Constant parameters and *g(x)* function are defined as in the deterministic case, in Section 4.3.1.2.

Equations from the deterministic definition of the CPT7 problem have been modified adding stochastic terms $\omega_i(\xi)$. These terms introduce a set of values into the equation which lead to its stochastic definition. Stochastic terms have been defined through their mean (μ) and standard deviation (σ). The following values have been defined for a Gaussian distribution:

$$\mu(\omega_1(\xi)) = 3$$
$$\sigma(\omega_1(\xi)) = 0,5$$
$$\mu(\omega_2(\xi)) = 1$$
$$\sigma(\omega_2(\xi)) = 0,01$$

The μ value for each stochastic term has been selected to clearly identify the effects of introducing it in the fitness functions. They enable an easy comparison between the results highlighting the differences in shape and position of the whole population and the Pareto front.

Figure 4-4 shows the solution of the CTP7 test case with a stochastically defined fitness function.
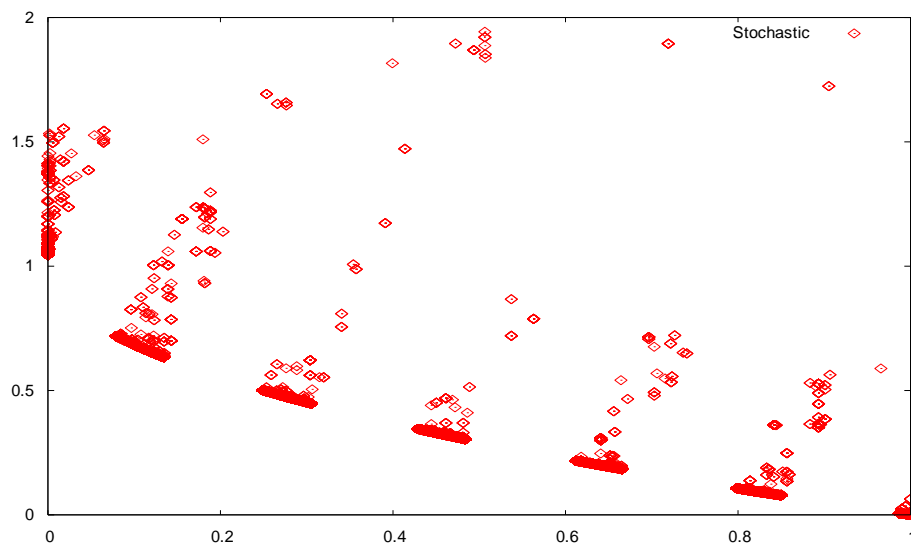
Figure 4-4.- CTP7 problem with stochastically defined fitness function
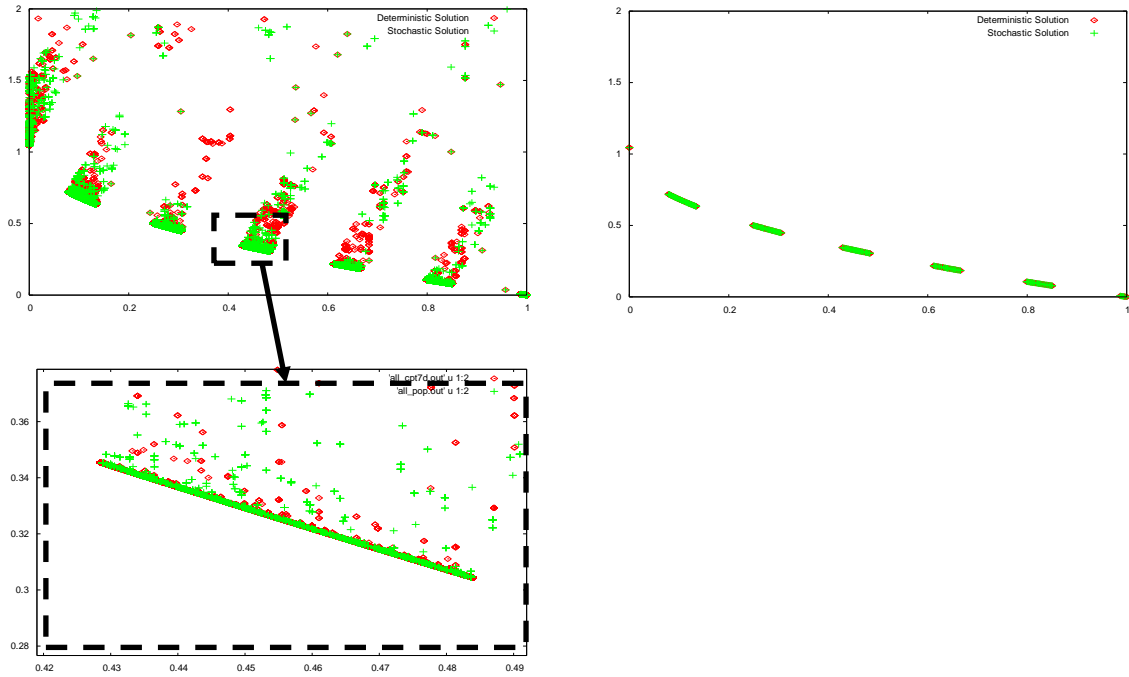
Figure 4-5.- Comparison between CTP7 problem with stochastically defined fitness function and the deterministic solution

Figure 4-5 is a comparison between the deterministic solution of the CTP7 test case and the stochastic solution of the same mathematical test case. It shows the constrained solution space. Figure 4-5 shows how adding a stochastic term in the fitness function the total number of evaluations on the front is reduced. Former best individuals lose their dominance due to the stochastic term. Even though the shapes of total population and of Pareto front are almost the same, as it can be seen in Figure 4-5, the density of points in the Pareto front is lower in the stochastic case, as it can be seen in the bottom image of the Figure 4-5. This effect is produced due to the fact that the stochastic term introduces variability on the fitness values that means losing dominance and becoming a non-optimal solution.

- CTP7 Test Case with stochastic terms on the constraint function

The second stochastic definition of CPT7 problem modifies *a* and *b* parameters in the definition of constraint *c'(x)*. CTP7 problem has been described as:

Minimize	$f_1(x) = x_1$	4-5
	$f_2(x) = g(x)\left(1 - \dfrac{f_1(x)}{g(x)}\right)$	

Subject to	
$c'(x) \equiv \mu\left(\cos(\theta)(f_2(x) - e) - \sin(\theta)f_1(x) \geq a\left\|\sin\left(b\pi(\sin(\theta)(f_2(x) - e) + \cos(\theta)f_1(x))^h\right)\right\|^d\right)$	4-6

Parameters defining the constraint have been defined as:

$$x = \{x_{11},..., x_n\}$$
$$x_1 \in [0,1]$$
$$\theta = -0,05\pi$$
$$a = \omega'_1(\xi)$$
$$b = \omega'_2(\xi)$$

$$h = 1$$
$$d = 6$$
$$e = 0$$
$$g(x) = 1 - x_1$$

Equations 4-5 and 4-6 are the same as from the deterministic definition of the CPT7 problem. The stochastic terms $\omega'_i(\xi)$ have been introduced into the definition of the parameters of the constraint, which should be calculated as the mean value of set of values defined by the stochastic terms. The Gaussian distributions of the stochastic terms have been defined with the following parameters:

$$mean(\omega'_1(\xi)) = 40$$
$$Std\ dev(\omega'_1(\xi)) = 0,5$$
$$mean(\omega'_2(\xi)) = 5$$
$$Std\ dev(\omega'_2(\xi)) = 0,5$$

Values for the mean and the standard deviation have been selected according the deterministic value. They enable an easy comparison between the results highlighting the differences in shape and position of the whole population and the Pareto front.
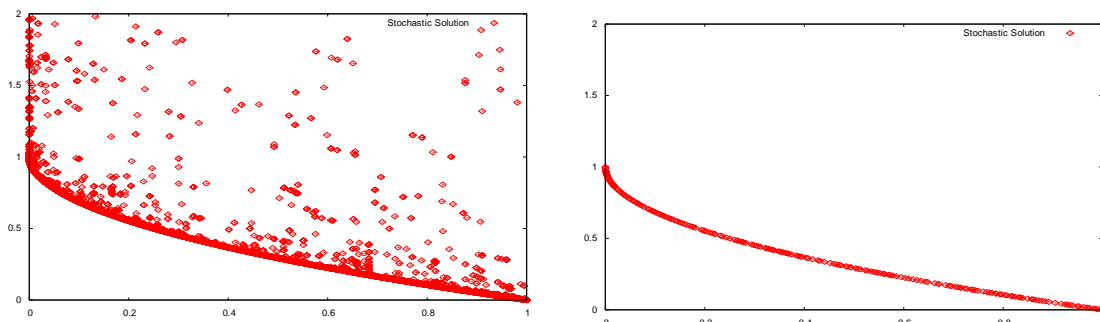
Figure 4-6.- CTP7 problem with stochastically defined constraint

This case presents a completely different behaviour. The stochastic terms are affecting the constraint definition in such a way that the final shapes of the total population and the Pareto front, shown in Figure 4-6, do not follow the guideline defined by deterministic CPT7 problem. Now, the Pareto front becomes a continuous line instead of a dashed line as in the deterministic case. This effect is produced by the variability of the constraints values, so the band-shaped plot loses its meaning.

4.3.1.4 OSY Test Case; Deterministic definition

The deterministic description of the OSY test case (Deb et Al, 2000) is based on two quadratic objective functions with 6 linear constraints.

OSY problem is described as:

Minimize	$$f''_1(x) = -\left(25(x_1 - 2)^2 + (x_2 - 2)^2 + (x_3 - 1)^2 + (x_4 - 4)^2 + (x_5 - 1)^2\right)$$ $$f''_2(x) = x_1^2 + x_2^2 + x_3^2 + x_4^2 + x_5^2 + x_6^2$$	4-7

Subject to	$$c_1(x) = x_1 + x_2 - 2 \geq 0$$ $$c_2(x) = 6 - x_1 - x_2 \geq 0$$ $$c_3(x) = 2 - x_2 + x_1 \geq 0$$ $$c_4(x) = 2 - x_1 + 3x_2 \geq 0$$ $$c_5(x) = 4 - (x_3 - 3)^2 - x_4 \geq 0$$ $$c_6(x) = (x_5 - 3)^2 + x_6 - 4 \geq 0$$	4-8

The parameters defining the constraints are:

$$x = \{x_1, ..., x_n\}$$
$$0 \leq x_1, x_2, x_6 \leq 10$$
$$1 \leq x_3, x_5 \leq 5$$
$$0 \leq x_4 \leq 6$$

To set up the NSGA-II optimizer in all OSY test cases the following values have been used:
- Population size: 200
- Number of generations: 1000
- Probability of Crossover: 0,99
- Probability of Mutations: 0,16667
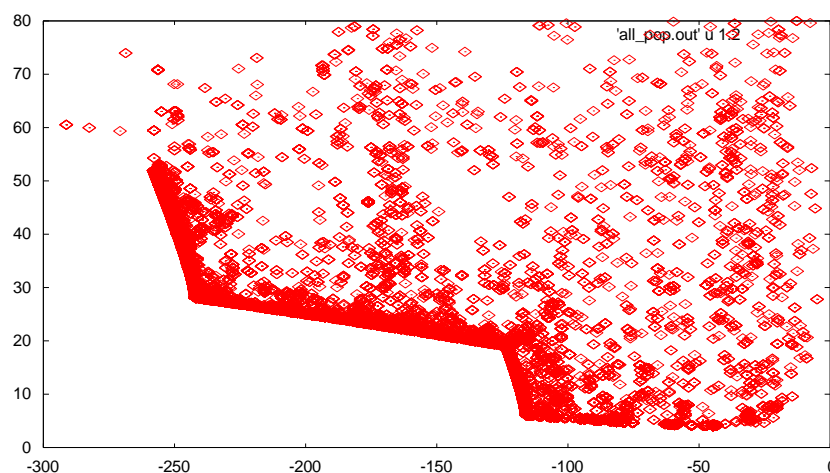
Figure 4-7 shows the problem solution and its Pareto front. The reader can observe how linear constraints define the feasible area, and how the optimal solutions in the Pareto front follow the defined restrictions.
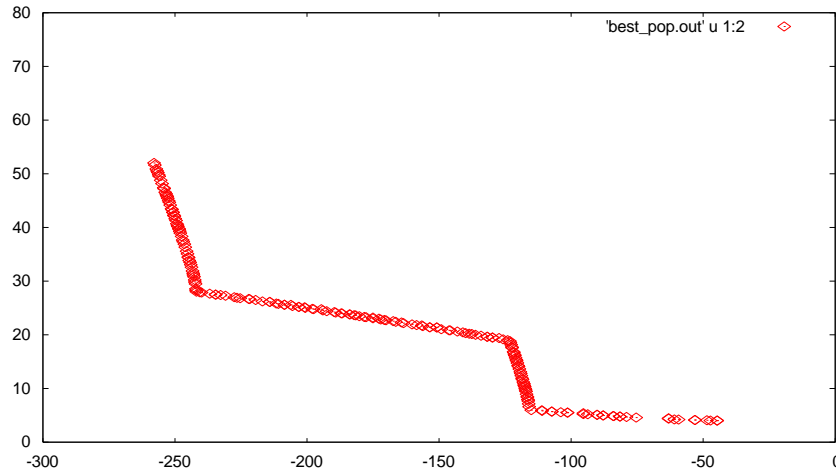
Figure 4-7.- OSY constrained test problem solution and Pareto front

4.3.1.5   OSY Test case; stochastic definition

OSY test case has been modified from its deterministic description to a non-deterministic version with the introduction of stochastic components in the former fitness functions f''_1 and f''_2, plus considering as new fitness functions the mean of the new functions f'''_1 and f'''_2.

OSY problem is now described as:

Minimize $$f'''_1(x) = \mu\left(\omega''_1(\xi) - \left(25(x_1 - 2)^2 + (x_2 - 2)^2 + (x_3 - 1)^2 + (x_4 - 4)^2 + (x_5 - 1)^2\right)\right)$$ $$f'''_2(x) = \mu\left(x_1^2 + x_2^2 + x_3^2 + x_4^2 + x_5^2 + x_6^2 + \omega''_2(\xi)\right)$$	4-9

	$$c_1(x) = x_1 + x_2 - 2 \geq 0$$ $$c_2(x) = 6 - x_1 - x_2 \geq 0$$ $$c_3(x) = 2 - x_2 + x_1 \geq 0$$ Subject to $$c_4(x) = 2 - x_1 + 3x_2 \geq 0$$ $$c_5(x) = 4 - (x_3 - 3)^2 - x_4 \geq 0$$ $$c_6(x) = (x_5 - 3)^2 + x_6 - 4 \geq 0$$	4-10

The value ranges for x_i parameters have been defined as done in Section 4.3.1.4. The stochastic terms have been defined in two different ways. A Gaussian probability density function has been applied in the first case, while in the second case a Uniform distribution has been applied.

- OSY Test Case with Gaussian stochastic terms

Gaussian distributions have been applied to the stochastic terms, considering the stochastic parameters:

$$\mu\bigl(\omega''_1(\xi)\bigr) = 5,0$$
$$\sigma\bigl(\omega''_1(\xi)\bigr) = 0,05$$
$$\mu\bigl(\omega''_2(\xi)\bigr) = 5,0$$
$$\sigma\bigl(\omega''_2(\xi)\bigr) = 0,02$$

Population size has been defined equal to 200 individuals and the number of generations equal to 1000, as done in the deterministic case.

The new definition of the fitness functions produces a displacement of the fitness value, as the reader can observe in Figure 4-8. The mean value suffers a displacement of 5 units in both functions, and considering how small the standard deviation values are, the expected result would be a displacement of the entire Pareto front up and right.
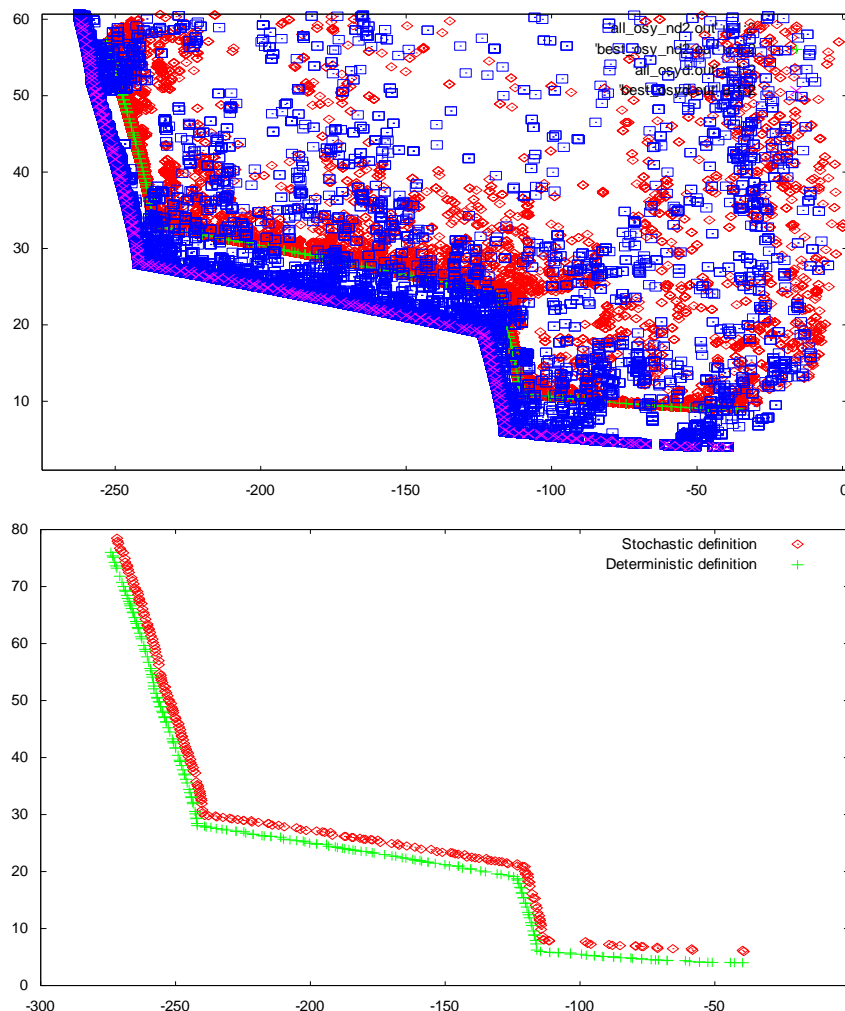
Figure 4-8. OSY test case: deterministic and stochastic definition

- OSY Test Case with stochastic terms defined by a Uniform distribution

In the second test case the stochastic parameters have been defined following a uniform density function with the defined lower and upper bounds of:

$$Lower\,bound\big(\omega''_1(\xi)\big)=3,5$$
$$Upper\,bound\big(\omega''_1(\xi)\big)=6,5$$
$$Lower\,bound\big(\omega''_2(\xi)\big)=3,8$$
$$Upper\,bound\big(\omega''_2(\xi)\big)=6,2$$

Values for the upper and lower bounds have been selected to define a similar stochastic range compared with the previous case which has defined a Gaussian distribution.

Figure 4-9 shows a comparison of the two defined test cases; the one using a normal or Gaussian distribution, and the one using a uniform distribution. Taking as reference the Pareto front of the Gaussian distribution case, the Pareto front obtained in the stochastic case using uniform distribution moves forward the small difference between the mean of Gaussian distribution and lower bound of the uniform distribution. Even though Gaussian distribution and uniform one obtain Pareto optimal individuals according to the dominance criterion, Gaussian PDF is centred on the mean value, and uniform is distributed along the whole range of values, and this behaviour is reflected on the Pareto front.
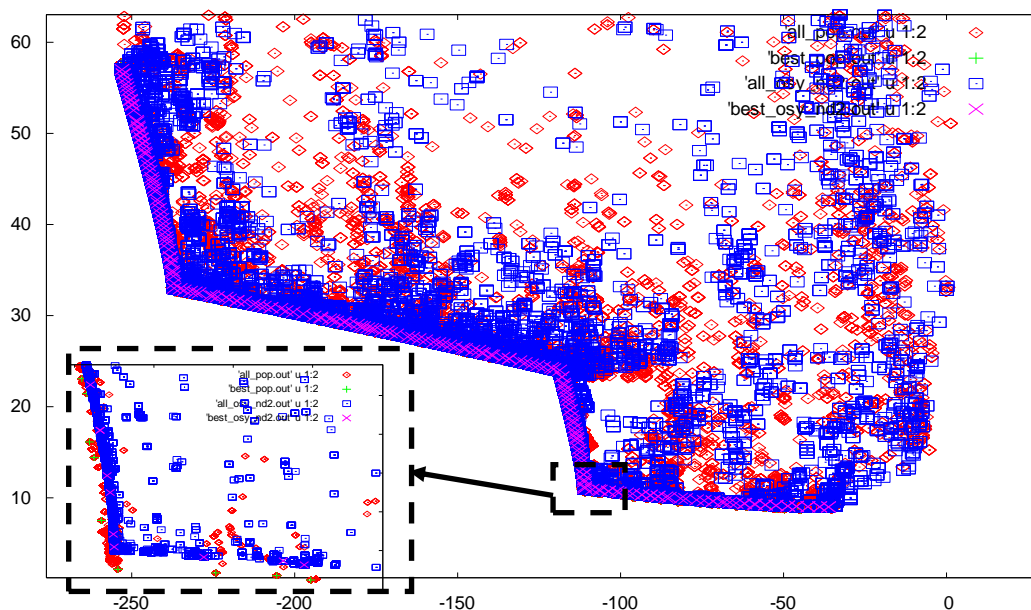
Figure 4-9. OSY test case: uniform and Gaussian PDF

The uniform PDF case is similar to the Gaussian definition if the central point of the uniform distribution is equal to the mean value for Gaussian distribution and the range of values is equivalent to the Gaussian one on its 95% confident range.

4.3.1.6 Conclusions

Stochastic terms have been introduced in both fitness functions and constraints of the selected mathematical test cases. The reader can observe how the consideration of stochastic terms in the constraint produces a completely new problem, while the

stochastic fitness function only produces a slight modification of the problem, providing similar results to the deterministic one. The stochastic definitions applied to both CTP7 and OSY test cases shows this behaviour, but CTP7 shows a completely new behaviour between the cases with the deterministic and the stochastic fitnees function and the stochastic constraints.

This is an important conclusion in order to understand a more complex problem and the effects that uncertainty definition can produce. As mentioned, in CFD problems several uncertainty sources can be selected and analysed. The comparison between the original problem and the one with uncertainties has to be fair. Both definitions and results should be comparable.

4.4 Deterministic, Stochastic and Robust Optimization

4.4.1 Introduction

In previous section, a couple of mathematical test cases has been analysed in order to compare the deterministic and the stochastic optimization results for the same problem. Taking advantage of the same problem definition, the comparison of these three types of results has been very useful to clarify the concepts and methodologies.

One of the main objectives of this section analyses has been to evaluate the differences between these three procedures; namely the deterministic, the stochastic and the robust ones. The deterministic solution of the deterministic problem does not take into account neither the stochastic definition of the input variables, nor the variability analysis of the output values. The result is always a single point. The stochastic case already takes into account the uncertainties in the definition of the input parameters. Uncertainties are modelled using a probabilistic density function. The stochastic case takes also into account the variability induced on the output parameters, but only considering the mean value of the cloud of results. Finally, the robust case defines the input variables with their associated uncertainties, but also analyse the variability of the results managing the mean and the standard deviation of the results.

4.4.2 Single Objective test case

4.4.2.1 Problem definition

In order to compare the deterministic, stochastic and robust procedures, a test case with the same problem definition has been used through the three test cases. A profile has been analysed using Eulerian solver PUMI (Flores and Ortega, 2007). The baseline design has been selected as the RAE2822 profile as shown in Figure 4-10. Six control points have been used to generate and to control the geometry of the shape optimization problem. Although one of the most usual ways to define aeronautical profile shapes is using chord curvature and thickness of the profile, the definition of the shape using the coordinates of the knots or control points of the Bezier curve is also an accepted procedure. It provides great flexibility, mainly when dealing with optimization methods which require a good control of the shape to be optimized. The search space of the values has been defined by the following range of values for each parameter:

- Upper Profile:
  - First control point, y-coordinate of the control point located at x = 0,25: [0,05 0,085]
  - Second control point, y-coordinate of the control point located at x = 0,5: [0,03 0,0599]
  - Third control point, y-coordinate of the control point located at x = 0,75: [0,001 0,0199]
- Lower profile:
  - First point, y-coordinate of the control point located at x = 0,25: [-0,0499 -0,03]
  - Second point, y-coordinate of the control point located at x = 0,5: [-0,035 -0,02]
  - Third point, y-coordinate of the control point located at x = 0,75: [-0,0149 -0,005]

This search space has been constructed in such a way that a constrain on a minimum thickness of the profile is automatically accomplished.

The main parameters of the CFD analysis are:
- Reynolds number: $6,5*10^6$
- Angle of attack: 4º
- Mach number: 0,704

The stochastic and the robust cases also define the probabilistic density function of angle of attack and Mach number as Gaussian distributions with the mean values equal to the previous defined values and the standard deviation equal to:
- Standard deviation of Angle of attack: 0,5
- Standard deviation of Mach number: 0,08

Standard deviation values have been selected as a 10% of the mean value to define a large stochastic range of values. It enables the generation of a stochastic range large enough to clearly modify the deterministic results.
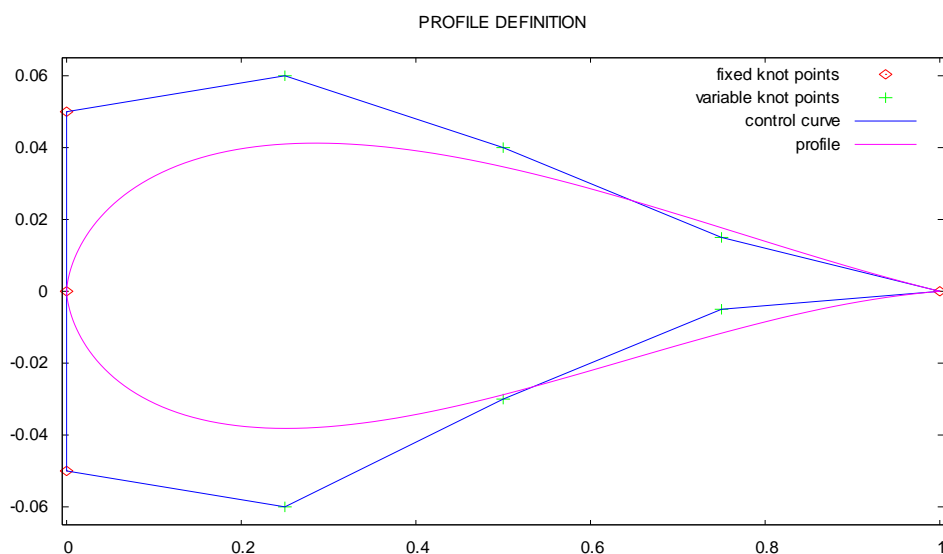
Figure 4-10.- Geometry definition

The objective functions for each case (deterministic, stochastic and robust design) have been defined in equations 4-11, for the deterministic test case, 4-12, for the stochastic, and 4-13, for the robust one:

- Deterministic case:

Minimise	$f_{1d}(x) = C_d / C_l$	4-11

- Stochastic case:

Minimise the mean of	$f_{1s}(x) = \mu\left(C_d / C_l\right)$	4-12

- Robust case:

Minimise	$f_{1r}(x) = \mu\left(C_d / C_l\right)$ $f_{2r}(x) = \sigma\left(C_d / C_l\right)$	4-13

The reader can observe that the robust case cannot be defined as a single-objective problem if mean (μ) and standard deviation (σ) should be taken into account. The use of the ratio μ/σ has not been considered as an option because it cannot be directly compared with the deterministic and stochastic objective functions.

On the other hand, the evolutionary algorithm, NSGA-II, for optimization has been set-up with the following parameters:
- Population size: 24
- Number of generations: 300
- Probability of Crossover: 0,95
- Probability of Mutation: 0,166667

A surrogate model, based on the Artificial Neural Network, has been used to accelerate the evaluations. In order to train the network a set of 400 samples has been used, which sample the search space of the design variables of the optimization process. The validation set has been defined with 40 additional samples. The obtained validation error is lower than 1.5%. The surrogate model has been trained previously to perform the optimization analysis. This fact helps to greatly reduce the total computational cost of the whole process.

An important remark is the specific definition of each case. The deterministic objective function has been just defined by the use of the drag-lift ratio, while the stochastic objective function and robust one have been defined by the mean value of a set of evaluations of the drag-lift ratio. At the end of the process, for this research both values, the deterministic one and the stochastic mean, are considered as fully equivalent whichever the number of evaluations to calculate the stochastic mean is. A second remark is that the robust case is no longer a single-objective problem due to the mandatory introduction of the standard deviation. The robust test case is aimed to

reduce the variability, as well as the mean value. This issue has been considered when comparing with the results of the other test cases.

4.4.2.2 Results of the single objective test case

Figure 4-11 shows the convergence of the three cases, while Table 4-1 lists the converged values. Some clear differences can be appreciated. The first one is the difference between the converged value of the deterministic case and the stochastic and robust cases. There is a big difference between the deterministic and the stochastic optimal values, while the stochastic and the robust optimal values are closer between them. A second difference is the convergence rate. Deterministic and stochastic cases are only dealing with one objective function, namely the deterministic value and the mean value, whereas the robust case is dealing with two objective functions, namely the mean and the standard deviation. Then, the convergence rate of the robust case is slower than in the other two cases. This is mainly due to the larger complexity of solving a multi-objective optimization problem compared with single objective ones.
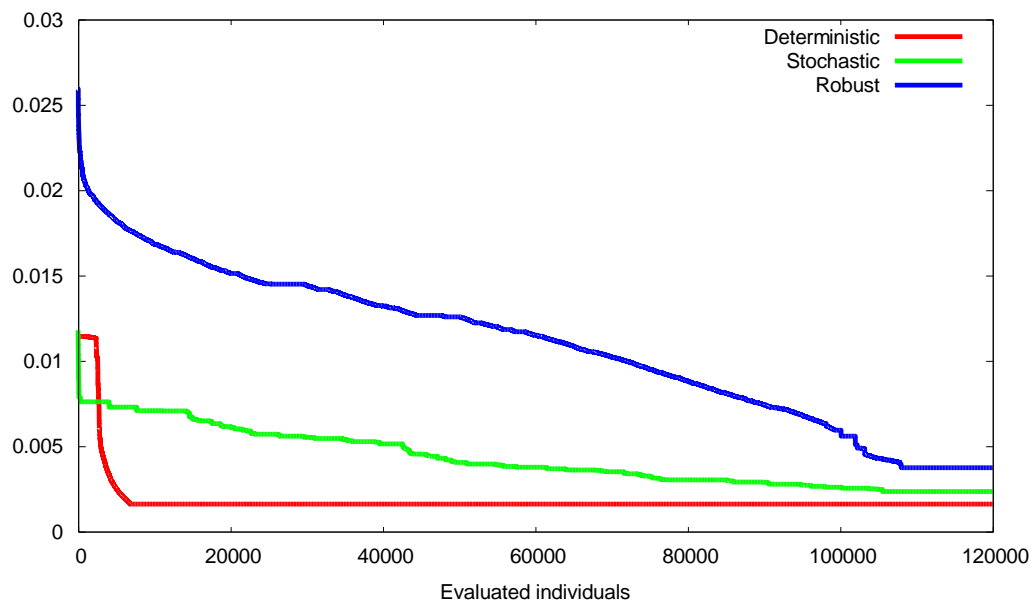
Figure 4-11.- Convergence for Deterministic, Stochastic and robust case

Test Case	Converged Value
Deterministic	1,605e-003
Stochastic	2,342e-003
Robust	3,737e-003

Table 4-1: Converged values of the single objective test cases

Figure 4-12 shows the convergence of the standard deviation of the drag-to-lift ratio, which has been defined as the second fitness function of the robust test case. Figure 4-13 shows the geometrical shape of the obtained profiles for each optimization process. As it can be anticipated by the obtained values, each of them has a different shape. The stochastic and robust solutions are closer between them than with the deterministic ones.
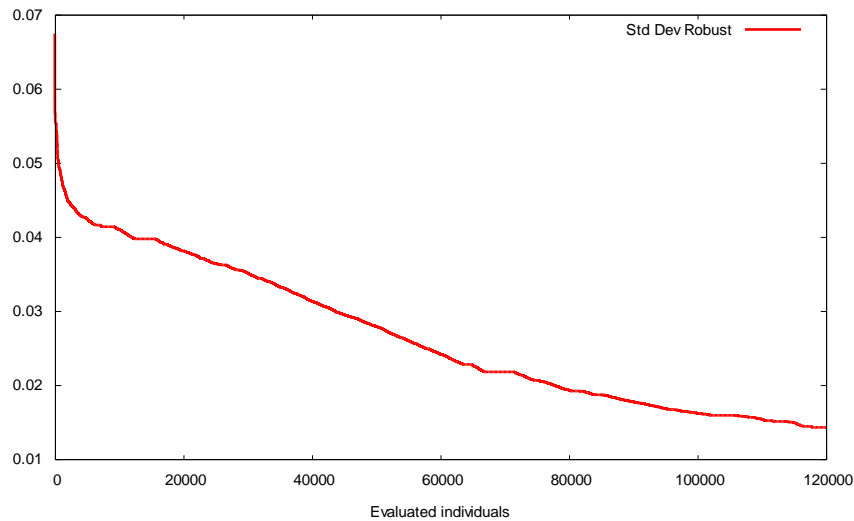
Figure 4-12.- Convergence for Deterministic, Stochastic and robust case
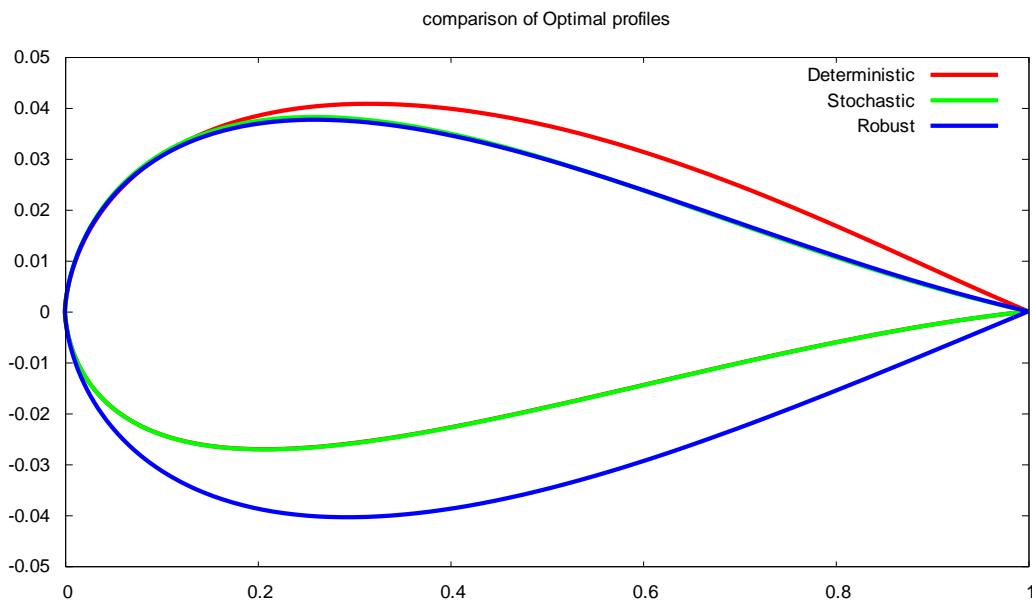
Figure 4-13.- Comparison of the optimal profile for Deterministic, Stochastic and robust case

In order to better understand the results and how the results are affected by the stochastic definition, Figure 4-15 and 4-16 show a comparison of the behaviour of the obtained optimal individuals for each case when analysed under uncertainty conditions. Figure 4-15 shows the evolution of the drag to lift ratio under uncertainties on the Angle of Attack. For small values of the angle of attack the reader can observe a larger difference between the behaviour of the three cases. The stochastic case presents a more constant slope, but larger than the slope of the robust case, which after a fast increment from 0 to 2, it reaches a constant and smaller slope. For a certain range of values, close to the stochastic mean value of the angle of attack, the robustness of the objective function can be ensured and the results of the stochastic and the robust test cases improve those obtained by the deterministic test case. Due to the fact that the robust test case has provided a whole Pareto front as the optimal solution, some of the Pareto members have been plotted in order to better compare how the solution behaves. The curves marked as "Robust PM" are:

- Robust PM1; the member with the largest variability
- Robust PM10 and Robust PM12; the central members of the Pareto front, id est, those with the better balance between both objectives functions.
- Robust PM24; the member with the lowest variability.

The reader can compare how the member with the largest variability has a similar behaviour as the stochastic test case result. The member presenting the lowest variability shows a more stable value of the drag-to-lift ratio along the whole range of angle of attack.
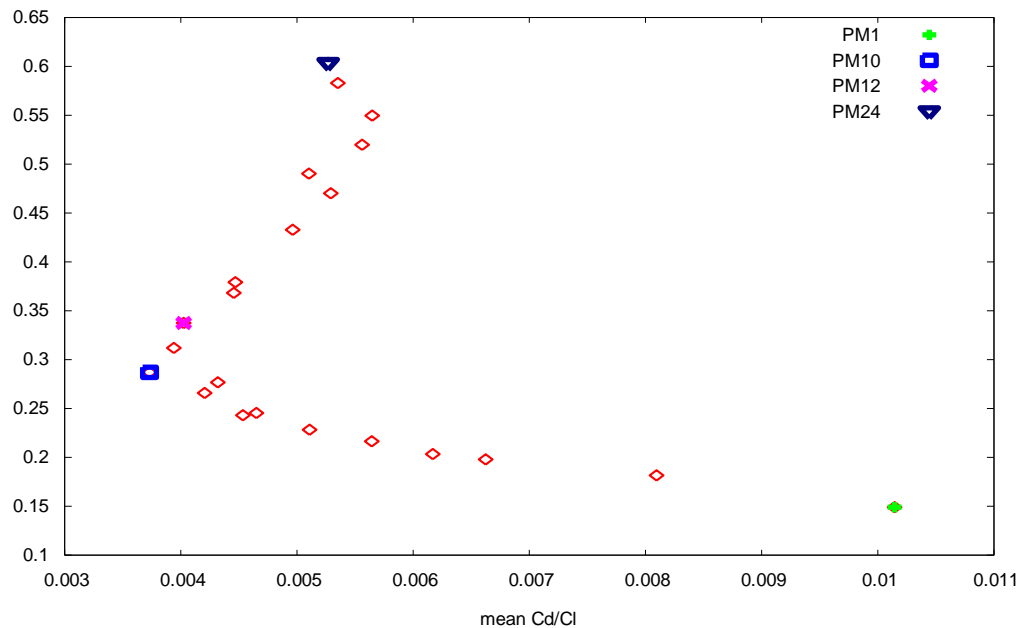
Figure 4-14.- Pareto front of the robust test case

Figure 4-14 shows the Pareto front of the robust test case, and the selected Pareto members which have been analysed.

Figure 4-16 shows the equivalent comparison when the Mach number is the uncertain parameter. Mach number has a larger effect on the vicinity of the stochastic mean value due to the shock wave phenomena. On the subsonic region, the differences between the three test cases are insignificant. But on the transonic region, the drag to lift ratio increases quickly due to the drag increment. The deterministic test case is not considering the vicinity of the evaluated point, so it cannot detect this phenomena and the optimal value is not robust under this circumstance. On the other hand, the stochastic and the robust test cases are considering the vicinity of the evaluated point during the optimization and they are able to improve the search. Obviously, the robust test case provides the mist uniform behaviour.

The reader can observe how the angle of attack and the Mach number introduce a different variability to the objective function. In Figure 4-16 the reader can observe how the Pareto member with the lowest variability shows an equivalent behaviour to the Pareto member 10 with a balanced equilibrium between mean value and variability.
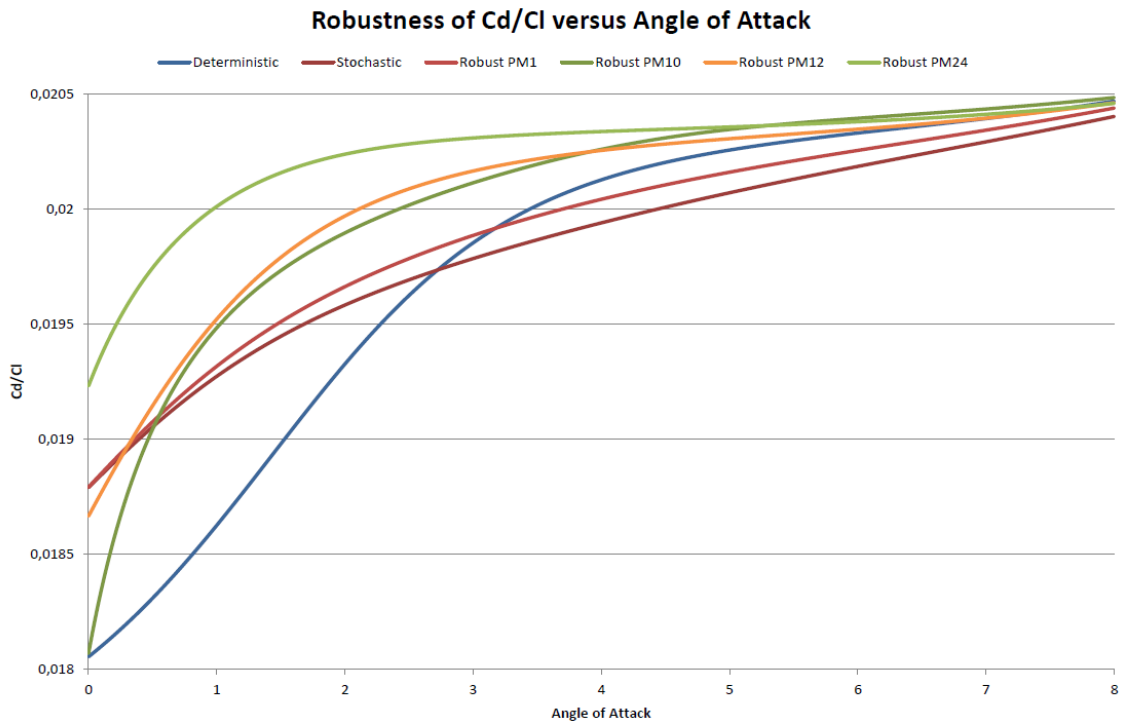
Figure 4-15.- Robustness of drag/lift versus Angle of Attack number for Deterministic, Stochastic and robust case
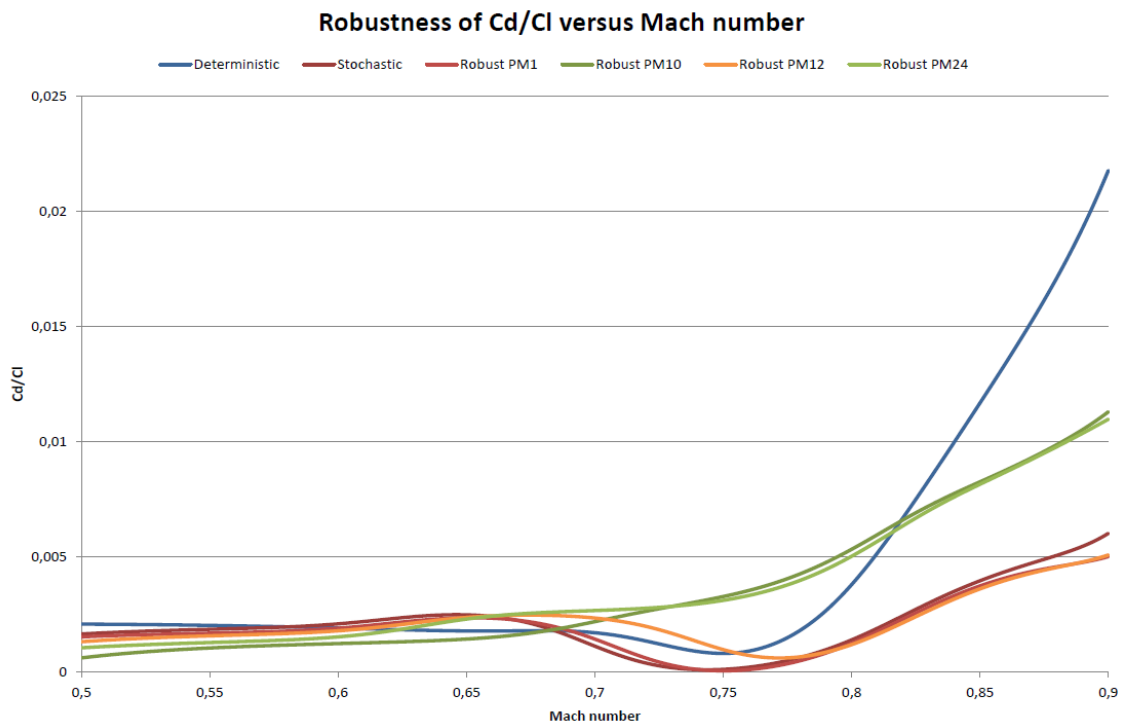
Figure 4-16.- Robustness of drag/lift versus Mach number for Deterministic, Stochastic and robust case

4.4.3 Multi-Objective test case

4.4.3.1 Problem definition

As it has been done in the previous section, the deterministic, the stochastic and the robust test cases have been defined and compared. The same problem definition has been used through the three test cases. A profile has been analysed under transonic regime conditions.

The main parameters of the analysis are:
- Reynolds number: $6,5*10^6$
- Angle of attack: 4º
- Mach number: 0,704

The stochastic and the robust cases applies a Gaussian distribution to angle of attack and Mach number with:
- Standard deviation of Angle of attack: 0,5
- Standard deviation of Mach number: 0,08

The NSGA-II optimizer has been set-up with the following parameters:
- Population size: 24
- Number of generations: 300
- Probability of Crossover: 0,95
- Probability of Mutation: 0,16667

The surrogate model, which has been trained for the single objective test case, has been used in the multi-objective test case. The training and validation processes have been performed in advance to the use of the surrogate model within the optimization process.

The objective functions for each case have been defined in equation 4-14 for the deterministic case, in 4-15 for the stochastic case, and in 4-17 for the robust design case:

- Deterministic case:

Minimise	$f_{1d}(x) = \dfrac{1}{C_l}$ $f_{2d}(x) = C_d$	4-14

- Stochastic case:

Minimise the mean of	$f_{1s}(x) = \mu\left(\dfrac{1}{C_l}\right)$ $f_{2s}(x) = \mu(C_d)$	4-15

- Robust case:

Minimise		
	$f_{1r}(x) = \mu\left(\dfrac{1}{C_l}\right)$ $f_{2r}(x) = \mu(C_d)$ $f_{3r}(x) = \sigma\left(\dfrac{1}{C_l}\right)$ $f_{4r}(x) = \sigma(C_d)$	4-16

4.4.3.2 Results of the Multi-objective test case

The comparison of the results of the multi-objective test cases has been done only considering the f_{1d} and f_{2d}, f_{1s}, f_{2s}, f_{1r} and f_{2r} objective functions, i.e., the deterministic and the mean values of $1/C_l$ and C_d coefficients for the stochastic and robust test cases.

Figure 4-17 shows the whole set of populations obtained for the three cases, when using an evolutionary algorithm optimizer, the modified NSGA-II, combined with the deterministic, the stochastic and the robust design procedures. The deterministic case presents a more concentrated population, while the stochastic case spreads values in a larger range, due to the fact that the introduction of uncertainties can lead to an increment on the output variability. If the robust design case is added to the comparison, a significant increase of the variability can be observed. It should be taken into consideration that the robust case is using four objective functions, including the standard deviation values, while the previous two cases only use two objective functions (mean values).

The effect of defining four objective functions can be clearly observed in Figure 4-18. It shows the Pareto fronts for each case. Those cases which have defined only two objective functions have a 2D front, while the robust case has a 4D front. The comparison between a case defining 2 objective functions and a case defining 4 objective functions is not an easy task. The 2-functions case defines a 2D result space while the 4-functions case defines a 4D space. The comparison can be done only by pairs of objective functions, which is not a fair comparison due to the fact the 4D case is dismissing two dimensions. The use of Self Organizing Maps (SOM) can be evaluated when dealing with high dimensional data, which cannot be easily plotted and compared (see references Obayashi and Sasaki, 2003; Obayashi, Jeong and Chiba, 2005; Pediroda and Poloni, 2006; Parashar, Pediroda and Poloni, 2008).
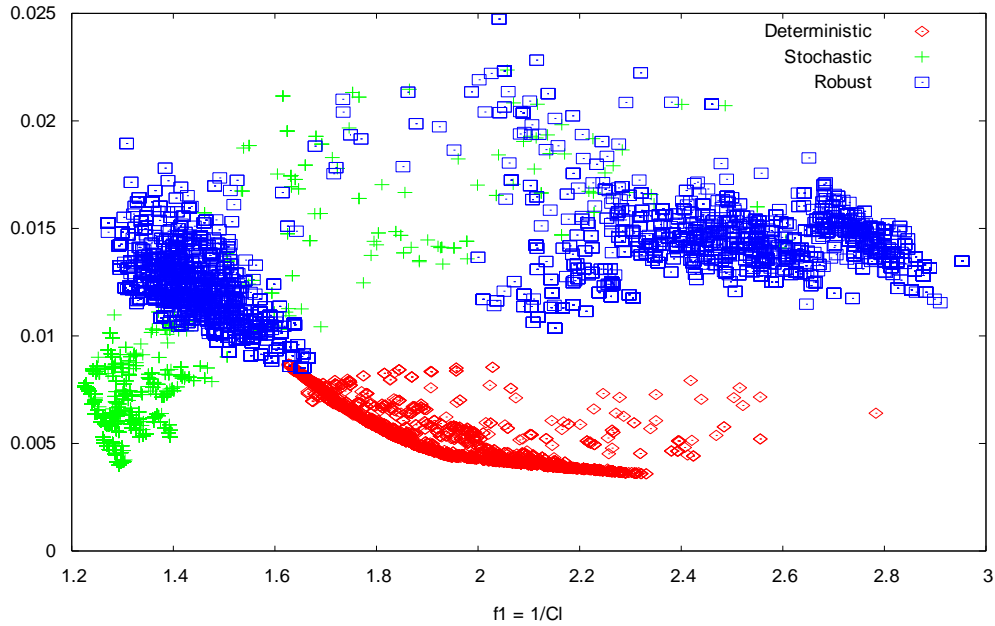
Figure 4-17.- All populations comparison for Deterministic, Stochastic and robust case
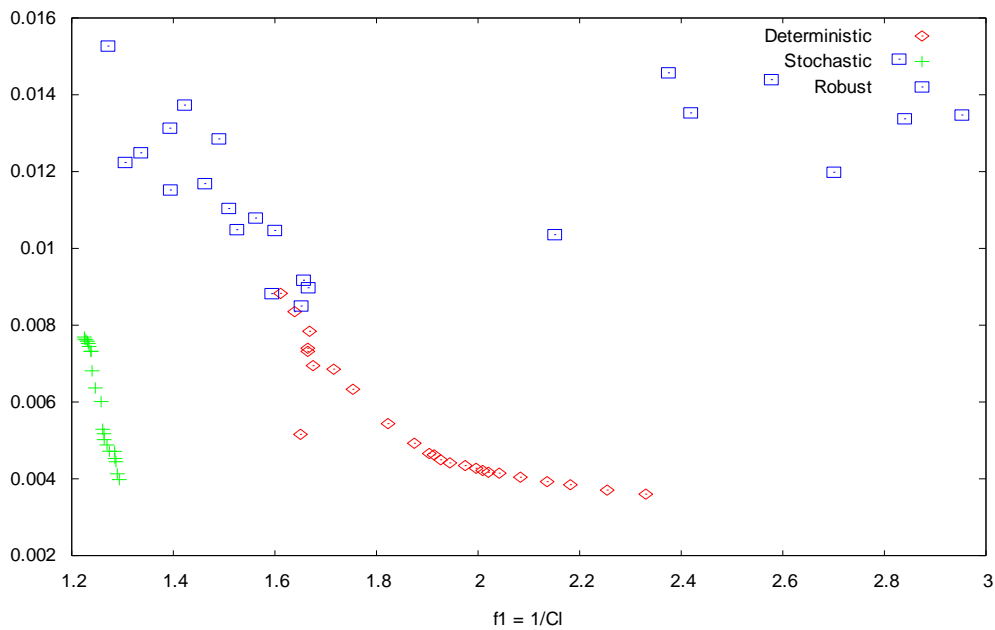
Figure 4-18.- Best population comparison for Deterministic, Stochastic and robust case

The robustness of the optimal individuals obtained in each test case has been evaluated through the comparison of its behaviour under uncertain conditions. The lift and drag coefficients have been analysed under uncertain values of Mach number and Angle of attack, in a similar way the optimization process did.

The figures show the most balanced Pareto members, which can be considered the optimal values from the point of view of both fitness functions. The represented individual by the profile has been selected from those with a balanced optimality on all the objective functions, i.e. from the central area of the Pareto front.

Figure 4-19, 4-20, 4-21 and 4-22 show lift and drag coefficients versus angle of attack and Mach number. The reader can observe how the lift coefficient values are bigger and

with a larger line slope for the stochastic and robust test cases than for the deterministic cases

Taking into consideration that the objective of the optimization was defined as the minimization of the inverse value of the lift coefficient, and the minimization of the drag value, what the reader can observe in Figure 4-19, 4-20, where lift values are bigger in the stochastic and robust cases, and drag value is bigger in the deterministic case fulfils the expectations of the analysis; the maximization of lift and minimization of drag while taking into account the variability.

In Figure 4-21 and 4-22, the reader can observe that in the case of variability on the angle of attack the lift and drag values are not improved as much as in the Mach number case. This is also a penalty the engineer should pay due to the introduction of the uncertainty analysis.
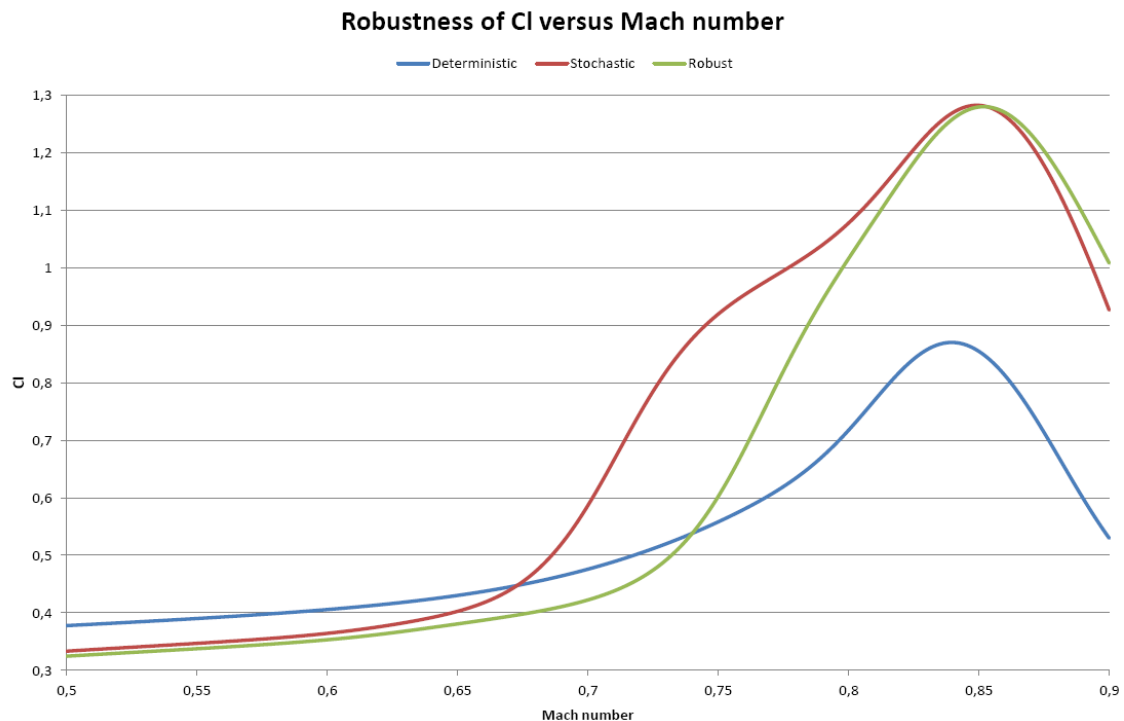
Figure 4-19.- Robustness of lift versus Mach number for Deterministic, Stochastic and robust case

Robustness of Cd versus Mach number
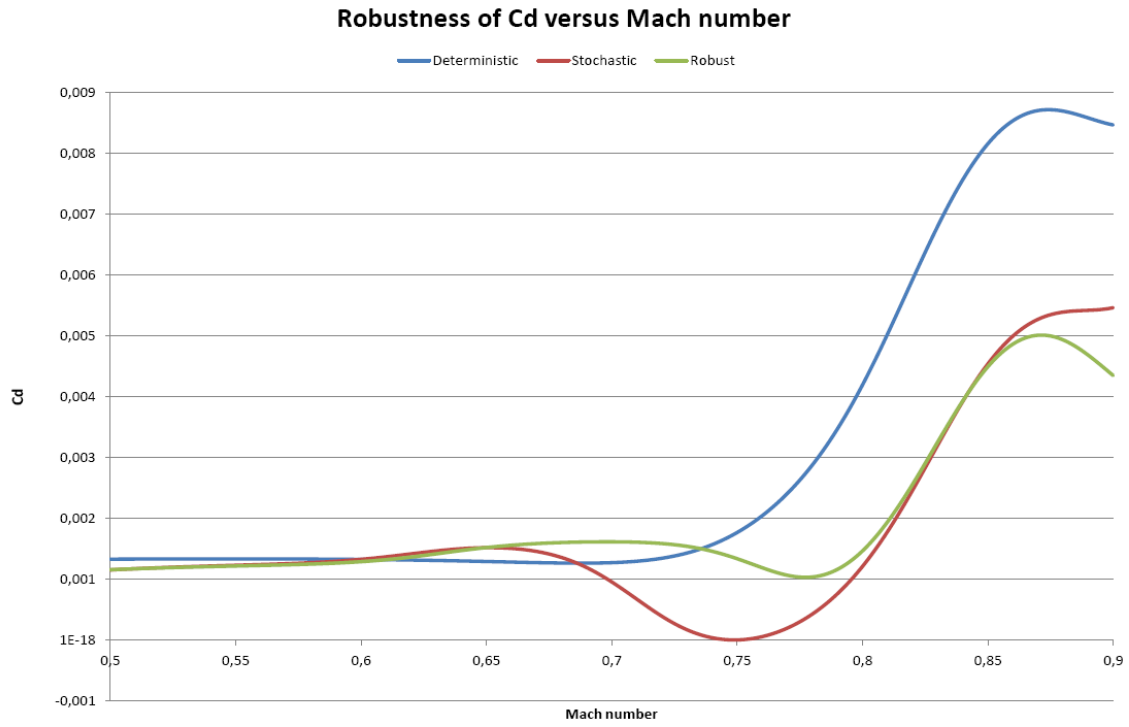
Figure 4-20.- Robustness of drag versus Mach number for Deterministic, Stochastic and robust case

Robustness of Cl versus Angle of Attack
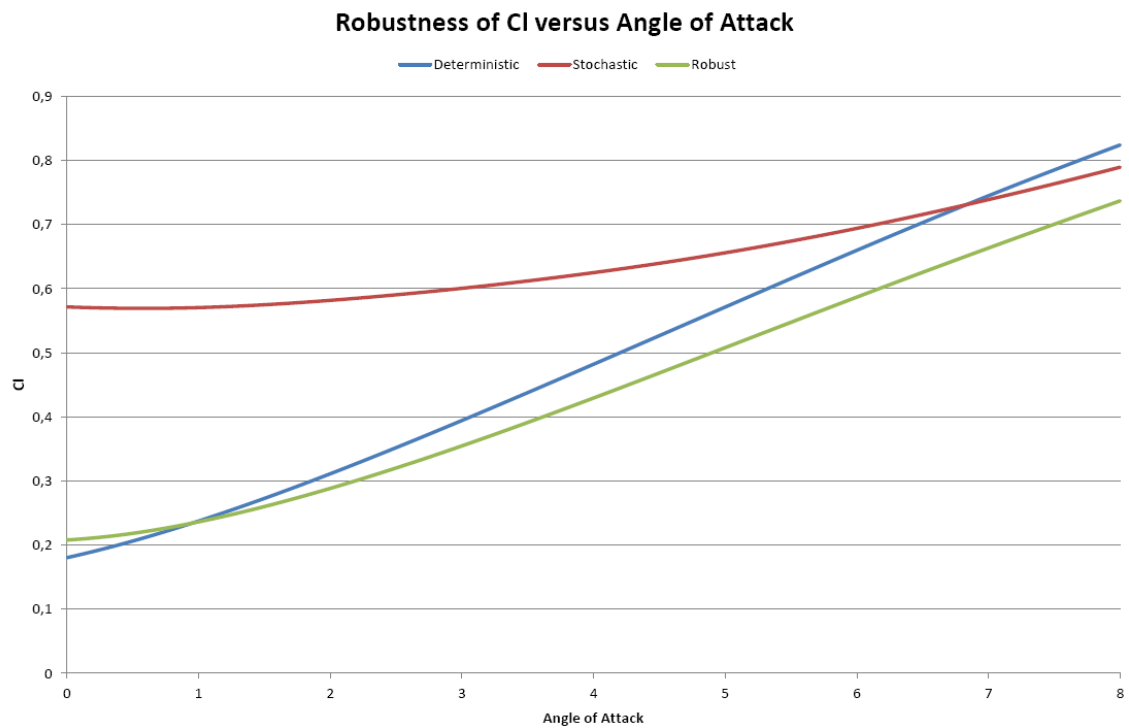
Figure 4-21.- Robustness of lift versus angle of attack for Deterministic, Stochastic and robust case
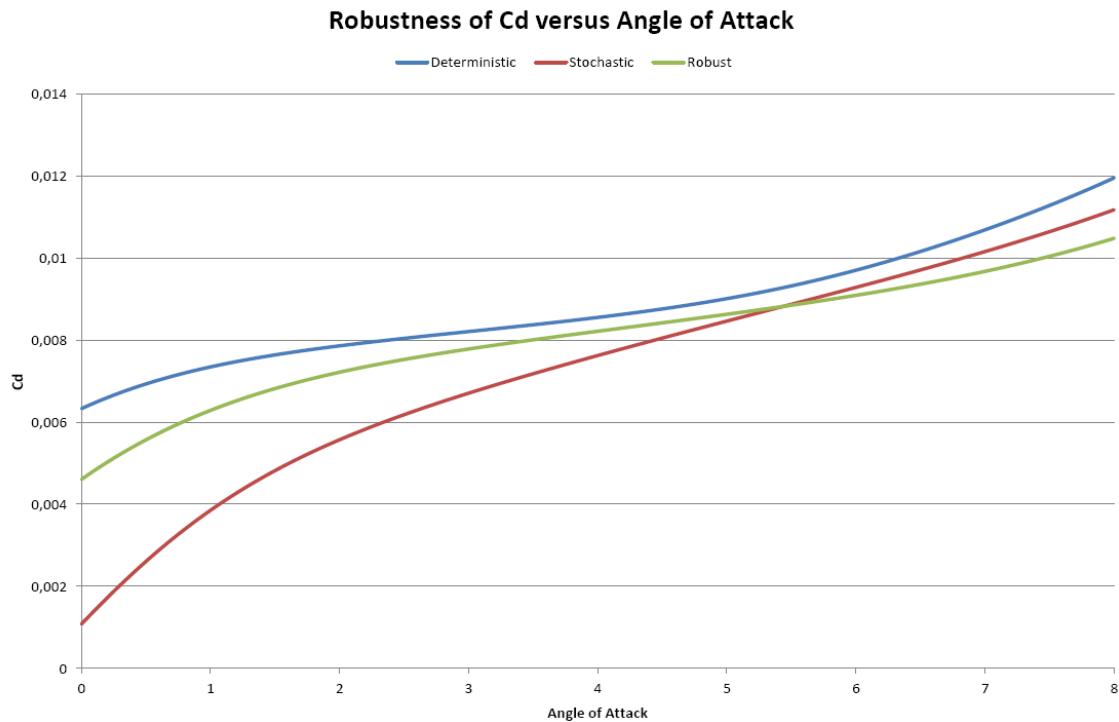
Figure 4-22.- Robustness of drag versus angle of attack for Deterministic, Stochastic and robust case
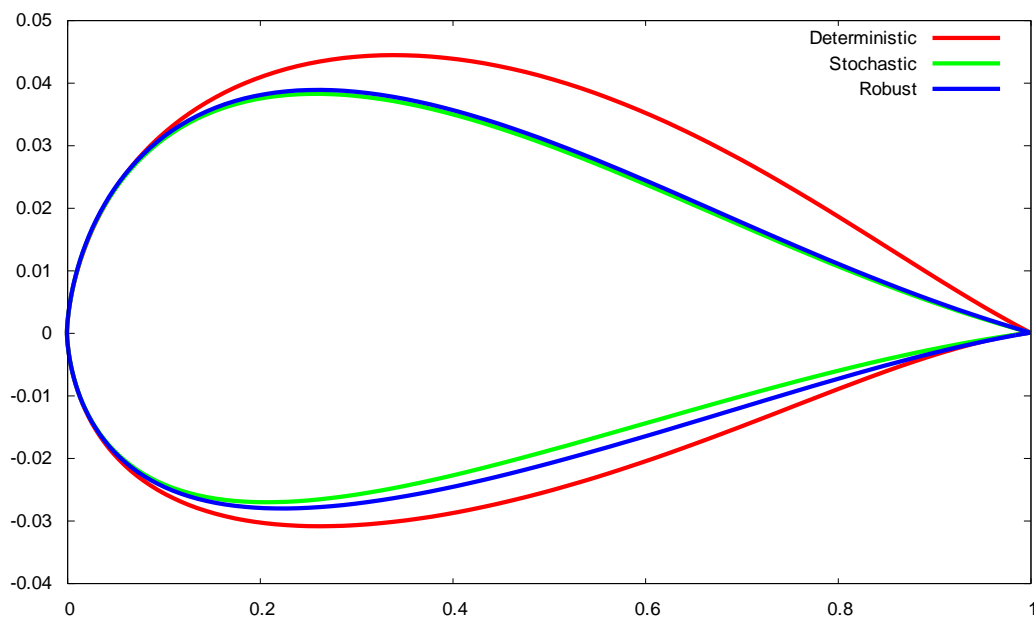
Figure 4-23.- Comparison of the optimal profile for Deterministic, Stochastic and robust case

Figure 4-23 shows the profile representation of three optimal results. Each of them has been selected from the best population of each analysed cases; namely one profile for the deterministic case, one for the stochastic case, and one for the deterministic case. It can be observed the similarities between deterministic and stochastic optimal profiles, while the difference with the robust optimal profile. Although, these three cases cannot be considered as the best representation of the general behaviour of the results, it can be taken as a good example. The deterministic case can be easily compared with the stochastic one. The objective functions they use are more similar than compared with the robust case.

The reader can observe how the resulting shape is modified when applying robust methodologies.

4.4.4 Conclusions

From the obtained results the reader could wonder which the best method is. The deterministic method is only using a single point value, which could miss information about variability under uncertain conditions. The stochastic method is already using the variability information to produce the mean value as its objective function. It can be seen as an improvement due to a better representation of the actual behaviour of the optimized phenomena. Finally, the robust method is using both the mean and the standard deviation. It means it is not only considering the input variability, or uncertainty, but also the output variability. The complexity of the method is increased, the computational cost is also increased, but the quality of the results, regarding the uncertainty quantification is greatly improved.

The simple set of three parallel test cases has enabled the comparison of the different behaviour of a CFD analysis under deterministic, stochastic or robust definition. Anyway, engineers should take into account that the more simplified the model is, the less accurate it is. The computational cost associate to uncertainty quantification techniques is a drawback, but if the phenomenon has a large stochastic component the computational cost is no longer a drawback compared with the accuracy the designer obtains.

Deterministic and Stochastic cases can be easily compared, mainly because of the fact that both of them define only two objective functions. The objective functions have a comparable meaning; the deterministic value and the stochastic mean are almost the same. The robust case, which includes the standard deviation values, introduces new dimensions on the result space. If the space of results has a large dimension, methods as SOM (Self-Organized Maps) should be used.

Both stochastic and robust cases use the variability information as an input. It means that both of them take into account the variability and the robustness of the solution. The main difference is the definition of the standard deviation as an objective function, which not only ensures the analysis of the variability of the input variables, but also ensures taking into consideration the variability of the objective functions.

The reader can appreciate how the stochastic and the robust test cases can provide lower optimal values compared with the deterministic cases. But on the other hand, the robustness of these solutions of the stochastic and robust cases improves the obtained for the deterministic case.

Comparing the stochastic and the robust case, the designer should select if it is required to deal with the standard deviation as an additional objective function, which increase the complexity of the solution space, or if it is enough to consider the mean value.

4.5 Definition of the initial population on the optimization process

4.5.1 Introduction

The main objective of the analysis in this section has been to check the influence of the initial population guess. Usually, the initial population is randomly generated. Here two extreme cases have been defined: the first one has defined a regular distribution of population members across the search space, and the second one has defined a concentrated location of the members of the population.

4.5.2 Procedure and results

The problem takes the profile definition shown in Figure 4-10 as the base line. The geometry is modified thanks to the use of Bezier curves. The knot coordinates of the Bezier curves defining the profile are listed in Table 4-2. The optimization problem is defined as the maximization of the lift to drag ratio. No restrictions have been applied.

The optimization problem is defined as a maximization problem, so it can be written as:

Maximise	$f_1(x) = C_l / C_d$	4-17

The optimizer has been set-up with the following parameters:
- Number of populations: 45
- Population size: 10
- Probability of crossover: 0,95
- Probability of Mutation: 0,02

Name of the variable value	Control Points		Value ranges	
	X coordinate	Y coordinate	Lower Limit	Upper limit
Coordinates x1s, y1s	0	0	-	-
Coordinates x2s, y2s	0	0,05	-	-
Coordinates x3s, y3s	0,25	Random	0,05	0,085
Coordinates x4s, y4s	0,5	Random	0,03	0,06
Coordinates x5s, y5s	0,75	Random	0,01	0,02
Coordinates x6s, y6s	1	0	-	-
Coordinates x2l, y2l	0	-0,05	-	-
Coordinates x3l, y3l	0,25	Random	-0,06	-0,03
Coordinates x4l, y4l	0,5	Random	-0,035	-0,02
Coordinates x5l, y5l	0,75	Random	-0,015	-0,005
Assigned Values				
Angle of attack	4			
Mack number	0,7			

Table 4-2: Problem definition values

In order to compare the sensitivity of the optimization algorithm with respect to the initial population two types of initial population have been defined. The first one is

regularly distributed across the search space. The second one is located in a random location concentrating all the members of the initial population within a small area of the search space. The solutions for both cases present a similar optimum value.

Figure 4-24 shows the results for the regularly distributed initial population. The reader can observe how the maximum values remain almost constant along the generations, while the mean value of the C_l/C_d ratio tends to the optimal value. Figure 4-25 shows the results for the concentrated initial population. Both the maximum and the mean value of each generation show a clear trend to the optimum value.

As mentioned, Figure 4-24 does not show a clear trend, while the values remain around the optimum one from the beginning of the analysis. Some of the analysis present a lost of quality, decreasing their values and not improving the previous generation. These poor values are a consequence of the search strategy of the Evolutionary Algorithm, which uses the mutation as the mechanism to avoid local minima. The mutation ensures that all the search space is scanned, while the convergence to the optimum is recovered in few next generations.

On the other side, when the initial population is located close to a certain area, the behaviour of the analysis is completely different. The evolution of the maximum values converges to the optimum in an asymptotic way, reaching quite the same optimum value as in the previous case. Both analyses can be said to converge to same optimum value. Figure 4-25 shows the maximum and the mean values evolution of each calculated generation for the concentrated initial population.

Figure 4-25 shows the evolution of the C_l/C_d means of each generation. It can be observed both maximum and mean values are representative of the general trend to the optimum; although the maximum has been considered as our final objective function.
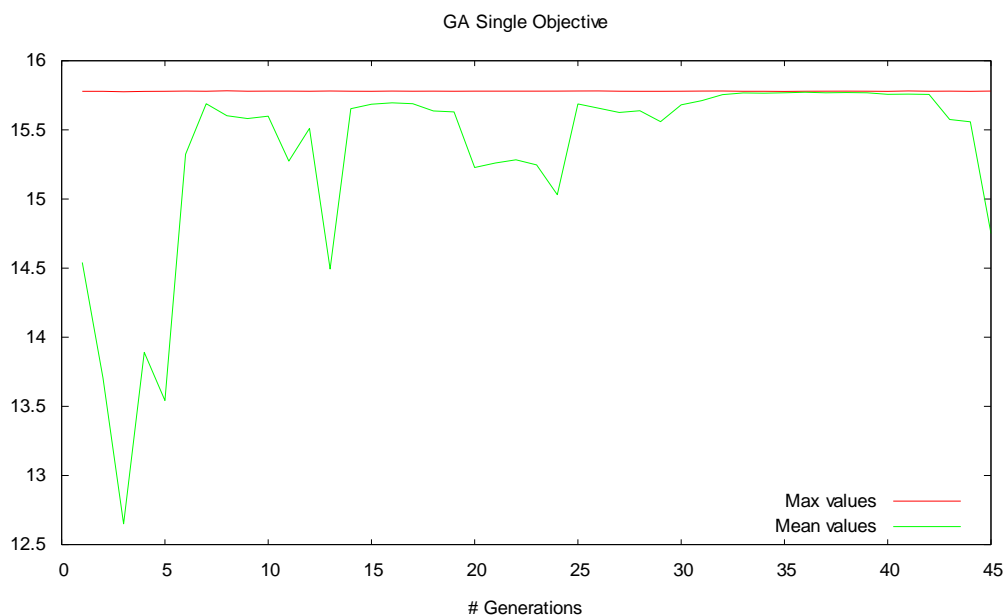
Figure 4-24.-Cl/Cd evolution with a regularly distributed initial population
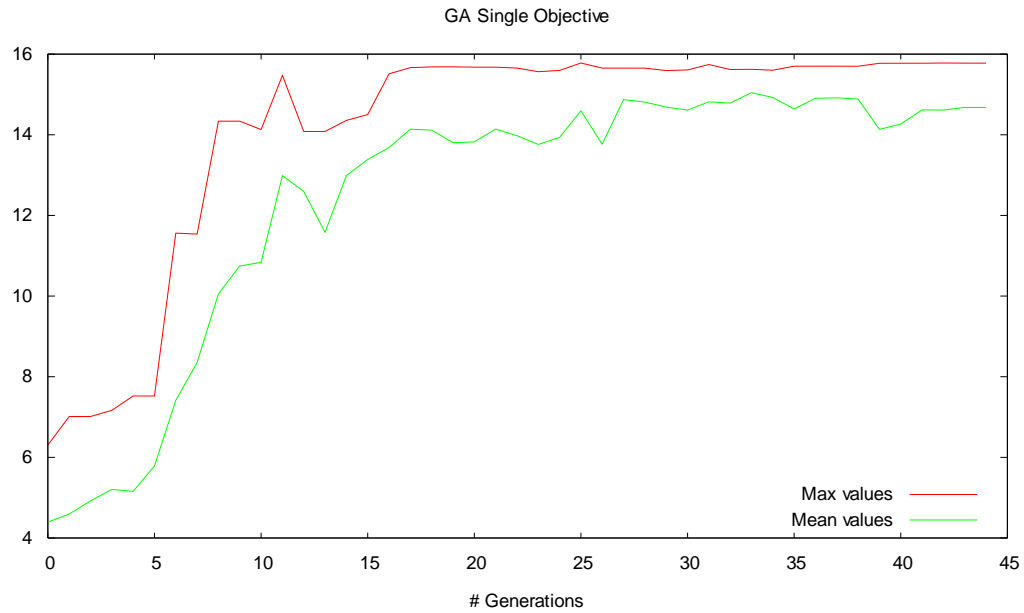
Figure 4-25.- Cl/Cd maximums evolution; concentrated initial population

4.5.3 Conclusions

The main difference is that the case using a regularly distributed initial population seems to converge to a value similar to the initial one. While the other case present a clear convergence to an optimum value.

Two strategies for the definition of the initial population have been compared. The random generation of the initial population that Evolutionary Algorithms mainly uses is switched to a user-defined initial population. It enables the comparison of two extreme cases of the random generation, in order to ensure if both reach the same optimum value.

It can be concluded that evolutionary algorithms are robust enough to converge to an optimum solution whichever the initial population is generated. Both random and fixed generation of the initial population produce similar effects and no improvement is introduced in the results.

4.6 Applying enhancements to the stochastic method

4.6.1 Deterministic procedure

4.6.1.1 Introduction

Taking advantage of a multi-objective definition of the CFD problem, several enhancements have been tested and evaluated. An improvement on the efficiency of the method has been looked for thanks to the use of surrogate models, and the Latin Hypercube sampling technique.

The deterministic solution of the problem has been defined as the reference point to

validate the new results.

4.6.1.2 Procedure

The problem to be solved is basically the optimization of a 2D profile (Clarich et al, 2004; Pediroda et al, 2004), as it has been made in the previous single-objective problem. Two objective functions have been defined to be minimized; the first one is the inverse of the lift coefficient, C_l, in order to maximize its value, and the second one is the drag coefficient, C_d. Bezier curves have been used to define the profile shape in order to ensure a smooth shape (see Figure 4-10). Coordinates of the knot points which define the upper and lower profiles have been selected as the input values of the genetic algorithm. In addition, the flow conditions have been defined as secondary input parameters. These parameters are the angle of attack and the Mach number, which take the values in Table 4-3. The selection is mainly intended to reproduce the flight conditions during straight and stabilized flight in a transonic regime.

In order to decrease the computational time of each solver evaluation, and, consequently, the computational effort of the global optimization process, an Artificial Neural Network has been used as surrogate model of the solver.

The parameter values for the configuration of the evolutionary algorithm are:
- Number of populations: 500
- Population size: 24
- Probability of Crossover: 0,95
- Probability of Mutation: 0,16667

The problem has been defined as:

Minimise	$$f_1(x) = \frac{1}{C_l}$$ $$f_2(x) = C_d$$	4-18

No restrictions or constraints are applied. The search space is defined according the range of values in Table 4-3.

Name of the variable value	Control Points		Value ranges	
	X coordinate	Y coordinate	Lower Limit	Upper limit
Coordinates x1s, y1s	0	0	-	-
Coordinates x2s, y2s	0	0,05	-	-
Coordinates x3s, y3s	0,25	Variable	0,05	0,085
Coordinates x4s, y4s	0,5	Variable	0,03	0,06
Coordinates x5s, y5s	0,75	Variable	0,01	0,02
Coordinates x6s, y6s	1	0	-	-
Coordinates x2l, y2l	0	-0,05	-	-
Coordinates x3l, y3l	0,25	Variable	-0,06	-0,03
Coordinates x4l, y4l	0,5	Variable	-0,035	-0,02
Coordinates x5l, y5l	0,75	Variable	-0,015	-0,005
	Assigned Values			
Angle of attack	2,79			
Mack number	0,734			

Table 4-3: Problem definition values

The neural network has been trained with evaluation data from TDYN and PUMI solvers. TDYN has provided subsonic data, and PUMI has provided transonic data. Two different surrogate models have been generated to ensure the accuracy. One of them has been trained with the subsonic regime data, and another one has been trained with the transonic regime data.

In order to train the Neural Network (ANN) 400 evaluations have been required. To ensure the quality of the training process this is the minimum amount of evaluation, and all of them must be representative of the search space. Table 4-3 shows a comparison for a fixed number of evaluations when the ANN is already trained, and when the direct evaluation of the solver is used.

	EA run defining 750 generations and 8 individuals	
	Using ANN	Using the analysis tool
Generation of training Values (400 samples)	12h	--
Training Process	1h	--
Validation process	0,5h	--
EA calculation	1,5h	200h
Total	15h	200h
	-92,5%	

Table 4-4: Cost comparison for a fixed number of evaluations using ANN or the analysis tool

In this example, the Artificial Neural Network has been trained before the integration into the optimization loop. It could be trained during the execution of the optimization analysis, taking advantage of the evaluation of the individuals to train the network. It means that the training process and the validation process would take longer, because of the fact they would have been repeated several times.

4.6.1.3   Results of the deterministic procedure

Figure 4-26 shows the best population, the initial population and the whole set of result values of this analysis. The solutions on the Pareto Front have been plotted in Figure 4-27. Figure 4-27 shows the shape of the optimum profiles, while Figure 4-28 shows the profiles of the initial population and the values of the objective functions.

Figure 4-26 includes the plot of the non-dominated solutions, the optimal ones in green, the whole population, in red, and the initial values obtained from the multi-objective problem.

Comparing the shape of the best profiles and the initial ones, Figure 4-27 and 4-28, the reader can observe that the best ones define specific characteristics to the profile that the initial ones do not consider. A clear example is the trailing portion, which is thinner. In addition, the best profiles define a trend to two or three best shapes.
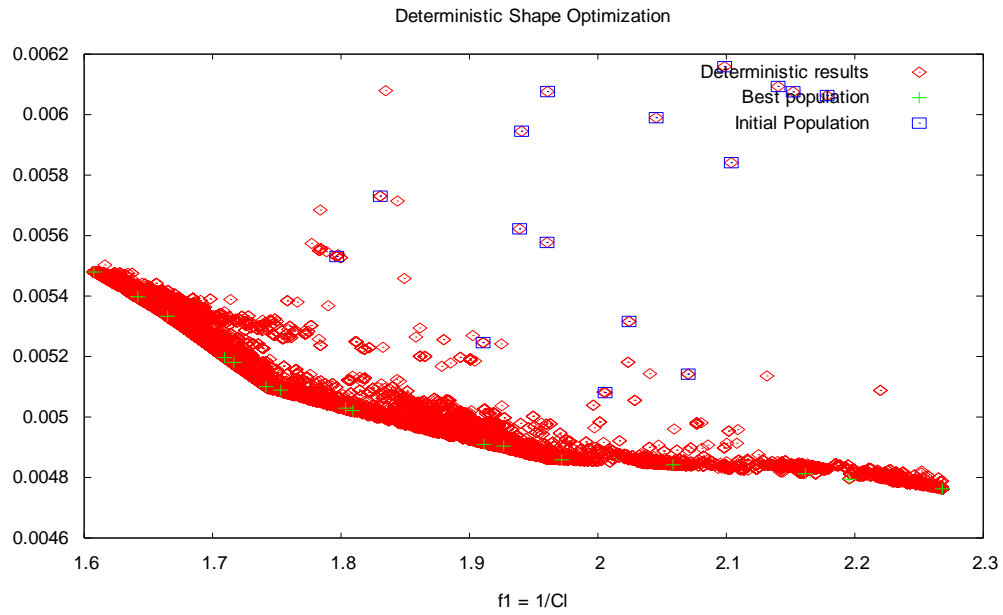
Figure 4-26.- Pareto Front, whole population and initial population; deterministic case
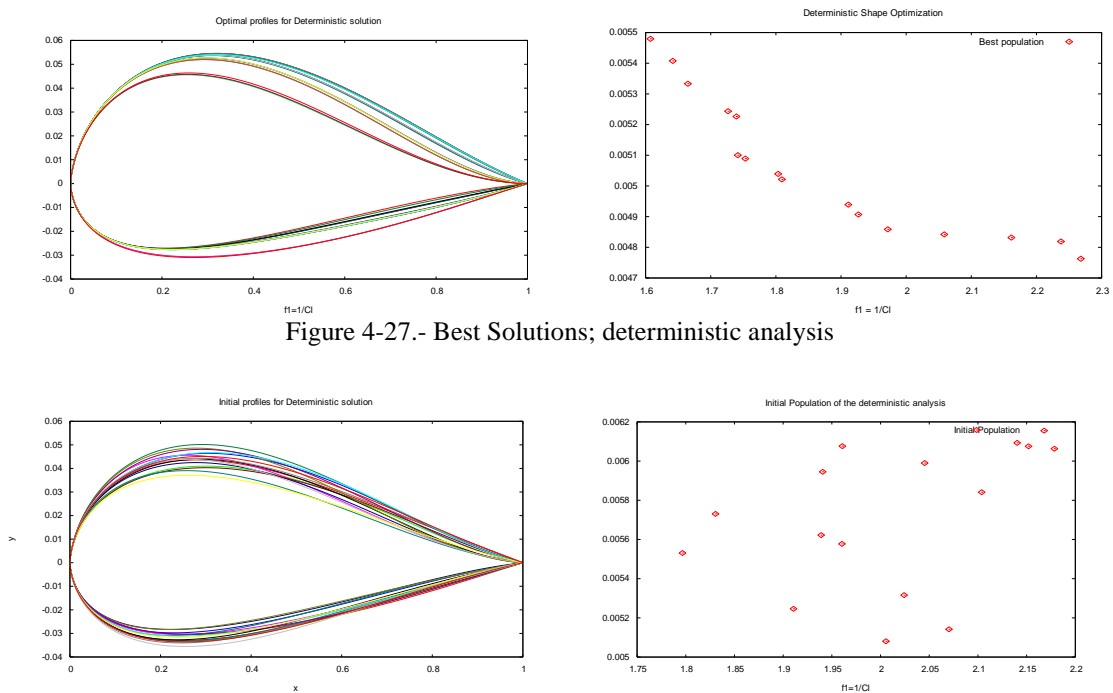
Figure 4-27.- Best Solutions; deterministic analysis

Figure 4-28.- Initial Population

4.6.2 Stochastic procedure

4.6.2.1 Introduction

The stochastic procedure has now been applied to a CFD optimization problem. The results from this analysis have been used as a comparative point when the same problem has been solved using a surrogate model.

4.6.2.2 CFD problem definition

The optimization problem has been defined as:

Minimize	
$$f_1 = \mu\left(\frac{1}{C_l}\right)$$ $$f_2 = \mu(C_d)$$	4-19

RAE2822 has been selected as the baseline design, and it has been parameterized using Beziers curves. See Figure 4-10 form details.The constraints for the knot points have been defined as in the previous section.

The parameter values for the configuration of the evolutionary algorithm are:
- Number of populations: 150
- Population size: 24
- Probability of Crossover: 0,95
- Probability of Mutation: 0,16667

Applying the values on the Table 4-3, additional constraints are stochastically defined on Table 4-5 in order to define a Gaussian distribution for Angle of attack and Mach number.

	Mean	Standard Deviation
Angle of attack	2,79	0,279
Mach number	0,734	0,05

Table 4-5: Stochastic Constraints

The geometry related variables are controlled by the optimization algorithm itself. They have been defined as the design variables. The stochastic samples have been used to define a set of evaluations for each individual to calculate the fitness function as the mean of all the evaluations.

The total number of samples used to evaluate each individual has been 250. The selection has been done due to the fact that previous tests have shown that the accuracy of a 250 samples set is accurate enough for this research purpose compared with the real mean value.

4.6.2.3 Results of the stochastic procedure

Figure 4-29 and 4-30 show the results obtained with the stochastic analysis, using 250 samples for the stochastic definition of the variables. Both plots of the whole population and the Pareto front have been obtained from the same analysis.
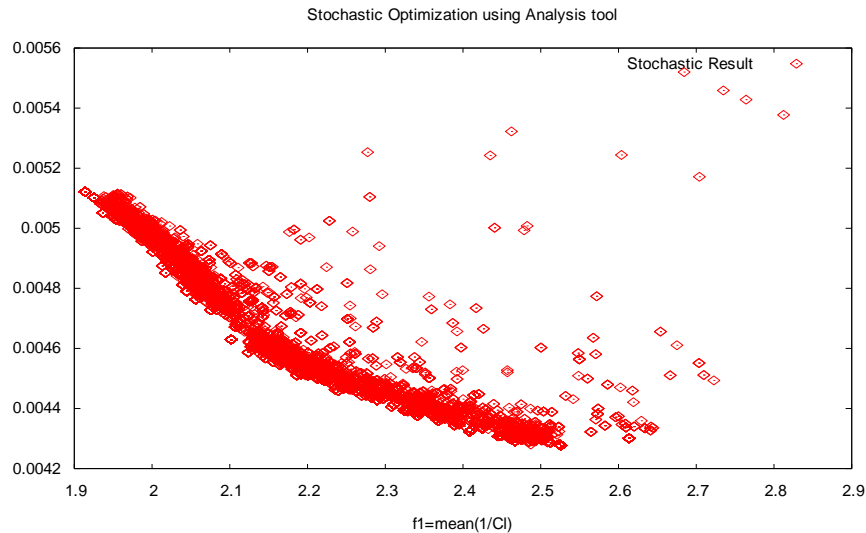
Figure 4-29. Stochastic result
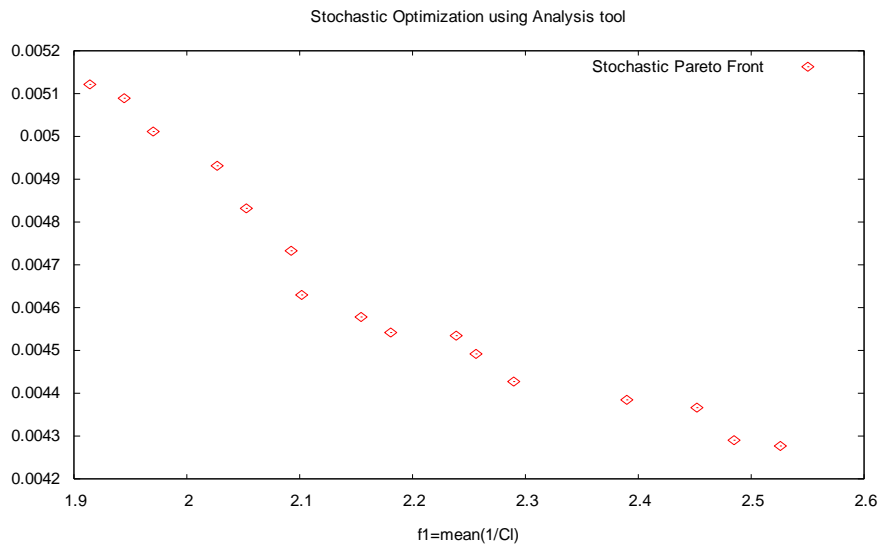
Figure 4-30. Stochastic Optimal Pareto Front

Figure 4-31 shows a comparison between the deterministic and the stochastic optimization solutions. Both of them use the same problem definition except for the angle of attack and the Mach number, which are the stochastic variables. Both use ANN coupled with the optimizer.

The reader can observe that the shapes of both Pareto fronts are similar, but one front is displaced with respect to the other one. The stochastic front is clearly forwarded, as it can be seen in the amplified picture. Solutions are different because the stochastic solution is dealing with the mean of a cloud of evaluations instead of a single value as in the deterministic case. Some of these points are affected by the presence of a shock wave whereas the deterministic optimization does not take into account the possibility of having this shock wave. From this point of view, the stochastic definition produces a more robust solution. Closest Pareto fronts could be obtained in low subsonic situations, but when the research is focused on transonic flow fields the differences are relevant.

The same behaviour, just described, can be observed in the mathematical test cases in section 4.3. The front of the stochastic solution has displaced in comparison with the deterministic one.
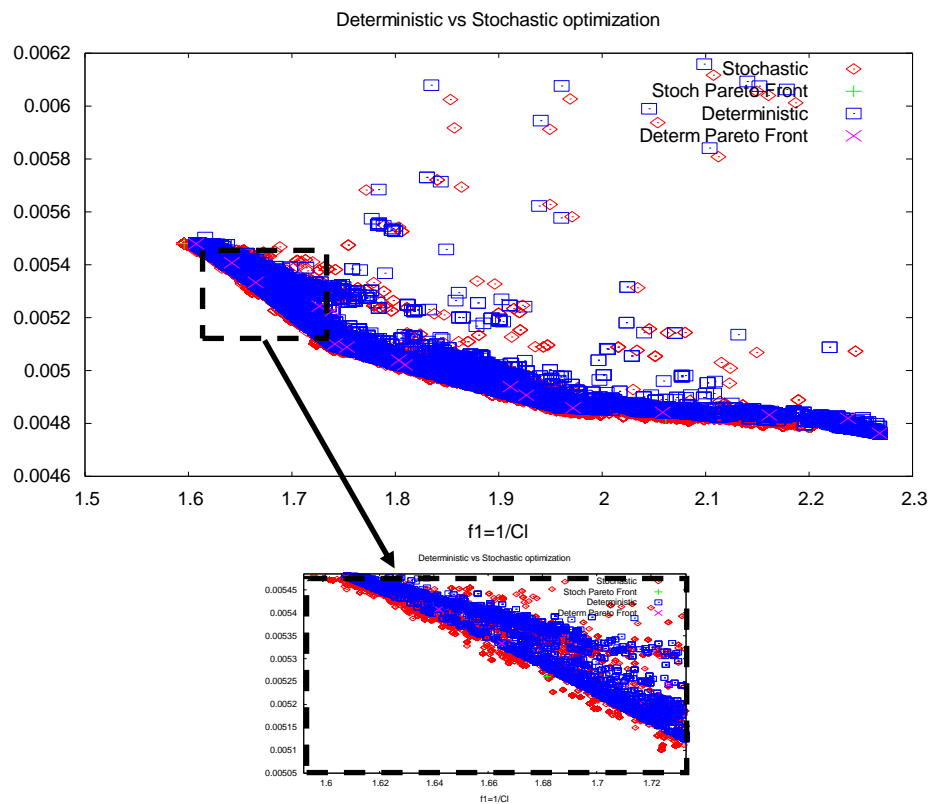
Figure 4-31. Comparison between deterministic and stochastic results

Figure 4-32 show the solution to the same problem but using only 10, 50, 100 or 150 stochastic evaluations of each individual. Figure 4-32 shows the whole populations and Figure 4-33 shows the Pareto fronts.

The reader can observe that 10 samples analysis produces results with low accuracy; both the whole population and the Pareto front show bigger dispersions. The accuracy increases with the number of samples, but the reader can observe that those cases using 100, 150 or 250 samples are pretty similar, and only intrinsic variability of sampling can be detected.

Figure 4-32. Stochastic sampling comparison

Figure 4-33. Stochastic sampling comparison
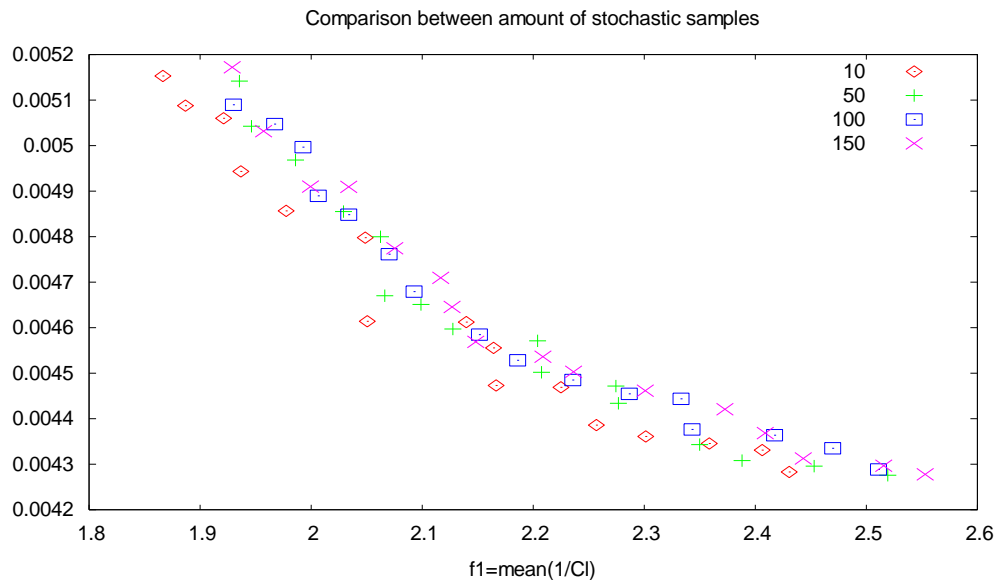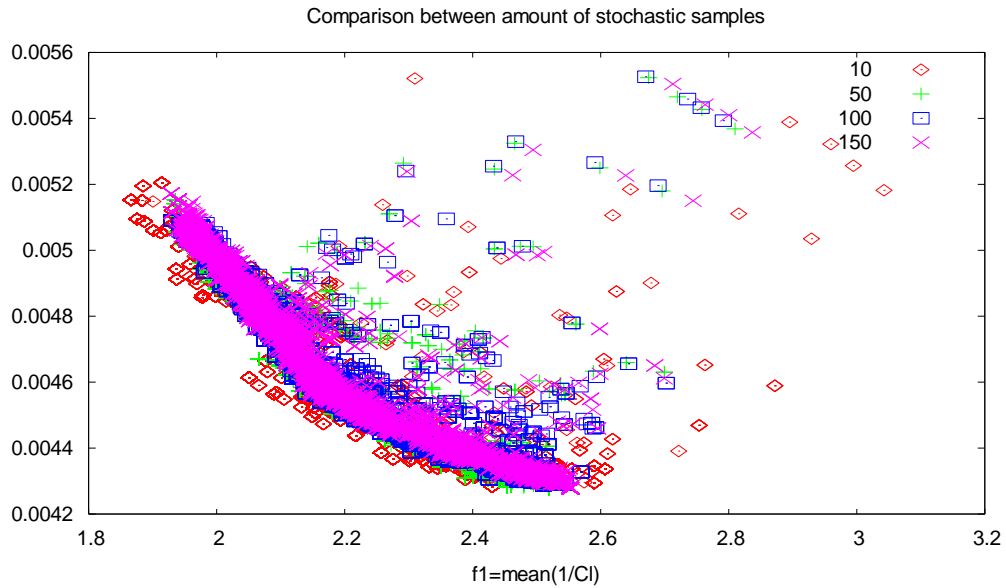
Comparing the obtained optimal solutions, it can be observed that a lower number of samples produces a more discrete dispersion of the geometries within the optimal range. On the other hand, increasing the number of samples a richer population of optimal solutions is obtained. Richer population means the optimal individuals differ from each other in a more significant way, so the optimal set better represents its optimality. When comparing the same analysis using several stochastic samples, expected result can be that all the optimal values belongs to the same Pareto front. Figure 4-33 shows it is not exactly true because the sampling variability must be taken into consideration in addition to the poor statistical definition when the number of samples is low.

Figure 4-34 to 4-37 show the profile shapes of the optimum individuals when using different number of stochastic samples. Figure 4-34 shows the 10 stochastic sample solutions, Figure 4-35 shows the 50 stochastic sample solutions, Figure 4-36 shows the

100 stochastic sample solutions, and Figure 4-37 shows the 150 stochastic sample solutions.
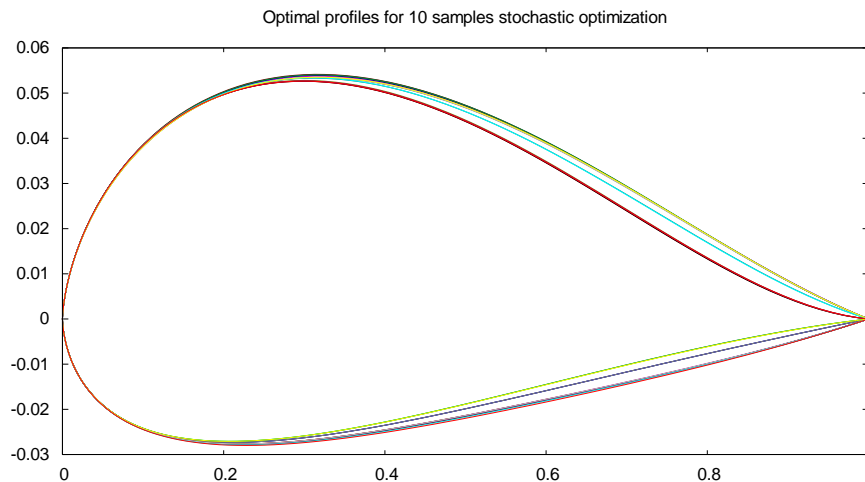
Figure 4-34. Stochastic sampling comparison; optimal geometries with 10 stochastic samples
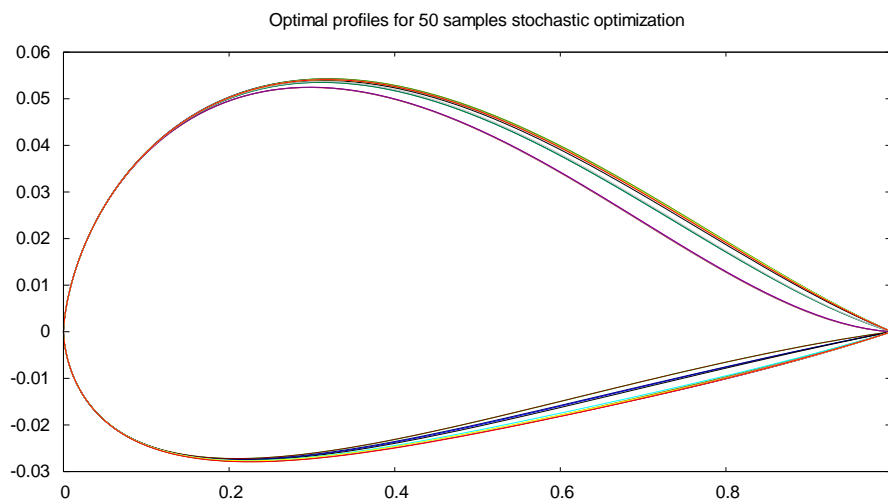
Figure 4-35. Stochastic sampling comparison; optimal geometries with 50 stochastic samples

Comparing a multi-point method to the one applied here is worst to mention that, first of all, almost all the multi-point methods use a simple discretization of the search space. In this research, sample values are taken from the statistical definition of the stochastic variables. It means they follow a mean and standard deviation when a Gaussian distribution is used, or uniformly and randomly spread along the search space when a uniform distribution is defined. The procedure selects the stochastic samples according the definition of the variable. On the other hand, usual multi-point discretization uses few points. As it has been demonstrated, the lower the number of stochastic samples is, the lower the accuracy is. From statistical theory, it is clear that variance of a set of samples strongly depends on the number of samples.
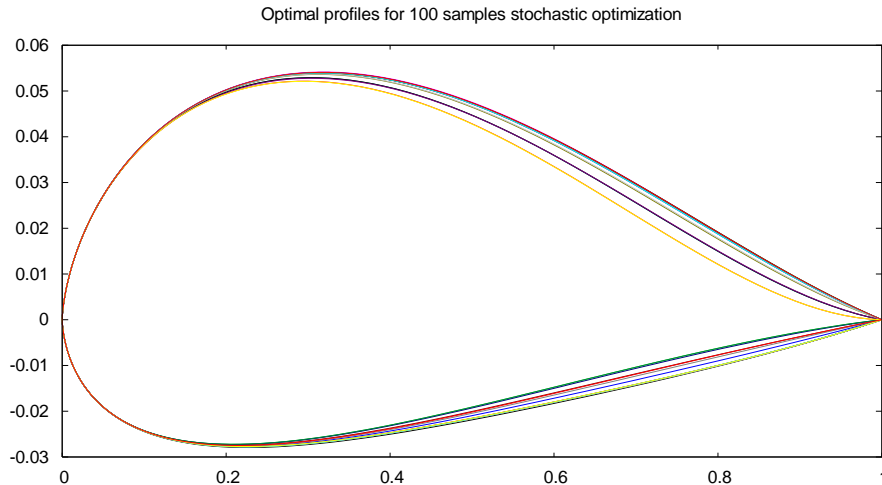
Figure 4-36. Stochastic sampling comparison; optimal geometries with 100 stochastic samples
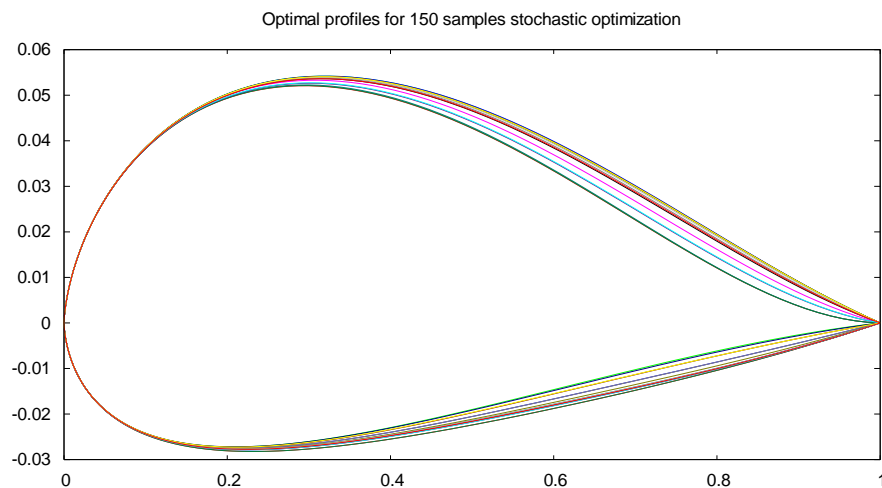
Figure 4-37. Stochastic sampling comparison; optimal geometries with 150 stochastic samples

4.6.3 Stochastic procedure using a surrogate model

4.6.3.1 Introduction

Previous research has demonstrated how expensive a CFD analysis can be. Stochastic procedure for optimization requires the calculation of a big amount of individuals, which are highly increased when dealing with uncertainty quantification techniques, mainly if they are based on Monte Carlo method. The use of a surrogate model has been considered to keep the computational cost under reasonable limits. The Artificial Neural Networks have been selected due to their capability to deal with a vast type of problems. It will be integrated in the evolutionary algorithm and the stochastic tool.

Neural Networks provide a powerful tool for reducing the calculation time. After a required training, the network will obtain a result much faster than performing the calculation itself. Based on the research of Lopez (2007), a Neural Network has been embedded into the evolutionary algorithm code. The Multilayer Perceptron Model ((Lopez and Oñate, 2006), (Lopez, Balsa-Canto and Oñate, 2008)) is the type of

Artificial Neural Network selected due to its good performance dealing with regression and model generation problems.

Exactly the same problem as defined in section 4.6.2.2 has been analysed used the surrogate model. The only difference is that a surrogate model has been previously trained and used instead of the solver. In order to train the networks parameters have been defined within the same range as defined in **¡Error! No se encuentra el origen de la referencia.** and Table 4-5.

4.6.3.2   Results of the stochastic procedure using a surrogate Model

The usual procedure when working with surrogate models is to use them only for around the 25% of the evaluations. The stochastic robust procedure quickly increases the total amount of evaluations, so even reducing them to 25% does not mean a significant increase of speed. What has been proposed is to completely substitute the analysis tool with the surrogate model. It implies to ensure and control the surrogate model accuracy.

The used Artificial Neural Network (ANN) has been trained in order to provide results with less than 1% of error. In order to ensure ANN feasibility, it has been compared the Pareto fronts obtained using the direct analysis tool and the ANN. Figure 4-38 shows both Pareto fronts and the difference existing between them. This difference remains below a 3% at maximum, which has been considered as acceptable.
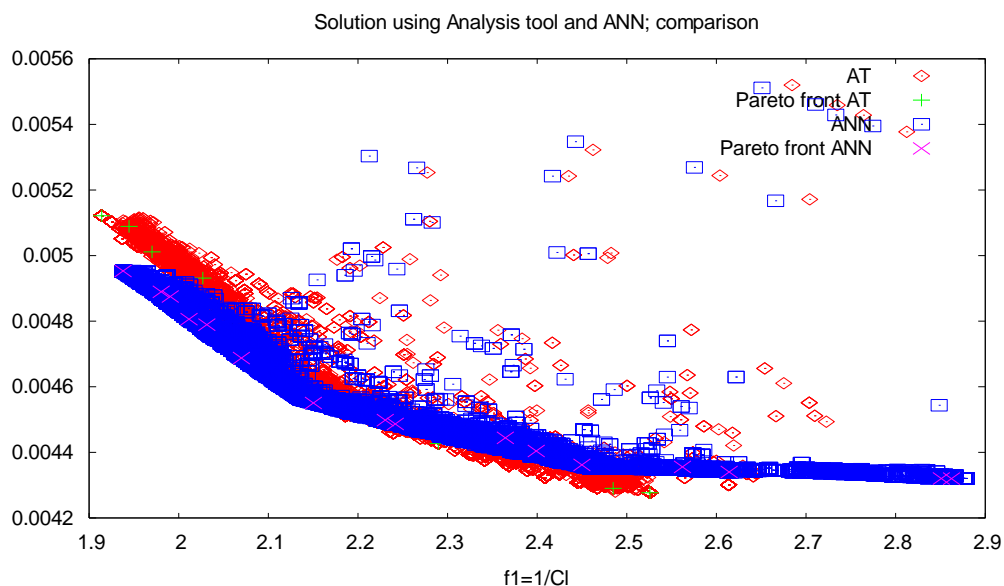
Figure 4-38. Analysis tool and Surrogate model comparison

4.6.4 Variability of the stochastic samples

4.6.4.1   Introduction

In Section 3.5 a variability analysis has been performed in order to detect how sampling affects the results. Two sampling techniques have been compared; namely Monte Carlo and Latin Hypercube. In the present chapter, similar analysis has been performed into

an optimization process. The previous results have pointed out two main conclusions; namely the low effect sampling variability has on the stochastic analysis, and the negligible difference between Monte Carlo and Latin Hypercube sampling techniques. Similar tests have been performed when applying the stochastic and the robust procedure into the optimization process, in order to confirm what the previous analysis pointed out.

A brief summary of the comparative results between Monte Carlo and Latin Hypercube stochastic sampling is presented. Stochastic and robust procedures have been applied to the optimization process. The robust procedure has been seeking to evaluate if the best convergence of the variance of the Latin Hypercube technique produces some improvement in the optimization results.

4.6.4.2 Problem definition

The same problem as defined in section 4.6.1 has been analysed using Monte Carlo and Latin Hypercube sampling techniques. To define the stochastic and robust test cases several amount of samples have been defined and compared. Comparative data for 10, 50, 100, 150 and 250 samples have been used, in both Monte Carlo and Latin Hypercube sampling techniques.

- **Stochastic definition**

The objective functions are defined as follow:

Minimize		
	$$f_{1s} = \mu\left(\frac{1}{C_l}\right)$$ $$f_{2s} = \mu(C_d)$$	4-20

- **Robust definition**

The stochastic test case has used the mean values as fitness function. A robust test case has been performed using both mean and standard deviation. It has been already pointed that Latin Hypercube improves the convergence of the variance with low number of samples in comparison to the Monte Carlo sampling technique. The test case aims to check the influence of the standard deviation if it is used as a secondary fitness function.

The robust formulation of the fitness functions of the problem is:

Minimize		
	$$f_{1r} = \mu\left(\frac{1}{C_l}\right)$$ $$f_{2r} = \sigma\left(\frac{1}{C_l}\right)$$ $$f_{3r} = \mu(C_d)$$ $$f_{4r} = \sigma(C_d)$$	4-21

The applied constraints and stochastic definition of the parameters are the same as in the previous case. The number of used samples is 10, 50, 100, 150 and 250 samples in both MC and LHS cases.

4.6.4.3   Random and fixed stochastic sampling

A comparison is now established between the results of equivalent analysis when using a random stochastic sampling or a fixed stochastic sampling. A fixed stochastic sampling defines an initial set of stochastic random samples which is used all long the analysis. A random stochastic analysis generates the set of stochastic samples for each generation, or even for each individual to be evaluated.

In fact, the fixed sampling can be considered an extreme case of a multi-point optimization problem, but with a very high number of points. On the other hand, random sampling takes into account the statistical variability to ensure additional robustness of the solution.

Several tests have been performed regarding the sampling variability, the Monte Carlo and the Latin Hypercube techniques or the number of samples used to define the stochastic variables. All of these issues have been analysed and conclusions have been taken. An additional test has been performed regarding the definition of the initial population. It is usually randomly defined by the optimization method itself. What is done in this test is to analyse the result behaviour if the initial population is prescribed.

4.6.4.4   Defining the initial population

A comparison has been also established when initial populations are predefined. It has been compared how the optimization behaves if it uses Monte Carlo sampling with an initial population equal to the optimal one obtained by an analysis which uses Latin Hypercube sampling, and vice versa. Table 4-6 is a brief description of all the performed analysis in order to determine the variability effects on the results.

	Monte Carlo Analysis (MC)	Latin Hypercube Analysis (LHS)
Initial populations	- From MC sampling - From LHS previous analysis	- From LHS sampling - From MC previous analysis
Applied to	- Stochastic optimization - Robust optimization	- Stochastic optimization - Robust optimization
Objective	- Analysis of the variability induced by sampling - Comparison between MC and LHS	- Analysis of the variability induced by sampling - Comparison between MC and LHS

Table 4-6. Performed analyses

All these analyses have used a meta-model to surrogate the solver evaluation.

4.6.4.5   Results of the analysis of the Variability of the stochastic samples

4.6.4.5.1   Monte Carlo and Latin Hypercube sampling applied to stochastic optimization

- **Stochastic definition**

Firstly, the results using only two objective functions are shown. Fitness function values, C_l and C_d coefficients, are shown in Figure 4-39 and 4-40 with the entire population or only the Pareto front. Comparing the plots, the reader can observe no significant improvement can be obtained.
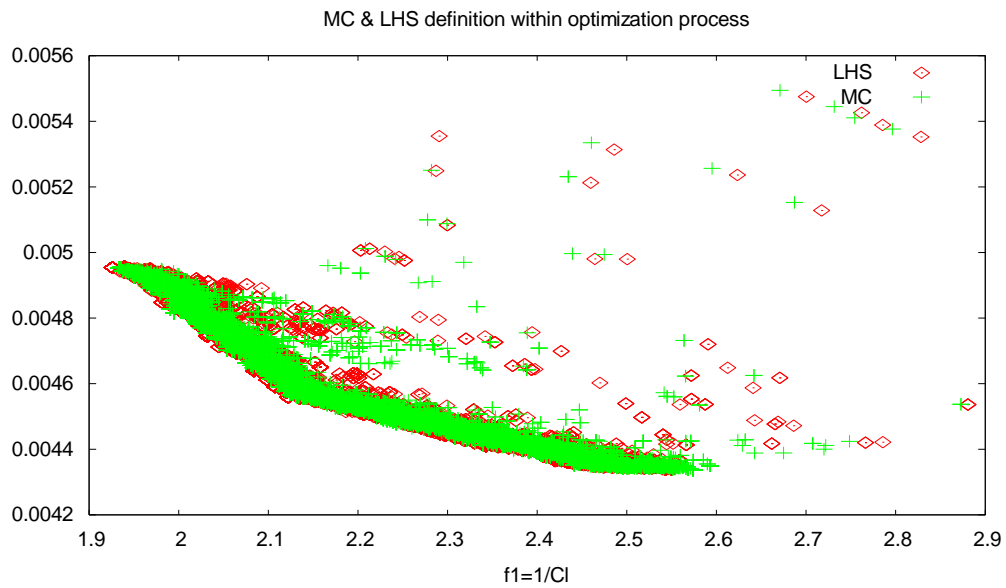
Figure 4-39. Comparison between MC and LHS.
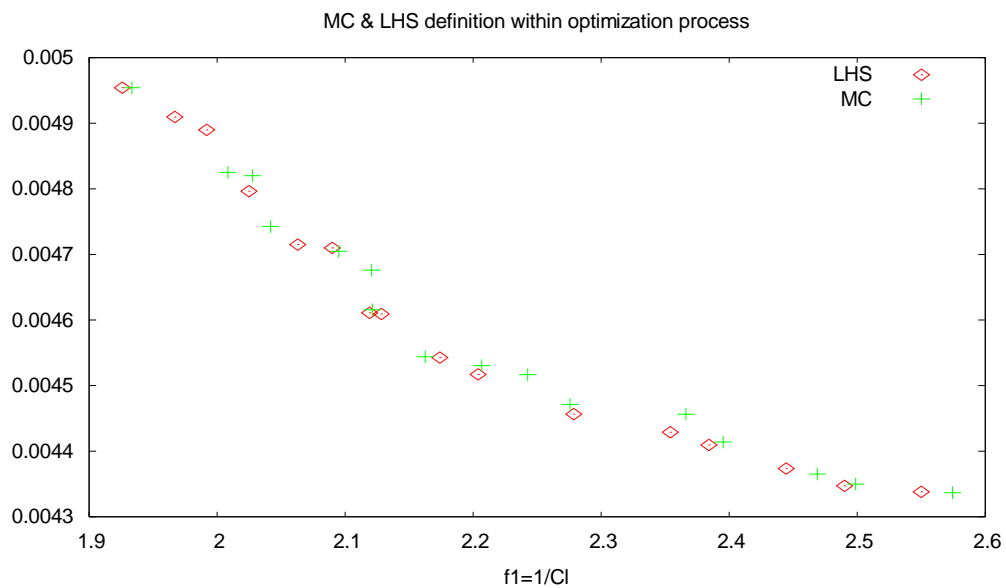
Figure 4-40. Pareto Front comparison between MC and LHS.

Monte Carlo (MC) and Latin Hypercube (LHS) comparison has been performed defining several amounts of samples. Comparative data for 10, 50, 100, 150 and 250 samples have been used, in both Monte Carlo and Latin Hypercube sampling techniques. Again, previous results are confirmed and negligible difference can be detected.

- **Robust definition**

The shape of the result is completely different when dealing with 4 objective functions. The introduction of two additional fitness functions creates a new problem, but slight differences between MC and LHS are detected.

Figure 4-41 to 4-46 show the Pareto front that combines the fitness functions. Figure 4-41 is the Pareto front combining f_{1r} and f_{2r} fitness functions. Figure 4-42 is the Pareto front combining f_{1r} and f_{3r} functions. Figure 4-43 is the Pareto front combining f_{1r} and f_{4r}. Figure 4-44 is the Pareto front combining f_{2r} and f_{3r} fitness functions. Figure 4-45 is the Pareto front combining f_{2r} and f_{4r} functions. And finally, Figure 4-46 is the Pareto front combining f_{3r} and f_{4r}.
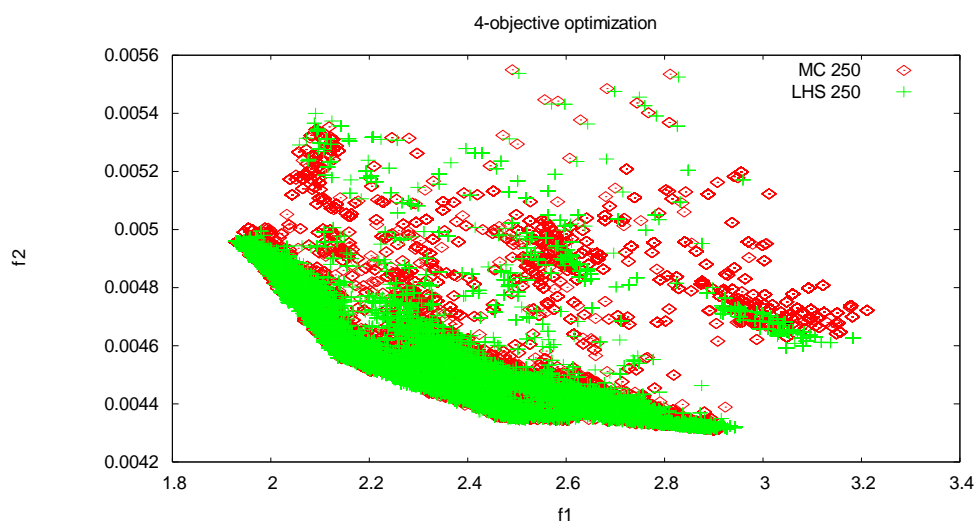
Figure 4-41. 4-objective results; plots of f_{1r} and f_{2r} fitness functions
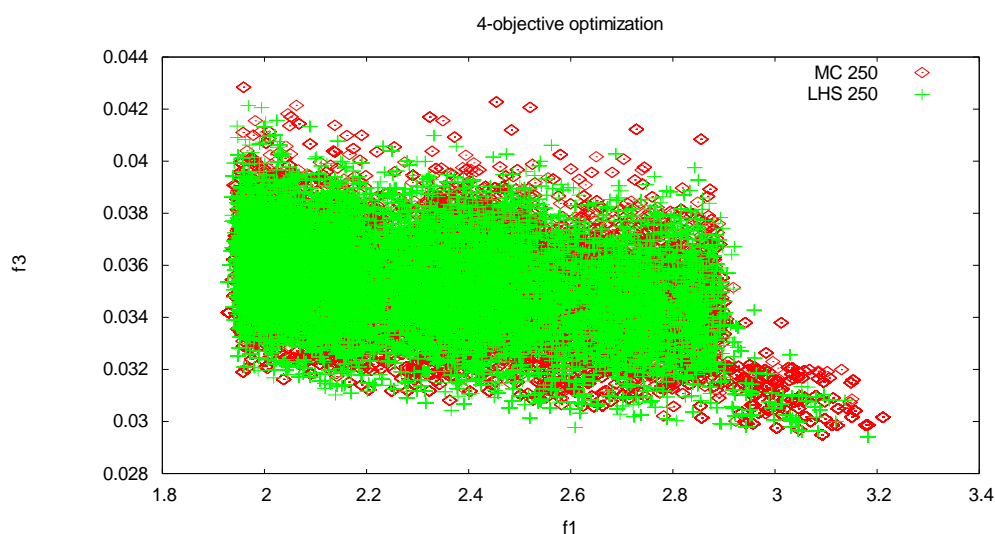
Figure 4-42. 4-objective results; plots of f_{1r} and f_{3r} fitness functions
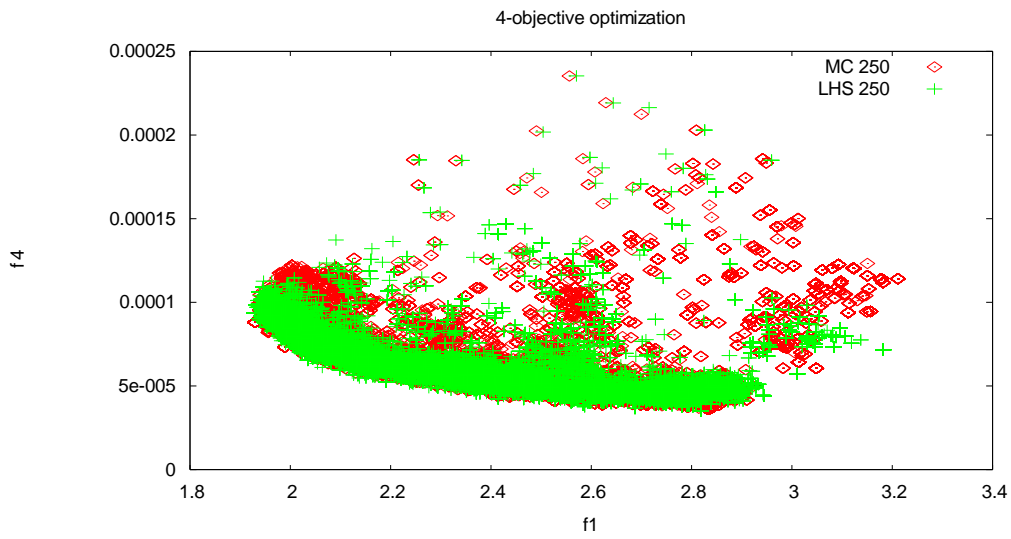
Figure 4-43. 4-objective results; plots of f_{1r} and f_{4r} fitness functions
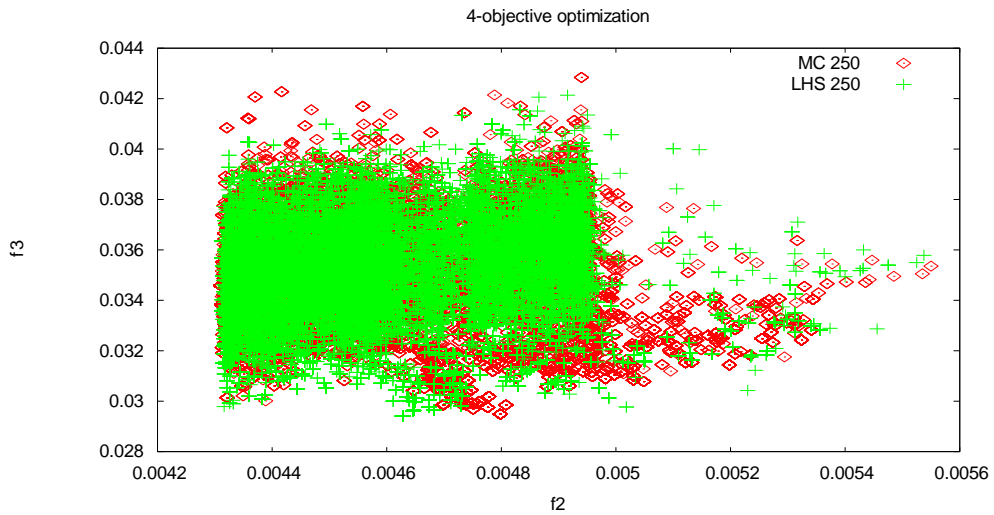
Figure 4-44. 4-objective results; plots of f_{2r} and f_{3r} fitness functions
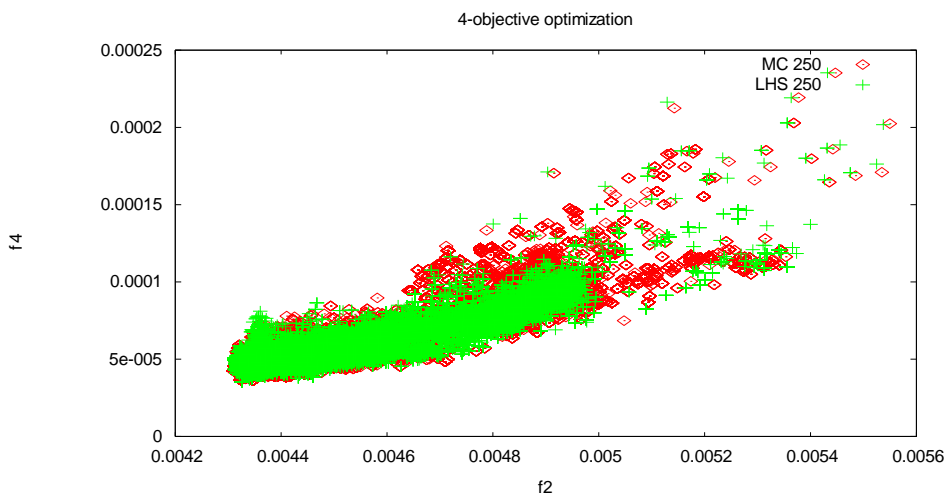
Figure 4-45. 4-objective results; plots of f_{2r} and f_{4r} fitness functions
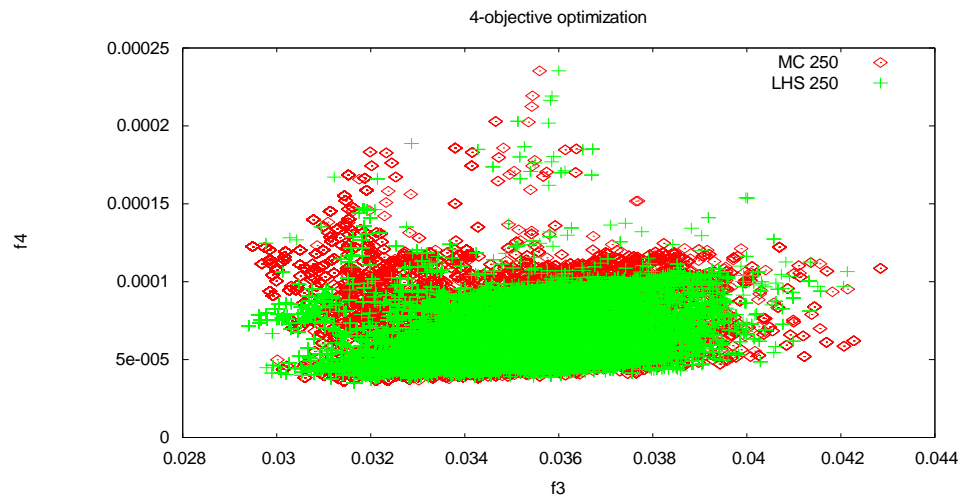
Figure 4-46. 4-objective results; plots of f_{3r} and f_{4r} fitness functions

The lift and drag's mean and standard deviation obtained in a four (4) objective optimization is represented by a four dimensional graph. To be able to plot it, the graph is split into pair of fitness functions. In all of them there are no significant differences between a 250 Monte Carlo samples analysis and a 250 Latin Hypercube samples one.

Other analyses that define less samples increase the variability due to intrinsic sampling variability, but both Monte Carlo and Latin Hypercube show a similar behaviour.

4.6.4.5.2 Random and fixed stochastic sampling

To compare the results using a random or a fixed set of samples the reader can focus on the shape of the Pareto fronts, Figure 4-47 shows how optimal results for the fixed definition lead to a poor number of individuals compared with those existing in the Pareto front obtained with the variable definition. The variable definition leads to a narrower front, producing results with lower values for f_1.
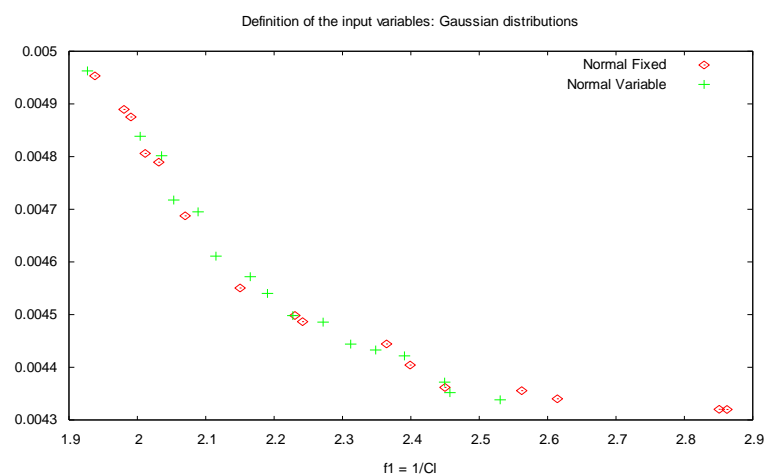
Figure 4-47. Comparison between Pareto fronts for Random variable and fixed definition.

Figure 4-48 shows the comparison between the fixed random definition and the variable random definition for each individual. It can be detected how the fixed definition also fixes the front of the solution, clearly defining a linear trend, while the variable

definition breaks this regularity. It means that the variable definition affects the evaluation of the fitness function enabling to capture better results.

A comparison of two different types of PDF has also been done. The Gaussian and the uniform PDF have been used and applied to the analysis of each individual during the optimization loop and it has not been detected any relevant difference between them.
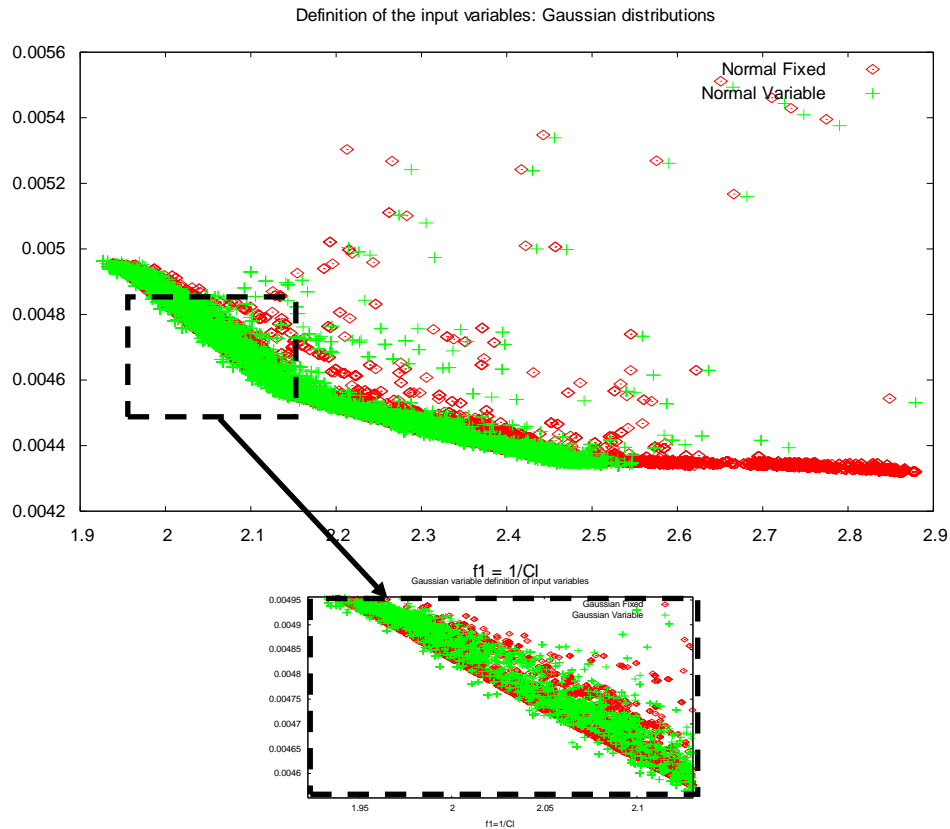
Figure 4-48. Comparison between Random variable and fixed definition and detail on random variable definition effects on the front.

4.6.4.5.3 *Defining the initial population*

First of all, two tests have been done to obtain the best population of one analysis using Monte Carlo sampling, and to obtain the best population using Latin Hypercube sampling. These two optimum populations have been prescribed as initial populations for an analysis using Latin Hypercube sampling, and for one using Monte Carlo sampling respectively. Figure 4-49 shows the optimal profile obtained in each case. These are the profiles that have been defined as the initial populations.
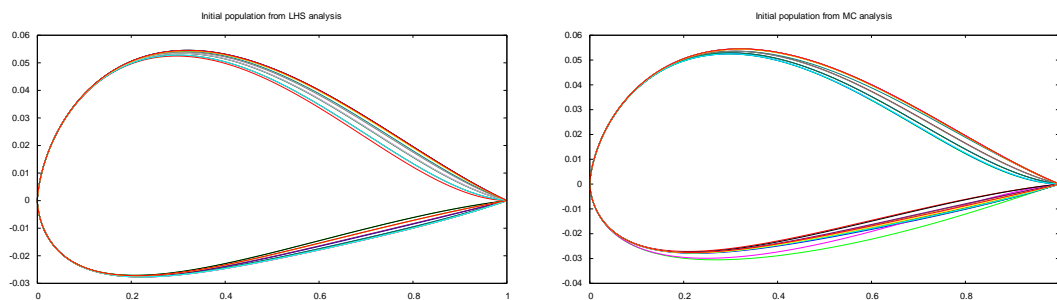
Figure 4-49. Optimal solution for LHS and MC sampling.

The same test is repeated three times to ensure robustness and convergence to the same results. Even though each analysis has been affected by the variability of the samples; the final result has almost been the same. Figure 4-50 shows a combined plot of the three whole populations, and the three Pareto fronts. It can be observed how similar they are. The robustness of the analysis is demonstrated. The third image in the Figure 4-50 is the optimal profiles of an analysis which uses Latin Hypercube samples, and an initial population from a Monte Carlo analysis.
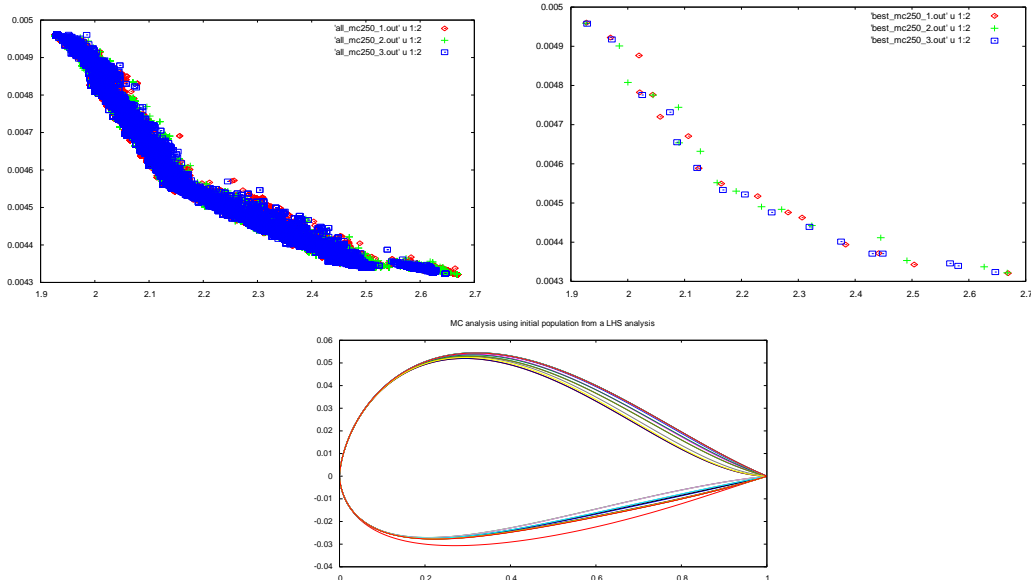
Figure 4-50. Results for LHS analysis using MC initial population.

The same procedure has been followed when applying Monte Carlo samples into the analysis which uses the Latin Hypercube optimal population as its initial population. It has been repeated three times to ensure its convergence and robustness, as well. Figure 4-51 shows similar images as in Figure 4-50. The first two images are the set of three whole populations, and the set of three Pareto Fronts. All three are pretty similar, and no relevant differences can be detected. The third image in Figure 4-51 is the set of optimal profiles.
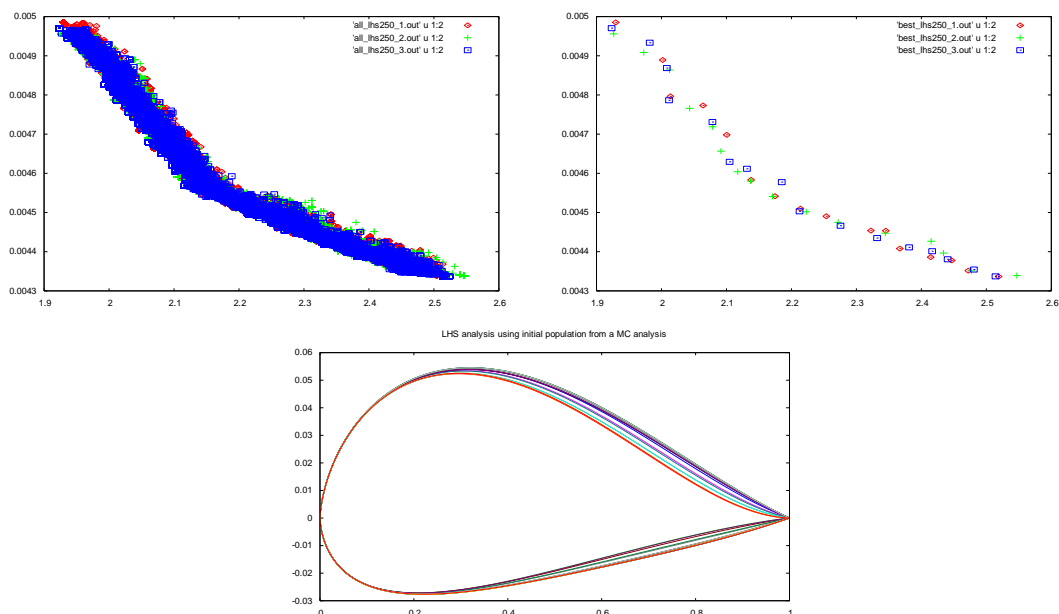
Figure 4-51. Results for MC analysis using LHS initial population.

Regarding the definition of the initial population, improvements cannot be detected on the optimal solution. However, it can be observed that the use of an optimal solution as the initial population will lead to a narrow distribution of the results, closer to the Pareto front; although Pareto front itself does not improve. The whole population is located near the Pareto Front, instead of being spread across a large area.

4.6.5 Probabilistic Collocation method

4.6.5.1 Introduction

The Probabilistic Collocation method is an uncertainty quantification method based on quadrature techniques. It calculates a set of fixed points using the information of the probability density function (PDF) of each variable. It can be considered a multi-point method because, given a PDF, it always produces the same points with the same weight.

Due to the fact the probabilistic collocation method is becoming a common method it has been compared with the stochastic method developed in this research.

4.6.5.2 Procedure

The optimization problem to be solved is the same as in previous sections. The evolutionary algorithm is controlling the geometry, and flow conditions are defined as stochastic variables. Stochastic variables have been defined using mean and standard deviation of a truncated Gaussian distribution. It is truncated at the 99.7% confidence interval.Same mean and standard deviation values as in the previous test case have been applied in order to enable the comparison. Evaluation points are now fixed to the following values:

	Mean	Standard Deviation	
Angle of attack	2,79	0,279	
Mach number	0,734	0,05	
Collocation point #	Angle of Attack	Mack number	Weight
1	1,034	-0,009	0,0026
2	1,792	0,312	0,0886
3	2,464	0,596	0,4088
4	3,116	0,872	0,4088
5	3,788	1,156	0,0886
6	4,546	1,477	0,0026

Table 4-7: Collocation points

The calculation method for mean and standard deviation of the outputs is described in equations 4-22 and 4-23 for one and two stochastic variables.

One single stochastic variable:

$$\mu_u = \sum_i^{N_p} u_i(x,t) w_i$$

$$\sigma_u{}^2 = \sum_i^{N_p} \left(u_i(x,t)\right)^2 w_i + \left(\sum_i^{N_p} u_i(x,t) w_i\right)^2$$

4-22

Two stochastic variables:

$$\mu_u = \sum_i^{N_p}\sum_j^{N_p} u_{ij}(x,t) w_i w_j$$

$$\sigma_u{}^2 = \sum_i^{N_p}\sum_j^{N_p} \left(u_{ij}(x,t)\right)^2 w_i w_j + \left(\sum_i^{N_p}\sum_j^{N_p} u_i(x,t) w_i w_j\right)^2$$

4-23

4.6.5.3 *Probabilistic Collocation Method*

A comparative plot can be drawn between deterministic case, which means standard evolutionary algorithm execution, stochastic case, which uses stochastic definition of the input variables, and Probabilistic Collocation method (PCM) that defines stochastic variables using quadrature techniques. Figure 4-52 shows the comparison among the three methods. Figure 4-52 shows the three whole populations of the solutions, and Figure 4-53 shows the Pareto Fronts of the three cases.

The first difference comes from the use of a truncated distribution in the PCM case. It produces values in a narrow range. The second difference is that it improves results in a range of f_1 values.
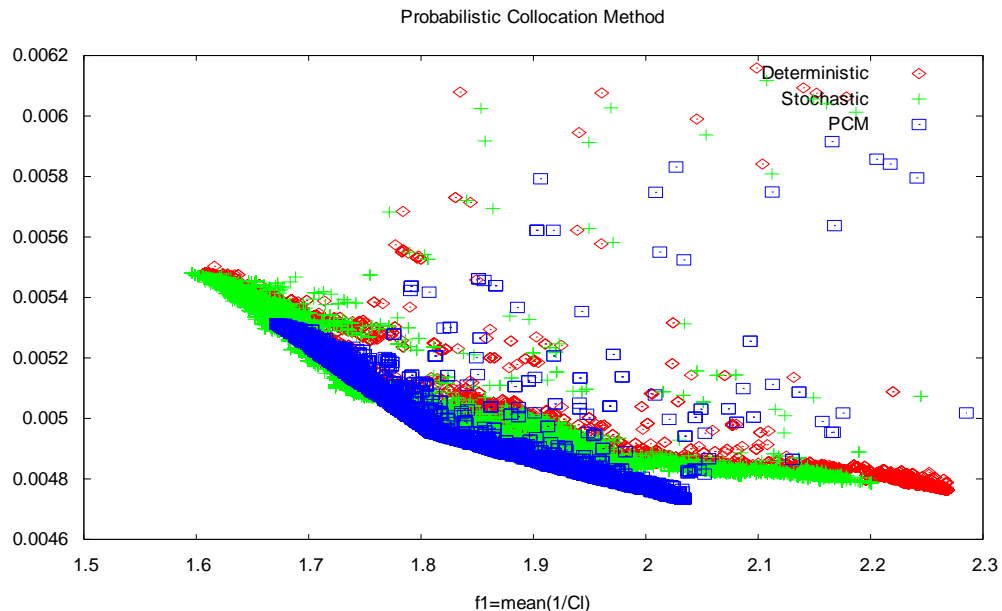
Figure 4-52. Comparative plot of whole populations.
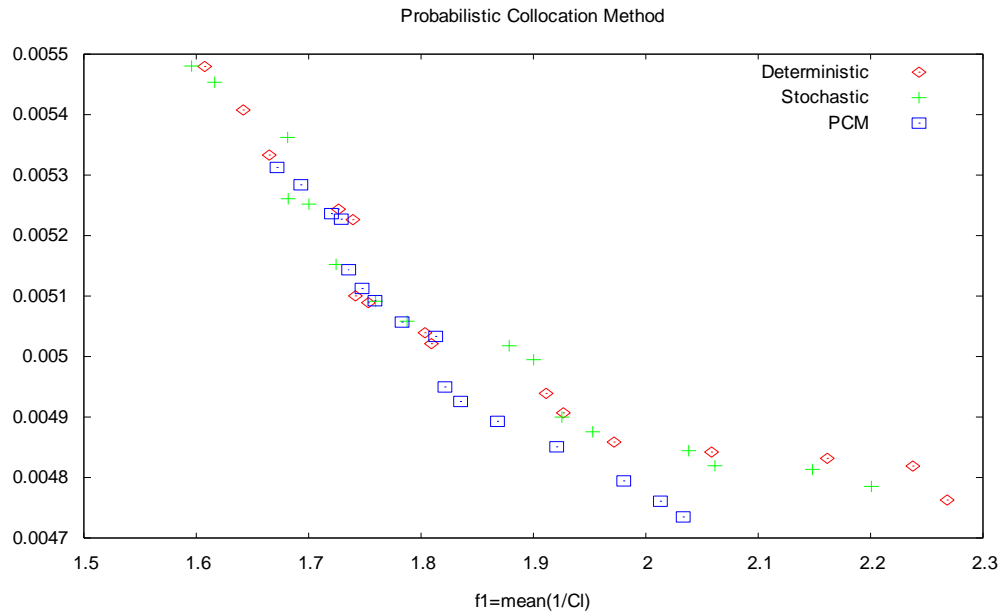
Figure 4-53. Comparative plot of best populations.

The reader should take into account the evaluation point obtained by the quadrature technique. In the case of the Mach number a negative value is obtained, which is has no physical sense. In order to define the same PDF and to enable a comparison this evaluation point should be taken into consideration, even its weight is almost zero.

4.6.6   Conclusions

Evolutionary algorithm coupled with Artificial Neural Networks meta-model has provided a powerful combination of tools to reduce the computational effort. It does not require major changes on the procedure. Although the training cost have to be taken into account, the save of time is still remarkable. In order to ensure the best accuracy with the fewer training effort, a good Design of Experiments should be required.

Deterministic and stochastic cases have been compared in order to validate stochastic procedure. The stochastic robust procedure has been fully integrated into the optimization process. But an important issue arises after this test; as expected the total computational time required for the evaluation of 1250 generations of 16 individuals takes several days.

The total time required is clear a big issue concerning stochastic robust procedure. Table 4-8 is an approximate overview of the computational cost of the coupling between evolutionary algorithms and stochastic analysis, when using a direct evaluation of the analysis tool. The computer used is a calculation server Intel Xeon 16 CPU @ 3,2GHz RAM 15,2Gb.

Stochastic samples	Computational time
10	7.5h
50	40h
100	80h
150	115h
250	190h

Table 4-8: Computational time

The use of a surrogate model has demonstrated its capability to reduce the computational effort while ensures the accuracy in an easy way. Table 4-9 shows a comparison of the computational cost with a calculation server Intel Xeon 16 CPU @ 3,2GHz RAM 15,2Gb.

Stochastic samples	Computational time	Using ANN
250	190h	29h

Table 4-9: Computational time using a surrogate model

Then, it is clear that it is better to find a new strategy to face such a costly effort. A surrogate model is a good option to reduce the total time required for each analysis. Other possibilities are the parallelization of the code, and take advantage of the new developments in GPU computing.

The final decision of using a surrogate model instead of direct evaluations of the solver has been taken; the computational cost is the main reason. But accuracy is always an important issue, as well. The literature about the use of a surrogate model always leads to a combined use of the model and the solver (Chiba et al, 2003; Desideri and Janka, 2004). But stochastic and robust optimization that is defined in this research is really expensive. Evolutionary algorithms use a population based search with pseudo-random generation of the new individuals. Its combination with Monte Carlo techniques for stochastic definition means a huge number of evaluations. Deterministic analyses tend to limit the use of the surrogate model to the 25% of the evaluations. This is not a good solution for the stochastic and robust procedures. Then, a full-surrogated evaluation has been selected. It leads to seek the best accuracy of the meta-model. With this comparative study, it has been demonstrated that a good training and validation process can ensure a tight accuracy. It enables an optimization process completely based on surrogate model evaluations.

The stochastic and robust optimization is strongly related to sampling techniques. It has been expected that Latin Hypercube helps to reduce the total amount of samples required, but the results show it produces slight improvement compared to Monte Carlo sampling. As done in chapter 3, the comparison between MC and LHS has been expected to provide some improvement regarding the computational cost while reducing the amount of samples evaluated. As resulted in the stochastic analysis in chapter 3 this has not been the case.

A relevant conclusion is that regarding the random definition of the samples. The stochastic analysis should not be confused with a multi-point analysis. The uncertainty

of the input variables should be taken into consideration in all its statistical sense. This is the main reason that the stochastic samples are regenerated for each individual of the optimization process. This "variable" generation of samples does not decrease accuracy but ensures a larger robustness of the solution. The computational cost in both fixed and variable sample definition has been the same.

The Probabilistic Collocation method is an interesting method for uncertainty quantification. It is very useful to introduce the input variability in the analysis. It demonstrates a good performance in comparison to Monte Carlo based stochastic procedure. However, the Probabilistic Collocation Method can be considered a multi-point method because it fixes the evaluation points for a given density function. In addition, the user should take care of the values of the evaluation points, because they could be completely meaningless. Quadrature technique spreads the values along the range, and it defines weight without taking care of real and physical limits of the variable. Another handicap is the increasing computational cost the method has when increasing the number of stochastic variables or when increasing the degree of the collocation polynomial.

Even with a low degree value, degree 5 for example, for 1 stochastic variable 6 evaluations are required, for 2 variables 36 evaluations. In a general case, if N_p is the degree of the collocation, and n the number of variables it requires $(N+1)^n$ evaluations. The increase is exponential, so the computational cost also exponentially increases.

All these tests confirmed that the stochastic method produces robust results, but at the same time at a high computational cost.

4.7 Multi-objective optimization of an Aero-elastic problem

4.7.1 Deterministic procedure

4.7.1.1 Introduction

The same strategy of section 4.4 has been applied to an aero-elastic problem. The deterministic, the stochastic and the robust procedures have been applied to a Fluid Structure Interaction (FSI) problem. A multi-objective optimization problem has been defined to analyse the flutter phenomena and to optimize the structural behaviour. The objective functions of the optimization problem have been defined as the smoothness (the second derivative) of the evolution of a structural parameter and of the evolution of an aerodynamic parameter of the profile over the time.

The deterministic, the stochastic and the robust test cases are mainly intended to search the smoother behaviour of the angular spin of the profile ($\theta_i(t)$); not only the smoothest but also the robustest behaviour. In the stochastic and the robust test cases, the mean value of the curvature is considered as the objective function. Figure 4-54 and 4-55 shows two examples of how the curvature of the time evolution of $\theta_i(t)$ is improved. Figure 4-54 shows only one curve, as considered in the deterministic test case, and Figure 4-55 shows a set of stochastic curves, as considered in the stochastic and the robust test cases.
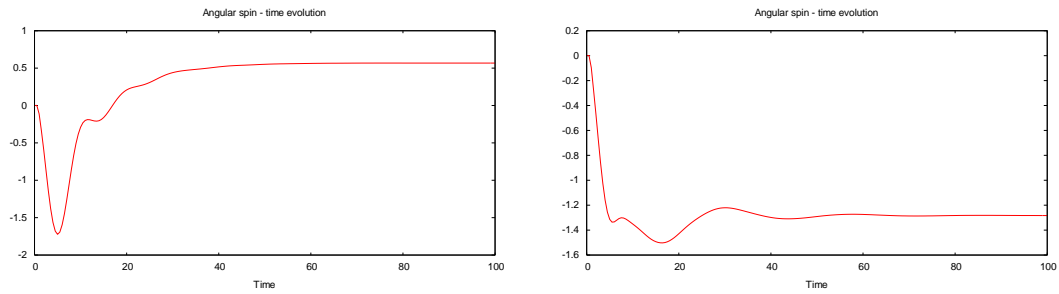
Figure 4-54.- Angular movement examples
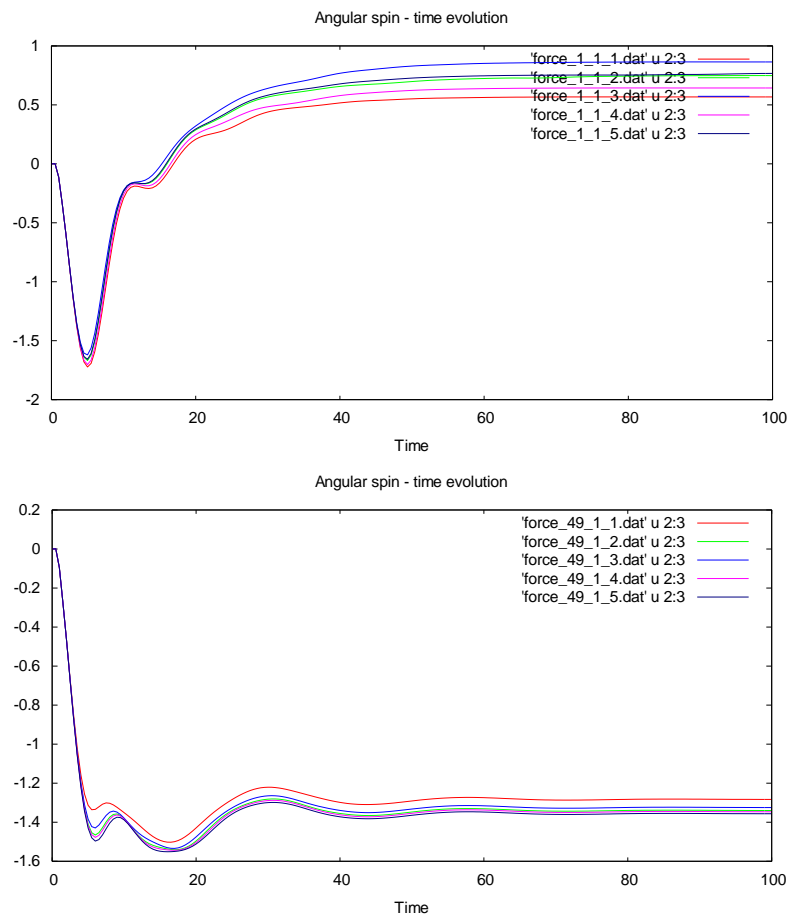
Figure 4-55.- Angular movement for two sets of individuals

The deterministic problem has been solved in order to be used as the reference for a stochastic and robust optimization.

4.7.1.2 Procedure

The selected FSI problem for this research has been based on a RAE2822 profile. The main objective has been defined to search the smoother behaviour of the time evolution of the angular spin ($\theta_i(t)$) and the time evolution of the pressure drag coefficient ($C_{dp}(t)$); smoother in the sense to reduce the total integral of the curvature, the second derivative of each time dependant function. The problem has been formulated as:

| Minimize | $$f_{1d} = \sum_{i=0}^{N_t} \frac{\partial^2 \theta_i(t)}{\partial t^2}$$ $$f_{2d} = \sum_{i=0}^{N_t} \frac{\partial^2 C_{di}(t)}{\partial t^2}$$ | 4-24 |

N_t is the number of time steps used to calculate both time dependant variables, so the total sum of the curvature values has been obtained and used as fitness functions. The reader can refer to Appendix I for further details on the formulation of the aero-elastic equations and how they are coupled and solved.

Considering the following bounds for the design variables:
- Range of the x-coordinate of the elastic axis; x_ea: [0,25 0,65]
- Range of the x-coordinate of the centre of gravity; x_cg: [0,35 0,60]
- Range of the mass ratio, μ_r: [30,0 65,0]
- Range of the damping coefficient for the vertical deformation, ξh: [0,15 0,35]
- Range of the damping coefficient for the angular spin, ξθ: [0,15 0,45]

The angle of attack and the Mach number have been defined as constant values at:
- Angle of attack: 2,79
- Mach number: 0,734

The evolutionary algorithm has been configured with the following parameters:
- Population size: 8
- Number of populations: 100
- Probability of Crossover: 0,99
- Probability of Mutation: 0,25

Finally, no surrogate model has been used during the optimization.

4.7.2 Stochastic procedure

4.7.2.1 Introduction

In order to take into consideration the variability on the input values each individual has been stochastically analysed. It means a cloud of points has been obtained instead of a single value. The mean value has been used as the objective function.

4.7.2.2 Procedure

In this case, both objective functions are the mean values of the total sum of the curvature of two different outputs: the time evolution of the angular spin of the aero-elastic airfoil ($\theta_i(t)$) and the time evolution of the drag coefficient ($C_{dp}(t)$). The analysis has been aimed to compare if the stochastic procedure is able to find robust solutions without defining standard deviation of the main output as one of its objective functions (as in a robust design case), which would be the case in a classical robust design problem.

The problem is now defined as:

$$
\begin{array}{ll}
\text{Minimize} &
\begin{aligned}
f_{1s} &= \mu\left(\sum_{i=0}^{N_t} \frac{\partial^2 \theta_i(t)}{\partial t^2} \right) \\
f_{2s} &= \mu\left(\sum_{i=0}^{N_t} \frac{\partial^2 C_{dp}(t)}{\partial t^2} \right)
\end{aligned}
& \text{4-25}
\end{array}
$$

The design variables are defined as in the previous deterministic aero-elastic case. Finally, angle of attack and Mach number are defined as stochastic variables:
- Angle of attack follows a Gaussian distribution;
  $\mu = 2,79$, $\sigma = 0,01$
- Mach number follows a Gaussian distribution;
  $\mu = 0,734$, $\sigma = 0,01$

Five stochastic samples have been generated on each individual evaluation. The NSGA-II evolutionary algorithm has been configured with the following parameters:
- Population size: 8
- Number of populations: 50
- Probability of Crossover: 0,99
- Probability of Mutation: 0,2

As did on the deterministic test case, no surrogate model has been used during the optimization.

4.7.3 Robust procedure

4.7.3.1 Introduction

The aero-elastic problem has been used as basis of the robust optimization as the third step on the present analysis. It has been based on the same problem definition already used in Section 4.7.1. Further details regarding the problem formulation, as well as about coupling strategy, can be found in Appendix I. Direct evaluations of the analysis tool are used instead of a surrogate model.

The problem has been described as a robust optimization due to the fact that the mean and the standard deviation of the solution have been considered as objective functions. From the stochastic procedure defined in Section 4.7.2 one step forward is done including an additional robust criteria.

4.7.3.2 Procedure

The problem RAE2822 profile has again been defined as the baseline design to solve the following optimization problem:

Minimize	
$$f_{1r} = \mu\left(\sum_{i=0}^{N_t} \frac{\partial^2 \theta_i(t)}{\partial t^2}\right)$$ $$f_{2r} = \sigma\left(\sum_{i=0}^{N_t} \frac{\partial^2 \theta_i(t)}{\partial t^2}\right)$$	4-26

Considering the following constraints:
- Range of the x-coordinate of the elastic axis; x_ea: [0,25 0,65]
- Range of the x_coordinate of the center of gravity; x_cg: [0,35 0,60]
- Range of the mass ratio, μ_r: [30,0 65,0]
- Range of the damping coefficient for the vertical deformation, ξ_h: [0,15 0,35]
- Range of the damping coefficient for the angular spin, ξ_θ: [0,15 0,45]

Finally, the angle of attack and the Mach number have been defined by 5 stochastic samples from the Gaussian distributions defined as:
- Angle of attack follows a Gaussian distribution;
  $\mu = 2,79$, $\sigma = 0,01$
- Mach number follows a Gaussian distribution;
  $\mu = 0,734$, $\sigma = 0,01$

The evolutionary algorithm has been configured with the following parameters:
- Population size: 8
- Number of populations: 50
- Probability of Crossover: 0,99
- Probability of Mutation: 0,2

As did on the previous test cases, no surrogate model has been used during the optimization.

4.7.4   Results

4.7.4.1   Results of the Deterministic test case

The optimization method searchs for a shape providing the angular spin ($\theta_i(t)$) and the shock pressure drag ($C_{dp}(t)$) curves that should look similar to that shown in Figure 4-56 right, which is smoother that the one shown in Figure 4-56 left. Optimal results should reach smooth shapes for both fitness functions. From the point of view of the analysed application, the flutter phenomena, the optimal results would provide a more stable behaviour. The flutter phenomena would not disappear at all, but it should occur more rarely.
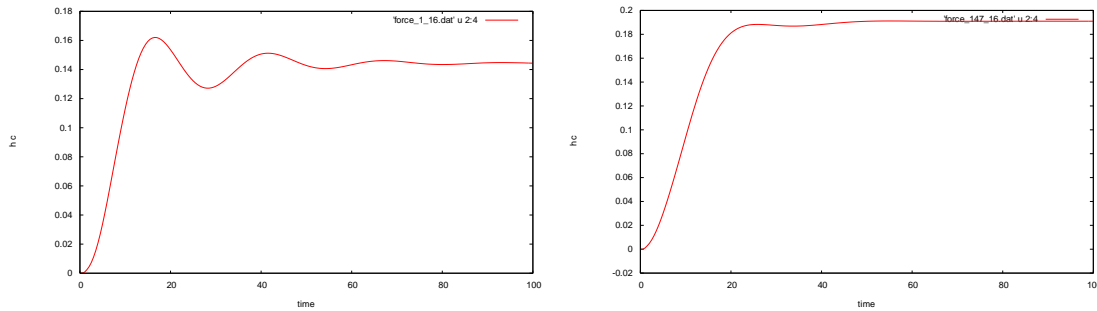
Figure 4-56.- Vertical movement examples

The optimization procedure has defined initial populations that present a wide variability, as shown in Figure 4-57 (a) and (b). After the optimization process, the best population that fulfil the optimization criteria has been obtained. Figure 4-58 shows a set of curves with a smoother time evolution.

But not only the smoothness of the curves has been improved; also the dispersion of the population has been reduced. Both $\theta_i(t)$ and $C_{dp}(t)$ initial populations present a large variability: a large dispersion between members of the population, but also a significant difference between the behaviour of each member. Some of them present an early converge in time, but others converge after a larger amount of time steps. On the other hand, the behaviour of the best populations is much homogeneous, as it can be seen comparing Figure 4-57 with 4-58.
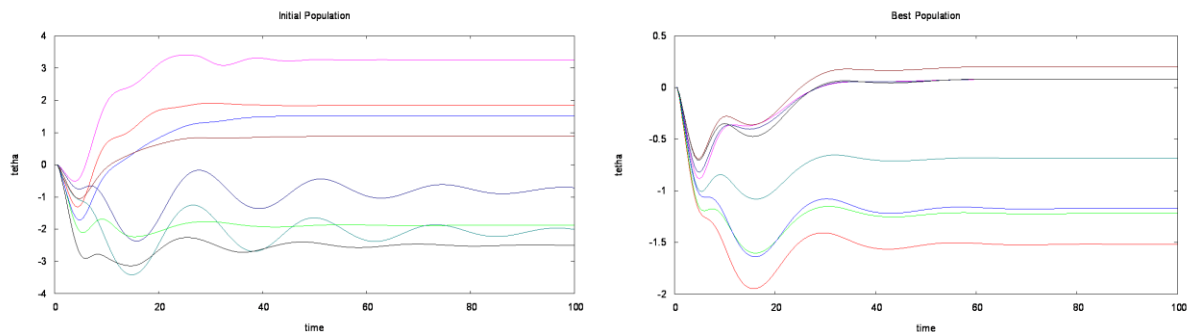
Figure 4-57.- Representation of the behaviour of the (a) initial population for $\theta_i(t)$, and the (b) optimal population for $\theta_i(t)$.
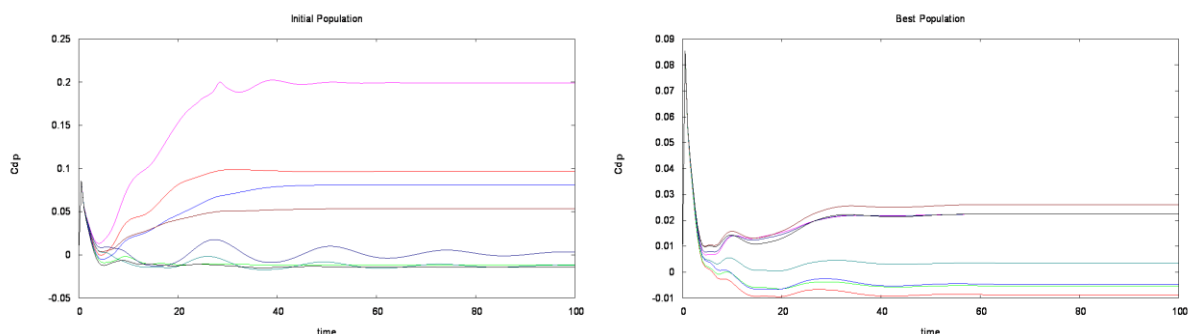
Figure 4-58.- Representation of the behaviour of the (a) initial population for $C_{dp}(t)$. and the (b) optimal population for $C_{dp}(t)$

Figure 4-59 shows the results and the Pareto front of the robust test case.

The analysed deterministic optimization has been performed as a validation of the problem definition. It defines a comparison point with the next analyses done. Comparing the obtained results for the best and the initial populations, the reader can

observe the closer behaviour of all the optimal members compared with the initial ones. Even the dispersion has been reduced; each of the optimum members has his own shape.
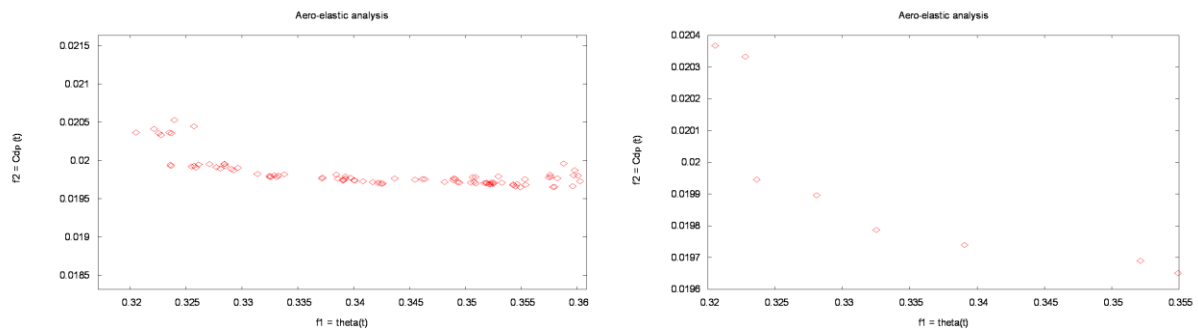
Figure 4-59.- Detail on (a) the whole population and (b) Pareto front from the optimization process.

4.7.4.2   Results of the Stochastic test case

Again, the problem has been mainly intended to look for the smoother behaviour of both curves. Results can be analysed using a similar scheme as it has been done in the previous case. In Figure 4-60, the detail showing the whole population identifies the main fitness function as the one with larger dispersion. The range of obtained values is larger in f_{1s} case than in f_{2s} case. When the attention is focussed only on the Pareto front it can be observed that both value ranges have similar dispersion.
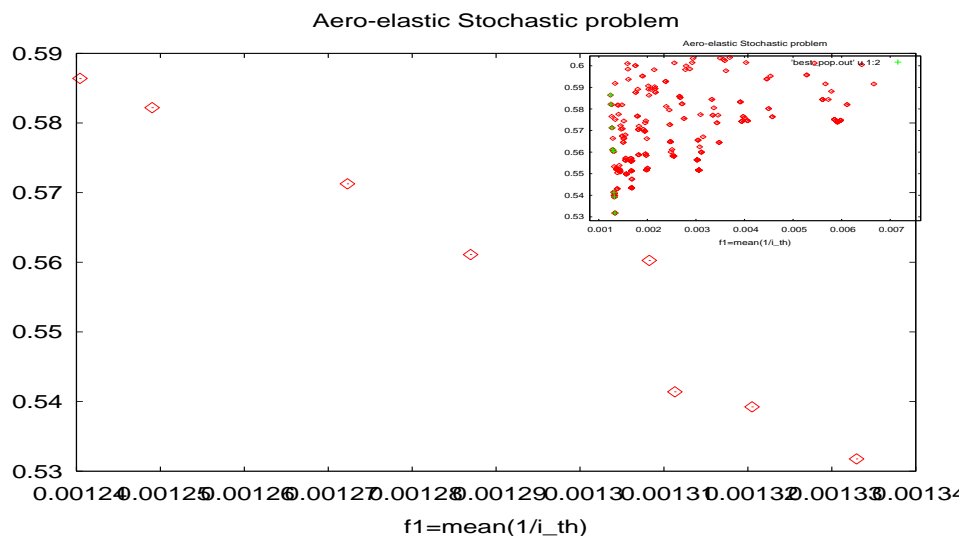
Figure 4-60.- Whole population and Pareto front for an aero-elastic stochastic analysis.

Another comparison can be established between the time evolution of each initial individual, showing its five stochastic evaluations, and the same time evolution for the optimal individuals. Figure 4-61 shows the time evolution of $\theta_i(t)$ and $C_{dp}(t)$. In this case, even not defining the standard deviation as one of the objective functions, the final aim is reached. Both $\theta_i(t)$ and $C_{dp}(t)$ curves became smoother after the optimization.
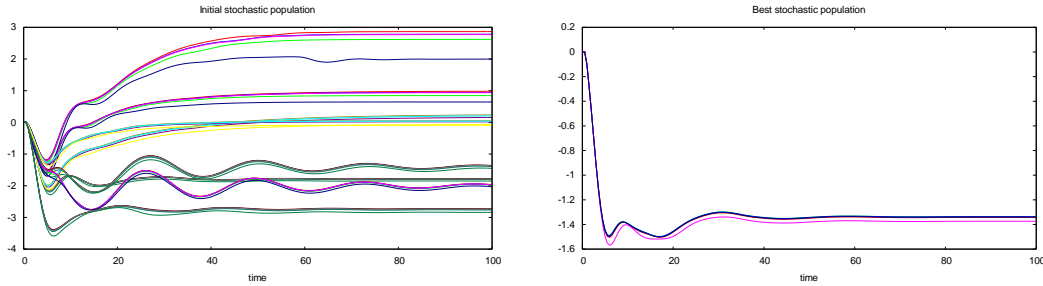
Figure 4-61.- (a) Initial and (b) best populations of Tetha, $\theta i(t)$, evolution.
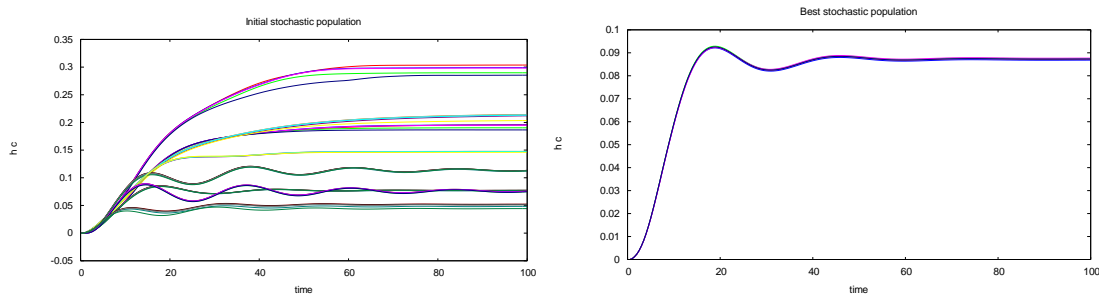
Figure 4-62.- (a) Initial and (b) optimal populations of $C_{dp}(t)$ evolution.

Similar conclusions can be taken from Figure 4-61 and 4-62, as it has been done in the previous test case. Comparing initial and best populations the reader can observe how the optimization process tends to search the fittest individuals. Compared with the deterministic results, the dispersion between optimal members has been reduced and the shapes of all the optimal members tend to be pretty similar.

4.7.4.3   Results of the Robust test case

The results can be analysed using a similar scheme as it has been done in the deterministic and the stochastic case. First of all, a comparison between initial population and the optimal one has been done. The plot showing the whole population demonstrates that the initial individuals are far from the optimal values. Again, the optimization process has been able to tend to the optimum.

The coupling between the stochastic procedure and the aero-elastic analysis tool has performed as expected, without any major issue. Figure 4-63 shows the whole solution, including a detail of the area closest to the optimum values. Figure 4-64 shows the Pareto front.
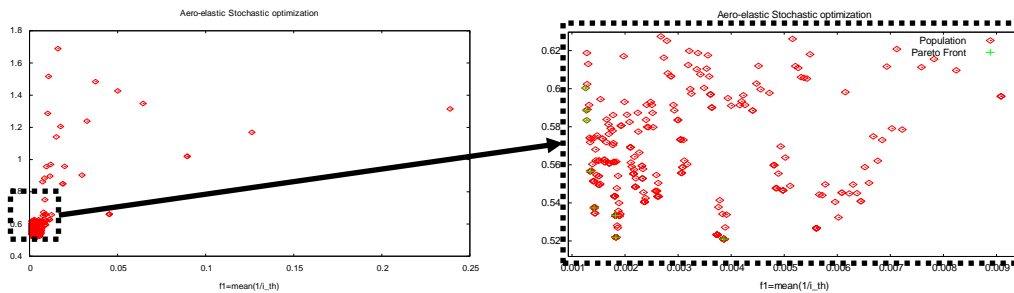
Figure 4-63.- Whole population for an aero-elastic robust analysis
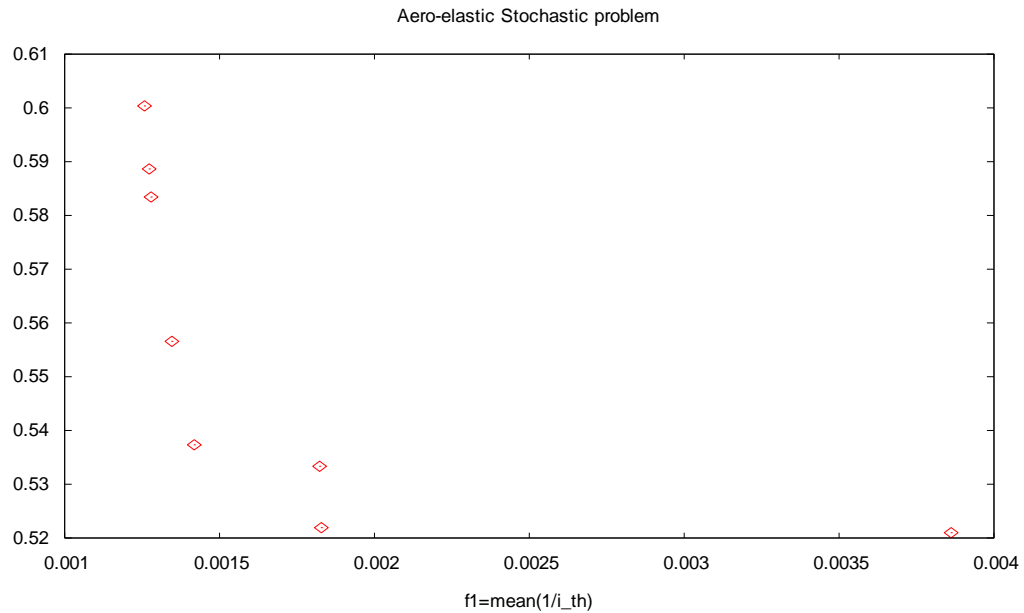
Figure 4-64.- Pareto front for an aero-elastic robust analysis

Another comparison can be established between the time evolution of each initial individual, showing its five stochastic evaluations, and the same time evolution for the optimal individuals. It is easy to observe how the initial population is more disperse, in all the senses. Each individual differs a lot from the other ones, but also each stochastic evaluation of individuals also presents bigger variability. On the other hand, the set of best solutions tend to the same shape, with lower variability comparing both individuals and stochastic evaluations. Figure 4-65 shows the comparison between the initial population and the best one.
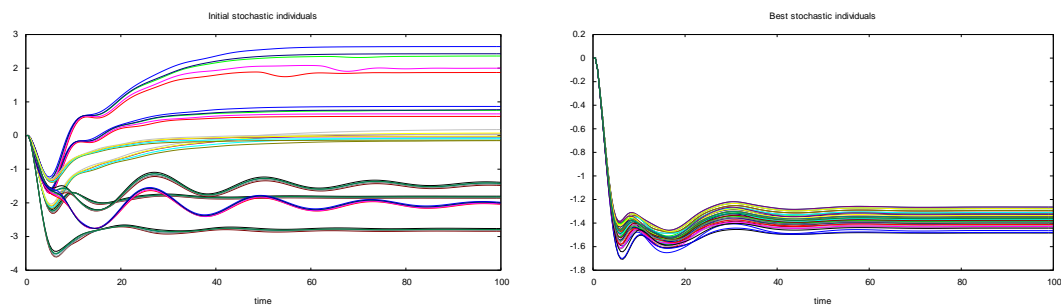
Figure 4-65.- Initial and optimal population comparison

A comparison can be established between the results from the deterministic analysis and those obtained applying the robust procedure. Comparing Figure 4-64 and 4-66 it can be observed that in the deterministic case the final curves are smoother than in the stochastic case. It is easy to understand that one of the main reasons is due to the uncertainty on the input parameters, which makes more difficult to identify an optimum value as the deterministic does.

Comparing with stochastic test case both the dispersion of the optimal individuals and the smoothness of the curves of the time evolution of the fitness functions have been improved.
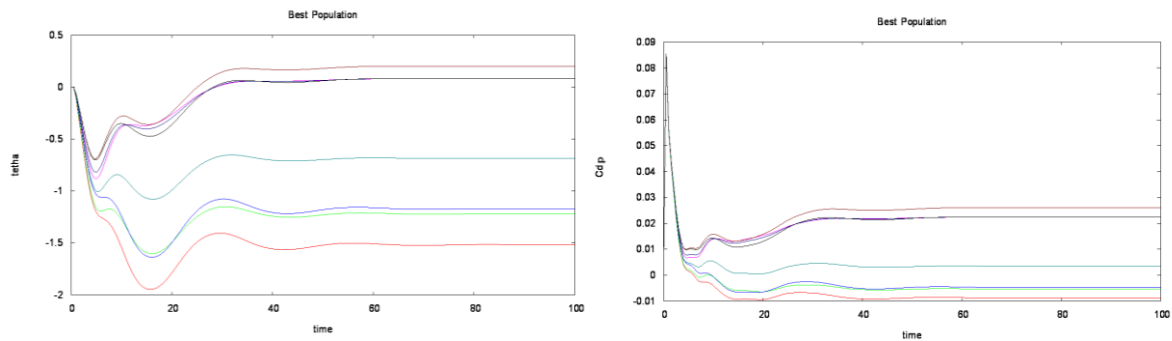
Figure 4-66.- θ_i and C_{dp} time evolution for and optimal populations (taken from the deterministic case)

4.7.5   Conclusions

Flutter problem is one of the biggest structural issues during flight. The aircraft wings must be designed to deform in order to absorb wing gust or impact during landings. But the aero-elastic problem can arise if the wing is perturbed in its resonance frequency. Then, the wing can reach an unstable oscillation that can produce its structural failure. Flutter is a structural problem which can appear in high aspect ratio wings; id est., large spanwise and short chord (a narrow and long wing). The results are quite interesting in the physical sense, but also from the point of view of the application itself.

Physically speaking, the aero-elastic parameters have been optimized to ensure a quick convergence of the aero-elastic behaviour. It means that flutter, or structural instability, is minimized straight when using one of the optimum individuals.

From the point of view of the application, it is interesting to note the definition of the fitness functions, which leads to an easy representation of the smoothness over the time. Of course, the same problem definition has been used for a stochastic and a robust design optimization problem.

The stochastic definition of the input variables introduces the uncertainty on the analysis. Although only the mean of the output values has been considered, it already means a best focus on the solution of the problem under uncertainties. Comparing the final results, it can be seen that dispersion on the optimal populations is lower than in the deterministic case. When facing uncertainty or variability on the parameters, the use of this procedure will lead to a better solution compared to the deterministic case. It should be taken into consideration by engineers, who should balance between getting a robust design and the computational cost associated.

The fact that only the mean value has been used in the stochastic case can be understood as a lost of information about variability of the output values. It leads to use the robust procedure which is taking both mean and standard deviation as objective functions.

Additional information taken from Figure 4-59 of the time evolutions of Theta $\theta_i(t)$ is of upmost interest to validate the final results of this test case.

Figure 4-65 and 4-66 showing fitness functions clearly identify how the optimization process behaves. But in this particular case, where the fitness function is strongly related to a time dependant function, it is also important to confirm that results adjust to the desired behaviour.

A perfect coupling between aero-elastic problem and stochastic robust procedure has been performed. The test case does not use any geometrical information; it only uses a fixed geometry of a RAE2822 profile. Evolutionary algorithm controls other kind of input parameters like mass ratio or damping coefficient, which are directly related with this type of problem.

The robustness of the solution has been reinforced using the stochastic definition of the input variables, which introduces uncertainty on the parameters into the analysis, but also using the variability as an objective of the optimization, which ensures the stability of the performance.

A central Pareto member of each analysed test case has been analysed to evaluate its angular spin behaviour. Next figures show these results. Figure 4-67 shows the time evolution of the deterministic Pareto member, Figure 4-68 shows the stochastic Pareto member and Figure 4-69 the robust Pareto member when the Mach number remains equal to 0,734, and the angle of attack is stochastically defined. Figure 4-70 shows a comparison of the three test cases. The reader can observe how the time evolution of the deterministic test case has a large variability between their members. The stochastic and the robust test cases present a similar behaviour, reducing the variability of the deterministic test case.
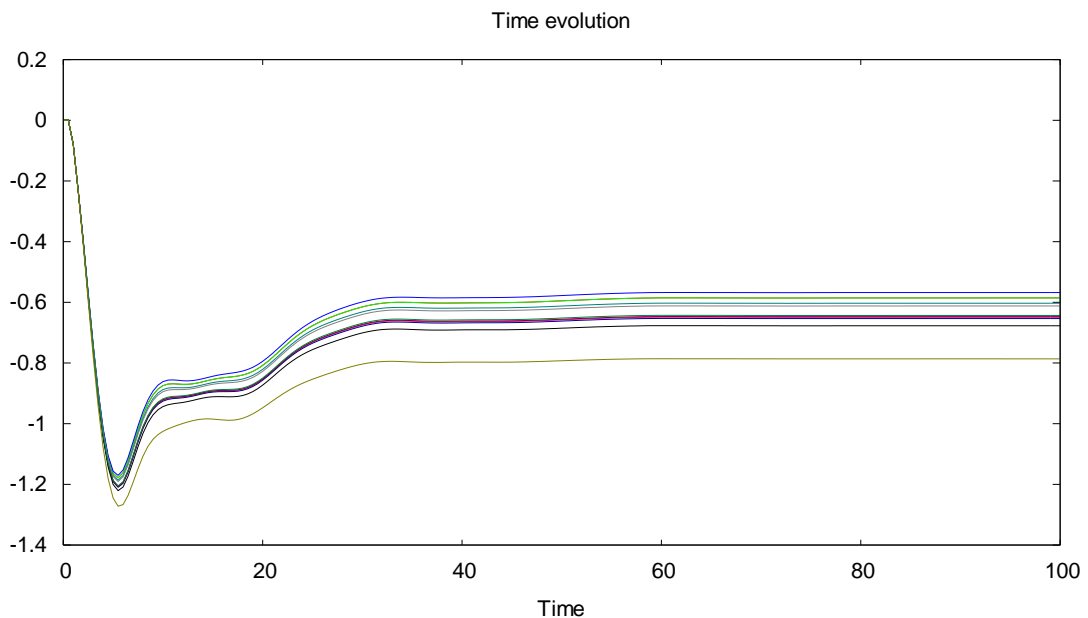
Figure 4-67.- Time evolution of θ_i for the deterministic test case with constant Mach number
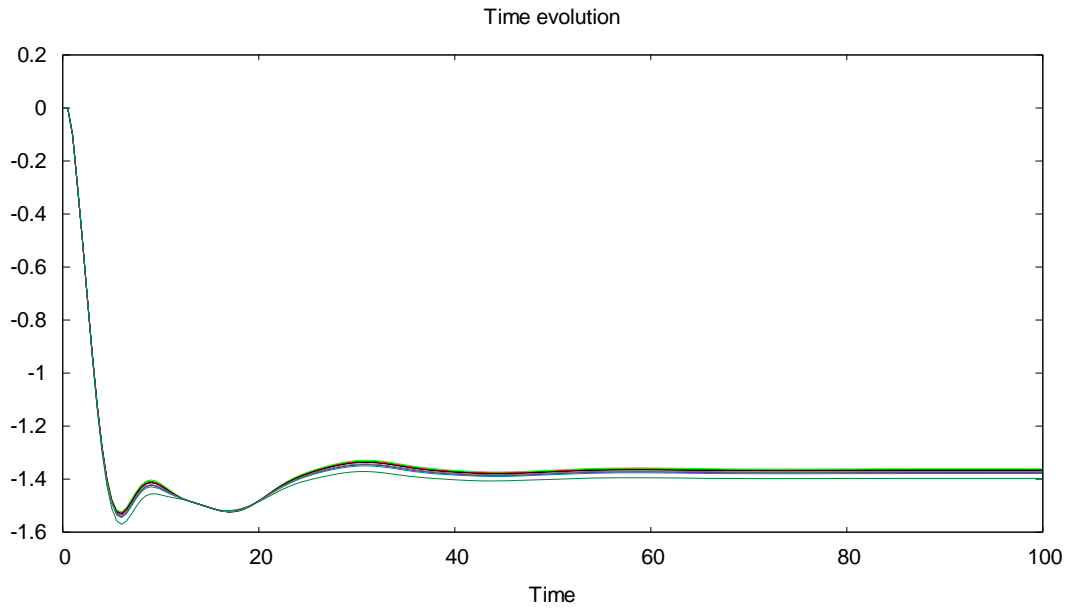
Time evolution

Figure 4-68.- Time evolution of θ_i for the stochastic test case with constant Mach number
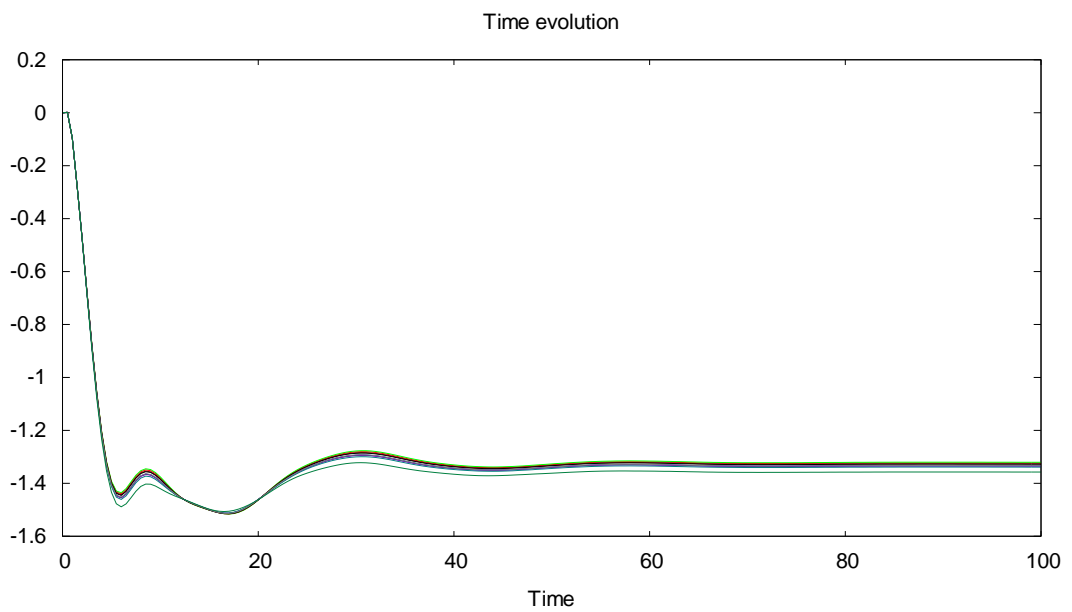
Time evolution

Figure 4-69.- Time evolution of θ_i for the robust test case with constant Mach number
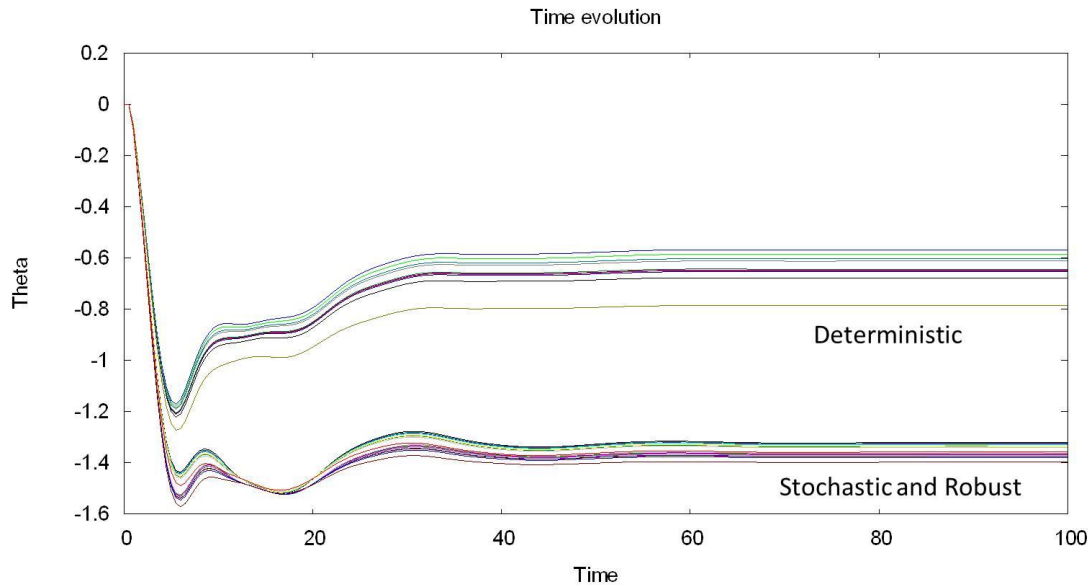
Time evolution

Figure 4-70.- Comparison of the deterministic, the stochastic and the robust time evolutions

Figure 4-67, 4-68 and 4-69 are a clear example of how the stochastic and the robust procedures are able to obtain a more stable behaviour of time evolution of the angular spin $\theta_i(t)$ for different values of the angle of attack and the Mach number. From the application point of view, the aero-elastic behaviour of a wing should be kept. The stochastic and robust results lead to a more predictable values of the angular spin $\theta_i(t)$ which can help to improve the flight performance of the wing.

If the analysis focus its attention on a constant value of angle of attack, equal to 2,79, and an uncertain Mach number, the next figures are obtained. Figure 4-67 shows the time evolution of the deterministic Pareto member, Figure 4-68 shows the stochastic Pareto member and Figure 4-69 the robust Pareto member. The reader can observe how the variability of the deterministic case is similar in the three test cases when angle of attack remains constant. The stochastic and the robust test cases present a similar behaviour, reducing the variability of the deterministic test case, although the converged value is not the same, being a little bit higher in the robust case.
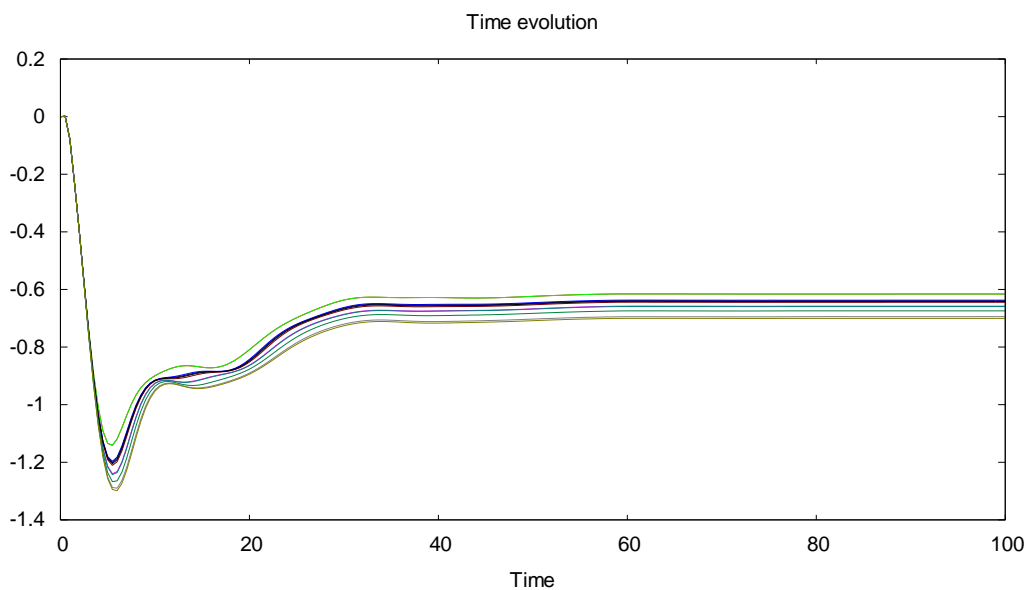
Time evolution

Figure 4-71.- Time evolution of θ_i for the deterministic test case with constant angle of attack
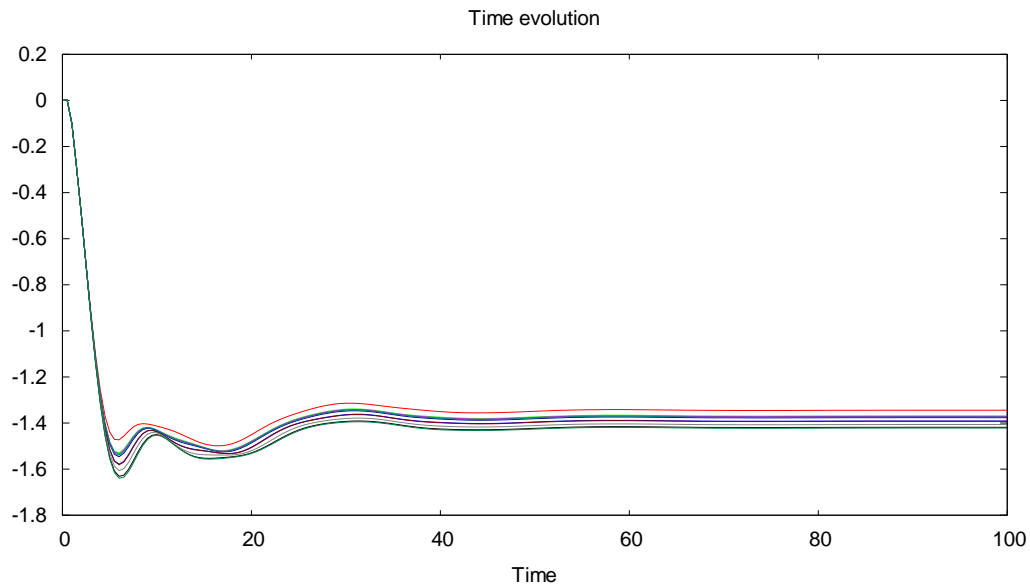
Time evolution

Figure 4-72.- Time evolution of θ_i for the stochastic test case with constant Angle of attack
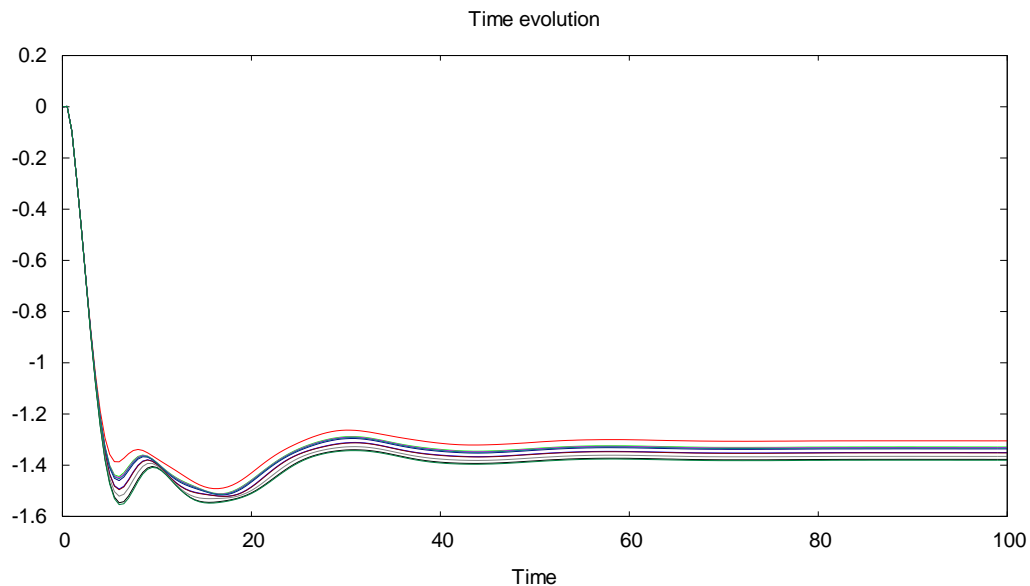
Time evolution

Figure 4-73.- Time evolution of θ_i for the robust test case with constant Angle of attack

Figure 4-67, 4-68 and 4-69 are a clear example of how the stochastic and the robust procedures are able to obtain a more stable behaviour of time evolution of the angular spin $\theta_i(t)$ for different values of the angle of attack and the Mach number. From the application point of view, the aero-elastic behaviour of a wing should be kept. The stochastic and robust results lead to a more predictable values of the angular spin $\theta_i(t)$ which can help to improve the flight performance of the wing.

4.8 Multi-objective optimization of a Mission Planning problem

4.8.1 Introduction

A project proposal to an air carrier company has opened the opportunity to develop the present test case. The main aim of the proposal has been to define an optimization

problem that helps to define the optimum flight procedures in order to reduce the fuel consumption. Some good ideas has been described in Lee et al (2010) where a mission path planning problem for Unnamed air vehicles (UAV) and a fuel reduction problem have been analysed through the definition of an optimization problem.

The provided information from the air carrier leads to the definition of a rough model of the fuel consumption. The model used in this section is an approximation to the real one due to the confidentiality agreement with the company. Anyway, the concept is the same and the results are accurate enough to provide the opportunity to enlarge the test case portfolio.

The mission profile has been defined in several phases. For each phase the time, the fuel consumption, and the distance have been calculated. The fuel consumption has been calculated using parameters like the climb ratio and the fuel flow of the engines described later on. The distance has been calculated based on the distance trip between waypoints. And the time has been defined by the ratio of distance and velocity. As in previous test cases, this problem has been solved using the deterministic, the stochastic and the robust procedures.

4.8.2 Definition of the problem

The mission planning problem has been based on the optimization of a flying route between two points. The restrictions are applied to the intermediate points, the so-called waypoints, but also to the parameters that define the vertical profile of the mission. Parameters like climb rate, acceleration and cruise altitudes are restricted within feasible range of values, according to the aircraft performances and air traffic restrictions. Thew defined model has been based on the guidelines by AIRBUS, 2008 and BOEING, 2007.

Three objective functions have been considered; namely the fuel consumption, the time of the mission and the length of the mission. The mission has been divided into mission phases; taxi, take-off, initial ascent, acceleration at acceleration altitude, ascent to cruise altitude, cruise at first cruise altitude, ascent/descent to second cruise altitude, cruise at second cruise altitude, descent, descent in final approach, and finally landing, as described in Figure 4-74.
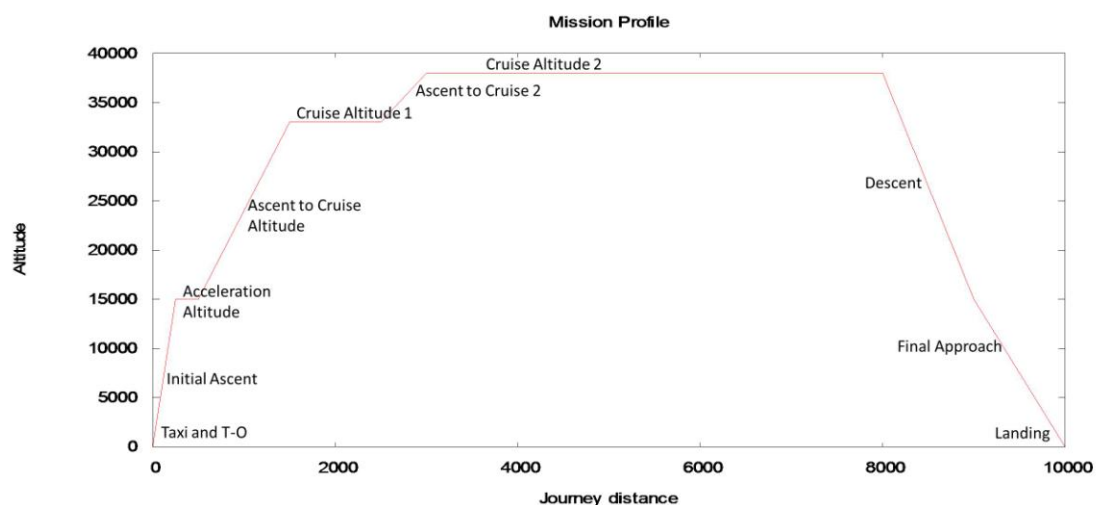
Figure 4-74.- Mission phases

The model for the time and the distance has been obtained by means of the calculation of the distance between waypoints depending on the flying phase. The time has been calculated using the velocity information. And the fuel consumption model has been defined as an approximation from the data of the customer. Parameters used to calculate the fuel consumption are only a representative set of all the parameters that could be used.

Several simplification have been decided to reduce the total amount of variables of the problem: limited number of flight phases have been defined, some variables have been considered as equal (throttle during cruise and levelled flight phases, Mach number for both first and second cruise are some examples).

This specific application has defined Barcelona as departure airport and Athens as destination. The waypoints are 4, and they have been selected from a list of 4 options each one. A discrete list of waypoints has been defined:
- Departure Point, Barcelona.
  o Waypoint 1: Girona, Lleida, Palma de Mallorca, Alghero.
  o Waypoint 2: Marseille, Cagliari, Tunis, Porto-Vecchio.
  o Waypoint 3: Torino, Genova, Roma, Palermo.
  o Waypoint 4: Split, Bari, Patra, Kalamata.
- Destination Point: Athens.

Examples of the possible mission profiles and routes are given in Figure 4-75.
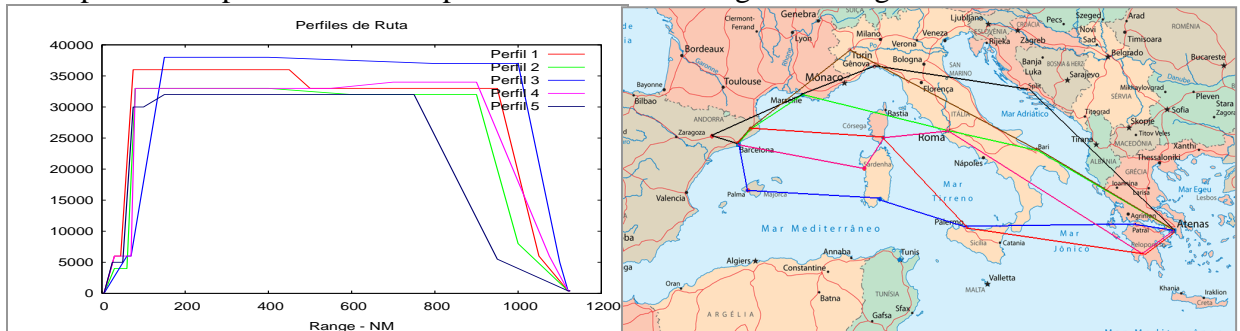
Figure 4-75.- Mission profiles and routes

4.8.3 Deterministic procedure

The problem to solve has been defined as described in equation 4-27:

Minimize $$f_{1d} = fc_{tx} + fc_{to} + fc_{a2aa} + fc_{aa} + fc_{aa2c} + fc_{c1} + fc_{c2c} + fc_{c2} + fc_{d2a} + fc_{fa}$$ $$f_{2d} = t_{tx} + t_{to} + t_{a2aa} + t_{aa} + t_{aa2c} + t_{c1} + t_{c2c} + t_{c2} + t_{d2a} + t_{fa}$$ $$f_{3d} = d_{tx} + d_{to} + d_{a2aa} + d_{aa} + d_{aa2c} + d_{c1} + d_{c2c} + d_{c2} + d_{d2a} + d_{fa}$$	4-27

For the first phase, taxi, the time value is considered as fixed at a value equal to 5 min. The distance is not considered in the overall journey. Fuel consumption during Taxi phase, fc_{tx} is computed as:

$$fc_{tx} = (1 + SE) \cdot ffr \cdot (1 + th_{tx}) \cdot t_{tx} \qquad \text{4-28}$$

t_{tx}: duration of taxi, fixed to 5 minutes.
ffr: fuel flow reference; minimum fuel flow of each engine (kg/h).
SE: single engine taxi; 0= taxi with only one engine, 1= taxi with two engines
th_{tx}: throttle adjustment (% of full throttle).

Time, t_{to}, and Fuel consumption, fc_{to}, of Take-off phase are computed as:

$$t_{to} = \frac{l_r \cdot 2}{1852 \cdot v_{to}}$$

$$fc_{to} = \left(2 ffr - h_{to} \cdot 10^{-3} + w_{to} \cdot 10^{-3}\right) \cdot 2 \cdot t_{to} \qquad \text{4-29}$$

v_{to}: take-off speed (kt)
l_r: runway length (m)
h_{to}: altitude of departure airfield (ft)
w_{to}: wind during take-off (kt)

Time, t_{a2aa}, distance, d_{a2aa}, and Fuel consumption, fc_{a2aa}, of Ascent phase after take off are computed as:

$$t_{a2aa} = \frac{(AA - h_{to})}{CR2AA \cdot 60}$$

$$d_{a2aa} = v_{to} \cdot t_{a2aa} \cdot \cos\left(a\sin\left(\frac{\frac{AA - h_{to}}{6076.115}}{v_{to} \cdot t_{a2aa}}\right)\right)$$

$$fc_{a2aa} = \left(2 ffr - AA \cdot 10^{-3} + w_{to} \cdot \left(1 + \frac{AA}{1000}\right) \cdot 10^{-3} + \frac{AA}{609 \cdot \sqrt{1 + \frac{15 + 1.98 \cdot \frac{AA}{1000}}{273.15}}}\right) \cdot 2 \cdot t_{a2aa} \qquad \text{4-30}$$

AA: Acceleration altitude (ft)
$CR2AA$: climb ratio to acceleration altitude (ft/min)

Time, t_{aa}, distance, d_{aa}, and Fuel consumption, fc_{aa}, of flight at acceleration altitude are computed as:

$$t_{aa} = \frac{\left(v_{aa} \cdot 609 \cdot \sqrt{1 + \frac{15 + 1.98 \cdot \frac{AA}{1000}}{273.15}} - v_{to}\right)}{\left(12596 \cdot \frac{1 - CI_{aa}}{100}\right)}$$

$$d_{aa} = v_{to} \cdot t_{aa} + 0.5 \cdot \left(12596 \frac{1 - CI_{aa}}{100}\right) \cdot t_{aa}^2 \qquad \text{4-31}$$

$$fc_{aa} = \left(2 ffr - AA \cdot 10^{-3} + w_{to} \cdot \left(1 + \frac{AA}{1000}\right) \cdot 10^{-3} + \frac{v_{to}}{609 \cdot \sqrt{1 + \frac{15 + 1.98 \cdot \frac{AA}{1000}}{273.15}}}\right) \cdot 5 \cdot (1 + th_{aa}) \cdot t_{aa}$$

v_{aa}: Mach number at acceleration altitude (% Mach)
CI_{aa}: Cost Index during flight to acceleration altitude
th_{aa}: throttle position during flight at acceleration altitude

Time, t_{aa2c}, distance, d_{aa2c}, and Fuel consumption, fc_{aa2c}, of ascent to cruise altitude are computed as:

$$t_{aa2c} = \frac{(CA_1 - AA)}{CR2C \cdot 60}$$

$$d_{aa2c} = v_{aa} \cdot 609 \cdot \sqrt{1 + \frac{15 + 1.98 \cdot \frac{CA_1}{1000}}{273.15}} \cdot t_{aa2c} \cdot \cos\left(a\sin\left(\frac{\frac{CA_1 - AA}{6076.115}}{v_{aa} \cdot 609 \cdot \sqrt{1 + \frac{15 + 1.98 \cdot \frac{CA_1}{1000}}{273.15}} \cdot t_{aa2c}} \right) \right)$$

$$fc_{aa2c} = \left(2\,ffr - CA_1 \cdot 10^{-3} + w_{c1} \cdot 10^{-3} + v_{c1} \right) \cdot \left(1 + th_{aa} \right) \cdot t_{aa2c}$$

4-32

CR2C: climb ratio to cruise altitude (ft/min)
CA_1: Cruise altitude 1 (ft)
w_{c1}: wind at cruise level 1 (kt)

Time, t_{c1}, distance, d_{c1}, and Fuel consumption, fc_{c1}, of first cruise phase are computed as:

$$t_{c1} = \frac{d_{c1}}{\left(v_{c1} \cdot 609 \cdot \sqrt{1 + \frac{15 + 1.98 \cdot \frac{CA_1}{1000}}{273.15}} \right)}$$

$$d_{c1} = \frac{\left(d_{od} - \left(d_{a2aa} + d_{aa} + d_{aa2c} + d_{c2c} + d_{c2a} + d_{fa} \right) \right)}{2}$$

$$fc_{c1} = \left(\left(2\,ffr - CA_1 \cdot 10^{-3} + w_{c1} \cdot 10^{-3} + v_{c1} \cdot 5 \right) \cdot \left(1 + th_{aa} \right) + \left(100 - CI_{c1} \cdot 2 \cdot ffr \right) \right) \cdot t_{c1}$$

4-33

v_{c1}: Mach number at cruise level 1
d_{od}: distance from departure to destination airfields (NM)
CI_{c1}: cost index during cruise 1

Time, t_{c2c}, distance, d_{c2c}, and Fuel consumption, fc_{c2c}, of ascent/descent from cruise altitude 1 to cruise altitude 2 are computed as:

$$t_{c2c} = \frac{(CA_1 - CA_2)}{CRCC \cdot 60}$$

$$d_{c2c} = v_{c1} \cdot 609 \cdot \sqrt{1 + \frac{15 + 1.98 \cdot \frac{CA_2}{1000}}{273.15}} \cdot t_{c2c} \cdot \cos\left(a\sin\left(\frac{\frac{CA_1 - CA_2}{6076.115}}{v_{c1} \cdot 609 \cdot \sqrt{1 + \frac{15 + 1.98 \cdot \frac{CA_2}{1000}}{273.15}} \cdot t_{c2c}} \right) \right)$$

$$fc_{c2c} = \left(2\,ffr - CA_2 \cdot 10^{-3} + w_{c2} \cdot 10^{-3} + v_{c1} \cdot 5 \right) \cdot \left(1 + th_{aa} \right) \cdot t_{c2c}$$

4-34

CRCC: climb ratio to cruise altitude 2 (ft/min)
CA_2: Cruise altitude 2 (ft)
w_{c2}: wind at cruise level 2 (kt)

Time, t_{c2}, distance, d_{c2}, and Fuel consumption, fc_{c2}, of second cruise phase are computed as:

$$
t_{c2} = \dfrac{d_{c2}}{\left(v_{c1} \cdot 609 \cdot \sqrt{1 + \dfrac{15 + 1.98 \cdot \dfrac{CA_2}{1000}}{273.15}} \right)}
$$

$$
d_{c2} = \dfrac{\left(d_{od} - \left(d_{a2aa} + d_{aa} + d_{aa2c} + d_{c2c} + d_{c2a} + d_{fa} \right) \right)}{2}
$$

$$
fc_{c2} = \left(\left(2\,ffr - CA_2 \cdot 10^{-3} + w_{c2} \cdot 10^{-3} + v_{c1} \cdot 5 \right) \cdot \left(1 + th_{aa} \right) + \left(100 - CI_{c2} \cdot 2 \cdot ffr \right) \right) \cdot t_{c2}
$$

4-35

CI_{c2}: cost index during cruise 2

Time, t_{d2a}, distance, d_{d2a}, and Fuel consumption, fc_{d2a}, of descent phase to final approach altitude are computed as:

$$
t_{d2a} = \dfrac{\left(CA_2 - \left(h_d + 3000 \right) \right)}{CRFA \cdot 60}
$$

$$
d_{d2a} = v_{c1} \cdot 609 \cdot \sqrt{1 + \dfrac{15 + 1.98 \cdot \dfrac{h_d + 3000}{1000}}{273.15}} \cdot t_{d2a} \cdot \cos\left(a\sin\left(\dfrac{\dfrac{CA_2 - \left(h_d + 3000 \right)}{6076.115}}{v_{c1} \cdot 609 \cdot \sqrt{1 + \dfrac{15 + 1.98 \cdot \dfrac{h_d + 3000}{1000}}{273.15}} \cdot t_{d2a}} \right) \right)
$$

$$
fc_{d2a} = \left(2\,ffr - CA_2 \cdot 10^{-3} + w_{c2} \cdot 10^{-3} + v_{c1} \cdot 5 \right) \cdot \left(1 + th_{aa} \right) \cdot t_{d2a}
$$

4-36

CRFA: descent ratio to final approach altitude (ft/min)
h_d: altitude of the destination airfield (ft)

Time, t_{fa}, distance, d_{fa}, and Fuel consumption, fc_{fa}, of final approach phase are computed as:

$$
t_{fa} = 0.6
$$

$$
d_{fa} = 25
$$

$$
fc_{fa} = 2\,ffr \cdot \left(1 + th_{tx} \right) \cdot t_{fa}
$$

4-37

Optimization parameters are defined as follows:
- throttle taxi (%): [0.15: 0.3]
- take off speed (kt): [220: 260]
- Acceleration Altitude (ft): [3000: 6000]
- Cost Index at Acceleration Altitude: [0: 50]
- Acceleration Altitude Mach: [0.65: 0.82]
- Throttle at Acceleration Altitude: [0.5: 0.8]
- Climb rate post-AA (ft/min): [500: 1500]
- Cruise alt1 (ft): [30000 : 42000]
- Cruise 1 Mach (kt): [0.75 : 0.8]
- Climb rate cruise (ft/min): [300: 1000]
- Cruise alt2 (ft): [30000: 42000]

- Descent rate(ft/min): [300: 1000]
- Cost Index Cruise 1: [0: 100]
- Cost Index Cruise 2: [0: 100]
- Single engine taxi: Yes/No

Considering constant values:
- Reference Fuel Flow; *ffr* = 1000 kg/h
- Climb rate to Acceleration altitude; CR2AA = 1000 ft/min
- Runway length for take off; l_r = 2500 m
- Wind at Take off: w_{to} = 15 kt
- Wind at Cruise level 1: w_{c1} = 60 kt
- Wind at Cruise level 2: w_{c2} = 40 kt

The NSGA-II optimizer has been configured with the following values:
- Population size: 100
- Number of populations: 5000
- Probability of Crossover: 0,90
- Probability of Mutation: 0,06

4.8.4 Stochastic and Robust procedure

The Mission Planning problem, based on the criteria described in 4.8.2, has been used as basis of the robust optimization.

For the stochastic procedure standard deviation has not been defined as an objective function. But, as done in Section 4.7.3, the standard deviation values have been used as objective function of the robust procedure, in the same way as the mean values.

4.8.4.1 Problem definition

In this case, some of the parameters are uncertain, it means that have been defined by a probability density function, PDF (mean and standard deviation), or they have an uncertain term, also defined by a PDF.

Based on a real-case problem, the uncertain definition of the parameters reproduces the unknown behaviour of some of the conditions during the mission. Uncertainty on the cruise speed, cruise altitude which could be reached due to air traffic restrictions, and uncertainty on the weather conditions have been considered through the calculation of the fuel consumption, the mission time and the distance. The mission follows the same phases as described in the deterministic case.

Two cases have been analysed; the first one is a stochastic optimization problem, which considers 3 objective functions that are the mean values of fuel consumption, time, and distance. This first case is very similar to the deterministic one, but only considering the uncertainty as a perturbation of some of the parameters. The second one is a robust optimization problem, which considers 5 objective functions; namely the three mean values of fuel consumption, time and distance, and the two standard deviation values of

fuel and time. The standard deviation of distance has been discarded because previous results show an optimal value is reached.

Fuel consumption, fc_{tx}, during Taxi phase is now computed as:

$$fc_{tx} = (1 + SE) \cdot \xi_{ffr} \cdot (1 + th_{tx}) \cdot t_{tx}$$

| 4-38 |

ξ_{ffr}: uncertain fuel flow reference; minimum fuel flow of each engine (kg/h).

Time, t_{to}, is defined as in the deterministic case, and Fuel consumption, fc_{to}, of Take-off phase is now computed as:

$$fc_{to} = (2 \cdot \xi_{ffr} - h_{to} \cdot 10^{-3} + \xi_{w_{to}} \cdot 10^{-3}) \cdot 2 \cdot t_{to}$$

| 4-39 |

ξ_{wto}: uncertain wind during take-off (kt)

Time, t_{a2aa}, and distance, d_{a2aa}, are computed as in the deterministic case, and Fuel consumption, fc_{a2aa}, of Ascent phase after take off is now computed as:

$$fc_{a2aa} = \left(2\xi_{ffr} - AA \cdot 10^{-3} + \xi_{w_{to}} \cdot \left(1 + \frac{AA}{1000}\right) \cdot 10^{-3} + \frac{AA}{609 \cdot \sqrt{1 + \frac{15 + 1.98 \cdot \frac{AA}{1000}}{273.15}}} \right) \cdot 2 \cdot t_{a2aa}$$

| 4-40 |

ξ_{CR2AA}: uncertain climb ratio to acceleration altitude (ft/min)

Time, t_{aa}, and distance, d_{aa}, are computed as in the deterministic case and Fuel consumption, fc_{aa}, of flight at acceleration altitude is now computed as:

$$fc_{aa} = \left(2\xi_{ffr} - AA \cdot 10^{-3} + \xi_{w_{to}} \cdot \left(1 + \frac{AA}{1000}\right) \cdot 10^{-3} + \frac{v_{to}}{609 \cdot \sqrt{1 + \frac{15 + 1.98 \cdot \frac{AA}{1000}}{273.15}}} \right) \cdot 5 \cdot (1 + th_{aa}) \cdot t_{aa}$$

| 4-41 |

Time, t_{aa2c}, and distance, d_{aa2c}, are computed as in the deterministic case and Fuel consumption, fc_{aa2c}, of ascent to cruise altitude is now computed as:

$$t_{aa2c} = \frac{(CA_1 + \xi_{ca1} - AA)}{CR2C \cdot 60}$$

$$d_{aa2c} = v_{aa} \cdot 609 \cdot \sqrt{1 + \frac{15 + 1.98 \cdot \frac{CA_1 + \xi_{ca1}}{1000}}{273.15}} \cdot t_{aa2c} \cdot \cos\left(a\sin\left(\frac{\frac{CA_1 + \xi_{ca1} - AA}{6076.115}}{v_{aa} \cdot 609 \cdot \sqrt{1 + \frac{15 + 1.98 \cdot \frac{CA_1 + \xi_{ca1}}{1000}}{273.15}} \cdot t_{aa2c}} \right) \right)$$

$$fc_{aa2c} = \left(2\xi_{ffr} - (CA_1 + \xi_{ca1}) \cdot 10^{-3} + \xi_{w_{c1}} \cdot 10^{-3} + (v_{c1} + \xi_{v_{c1}})\right) \cdot (1 + th_{aa}) \cdot t_{aa2c}$$

| 4-42 |

ξ_{CA1}: Uncertainty added to Cruise altitude 1 (ft)
ξ_{wc1}: Uncertain wind at cruise level 1 (kt)
ξ_{vc1}: Uncertainty added to speed at cruise level 1 (Mach)

Distance, d_{c1}, is calculated as in the deterministic case. The time, t_{c1}, and Fuel consumption, fc_{c1}, of first cruise phase are now computed as:

$$t_{c1} = d_{c1} \Bigg/ \left((v_{c1} + \xi_{v_{c1}}) \cdot 609 \cdot \sqrt{1 + \frac{15 + 1.98 \cdot {}^{CA_1 + \xi_{ca1}}\!/\!_{1000}}{273.15}} \right)$$

$$fc_{c1} = \left((2\xi_{ffr} - (CA_1 + \xi_{ca1}) \cdot 10^{-3} + \xi_{w_{c1}} \cdot 10^{-3} + (v_{c1} + \xi_{v_{c1}}) \cdot 5) \cdot (1 + th_{aa}) + (100 - CI_{c1} \cdot 2 \cdot \xi_{ffr}) \right) \cdot t_{c1}$$

4-43

Time, t_{c2c}, distance, d_{c2c}, and Fuel consumption, fc_{c2c}, of ascent/descent from cruise altitude 1 to cruise altitude 2 are now computed as:

$$t_{c2c} = (CA_1 + \xi_{ca1} - CA_2) \Big/ CRCC \cdot 60$$

$$d_{c2c} = (v_{c1} + \xi_{v_{c1}}) \cdot 609 \cdot \sqrt{1 + \frac{15 + 1.98 \cdot {}^{CA_2}\!/\!_{1000}}{273.15}} \cdot t_{c2c} \cdot \cos\left(a\sin\left(\frac{{}^{CA_1 + \xi_{ca1} - CA_2}\!/\!_{6076.115}}{(v_{c1} + \xi_{v_{c1}}) \cdot 609 \cdot \sqrt{1 + \frac{15 + 1.98 \cdot {}^{CA_2}\!/\!_{1000}}{273.15}} \cdot t_{c2c}} \right) \right)$$

$$fc_{c2c} = (2\xi_{ffr} - CA_2 \cdot 10^{-3} + \xi_{w_{c2}} \cdot 10^{-3} + (v_{c1} + \xi_{v_{c1}}) \cdot 5) \cdot (1 + th_{aa}) \cdot t_{c2c}$$

4-44

ξ_{wc2}: Uncertain wind at cruise level 2 (kt)

Distance, d_{c2}, is computed as in the deterministic case, while Time, t_{c2}, and Fuel consumption, fc_{c2}, of second cruise phase are now computed as:

$$t_{c2} = d_{c2} \Bigg/ \left((v_{c1} + \xi_{v_{c1}}) \cdot 609 \cdot \sqrt{1 + \frac{15 + 1.98 \cdot {}^{CA_2}\!/\!_{1000}}{273.15}} \right)$$

$$fc_{c2} = \left((2\xi_{ffr} - CA_2 \cdot 10^{-3} + \xi_{w_{c2}} \cdot 10^{-3} + (v_{c1} + \xi_{v_{c1}}) \cdot 5) \cdot (1 + th_{aa}) + (100 - CI_{c2} \cdot 2 \cdot \xi_{ffr}) \right) \cdot t_{c2}$$

4-45

Time, t_{c2a}, is calculated as in the deterministic case. The distance, d_{c2a}, and the Fuel consumption, fc_{c2a}, of descent phase to final approach altitude are computed as:

$$d_{c2a} = (v_{c1} + \xi_{v_{c1}}) \cdot 609 \cdot \sqrt{1 + \frac{15 + 1.98 \cdot {}^{h_d + 3000}\!/\!_{1000}}{273.15}} \cdot t_{c2a} \cdot \cos\left(a\sin\left(\frac{{}^{CA_2 - (h_d + 3000)}\!/\!_{6076.115}}{(v_{c1} + \xi_{v_{c1}}) \cdot 609 \cdot \sqrt{1 + \frac{15 + 1.98 \cdot {}^{h_d + 3000}\!/\!_{1000}}{273.15}} \cdot t_{c2a}} \right) \right)$$

$$fc_{c2a} = (2\xi_{ffr} - CA_2 \cdot 10^{-3} + \xi_{w_{c2}} \cdot 10^{-3} + (v_{c1} + \xi_{v_{c1}}) \cdot 5) \cdot (1 + th_{aa}) \cdot t_{c2a}$$

4-46

The time and the distance are calculated, as in the deterministic case, considering the flight phase parameters.

Same simplifications as in the deterministic case have been applied in the robust design. Optimization search space is defined using the same range of values as in the deterministic case, as well.

Uncertainties are defined as follows:

- ξ_{ffr}: uncertain fuel flow (kg/min)

Gaussian distribution, Mean = 1000, Standard deviation = 0.5
- ξ_{CR2AA}: uncertain climb ratio to acceleration altitude (ft/min)
  Uniform range = [800; 1500]
- ξ_{wto}: uncertain wind during take-off (kt)
  Gaussian distribution, Mean = 15, Standard deviation = 0.1
- ξ_{wc1}: Uncertain wind at cruise level 1 (kt)
  Uniform range = [-10; 60]
- ξ_{wc2}: Uncertain wind at cruise level 2 (kt)
  Uniform range = [-15; 40]
- ξ_{CA1}: Uncertainty added to Cruise altitude 1 (ft)
  Uniform range = [1500; 2500]
- ξ_{vc1}: Uncertainty added to speed at cruise level 1 (Mach)
  Gaussian distribution, Mean = -0.02, Standard Deviation = 0.02

- **Stochastic definition**

Minimize	
$$f_{1s} = \mu\left(fc_{tx} + fc_{to} + fc_{a2aa} + fc_{aa} + fc_{aa2c} + fc_{c1} + fc_{c2c} + fc_{c2} + fc_{d2a} + fc_{fa}\right)$$ $$f_{2s} = \mu\left(t_{tx} + t_{to} + t_{a2aa} + t_{aa} + t_{aa2c} + t_{c1} + t_{c2c} + t_{c2} + t_{d2a} + t_{fa}\right)$$ $$f_{3s} = \mu\left(d_{tx} + d_{to} + d_{a2aa} + d_{aa} + d_{aa2c} + d_{c1} + d_{c2c} + d_{c2} + d_{d2a} + d_{fa}\right)$$	4-47

- **Robust definition**

Minimize	
$$f_{1r} = \mu\left(fc_{tx} + fc_{to} + fc_{a2aa} + fc_{aa} + fc_{aa2c} + fc_{c1} + fc_{c2c} + fc_{c2} + fc_{d2a} + fc_{fa}\right)$$ $$f_{2r} = \mu\left(t_{tx} + t_{to} + t_{a2aa} + t_{aa} + t_{aa2c} + t_{c1} + t_{c2c} + t_{c2} + t_{d2a} + t_{fa}\right)$$ $$f_{3r} = \mu\left(d_{tx} + d_{to} + d_{a2aa} + d_{aa} + d_{aa2c} + d_{c1} + d_{c2c} + d_{c2} + d_{d2a} + d_{fa}\right)$$ $$f_{4r} = \sigma\left(fc_{tx} + fc_{to} + fc_{a2aa} + fc_{aa} + fc_{aa2c} + fc_{c1} + fc_{c2c} + fc_{c2} + fc_{d2a} + fc_{fa}\right)$$ $$f_{5r} = \sigma\left(t_{tx} + t_{to} + t_{a2aa} + t_{aa} + t_{aa2c} + t_{c1} + t_{c2c} + t_{c2} + t_{d2a} + t_{fa}\right)$$	4-48

4.8.5   Results

4.8.5.1   Results of the deterministic test case

The obtained results show how the optimizer has been able to define the best route, which is shown in Figure 4-79. It is not a strange situation because a shorter route exists within the whole set of options. The waypoints defined clearly identify it, and the effects of the vertical profile of the mission are not so relevant as to create another optimum route.

Figure 4-76 shows a 3D representation of the Pareto Front showing the three objective functions. As shown in Figure 4-77, the Pareto front belongs to a parallel plane of the

time-fuel plane, due to the fact that the optimal value for distance has been reached and it remains constant in the plot.
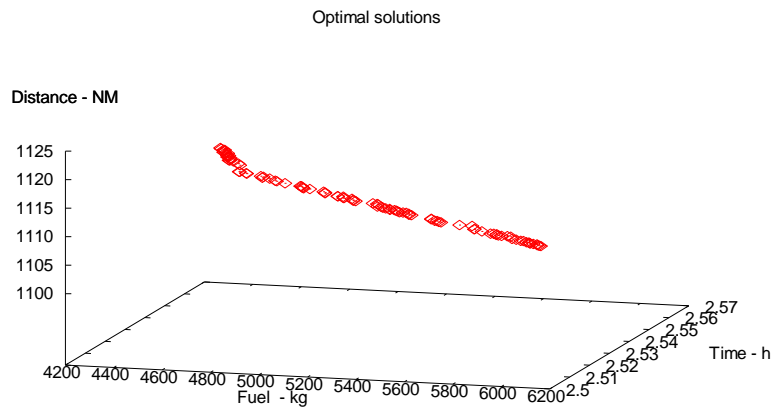
Figure 4-76.- Set of optimal solutions for the three objective functions
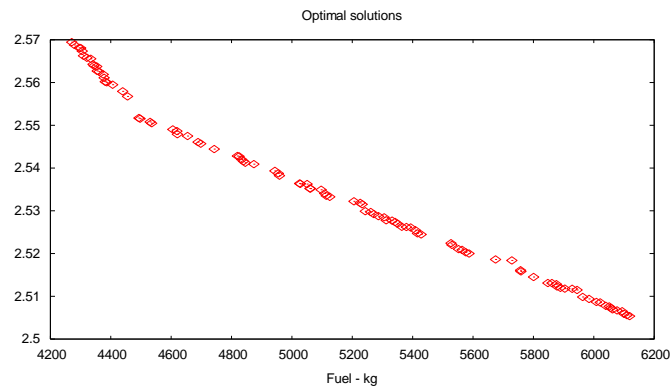
Figure 4-77.- Set of optimal solutions for the three objective functions

The information from the Pareto front can be translated to an application-specific representation. Figure 4-78 shows the profiles of some of the Pareto optimal members. It can be observed how climb to cruise level is directly related to cruise altitude in order to ensure the minimum fuel consumption. A significant result is that optimal solution which has defined the steepest climb to cruise level. In order to maintain low fuel consumption the second cruise level is one of the lowest. It demonstrates how the optimizer is seeking the best combinations of values to perform the optimal flight according to the defined objective functions.

The defined restrictions have enabled to obtain solutions with a long descent phase to final approach. In a more realistic scenario, air traffic restrictions would make unable such a descent ratio.
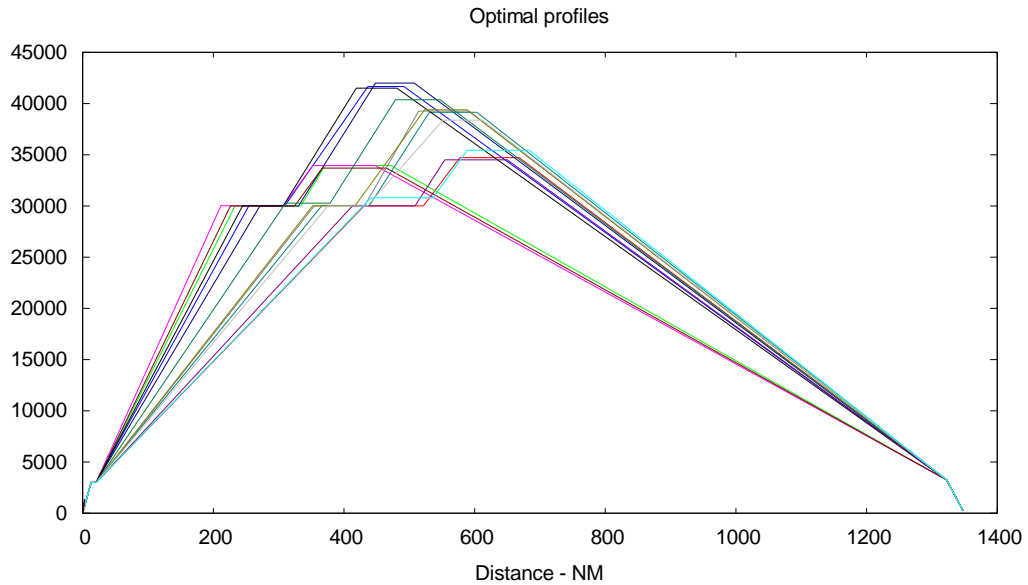
Figure 4-78.- Mission profiles for the best route

Figure 4-79.- Best route

4.8.5.2 Results of the stochastic test case

As in previous deterministic solution of the problem, the optimizer has been able to reach the optimum route, which minimizes the distance. In both stochastic and robust optimization cases the distance is fully optimized even considering uncertainty in the input parameters.

Figure 4-80 shows the Pareto Front of the Fuel and Time objective functions obtained with the stochastic procedure.

Figure 4-81 translates the information for some of the optimal members in the Pareto Front into the mission profile. Due to the introduction of the uncertainty on the input

parameters, a combination between steeper climb ratio and higher cruise altitude can be obtained. The main issue is to ensure the robustness of the solution when facing uncertainties in the parameters.
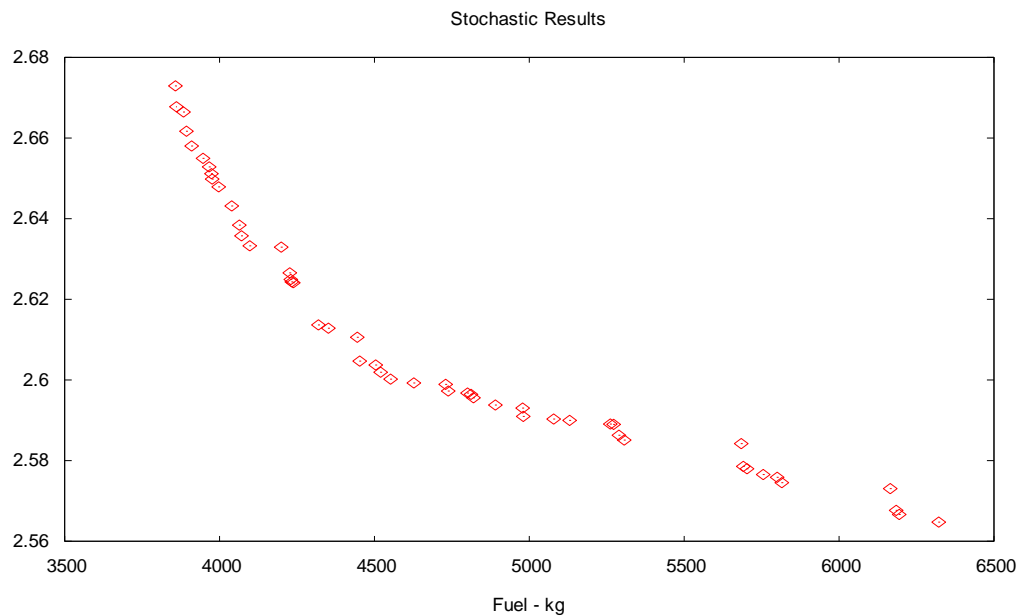
Figure 4-80.- Pareto Front for the stochastic analysis
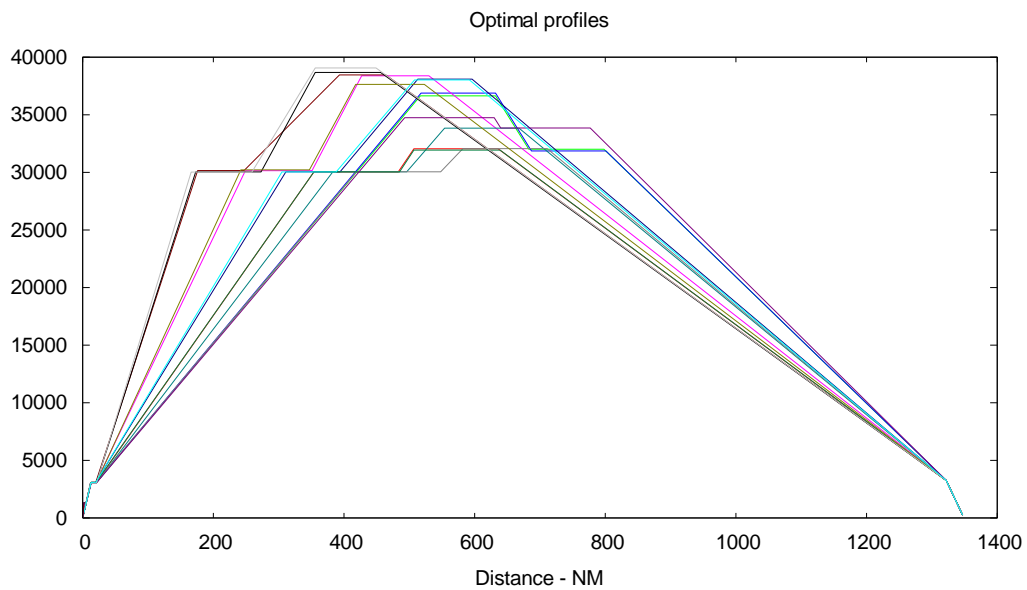
Figure 4-81.- Optimal Profiles for the stochastic analysis

4.8.5.3   Results of the robust test case

Figure 4-82 shows the Pareto Front of Fuel and Time objective functions for the robust analysis procedure. The front is no longer a line due to the fact that the problem is defined using 5 objective functions (means and standard deviations). Even plotting a 3D representation of the Pareto Front it would not be able to plot a Pareto surface because the dimension of the space of the solutions is larger than 3. Time and fuel consumption have been selected in order to compare with the deterministic and the stochastic results.

The definition of the standard deviation as one of the objective functions has produced optimum results far away from those obtained in the first case, where only mean values have been considered. In the robust analysis case, the solutions have not only taken into account the variability of the results, but also the output variability.
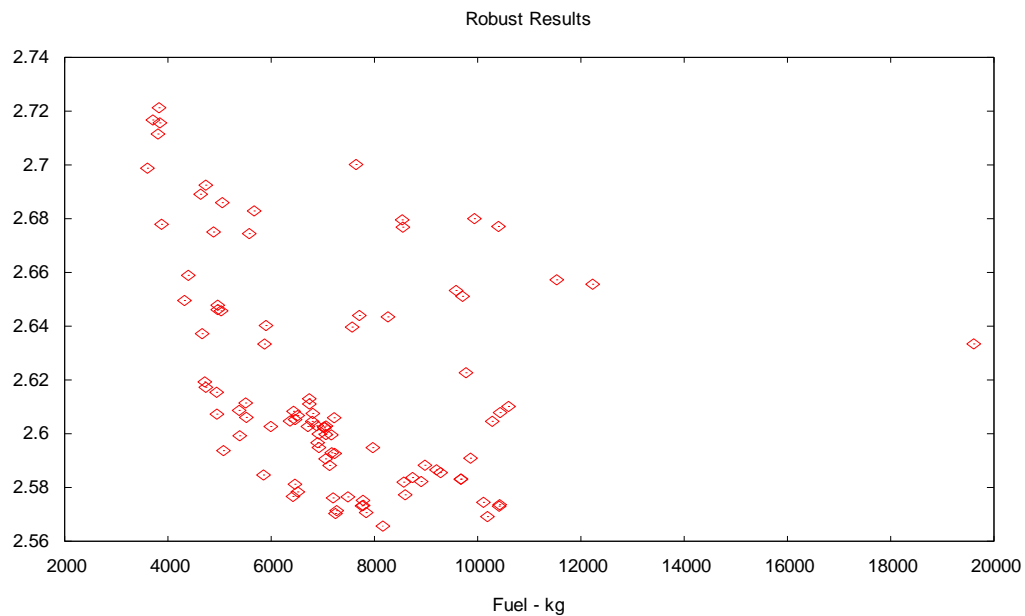
Figure 4-82.- Pareto Front for robust optimization analysis
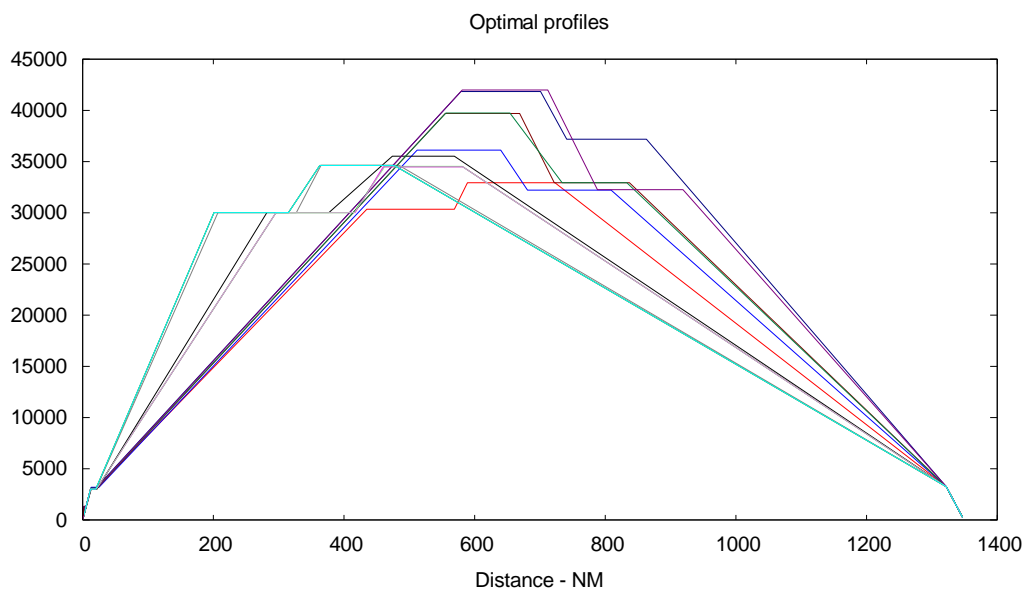
Figure 4-83.- Optimal Profiles for the robust optimization analysis

No significant differences can be detected in Figure 4-83 when it is compared with Figure 4-81. When considering the standard deviation as output, in the second case, values of climb rate and descent rates are not spread so regularly than in first case.

4.8.6 Conclusions

Taking into account the simplification that has been applied to the problem definition and the mandatory use of partial information to generate the model of the fuel

consumption, the results are accurate enough. Engineers from the air carriers have confirmed that the real problem behaves as described in this test case.

The study of the obtained results has been simplified thanks to the fact that distance gets a single optimum. The problem is simplified from a problem with three objective functions to a problem with two objective functions. This results has been obtained due to the definition of a low number of waypoints.

However, the test case has provided the opportunity to escape from fluid-dynamics applications and expand the application range to a topic with real commercial interest. It is directly related to the 2020 Vision (Busquin et al, 2001), which look for an important emission reduction, as well as an important noise reduction. Emission reduction is directly related to fuel consumption.

The results from the three analysed cases can be compared. Figure 4-84 compares the results obtained in the stochastic and the robust optimization procedures. The points from the Pareto Front obtained by the stochastic analysis are close enough to the cloud of points of the robust optimization analysis, so both results could be considered to be similar. But the standard deviation defined as an objective function introduces several new solutions. The solutions for the robust analysis do not belong to a 3D space, but to a 5D space, making the comparison more difficult.
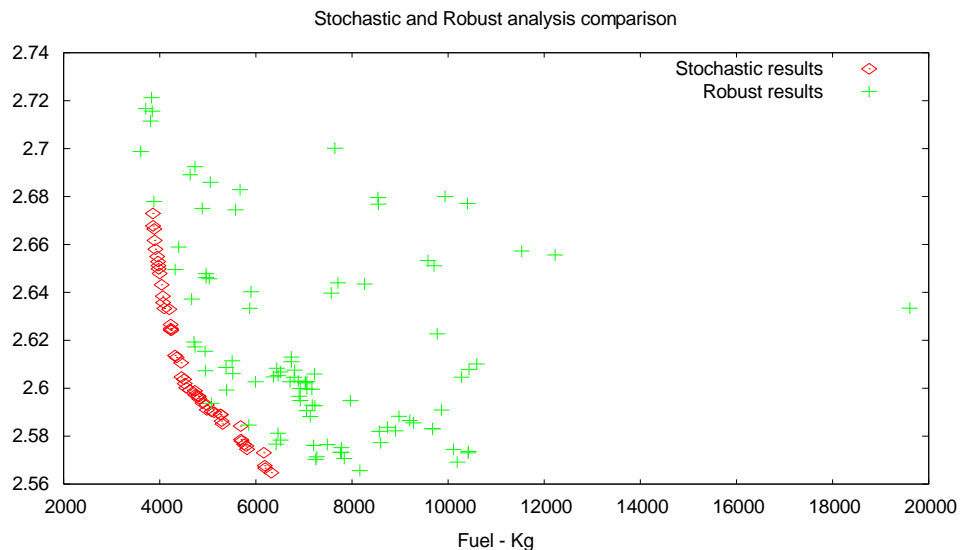
Figure 4-84.- Two non-deterministic case comparison

If the deterministic results are added to the comparison, as done in Figure 4-85, the reader can observe more differences. The deterministic solution seems to obtain a better solution, which minimizes more effectively fuel and time. But the robustness of the solution set cannot be ensured. This is the main issue to consider when comparing a deterministic solution and one taking into account uncertainty.

The use of a simplified model, based on mathematical relationship of the variables, has led to an easy computation of the individuals. Opposite to the previous applications, the actual Mission planning application does not present such a huge difference between the computational cost of the deterministic and the robust definition. Although the robust case is more expensive, now, the cost is not a limiting issue.

Figure 4-85.- Deterministic and non-deterministic cases comparison
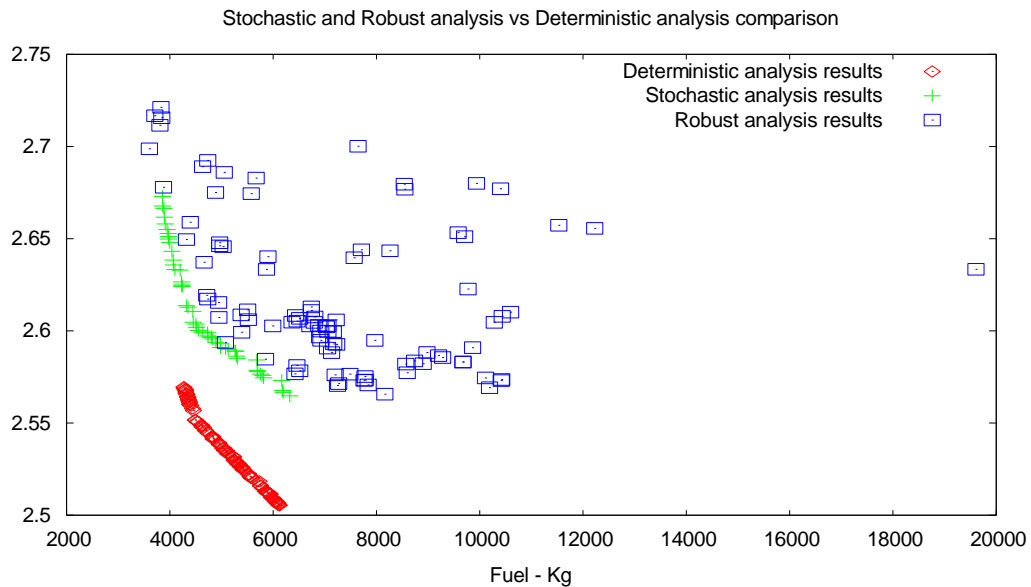
4.9 General conclusions on Stochastic and Robust Optimization

The test cases using CFD analysis tools have provided the opportunity to analyse several configurations of the management of uncertainties. The definition of the initial population, and of the stochastic set of samples has been taken into consideration. Additional test cases have been performed with the definition of a FSI aero-elastic problem, and a Mission Planning problem, as well.

The main conclusion come from the comparison between the deterministic and the stochastic and robust procedures. The results from all the test cases have demonstrated the robustness of the solution obtained by the stochastic and the robust procedures. The comparison of the deterministic results with the solutions provided by the Pareto members of the robust procedures shows how all the Pareto members are improving the robustness of the deterministic solution, even those Pareto members with the largest variability or standard deviation.

If the comparison is focussed on the stochastic and the robust procedures, the reader can conclude that the stochastic procedures is an intermediate point between the deterministic and the robust procedures. The stochastic is dealing with uncertainties but is not considering the variability of the results. Although a good performance can be obtained by using the stochastic, the robust solutions ensure a better control of the robustness, or at least a better measure of the robustness.

The reader should take into account the fact that pure mathematical cases can be easy to compute, but CFD or aero-elastic analyses take longer time. Due to the expensive cost of hundreds or thousands of evaluations required by an evolutionary algorithm, it is important to clearly identify the minimum number of individuals of each population and how many populations are required. The performed analysis in previous sections and the validation process of the used evolutionary algorithm described in the Appendix I help to find the best configuration.

Both fluid-dynamics and mission planning problems establish good examples on how to apply the stochastic procedure for robust design optimization to other kind of problems. The robustness of the solutions has been analysed. Stochastic and robust procedures have shown a good performance, dealing with the optimization of the variables involved in the phenomena while taking care of the uncertainty of the additional parameters. Although the robust procedure ensures the best control, with the definition of optimizing criteria based on the standard deviation of the fitness functions, in some cases, where the stochastic mean value improves the robust one for some of the Pareto members as happens in the multi-objective CFD test case, it can be considered that the stochastic procedure performed better. It is clear that the simplification that represents the stochastic case compared with the robust case, combined with the characteristics of each problem can produce different kinds of behaviour of the results. The engineer should carefully evaluate the analysed phenomena and decide which the most appropriate method to be applied is.

The stochastic method has been compared with a recent methodology applied for uncertainty propagation; the Probabilistic collocation Method. The Probabilistic Collocation method is a powerful method, which takes advantages of the probabilistic definition of the input variables, to define a multi-point evaluation of the solver. Thanks to a limited number of the input variables and its non-intrusive definition, it is a fast method to spread uncertainties across the analysis.

It is well known that the cost of the stochastic evaluations is high, due to the total number of the single evaluations, or shots, which must be performed. On the other hand, the stochastic method has a constant cost when increasing the number of stochastic variables and produces robust solutions thanks to its intrinsic variability. It should be taken into consideration that the introduction of stochastic samples means a significant increase of the total number of evaluations.

Using a surrogate model the cost is reduced, even taking into account the training time. Table 4-10 describes the time cost of direct evaluation of the solver or evaluations using an Artificial Neural network, including the training and validation time cost.

	Stochastic Evolutionary Algorithm coupled to ANN	Stochastic Evolutionary Algorithm coupled to the analysis tool
Generation of training Values (1000 samples)	30h	--
Training Process	1h	--
Validation process	0.5h	--
EA calculation with 250 stochastic samples	29h	190h
Total	60.5h	190h
	-69%	

Table 4-10: Direct solver evaluations vs ANN evaluations; cost comparison

Engineers need to face the issue to find the best balance between accuracy and fast evaluations. The use of a surrogate model is an option. But if a parallelized code is available, or new high performance computational resources, like GPU, both of them

are also good option to take into account. The final conclusion, anyway, is that robust design optimization is an expensive procedure, but it provides robust design solutions that ensure the stability of performances.

4.10 Summary

The research in this chapter is mainly devoted to the analysis of the performance of the stochastic procedure applied to the Robust Design problem.

Two kind of robust design problems have been defined. The first one does not account with the standard deviation as one of the fitness functions. Only mean values are used. It is the so-called stochastic method. The second one is the so-called robust method, which uses both mean and standard deviation as fitness functions. It ensures that not only the nominal value is optimized, but also its dispersion does.

Several test cases have been used. As done in the previous chapter, the Table 4-11 summarises the main test cases that have been analysed.

The structure of all the test cases is almost the same. A comparison is established among deterministic, stochastic and robust solution, in order to get the best understanding of the performance and accuracy of the stochastic and robust methods.

Stochastic Robust Optimization							
Name	Variables	Objectives	Method	UQ	Regime	ANN	Chapter
Math Test cases	Math variables	Compare and check methodologies	Deterministic Robust	MC	--	No	4.3
Single Objective CFD analysis	Initial and boundary flow conditions	Initial test and set-up configuration	Deterministic	--	Transonic	Yes	4.4.2 and 4.5
Multi-Objective CFD analysis	Initial and boundary flow conditions	Robust design	Deterministic Stochastic Robust	MC LHS PCM	Subsonic Transonic	Yes	4.4.3 and 4.6
Multi-objective Aero-elastic analysis	Structural and flow conditions	Robust design	Deterministic Stochastic Robust	MC	Transonic	No	4.7
Multi-objective Mission planning	Aircraft performance parameters	Robust design	Deterministic Stochastic Robust	MC	--	No	4.8

Table 4-11. Summary of analysed cases

5   Conclusions and further work

Uncertainty management and quantification is a problem of increasing interest in aeronautics. How to deal with uncertainties, taking into account the high computational cost the aeronautical related problems tend to face, is a challenging problem.

In this research stochastic procedure has been defined to analyse the sensitivity of the outputs with respect to the variability of the input parameters. This procedure has helped to establish robust optimization procedures.

The robust procedure has been applied to Computational Fluid Dynamics (CFD) problems, as well as to Fluid-Structure interaction (FSI) problems or Aircraft mission planning problems. Regarding optimization applications, they can be divided into stochastic applications, where only mean values have been taken as output, and robust ones, where the mean and the standard deviation values have been used as outputs, increasing the robustness of the solution.

The sensitivity analysis provides the capability to analyse the partial derivatives of the output function, without knowing anything about it. It takes advantage of the Monte Carlo Uncertainty Quantification method, that is largely used in the robust optimization technique developed in this study.

It is fully accepted, that cutting-edge design and optimization methodologies have to account with uncertainties. Several methodologies have been tested. Robust design optimization is becoming one of the top priorities in engineering design. Several research projects have been devoted to uncertainty quantification. The NODESIM-CFD project (Contract number 030959, www.nodesim.eu), co-funded by the 6th Framework European program is a clear example. Other projects want to define robust design methods and incorporate related tasks. The CRESCENDO project (Contract Number 234344), co-funded by the 7th Framework European program is one of them.

As already pointed in the partial conclusions of chapter 4, the reader should keep the main advantages from the stochastic, and mainly from the robust procedures. Dealing with uncertainties is becoming a great advantage when designing a new product. The robustness of the design will ensure the best performance in all the situations, which will lead to more confidence

by the user. In aeronautical applications, an improved and more stable efficiency in the overall flight can help to easily reach the environmental goals of the ACARE 2020 vision (Busquin et al, 1989). The robust procedures have demonstrated their capabilities to deal with the uncertainties in the input parameters, and to seek the most robust solution taking into account the variability of the output solutions.

Compared with the deterministic solutions, the stochastic and mainly the robust procedures are able to ensure a robust solution, which will provide a more stable behaviour. The more stable behaviour means an overall efficiency whatever the working conditions are. The analysed aeronautical applications have a working environment which is directly affected by the atmospheric weather. Almost all the conditions can be considered as uncertain; the wind speed and direction or the presence of air gust are some clear examples. The uncertainty on wind conditions will affect the aerodynamic performance of a wing, inducing a different aero-elastic behaviour, but also it will affect the fuel consumption and flight time in a commercial scheduled route.

The comparison between the stochastic procedure and the robust one concludes that the stochastic procedure means an improvement, from the point of view of the deterministic solution, but it does not reach the robustness levels of the robust procedure.

Several methodologies have been analysed and compared; Monte Carlo and Latin Hypercube stochastic sampling, but also Probabilistic Collocation Method have been used to propagate uncertainty and input variability through the CFD and FSI analyses. As shown in Table 3-28, each methodology has its own advantages.

The selection of the Monte Carlo method has been based on several issues. The main one is the capability to define a set of samples, instead of fixing the evaluation values. The definition of the stochastic samples at different steps of the optimization process helps to ensure the robustness. Another considered issue is the constant cost whatever the number of uncertainties are defined. It is well known that the main drawback of the Monte Carlo method is its high computational cost. The reader should keep in mind that other methods exponentially increase their cost with the number of uncertainties as happens with the Probabilistic Collocation method. It means that for a small amount of uncertainties these methods can provide a better performance regarding computational cost, while for a large number of uncertainties the performance decrease and the computational cost is not so competitive.

Although Monte Carlo techniques are considered expensive, their cost is almost constant even though the number of variables increases. This is an important issue to consider when comparing these techniques with newest ones, like Probabilistic Collocation Methods. The user should carefully evaluate the number of stochastic variables in his problem, the requirements about statistic information and the problem definition to select the most appropriate method.

The use of a surrogate model has been analysed and has demonstrated how it can improve the performance of the overall process. The computational cost is drastically reduced using a surrogate model, and the integration of the surrogate model with the stochastic process, or with the optimization process does not represent a major issue. The FLOOD Artificial Neural Network have been selected because the easy-to-use configuration they provide. The training and validation process are both an easy task, and they do not greatly increase the computational cost. The reader can conclude that the use of a surrogate model, like the neural network used in this

research, is quite a mandatory tool to be integrated within a stochastic analysis. But it becomes mandatory if an optimization process is performed.

In order to ensure the robustness of the solution several definitions have been tested. They refer to the initial population definition, but also to the definition of the stochastic samples during the optimization process. Firstly, regarding the initial population definition, standard methods use a random definition. In this research, the effects on pre-defining the initial population in order to evaluate the convergence of the solutions and to enable a greater flexibility on the problem definition have been tested. On the other hand, regarding the definition of the stochastic samples, several definition steps within the process have been evaluated; the first one has been at the beginning of the optimization process. Then, the samples remain constant along the whole process. The second step has been before each generation, which means that the samples remain constant at the generation level, but each generation is using different samples. Finally the last tested step has been at the individual level, defining new samples for each individual to be evaluated. The first one has been discarded due to the fact that it can be considered a multi-point evaluation, and the aim of this study is to ensure the robustness of the solutions. The last two ones, are appropriate for ensuring the robustness. The final conclusion points out that defining the samples at the level of the generations seems to be the most efficient step. The results do not improve when defining the samples at the individual level, and it introduces more complexity to the data management.

Optimization analysis usually has a high time cost, and also a high computational cost; both are directly related. When dealing with robust design optimization, the computational cost can increase one or two orders of magnitude, at least. It is a relevant increment. The use of surrogate models can be a helpful tool. The accuracy of the models and their validation are the main issues to take into consideration. The cost of the model generation is also relevant, and it should be added to the overall cost of the procedure.

But not only surrogate models can lead to a more competitive computational cost. The use of parallelized codes, at the level of the analysis tool, or at the level of evaluating the individuals within the optimization process, can help, as well. High performance computation resources, like GPU or multi-core and multi-nodal computers, are available. If the parallelized code is not available, a careful trade-off study should be established in order to evaluate the opportunity to parallelize it or not.

Engineers should take into account the best balance between cost and robustness of the solutions. The available methods for uncertainty quantification are expensive. To reduce their cost they should be limited in their application. Anyway, these methods have demonstrated their capability to provide a robust design solution, which ensures the stability of the performances.

Of course, the defined procedure has drawbacks. Parallelization is a big issue to take into consideration, which will improve the time cost. Uncertainty quantification models are the second big issue. Monte-Carlo methods are expensive, but produce full statistics, on the other hand collocation methods have a great dependency on the number of stochastic variables and they do not produce full statistics. Other methods, like fuzzy logics, could be evaluated. A specific statistical analysis concerning which kind of method better fits each kind of problem should be done.

5.1 Main contributions of this research

This research has focussed the attention of the reader on robust design and robust optimization techniques. The main contributions can be listed as follow:

- Implementation of a stochastic procedure based on Monte Carlo techniques
- Implementation of the stochastic procedure to stochastic and robust optimization
- Implementation of a methodology to reduce the computational cost of such procedure based on Artificial Neural networks
- Establish a comparison point between standard optimization methodologies, based on deterministic procedures, and new implementation of the stochastic and robust optimization methodologies.
- Apply the stochastic procedure, as well as the stochastic and the robust optimization procedure to Computational Fluid Dynamics (CFD), Fluid-Structure Interaction (FSI) and mission planning (MP) problems as a validation point.

5.2 Further research

The present research has opened lots of new questions to be investigated. As a summary of what is planned as future investigations the following list briefly describes the step forward:

- development of a parallelized code (or GPU) which can deal with solver evaluations reducing the required computational time.
- implementation of the stochastic and the robust optimization procedures to other optimization methods, such as Gradient-based ones, in order to compare the requirements from Evolutionary techniques and Gradient-based methods.
- integrate Self Order Maps (SOM) methodologies to analyse results when large number of output variables has been defined.
- further developments related to Uncertainty Quantification techniques should be investigated. In particular, further development of Monte Carlo techniques, which helps to reduce their computational cost but enabling the statistical accuracy of the results.

6 Appendix I: Numerical Methods and Tools

6.1 Introduction

This research is not devoted to the development of new numerical methods. It takes advantages of already existing methods and tools. However, the robust design and the robust methodologies developed in this work extensively use all these methods and tools, so it quite mandatory to briefly introduce them.

This section describes the tools used during the development of the present work. Numerical tools as the pre and post-processor GiD, and the CFD solvers TDYN and PUMI, or the aero-elastic code are described. A description of the artificial neural network is also provided.

The implementation of NSGA-II optimization algorithm is also described and validated. Some mathematical test cases are solved and validated with the available literature. Finally, a description of STAC, the stochastic management tools, is developed as an important milestone of the computations presented and discussed.

6.2 STAC description

STAC is a stochastic analysis management tool. Based on the developments by Zárate and Hurtado (1998), CIMNE team has created a tool which provides a very friendly and easy to use user interface, and which provides pre and post-processing capabilities.

The pre-processing capabilities include file management; i.e., selection of files containing input and output values, work folders definition, and number of total and error shots permitted. Finally, it can be included as a pre-processing capability the solver management.

Several probability density functions can be applied to the input variables. Gaussian, uniform, t-student, are some of the continuous variable distributions, and Binomial and Poisson two of the discrete ones.

The post-processing capabilities include statistical analysis of the input and output values, evolution of means and dispersion plots.

The most important capability is, without hesitation, the solver management. It provides the ability to apply the defined input values, and to execute all the required steps in order to correctly obtain the output data. All necessary calls to several programs, management of extra files, etc, can be defined in the batch file of STAC. Each one of STAC run, or shot, follows all the batch file instructions. STAC is able to manage any kind of solver that can be called from the command line, in windows as well as in Linux operating systems.

6.2.1 STAC Batch file

In order to better understand how to define a STAC batch file, an example is provided;

```
(1)  c:
(2)  cd C:\DOCUME~1\JORDIP~1\MISDOC~1\Doctorat\tesis\RAE2822\treball\
(3)  varatm
(4)  del r2822n1.fla
(5)  copy r2822n2.fla r2822n1.fla
(6)  cd C:\Users\JORDIP~1\DOCUME~1\Doctorat\Tesis\RAE2822\rae2822cp.gid
(7)  del rae2822cp.flavia
(8)  copy C:\Users\JORDIP~1\DOCUME~1\Doctorat\Tesis\RAE2822\treball\r2822cp1.fla rae2822cp.flavia
(9)  C:\PROGRA~1\COMPAS~1.8R3\PROBLE~1\Tdyn5.016\scripts\Tdyn.exe -2D -name rae2822cp.flavia
(10) cd C:\Users\JORDIP~1\DOCUME~1\Doctorat\Tesis\RAE2822\treball\
(11) copy C:\Users\JORDIP~1\DOCUME~1\Doctorat\Tesis\RAE2822\rae2822cp.gid\rae2822cp.flavia.for bezier.for
(12) lda_5
(13) del bezier.for
```

First of all, it is advisable to ensure you are in the appropriate location; lines (1) and (2) defines the path of work folder. Line (3) shows the call of the first program, including the required file management in the next lines. If it is required temporarily change the work directory it can be done, as in line (6), mainly to ensure a proper call of the second solver (line (9)). But come back to the working solver (10) is always required, in order to ensure the proper shot running.

It can be observed that what a list of command-line commands based in DOS standard language is provided. So, one of the STAC limitations come from this point: it is required that all solver or programs can be called using command line.

6.2.2 Stochastic definition

The most significant tool that STAC provides to the user is the capability to define input values according several probability density functions (PDF) embedded into STAC. From the defined probabilistic information input values samples are generated and applied to the solver in each single run, or shot.

Sampling techniques available are both Monte Carlo and Latin Hypercube, for all the available PDF.

STAC can also be used as a stochastic generator thanks to the generation of a file containing all the samples of the input values.

6.3 GiD and TDYN description

GiD is a pre and post-process software developed by CIMNE. All the simulations require three main steps: the first one is the so called pre-process which consists on the definition of the problem to be solved; the geometry, materials, boundary conditions definition and the mesh generation. The second one is the simulation itself, done by the solver. After the calculation is done, the presentation of its solution is needed in order to analyze and conclude whether it is correct and acceptable, thanks to the post-process of the results.

GiD provides the necessary capabilities to perform the first and third required steps for a FEM simulation; the so-called pre- and post-process. GiD is an easy-to-use geometric user interface, which includes cutting-edge mesh generation capabilities. The GiD environment can be customized to adapt the presentation, menus and windows in order to accelerate the definition of the geometry, its verification, and the generation of the mesh. It enables the definition of the boundary conditions, the problem data, and the mesh parameters, and always adapting this information to the solver requirements. Related to the post-process capabilities, GiD enhances the visualisation capabilities with powerful tools to show the analysis result. Almost all the used solvers on this work used GiD as its pre-processor. TDYN, PUMI and the Aero-elastic solver are based on a GiD customization mainly focused on creating the geometry and applying initial conditions to it, so the mesh will be generated and used by the solver.

At the first stages of this work, TDYN has been the selected solver. TDYN is a fluid dynamics solver developed by Compass and CIMNE in its initial version. It is based on the finite elements analysis method. TDYN solves the three dimensional, incompressible and slightly compressible Navier-Stokes equations. The spatial discretisation of the Navier-Stokes equations has been done by means of the finite element method, while for the time discretisation an iterative algorithm that can be considered as an implicit two steps "Fractional Step Method" has been used. Problems with dominating convection are stabilised by the so called "Finite Increment Calculus" method. TDYN, as many other solvers, are completely integrated with GiD. All the menus, and operations required by TDYN are called from GiD, so it is extremely easy to use, and friendly.

Both codes, GiD and TDYN, can be called using the STAC command line. In the GiD case, the definition of a batch file, which contains all the instructions to be performed, enables to avoid the interaction through the graphical interface. The language used in the batch file has a macro-style, so it is easily understandable, and it enables the definition of every single operation the user can call using the graphical user interface.

6.4 PUMI description

TDYN only manages slightly compressible problems, for more compressible problems PUMI has been used. PUMI is a CFD solver mainly addressed to obtain fast solutions for problems containing complex geometries. PUMI is a CIMNE development made by Dr. Roberto Flores. PUMI looks for the code efficiency in order to deal with complex geometries problems avoiding high computational demands, id est.; minimum memory requirements, fast single-treaded performance, and a good parallel scaling.

PUMI is structured as other CIMNE in-house codes. It uses a problem type that can be coupled with GiD, so the geometry and the problem conditions definition, even results visualization can be performed through GiD user interface. GiD interface is mainly used to create the mesh file. Other important files can be edited using notepad application, in order to define the calculation parameters like Mach number, number of time steps, turbulence model, and so many other parameters to set up the calculation. Again, it is an important fact the capability of use the command line.

PUMI is based on the solution of Euler equations, and uses a stabilization technique added to Galerkin scheme in order to avoid non physical solutions. An explicit multi-stage Runge-Kutta scheme has been selected as the time integration scheme so an increase of solution robustness is obtained. More details about PUMI solver can be found in Flores and Ortega (2007).

6.5 The Aero-elastic code

The used aero-elastic code is based on the Finite Point method. In this method, the computational domain Ω is discretized by a set of points only identified by their spatial coordinates.The numerical approximation to the strong form of the problem equations is computed in subdomains Ω_i called cloud of points (local approximation). Each cloud of points is composed by a point x_i called 'star point' (where the approximation is sought) and a collection of neighbour points which provide the support for the numerical approximation.

A particular case of the Weighted Least-Squares techniques (WLSQ), where the weighting function is fixed at each cloud, is employed in order to obtain the local approximation (Fixed Least-Squares). The Complete Polynomial Basis is used, which uses a collocation technique to select the evaluation points. If it is not accurate enough, the minimization problem is solved by a QR-factorization based algorithm in conjunction with an iterative adjustment of the weighting function parameters. The local cloud can also be enlarged if the quality test are not satisfied, (Ortega, 2007). Regarding the generation of the cloud of points, a suitable number of x_i neighbouring points are sought. A local Delaunay grid of the points falling into the search area is performed and the first layer of nearest neighbours is retained, (Lohner, 2002). The cloud is completed adding further points closest to x_i (restrictions are applied to boundary points).

The flow solver takes advantage of the Euler equations, which are solved in an ALE framework of reference. The equations are given by

$$\frac{\partial U}{\partial t} + \frac{\partial F^k}{\partial x_k} = -U \frac{\partial w^k}{\partial x_k}$$

6-1

where w denotes the velocity of the points. The conservative variables vector U and the convective flux vectors F are

$$U = \begin{bmatrix} \rho \\ \rho u_i \\ \rho e_t \end{bmatrix} \quad , \quad F^k = \begin{bmatrix} \rho(u_k - w_k) \\ \rho u_i(u_k - w_k) + \delta_{ik} p \\ \rho e_t(u_k - w_k) + u_k p \end{bmatrix}$$

6-2

and

$$p = \rho(\gamma - 1)\left[e_t - \frac{1}{2} u_i u_i\right]$$

6-3

In addition, proper initial and boundary conditions must be defined.

Using the low-order semi-discrete scheme

$$\frac{\partial U_i}{\partial t} = -2\sum_{j \neq i} \frac{\partial N_{ij}}{\partial x_k}\left[F_{ij}^k - F_i^k\right] - U_i \sum_j \frac{\partial N_{ij}}{\partial x_k} w_j^k$$

6-4

Where F_{ij} are the approximation Riemann solver of ROE.

$$F_{ij}^k = \frac{1}{2}\left(F_j^k + F_i^k\right) - \frac{1}{2}\left|A_n(U_i, U_j)\right|\left(U_j - U_i\right) \cdot \hat{n}^k$$

6-5

MUSCL extrapolation scheme plus limiters is used to increase spatial accuracy, (Ortega, 2009), (Lohner, 2002).

For time integration Jameson's dual time-steeping scheme (1991) is used.

The structural model is a 2 DoF (pitch and plunge) typical wing section model. In non-dimensional form this can be written as

$$\ddot{h} + x_\theta \cos\theta \, \ddot{\theta} - x_\theta \sin\theta \, \dot{\theta}^2 + 4k\beta\xi_h \, \dot{h} + 4k^2\beta^2 h = -\frac{2}{\pi\mu} C_l(t)$$

$$x_\theta \cos\theta \, \ddot{h} + \frac{1}{4} r_\theta^2 \, \ddot{\theta} + k r_\theta^2 \xi_\theta \, \dot{\theta} + k^2 r_\theta^2 \theta = \frac{2}{\pi\mu} Cm_{EA}(t)$$

6-6

Where
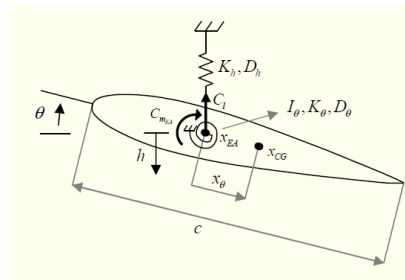
$$\beta = \frac{w_h}{w_\theta} \quad , \quad w_h = \frac{K_h}{m} \quad , \quad w_\theta = \frac{K_\theta}{I_\theta} \text{ are the uncoupled natural frequencies}$$

$k = \dfrac{w_\theta c}{2V_\infty}$ is the reduced frequency

$r_\theta^2 = \dfrac{4I_\theta}{mc^2}$ is the radius of gyration

$\xi_h = \dfrac{D_h}{2\sqrt{mK_h}}$, $\xi_\theta = \dfrac{D_\theta}{2\sqrt{I_\theta K_\theta}}$ are the damping ratios

$\mu = \dfrac{4m}{\pi\rho_\infty c^2}$ is the mass ratio

The coupling between the aerodynamic and structural models is performed as follows

do while structural time < maximum structural time
$t_n+1 = t_n + \Delta t$

1. Predict aerodynamic forces: $\boldsymbol{F^* = 3F_n - 3F_{n-1} + F_{n-2}}$ ($\boldsymbol{F}$=[Cl,Cmea])
2. Solve structure and compute body displacements (update points position)
3. Solve fluid in pseudo-time step
4. Re-compute aerodynamic forces. Go to step 2 if convergence is not achieved

end do

According to the problem under consideration, if the structural time increment is not large, inner iterations can be neglected without affecting the accuracy of the numerical results.

6.6 Meta-modelling

The optimization techniques and the meta-models usually work together. The use of meta-models are a good solution when the main solver requires long time calculations. The use of the meta-models provides an efficient way to obtain accurate results drastically decreasing the computation time. The Response Surfaces techniques, Kriging models or Artificial Neural Networks are some examples of them. Taking care of the definition of the constitutive parameters of models, and with appropriate initial values to define them, accuracy can be assured.

As mentioned, they are extensively used as an auxiliary tool on optimization procedures. Jeong, Murayama and Yamamoto (2004) have implemented a Kriging model in a Genetic Algorithms in order to optimize a 2D multi-elements airfoil. Chiba et al (2003) use an artificial neural network in order to model Navier-Stokes solver results avoiding calculation extra time on the first generations of the genetic algorithm progress. Papadrakis, Lagaros and Tsompanakis (1998) substitute the structural solver by a neural network, and applied it to an evolution strategy optimization problem. They saved computational resources within an acceptable accuracy.

6.6.1 Artificial Neural Networks

The multilayer perceptron model is an evolution of the perceptron model by Frank Rosenblatt, who developed a 3-layer model that used step transfer functions. In 1986,

David Rumelhart, Geoffrey Hinton and Ronald Williams used Rosenblatt's model to develop an improvement that used non-linear, but differentiable, transfer functions. It provided the ability to easily train the network, so it became more applicable.

Speaking about Neural Networks usually refers to a Multilayer Perceptron Network (López, 2008). However, there are many other types of neural networks, namely Probabilistic Neural Networks, General Regression Neural Networks, Radial Basis Function Networks, Cascade Correlation, Functional Link Networks, Kohonen networks, Gram-Charlier networks, Learning Vector Quantization, Hebb networks, Adaline networks, Heteroassociative networks, Recurrent Networks and Hybrid Networks.

6.6.1.1   The Multilayer Perceptron Neural Network Model

The Perceptron model uses a multilayer scheme. Each layer contains neurons, which are inter-connected with other neuron in the previous and the next layer. Each neuron executes a mathematical operation that in conjunction with all the other neurons will provide the solution or solutions. Briefly speaking, a multilayer scheme contains an input layer, where it can be assimilated each neuron to an input variable, and output layer, associated to output values, plus a number of intermediate layers, called hidden layers, that operate until the solution is reached. Although multilayer scheme can use several hidden layers, a 3-layer scheme is sufficiently accurate to face almost any problem. The 3-layer scheme is commonly used, so it is taken as example. The diagram in Figure 6-1 illustrates a perceptron network with three layers:
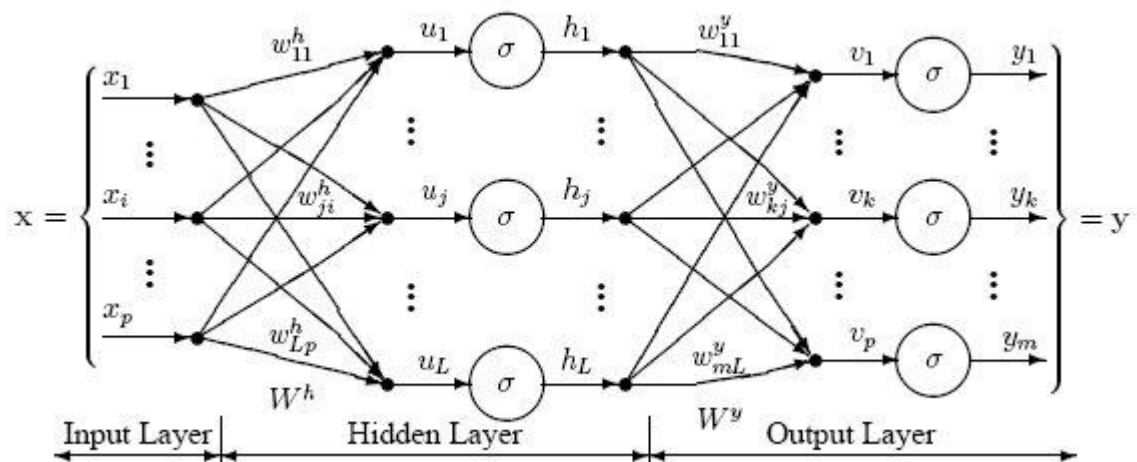
Figure 6-1. Perceptron scheme

This network has an input layer (on the left of the figure) with three neurons, one hidden layer (in the middle) with three neurons and an output layer (on the right) with three neurons.

There is one neuron in the input layer for each input variable. The main function of each layer is as follows:
- Input Layer — a vector of input variable values ($x_1...x_p$) is presented to the input layer. The input layer, or just before it in some cases with external processing, standardizes these values by subtracting the median and dividing by the

interquartile range as a first step. It distributes the values to each of the neurons in the hidden layer as a second step. The inputted value to the neuron in the hidden layer is the weighted sum of the standarized input values.

- Hidden Layer — arriving at a neuron in the hidden layer, the value from each input neuron is multiplied by a weight (w_{ji}), and the resulting weighted values are added together producing a combined value u_j. The weighted sum (u_j) is fed into a transfer function, σ, which outputs a value h_j. The outputs from the hidden layer are distributed to the output layer. Transfer function can be linear or non-linear (López 2008), depending on the case under study.
- Output Layer — arriving at a neuron in the output layer, the value from each hidden layer neuron is multiplied by a weight (w_{kj}), and the resulting weighted values are added together producing a combined value v_j. The weighted sum (v_j) is fed into a transfer function, σ, which outputs a value y_k. The y values are the outputs of the network.

If a regression analysis is performed with a continuous target variable, then there is a single neuron in the output layer, and it generates a single y value.

Mainly, the setup of a Neural Network includes the definition of the number of hidden neurons in each hidden layers of the network. For nearly all problems, one hidden layer is sufficient. Two hidden layers are required for modelling data with discontinuities such as a saw-tooth wave pattern. Using two hidden layers rarely improves the model, and it may introduce a bigger risk of converging to a local minima. There is no theoretical reason for using more than two hidden layers.

Another parameter to set-up is the number of hidden neurons. This value defines the precision of the solution, but high numbers produce an over-constrained function that does not approximate the function between two known points. A 2D example is shown in the Figure 6-2, where it can be appreciated that an over-constrained function perfectly approximates the known points but could not adjust the function in these areas where no points are defined.

6.7 Description and customization of the Neural network

The neural network used in this research is based on the FLOOD neural network open source code, by López (2007). FLOOD code provides all the capabilities and functions required to train, to evaluate and to validate the network. Additionally, FLOOD provides some pre-defined solutions to be used in typical test cases or problems like data linear regression application or Mean Squared Error application.
Everything is already defined and only a few work of customization is required. Mainly, the customization steps include the definition of the number of hidden neurons of the network, and the required definition of the number of input and output neurons.

The preliminary work before the use of the neural network is to define the number of hidden neurons. As explained, the number of hidden neurons defines the precision of the solution, but the use of high numbers produce an over-constrained function that does not approximate the function between two known points. Figure 6-2 is a clear example where can be appreciated that an over-constrained function perfectly approximates the

known points but produces an undesirable behaviour in these areas where no points are defined.
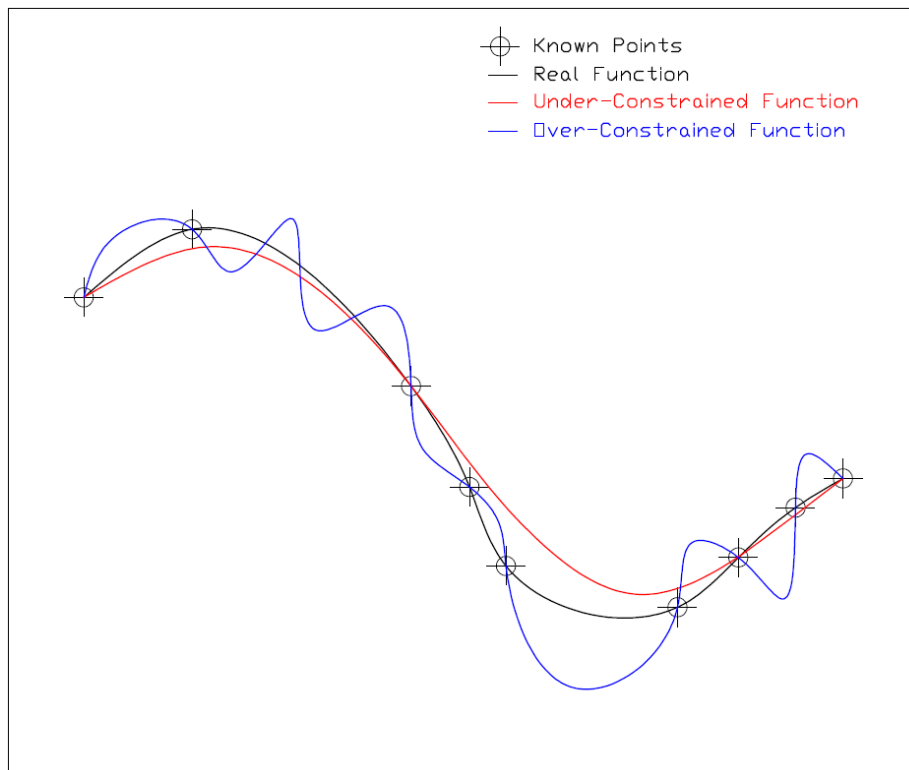
Figure 6-2. Function approximation

In order to define the best number of hidden neurons some tests have been performed. 4, 5, 6, 7, 8, 9, 10, 11 and 12 hidden neurons neural networks have been validated against the real values. The best results are obtained using an 11-hidden neurons network. Hidden neurons are directly related to the problem definition; its number directly depends on the number of inputs and outputs of the problem. Depending on the problem complexity, several layers of hidden neurons can be defined, so even if a preliminary guess can be done this neural network parameter should be check every time. Table 6-1 summarizes the values of correlation during the training process. Two outputs values have been considered, so each correlation and their mean value are considered.

Hidden Neurons	Correlation Cl	Correlation Cd	Mean Correlation
4	0,9885	0,9704	0,9795
5	0,9963	0,9956	0,9960
6	0,9988	0,9992	0,9990
7	0,9993	0,9992	0,9993
8	0,9997	0,9990	0,9993
9	0,9995	0,9995	0,9995
10	0,9987	0,9983	0,9985
11	0,9996	0,9997	0,9997
12	0,9980	0,9989	0,9985

Table 6-1. Correlation values

Figure 6-3 shows the evolution of the correlation values of each test.
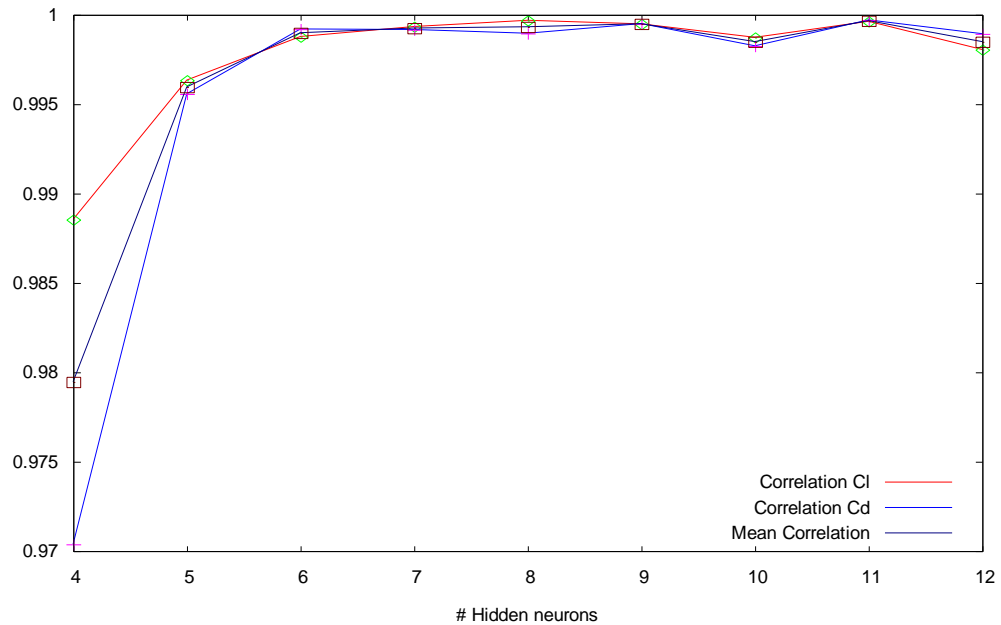
Figure 6-3. Correlation evolution

The training process needs sample data from real calculations of the solver. It is a usual practice, as done by Papadrakakis, Lagaros and Tsompanakis (1998) and Quagliarella and Vicini (1999), to train the artificial neural network using the previous generation data. When enough data is generated, it is used to train the neural network. The training process is embedded into the general optimization procedure. It should be taken into account the time required to train the network, and compared with the total time of the optimization process. Sometimes it is better to train the neural network independently of the general procedure, so advantage of previously calculated sample data can be taken in order to save computing time.

In this work, the usual procedure has been to previously train the neural network, because it is quite easy to obtain the required sample data from previous analysis, for example.

6.8 Evolutionary algorithm description

The core of the optimization procedure defined in this research is based on Evolutionary Algorithms techniques. Based on the Non-dominated Sorting Genetic Algorithm (NSGA-II) code described by Deb et al (2000), Deb et al (2000), Deb and Goel (2000), Deb, Pratap and Moitra (2000), the developments here implement several solutions to the core code.

Chafekar et al (2003) defined new approaches for solving constrained problems, which need to deal with a large number of constraints. It is not our case at this point of the research, but both approaches can improve NSGA-II results when the number of constraints increases.

The Evolutionary algorithms are considered stochastic optimization methods due to the random definition of the initial population and the mutation, and crossover strategies

that produce new members. But in the understanding of the present developments, it is considered that the evolutionary algorithms are deterministic processes. From the point of view of this work, all the methods which lead to an optimum point, without considering a stochastic probabilistic definition of the input parameters or uncertainties on the parameters, are considered as deterministic. Only those, defining a probability associated to the input values, or considering some kind of uncertainty on them has been considered as stochastic.

6.8.1 Validation of NSGA2

Introduction and objectives

NSGA-II algorithm is a development by K. Deb (Deb et al, 2000; 2003). It has been implemented as the optimizer to be used during this research. . In order to ensure the best performance on the applications, a validation process has been set-up.

These results complement those in section 4.3 where two mathematical test cases have been solved.

Procedure

The lift and the drag coefficient of a NACA0012 profile have been used as objective functions of the optimization process. Several tests have been established defining a different amount of generations and a different amount of individuals in each generation. The results have been compared by means of the convergence of the optimization.

The analysed cases include three different cases for the number of generations, and three cases for the number of individuals in each generation. The probabilities of mutation and cross-over have been fixed at the same value; cross-over equals to 0,92 and mutation equals to 0,16667.

Results of the validation with a General problem

Two main comparisons have been established. From the results, it can be noticed how an increase of the number of generations produces an increase of the total amount of points, but maintaining the same amount of points on the Pareto front. It can be also observed that the total amount of points near the frontier increase as effect of increasing total number of points, but without affecting the accuracy of the best solutions.

Analysing the whole population no major differences can be found, but if it is carefully checked the obtained frontiers, it can be evaluated the effect of the random definition in Genetic Algorithm, because each one of the frontier is slightly different from the others. In figure 6-4 to 6-6 it can be noticed these slight differences. Figure 6-7 is a comparison of the three Pareto Fronts.
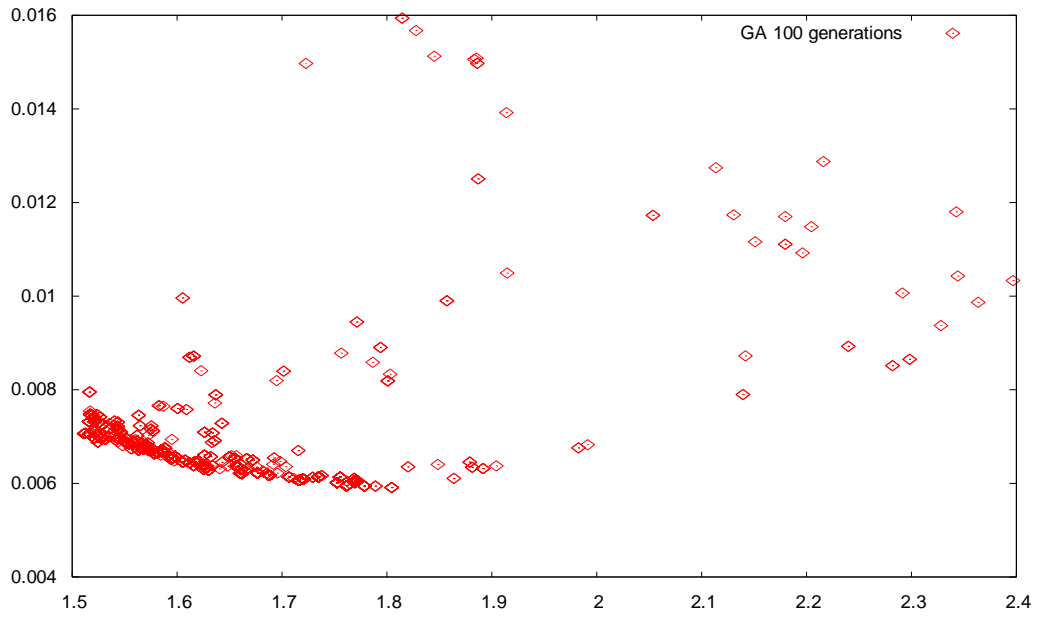
Figure 6-4.- 100 generations analysis
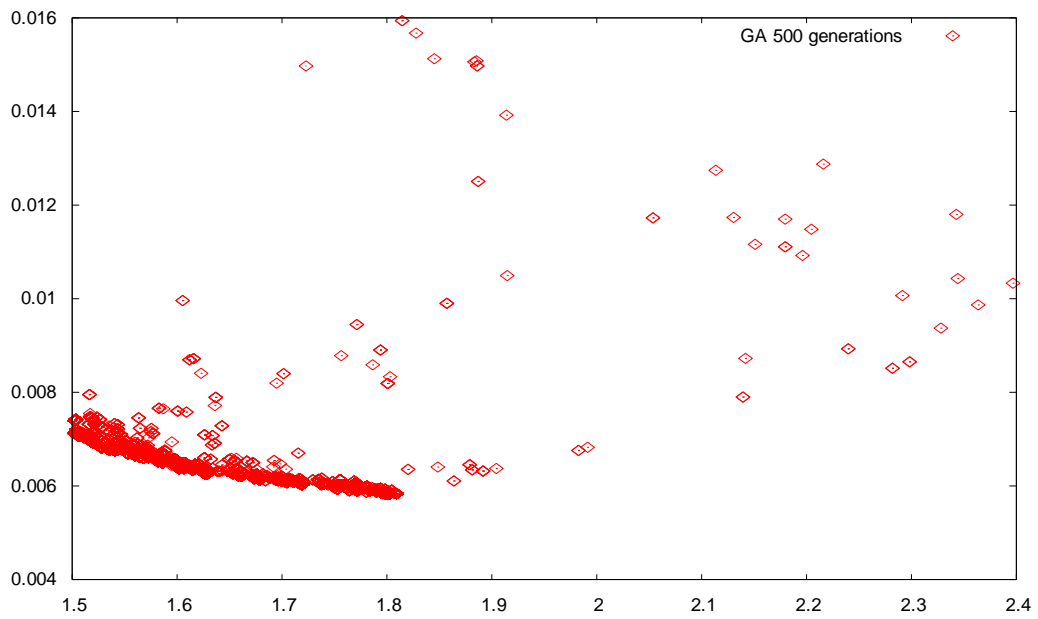
Figure 6-5.- 500 generations analysis
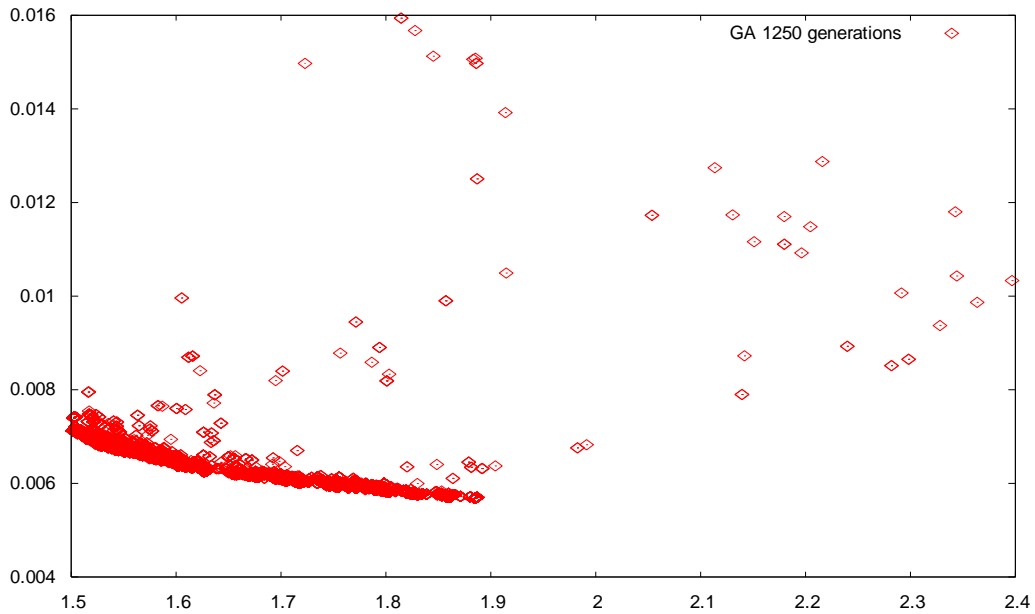
Figure 6-6.- 1250 generations analysis
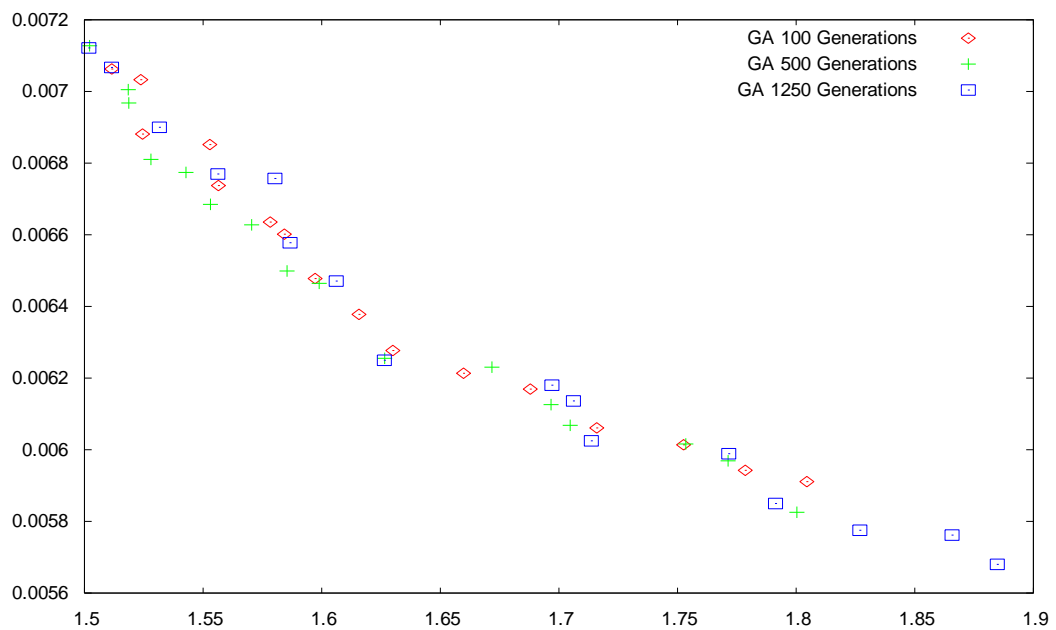
Figure 6-7.- Pareto front comparison; 100, 500 and 1250 populations

The analysis of the effect of increasing the number of individuals, and populations, reveals that, although the obtained results are quite similar, the Pareto front is better drawn when increasing the number of individuals.

In figure 6-7 the free parameter is the number of generations, and in figure 6-8 the free one is the number of members in each population, so the Pareto frontiers can be compared. Plotted values are pretty similar, and Pareto fronts are almost the same, which means that only the amount of best choices increase, but neither gain nor loss of accuracy is obtained.
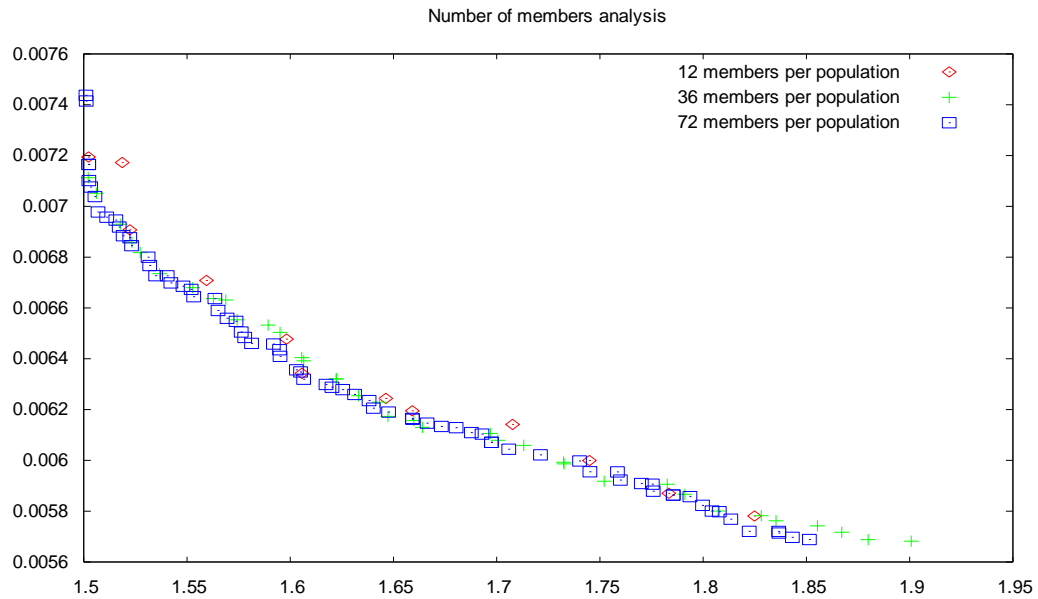
Figure 6-8.- Pareto front comparison; 12, 36 and 72 members per population

Of course, the definition of the required members, and generations is a problem-related issue. It means that accuracy is not related with the defined values.

Increasing the number of members and population the accuracy of the method is increased, but the time consumption is increased, as well. Analysing the shape of the Pareto fronts obtained when different number of members or populations are defined it can be observed that, even a clear difference is detected, it is not a great difference. It can be concluded, that if necessary the number of population can be reduced in order to decrease the computational effort without degrading the accuracy in a major way.

7   Appendix II: Aerodynamics

7.1 Introduction

In order to support the decisions taken during the developments of this research some aerodynamics concepts are introduced in this appendix. These concepts are well-known for people in the aerodynamical field, but could not be so clear for those coming from other fields.

7.2 Aerodynamic profiles

7.2.1 Definitions

a) Airfoil section: shape which results from cut the wing with a parallel plane of longitudinal axe of the aircraft.
b) Leading Edge: line that includes all initial points of all airfoil sections of the wing.
c) Trailing Edge: line that includes all final points of all airfoil sections of the wing.
d) Chord: fictitious line that joints the leading edge and the trailing edge.
e) Angle of attack: angle between the chord line and the direction of the relative wind. The relationship between lift and angle of attack depends on the airfoil shape, although the general shape of the function is the same in all airfoils.
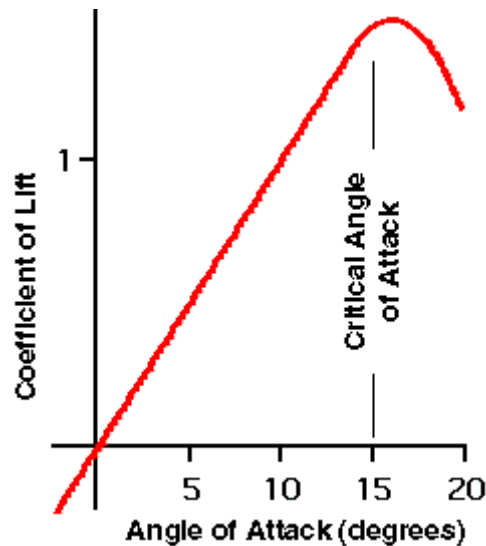
Figure 7-1. Polar curve

In all cases, the lift (or the coefficient of lift, which is the same in this context) increases while angle of attack also increases its values. When angle rounds approximately 13-17º, the lift no longer increases and it begins to decrease. This point is known as critical angle of attack. Critical angle of attack is a characteristic of each airfoil (see Figure 7-1).

Each airfoil is optimized in order to obtain the best relationship between lift and drag (or their coefficients) for the application to be developed.

f) Lift coefficient: dimensionless parameter that relates lift force and dynamic pressure;

$$C_L = L \Big/ q \cdot v^2$$

g) Centre of pressure or aero-dynamical centre: point where the aero-dynamical forces are applied.

h) Centre of gravity: point where mass forces are applied.

i) Aero-dynamical Forces: Four are the main aero-dynamical forces; Lift, Drag, Thrust and Weight. Third and fourth, which are thrust and weight, are a general characteristic of all aircraft and its engine. First and second, lift and drag, are airfoil characteristic. All four forces have a clear relationship for each of the stage of flight. In linear and straight flight, non-accelerated flight, thrust will be equal to drag, and weight equal to lift. In upward stage, weight should be considered as its components in longitudinal and transversal direction related to aircraft axis.
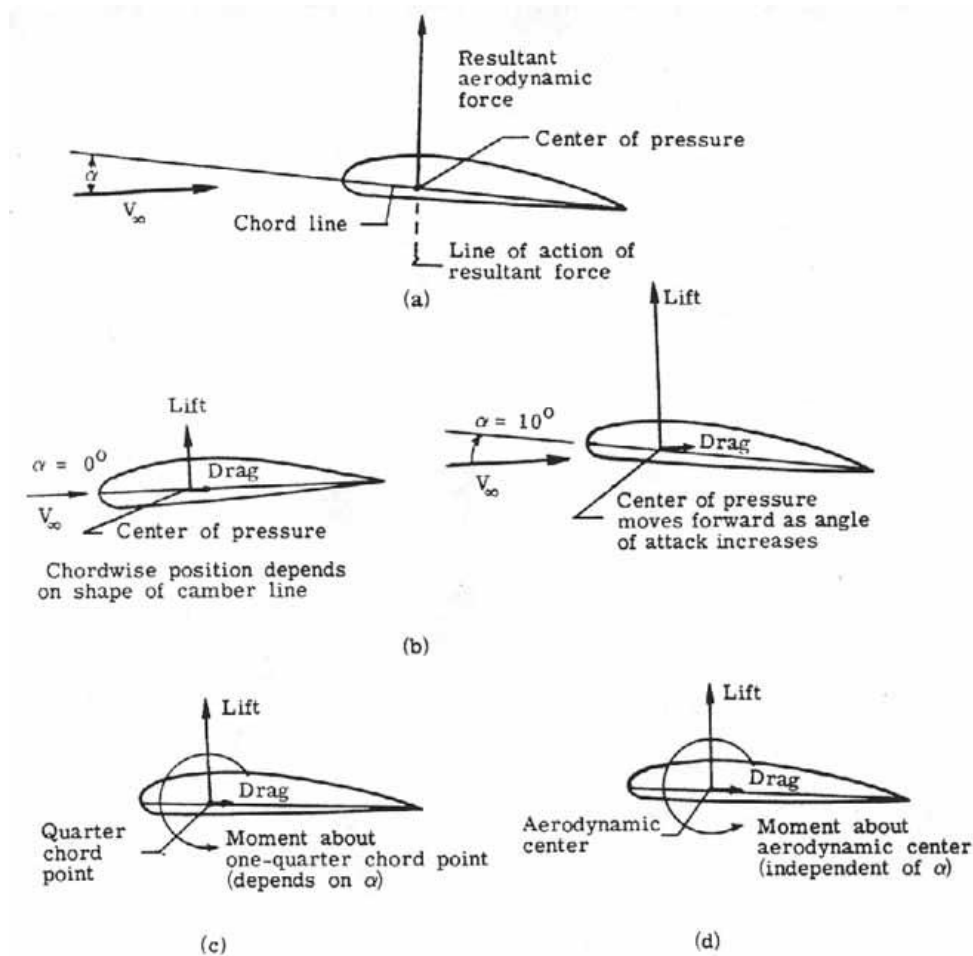
Figure 7-2. Aerodynamic Forces

Figure 7-2 shows force representation for some angle of attack. Lift and drag are always perpendicular and parallel to flow direction.

7.2.2 Bernoulli's principle

The Bernoulli's principle defines the equation that relates the amount of flow of a fluid, its pressure and its velocity.

$$\frac{v^2}{2} + \frac{P}{\rho} + g \cdot z = k \qquad \text{7-1}$$

First developed for the study and analysis of the fluid flow in a pipe, the equality of its formulae stands for the sum of the kinetic energy (related to velocity), the flow energy (related to pressure), the potential energy (related to its height) that is equal to a constant value k. The final meaning of the Bernoulli equation is that velocity and pressure of the fluid flow are related. Although there are several applications of the Bernoulli equation, some in aeronautical related applications like Pitot tube (Venturi application), if it is applied to an airfoil, the effect of the term $g \cdot z$ is negligible, so it can be understood that if the velocity increases, then the pressure decreases.

The shape of an airfoil produces an increment of the velocity in its upper surface and it can produce a decrement in its lower surface, producing lower pressures in the upper side and high pressures in the lower one. The total amount of the differential of pressure on the surfaces produces the lift force.

Although the Bernoulli principle is a good explanation of how the lift force is created, and it is used in many physics and aerodynamics courses to explain this phenomena, the theory cannot properly explain why the airflow in the upper side increases its velocity, even using geometrical reasons.

7.2.3 Newton's theory

The aerodynamic forces can be explained more efficiently using the Newton's laws.

Second Newton's law states that all action has its own reaction. Using this statement it can be completely justified the lift force, otherwise the action is missed. The lift is the reaction of the force produced by the downwash. The big amount of air diverted down by a wing changes the momentum of the air stream around the airfoil, and lift force is the reaction produced by the change in air momentum. Because the momentum is the product of the mass and the velocity of the air, the lift force is proportional to the amount diverted down and its velocity. Then the lift produced by a wing can be increased increasing the amount of air or increasing its velocity.

Of course, it must be taken into consideration other effects to completely understand the aerodynamics of a wing. From the previous explanation it can be guessed that increasing the amount of diverted air the lift can be increased, so increasing the angle of attack it increases. It must be observed that increasing angle of attack, drag is also increased due to the bigger surface facing the flow, which increases the pressure reaching maximum values in a bigger area. A second effect is that separation point approximates to the leading edge, increasing the turbulent flow area, which increases drag and reduces lift.

7.2.4 Potential Flow

All the above theories study the flow as a whole, but if the evaluation of pressure or the velocity distribution is required, the flow characteristics should be studied on each point of the control volume.

In this case, the governing equations are the laws of the mass conservation, the conservation of momentum and the conservation of energy. Including the viscosity effect, it will be obtained the Navier-Stokes equations that provide with the solution of a low viscous flow.

In order to finally obtain the potential flow equation the conservation of mass equations must be applied to a portion the control volume:

In x direction the input and output flow are:

$$\left(\rho \cdot u - \frac{\partial \rho\, u}{\partial x} \cdot \frac{dx}{2} \right) dy\, dz \quad and \quad \left(\rho \cdot u + \frac{\partial \rho\, u}{\partial x} \cdot \frac{dx}{2} \right) dy\, dz \qquad \text{7-2}$$

In the same way, in direction *y* are:

$$\left(\rho \cdot v - \frac{\partial \rho\, v}{\partial y} \cdot \frac{dy}{2} \right) dx\, dz \quad and \quad \left(\rho \cdot v + \frac{\partial \rho\, v}{\partial y} \cdot \frac{dy}{2} \right) dx\, dz \qquad \text{7-3}$$

And in *z* direction are:

$$\left(\rho \cdot w - \frac{\partial \rho\, w}{\partial z} \cdot \frac{dz}{2} \right) dx\, dy \quad and \quad \left(\rho \cdot w + \frac{\partial \rho\, w}{\partial z} \cdot \frac{dz}{2} \right) dx\, dy \qquad \text{7-4}$$

So the total flow is:

$$\dot{m}_{ext} = \left(\frac{\partial \rho\, u}{\partial x} + \frac{\partial \rho\, v}{\partial y} + \frac{\partial \rho\, w}{\partial z} \right) dx\, dy\, dz \qquad \text{7-5}$$

Considering the Reynolds transport theorem and the conservation of mass equation together, it can be obtained the continuity equation, which the only consideration is that velocity and density should be continuous in the portion of control volume considered.

The Reynolds transport theorems states:

$$\int_{CV} \frac{\partial \rho}{\partial t} dx\, dy\, dz + \dot{m}_{ext} = 0 \qquad \text{7-6}$$

Then the continuity equation is as follows:

$$\frac{\partial \rho}{\partial t} + \frac{\partial \rho\, u}{\partial x} + \frac{\partial \rho\, v}{\partial y} + \frac{\partial \rho\, w}{\partial z} = 0 \qquad \text{7-7}$$

In some cases, where rotational movement or radial motion flows are involved it is easy to uses the same equation but in cylindrical coordinates:

$$\frac{\partial \rho}{\partial t} + \frac{\partial \rho\, v_r}{\partial r} + \frac{1}{r}\frac{\partial \rho\, v_\theta}{\partial \theta} + \frac{\partial \rho\, w}{\partial z} = 0 \qquad \text{7-8}$$

Particular cases of the continuity equation are those where it is considered steady flow, or incompressible flow. Steady flow removes from general equation the time, so it states:

$$\frac{\partial \rho\, u}{\partial x} + \frac{\partial \rho\, v}{\partial y} + \frac{\partial \rho\, w}{\partial z} = 0 \qquad \text{7-9}$$

That is the same in cylindrical coordinates:

$$\frac{\partial \rho \, v_r}{\partial r} + \frac{1}{r}\frac{\partial \rho \, v_\theta}{\partial \theta} + \frac{\partial \rho \, w}{\partial z} = 0 \qquad\qquad \text{7-10}$$

The incompressible flow means that density is a constant value, so it can be simplified both equations to:

$$\frac{\partial u}{\partial x} + \frac{\partial v}{\partial y} + \frac{\partial w}{\partial z} = 0 \qquad\qquad \text{7-11}$$

Alternatively, in cylindrical coordinates:

$$\frac{\partial v_r}{\partial r} + \frac{1}{r}\frac{\partial v_\theta}{\partial \theta} + \frac{\partial w}{\partial z} = 0 \qquad\qquad \text{7-12}$$

Notice that incompressible flow uses the same equation both for steady and unsteady flow.

From this continuity equation the general Laplace equation can be obtained, introducing the concept of velocity potential.

$$u = \frac{\partial \phi}{\partial x} \quad , \quad v = \frac{\partial \phi}{\partial y} \quad , \quad w = \frac{\partial \phi}{\partial z} \qquad\qquad \text{7-13}$$

Or that is the same as, in cylindrical coordinates:

$$v_r = \frac{\partial \phi}{\partial r} \quad , \quad v_\theta = \frac{1}{r}\frac{\partial \phi}{\partial \theta} \quad , \quad w = \frac{\partial \phi}{\partial z} \qquad\qquad \text{7-14}$$

Then the Laplace equation can be obtained, or the Potential flow equation:

$$\frac{\partial^2 \phi}{\partial x^2} + \frac{\partial^2 \phi}{\partial y^2} + \frac{\partial^2 \phi}{\partial z^2} = 0 \qquad\qquad \text{7-15}$$

As in many other cases, the Laplace equations will provide with the solution of the flow around the airfoil. From this equation, it can be obtained the streamline equation, for the 2D and 3D case.

The 2D case really defines a line;

$$u \, dx + v \, dy = 0 \qquad\qquad \text{7-16}$$

But the 3D case defines stream-surfaces;

$$u \, dx + v \, dy + w \, dz = 0 \qquad\qquad \text{7-17}$$

Stream functions restrict the flow to be tangential to streamlines or surfaces, there is no flow across the streamline.

In order to calculate the lift around a body, it is calculated the pressure distribution combining Bernoulli equation, Lagrange equation and the circulation around the body Γ, defined as the total rotation around the body.

The conclusion is the Kutta-Jouskowski theorem, that states

$$Lift = \rho \cdot V_{\infty} \cdot \Gamma$$

| | 7-18 |

So, lift per area is:

$$Lift = \frac{1}{2} \cdot C_L \cdot \rho \cdot v^2$$

| | 7-19 |

and in the same way, drag per squared area is:

$$Drag = \frac{1}{2} \cdot C_D \cdot \rho \cdot v^2$$

| | 7-20 |

Potential flow has largely studied; Theodorsen (1940) and Theodorsen and Garrick (1949) describe the definition of equations to be used in numerical solutions. Working with the mathematical equations and comparing with experimental data, they develope a general theory that provide a clearer perspective, as mentioned by the authors.

7.2.5 Dimensionless coefficients

A tool to compare aerodynamic forces and momentum are the dimensionless coefficients. They were first developed to check similitude between scaled models and real ones. Dimensionless coefficients define equivalence between both models in order to estimate the forces in the full-scale model from the forces in scaled model. The main coefficients related with forces and moment are C_L, the lift coefficient, C_D, the drag coefficient, C_p, the pressure distribution coefficient, and C_m, the moment coefficient. There are other important coefficients; namely Mach number, M, Reynolds number, Re. Prandlt number, Pr, that are not so usual values as previous ones.

7.2.5.1 *Lift Coefficient*

The lift coefficient relates lift force, the dynamic pressure and the area of the airfoil. Equation 7-19 is the expression of lift per planform area of the airfoil.

The panform area is the orthogonal projection of the wing area in the horizontal plane.

Figure 7-1 shows a common polar curve. It represents the relationship between the lift and the angle of attack. As shown in the figure 7-1, lift tends to increase until stall angle, where a sudden and fast decrement of the force occurs.

Figure 7-1 represents lift versus angle of attack of a symmetric airfoil. When the angle of attack is zero, a symmetric airfoil does not produce any lift force. If the airfoil is not symmetric, for example chambered airfoils, its polar curve does not cross axes on the origin. Even angle of attack were zero, the airfoil is producing lift force due to its asymmetric shape.

7.2.5.2 Drag coefficient

The drag coefficient is the value that quantifies the drag of an object into a fluid flow. From the equation 7-21, the lower drag coefficient leads to lower drag force. The drag is related to the area faced against flow movement. This force has two main origins; skin friction and form drag. Form drag is related with the shape of the object, and skin friction is related to viscosity forces over the surface of the object.

For lifting surfaces, a third component appears. It is called induced drag, and is a consequence of the needed difference of pressure between upper and lower surfaces of the airfoil.

7.2.5.3 Pressure coefficient

The pressure coefficient is the ratio between relative pressure in a point and the dynamic pressure of the flow. For incompressible flows:

$$C_p = \frac{p - p_\infty}{\frac{1}{2}\rho_\infty v_\infty^2}$$

7-21

p: pressure at analysed point
p_∞: pressure of the free stream
ρ_∞: density of the free stream
v_∞: freestream velocity

It can also be written as:

$$C_p = 1 - \left(\frac{v}{v_\infty}\right)^2$$

7-22

The point with C_p equal to 1 is and stagnation point, where the velocity is equal to zero.

When the compressible effect cannot be neglected the formula above cannot be applied. In compressible case, C_p can be bigger than 1, meaning supersonic flow.

C_p and C_l are strongly related;

$$C_l = \int_{LE}^{TE} C_{pl}(x) - C_{pu}(x) d\frac{x}{c}$$

7-23

C_{pl}: is the pressure coefficient in the lower surface of the wing
C_{pu}: is the pressure coefficient in the upper surface of the wing
LE: means the leading edge
TE: means the trailing edge

7.2.5.4 Mach number

The Mach number is the relation between the velocity of an object and the velocity of the sound in the medium.

$$M = \frac{v}{u} \qquad \text{7-24}$$

v: velocity of the object
u: sound speed in the medium where object is travelling

Due to its dependence on the sound speed in the medium, the Mach number does not represent a constant value. It depends on temperature mainly.

The Mach number is a useful parameter because, even though it does not mean the same speed of the object, the fluid behaves similarly at the same Mach number, whichever the conditions are.

Using Mach number it can be defined the subsonic flow, M<0,5, the sonic flow, M=1, the transonic flow, M=[0,5-1,2], the supersonic flow, M=[1,2-5], and the hypersonic flow, M>5.

The transonic flow case is quite particular. In these conditions, flow usually presents zones where it is subsonic, zones where it supersonic, and a lines where flow speed is sonic (M=1), creating a normal shock. When this M=1 line reaches the trailing edge the normal shock becomes a weak oblique shock. When an aircraft exceeds Mach 1, it creates a great difference of pressure just in front, the so-called shock wave. The shock wave propagate backwards creating the so-called Mach cone.

In supersonic incompressible flow it can be computed Mach number using the following formulae:

$$M = \sqrt{\frac{2}{\gamma - 1}\left[\left(\frac{q_c}{P} + 1\right)^{\frac{\gamma - 1}{\gamma}} - 1\right]} \qquad \text{7-25}$$

q_c: impact pressure
P: static pressure
γ: ratio of specific heats

In a supersonic compressible flow:

$$M = 0.88128485 \sqrt{\left(\frac{q_c}{P} + 1\right)\left(1 - \frac{1}{7M^2}\right)^{2,5}}$$

7-26

q_c: impact pressure behind the normal shock.

7.2.5.5 Reynolds number

The Reynolds number is the dimensionless coefficient expressed by the ratio of the inertial forces and the viscous forces. It is used for both the dynamic and the thermal analysis, and it characterises the flow regime. For low Reynolds number flow is laminar, and it is turbulent for high values of Reynolds number.

$$\mathrm{Re} = \frac{\rho v l}{\mu}$$

7-27

μ: dynamic viscosity
ρ: density of the fluid
v: velocity of the flow
l: characteristic dimension; diameter for pipes, chord length for airfoils for example.

The Reynolds number is an important value for dynamic similitude. Using the same Reynolds number it can be tested an aircraft wing in a wind tunnel; if the linear dimensions of scaled model are $1/n$ times, the scaled model requires to adjust a velocity n times bigger than the real case.

In the case water tank is used instead of wind tunnel, a scaled model thirteenth the size in all dimensions must be used in order to maintain the same Reynolds number.

It is also important to define the drag characteristics of a defined body, an important parameter when optimizing cruise speed for low drag and long range profiles for example.

7.2.5.6 Prandlt number

The Prandlt number is the dimensionless coefficient that relates kinetic viscosity and thermal diffusity. It is the ratio of the viscous diffusion rate and the thermal diffusion rate.

$$\mathrm{Pr} = \frac{\upsilon}{\alpha} = \frac{c_p \mu}{k}$$

7-28

υ: kinetic viscosity
α: thermal diffusity
c_p: specific heat
μ: dynamic viscosity

k: thermal conductivity

In 2D case, where turbulence appear into the flow, the turbulent Prandlt number can be used. It relates the momentum eddy diffusity and the heat transfer eddy diffusity. In 3D turbulence it has no sense because both diffusities cannot be defined.

7.2.6 Compressible and incompressible flow

From its initial development regarding structural analysis, finite element method was first implemented in fluid problem during 70's. Viscous dominant, or non-viscous flows without considering convection (high Reynolds numbers), nor compressibility, were the first applications.

Nowadays, the finite element method (FEM) is largely applied in fluid dynamics problems, ranging over all kind of fluid problems. FEM has proven its better performance than the Finite Difference method or the Finite Volume method (Taylor and Zienkievicz, 1994).

The Navier-Stokes and The Euler equations are the basis of the development. Each one is better suited to a specific problem. Mainly speaking, the Euler equation is a simplification of the Navier-Stokes equation for non-viscous cases without heat transfer.

Navier-Stokes equation can be expressed as:

$$\frac{\partial U}{\partial t} + \nabla F + \nabla G + Q = 0 \qquad \text{7-29}$$

Where U is the velocity vector, F the forces matrix, G the viscosity matrix, and Q the massic forces matrix.

Euler equation can be expressed as:

$$\frac{\partial U}{\partial t} + \nabla F = 0 \qquad \text{7-30}$$

Both equations, the Navier-Stokes and the Euler one, are the origin of several particular cases. If the incompressible non-viscous flow is analysed, the starting point are the following equations, directly derived from Navier-Stokes.

$$\nabla U = 0$$
$$\frac{\partial u_i}{\partial t} + \frac{\partial}{\partial x_i}\left(u_i^2\right) + \frac{\partial}{\partial x_j}\left(u_i u_j\right) + \frac{\partial}{\partial x_k}\left(u_i u_k\right) + \frac{1}{\rho}\frac{\partial p}{\partial x_i} - f_{x_i} = 0 \quad i, j, k = 1,2,3 \qquad \text{7-31}$$

The formulation of the velocity potential needs to be introduced in order to improve the numerical solution.

$$U = -\nabla \phi \qquad \text{7-32}$$

So it can be easily deducted that

$$\nabla^2 \phi = 0 \qquad \text{7-33}$$

The need of the velocity potential imposes the irrotationality condition. The combination of the previous formula, equations 7-31, 7-32 and 7-33, it is obtained

$$\frac{\partial}{\partial x}\left(\frac{\partial \phi}{\partial t}\right) + \frac{\partial}{\partial x}\left(\frac{1}{2}\left(u^2 + v^2 + w^2\right) + \frac{p}{\rho} + P\right) = 0 \qquad \text{7-34}$$

P is the massic forces potential.

$$f_i = -\frac{\partial P}{\partial x_i} \qquad \text{7-35}$$

p is the pressure.

Equation 10-34 can be expressed in isothermic conditions as

$$\frac{\partial \phi}{\partial t} + \frac{1}{2}\left(u^2 + v^2 + w^2\right) + \frac{p}{\rho} + P = ct \qquad \text{7-36}$$

That is another confirmation that velocity potential has to exist. It becomes the Bernoulli equation in stationary state. It can be easily understood if it is considered the effect of the gravity, which convert P into gz.

Another typical case is Stokes problem, the viscous incompressible flow at low velocity. State equations can be written as

$$\nabla U = \overset{\bullet}{\varepsilon}$$
$$-\left(\frac{\partial}{\partial x_i}\left(\tau_{x_i x_i}\right) + \frac{\partial}{\partial x_j}\left(\tau_{x_i x_j}\right) + \frac{\partial}{\partial x_k}\left(\tau_{x_i x_k}\right)\right) + \frac{\partial p}{\partial x_i} - \rho f_{x_i} = 0 \quad i,j,k = 1,2,3 \qquad \text{7-37}$$

The study of the compressible flow is a complete chapter by itself. The finite element method provides the ability to better adjust to complex geometries and to make local mesh refinements in critical zones. But the first compressible flow solvers were based on the finite difference and the finite volumes methods.

It is considered that compressibility effects appears from Mach 0,3, but up to Mach 0,6 compressibility can be neglected without great lost of accuracy. From Mach 0,6 shock can appear creating discontinuities into the flow.

General equation for this case is:

$$\frac{\partial U}{\partial t} + \frac{\partial F}{\partial x_i} + \frac{\partial G_i}{\partial x_i} + Q = 0 \quad i = 1,2,3$$

7-38

Where ideal gas equation can be applied in order to evaluate density variation with pressure and temperature.

$$\rho = \frac{P}{RT}$$
$$R(C_p - C_v) = (\gamma - 1)C_v$$
$$\gamma = \frac{C_p}{C_v}$$

7-39

8 Appendix III: Shape Parametrization

8.1 Introduction

A short introduction to Bezier curves is presented in this appendix. The Bezier curves are extensively used in aerodynamical shape parametrization thanks to the capability they provide to accurately control the curves with small number of parameters.

8.2 Bezier Curves

Bezier curves were developed by Paul de Casteljau after defining the so-called Casteljau's algorithms. They are parametric curves first used by Renault engineer Pierre Bezier in the field of automotive design in 1962.

The Bezier curve can be written as:

$$B(t) = \sum_{i=0}^{n} b_{i,n}(t) \cdot P_i \qquad i = 0,1,2,...n$$

8-1

Where

$$b_{i,n}(t) = \binom{n}{i} \cdot t^i \cdot (1-t)^{n-i} \qquad i = 0,1,2,...n$$

$$P_i = \begin{pmatrix} x_i \\ y_i \\ z_i \end{pmatrix}$$

$$t \in [0,1]$$

8-2

n is the number of control points, P_i.

The polynomial $b_{i,n}(t)$ are the so-called Bernstein polynomials. Using lines to join each one of the control points P_i with the next one creates a polygon called the Bezier polygon or the control polygon. The final Bezier curve will be located on the convex side of the control polygon.

Some interesting characteristics of Bezier curves are:
-   Endpoint interpolation property: First and last control points are the first and last points on the curve.
-   If and only if all the control points are aligned the curve will be a straight line.
-   Bezier curve is tangent to the first and last section of the control polygon.
-   All the divisions of a Bezier curves are new Bezier curves.
-   Every quadratic Bézier curve is also a cubic Bézier curve, and more generally, every degree n Bézier curve is also a degree m curve for any $m > n$. In detail, a degree n curve with control points $P_0, \ldots, P_n$ is equivalent (including the parametrization) to the degree $n + 1$ curve with control points $P'_0, \ldots, P'_{n+1}$, where

$$P_k^{'} = \frac{k}{n+1} P_{k-1} + \left(1 - \frac{k}{n+1}\right) P_k \qquad \text{8-3}$$

Some of these characteristics are very helpful when defining the aerodynamic shape of a profile. It can be ensured the tangency of two curves defining appropriate initial and final sections of their control polygon. Then it can be created smoother shapes that will avoid turbulence, high drag values or flow separation, for instance.

9 References

Abbot H. I., Von Doenhoff A.E., 1959. *Theory of wing sections*, Ed. Dover Publications Inc., New York 1959

Anderson J.D., 2001. *Fundamentals of aerodynamics*, Ed McGraw Hill, 2001

AIRBUS, 2008. *Getting the grip with; Airbus A320 family, performance retention and fuel savings.* Flight Operations support and services, Airbus

Back T., Schwefel H-P., 1993. *An overview of evolutionary algorithms for parameter optimization*, University of Dortmund, MIT Press 1993

Badia S., Codina R., 2009. *On a multiscale approach to the transient Stokes problem: dynamic subscales and anisotropic space-time discretization* , Applied Mathematics and Computation 207 (2009) 415-433. Elsevier 2009.

Badia S., Codina R., 2000. *On some fluid-structure iterative algorithms using pressure segregation methods. Application to aeroelasticity*, Int. J. Numer. Engng 2000; 00; 1-6. John Wiley & Sons, Ltd, 2000.

Bazaraa M.S., Sherali H.D., 1993. Shetty C.M.; *Nonlinear programming: theory and algorithms.* John Wiley & Sons, New York, 1993.

Balsa-Canto E., Bugeda G., Thamotheram C., Oñate E., Zarate F., 2003. *A new probabilistic-stochastic search method: Application to optimal design*, 2003

Beyer H.-G., Deb K., 2000. *On the Desired Behaviors of Self-Adaptive Evolutionary Algorithms*. In M. Schoenauer et al., editors, Parallel Problem Solving from Nature, 6, pages 59-68, Heidelberg, Springer-Verlag, 2000.

Beyer H-G., Sendhoff B., 2007. *Robust optimization – A comprehensive survey*. Comput. Methods Appl. Engrg 196, pg 3190-3218. March 2007

Blatman G., Sudret B., 2008. *Sparse polynomial chaos expansions and adaptative stochastic finite elements using a regression approach*, Pre-print submitted to Elsevier Science, 2008

BOEING, 2007. *Fuel conservation strategies: cost index explained.* Boeing AERO quarterly, Seattle.

Broyden C.G., 1967. *Quasi-Newton's methods and their application to function minimization*, Mathematics of Computation, Vol. 21, No. 99 (Jul., 1967), pp. 368-381

Bugeda G., Balsa-Canto E., Thamotheram C., Oñate E., Zarate F., 2003. *Global search methods for nonlinear optimisation: A new probabilistic-stochastic approach,* EUROGEN 2003

Bugeda G., Ródenas J.J., Pahl E., Oñate E., 2006. *An adaptive mesh generation strategy for the solution of structural shape optimization problems using evolutionary methods,* Proccedings of III European Conference on computational mechanics, solids, structures and coupled problems in engineering, 2006.

Busquin P., et al., 1989. *European Aeronautics; a vision for 2020. Meeting society's needs and winning global leadership*, Report of the group of personalities, European Commission, January 2001.

Carmona A.I., 1989, *Aerodinámica y actuaciones del avión*, Ed Paraninfo, 1989

Cervera M., Codina R., Galindo M., 1996, *On the computational efficiency and implementation of block-iterative algorithms for non-linear coupled problems*, Engineering Computations, Vol. 13 No. 6, 1996, pp. 4-30. © MCB University Press, 0264-4401

Chafekar D., Xuan J., Rasheed K., 2003, *Constrained Multi-Objective Optimization Using Steady State Genetic Algorithms*, Lecture Notes in Computer Science, 2003 – Springer

Chiba K., Obayashi S., Nakahashi K., Giotis A.P., Giannakoglou K.C., 2003, *Design Optimization of the wing shape for the RLV Booster stage using Evolutionary Algorithms and Navier-Stokes computations on unstructured grid,* Proceedings of International Congress on Evolutionary Methods for Design, EUROGEN 2003.

Clarich A., Pediroda V., Padovan L., Poloni C., Periaux J., 2004, *Application Of Game Strategy In Multi-Objective Robust Design Optimisation Implementing Self-Adaptive Search Space Decomposition By Statistical Analysis.*,European Congress on Computational Methods in Applied Sciences and Engineering. 24-28. July. 2004.

Constantine P.G., Doostan A., Iacarrino G., 2009, *A hybrid collocation/Galerkin scheme for Comvective heat transfer problems with stochastic boundary conditions*, Int. J. Numer. Engng, 2009, DOI 10.1002/nme.2564

Crespo L.G., Kenny S.P., 1991, *Robust Control Design for systems with probabilistic uncertainty,* NASA/TP-2005-213531, 2005

Davis L., *Handbook of genetic algorithms*, Edited by Lawrence Davis, Van Nostrand Reinhold, New York, 1991

Deb K., 2002, Anand A., Joshi D., *A computationally efficient evolutionary algorithm for real parameter optimization,* KanGAL Report 2002003, 2002

Deb K., 2003, *Multi-Objective Optimization Using Evolutionary Algorithms.* Wiley, 2003.

Deb K., 2003, *A population-Based algorithm-generator for real-parameter optimization*, KanGAL Report 2003003, 2003

Deb K., 2005, *Practical optimization using evolutionary Methods*, KANGAL report 2005008

Deb k., Agrawal S., Pratap A., Meyarivan T., 2000, *A Fast Elitist Non-Dominated Sorting Genetic Algorithm for Multi-Objective Optimization: NSGA-II*, Kangal Report 200001, 2000

Deb K., Goel T., 2000, *Controlled Elistist Non-Dominated Sorting Genetic Algorithms for Better Convergence*, Kangal Report 200004, 2000

Deb K., Pratap A., Meyarivan T., 2000, *Constrained Test Problems for Multi-Objective Evolutionary Optimization*, Kangal Report 200002, 2000

Deb K., Pratap A., Moitra S., 2000, *Mechanical Component Design for Multiple Objectives Using Elitist Non-Dominated Sorting GA*, Technical Report 200002, 2000

Deb K., Padmanabhan D., Gupta S., Mall A.K., 2006, *Handling uncertainties through reliability-based optimization using evolutionary algorithms*, KANGAL report 2006009

Deuflhard P., 1974, *A modified Newton's method for the solution of ill-conditioned systems of non-linear equations with application to multiple shooting*, Numer. Math. 22, 289-315, Springer-Verlag 1974

Desideri J-A., Janka A., 2004, *Multilevel Shape parametrization for aerodynamic optimization – Application to Drag and Noise reduction of transonic/Supersonic Business Jet*, ECCOMAS 2004, Jyväskylä 2004

Dennis J.E., More J.J., 1977, *Quasi-Newton methods, motivation and theory*, SIAM review, V19, 1, January 1977

Dietz G., Vob R., De Breuker R., 2004, *Airfoil optimization based on an evolution strategy with respect to aeroelasticity*, ECCOMAS 2004

Durga Rao K., Kushwaha H.S., Verma A.K., Srividya A., 2006, *Quantification of epistemic and aleatory uncertainties in level-1 probabilistic safety assessment studies*, Reliability Engineering & System Safety 92 (2007) 947-956, Elsevier 2006

Drela M., 1989, *XFOIL - An analysis and design system for low Reynolds number airfoils,* Low Reynolds number aerodynamics; Proceedings of the Conference, Notre Dame, IN; GERMANY, FEDERAL REPUBLIC ; pp. 1-12. 1989

Eldred M.S.,Burkardt J., 2009, *Comparison of non-intrusive polynomial chaos and stochastic collocation methods for uncertainty quantification*, AIAA, paper 2009-0976

Eldred M.S., 2009, *Recent advances in non-intrusive polynomial chaos and stochastic collocation methods for uncertainty analysis and design* , AIAA, paper 2009-2274

Eppler R., 1990, *Airfoil design and data*, Ed Springer-Verlag, 1990

Foo J., Wan X., Karniadakis G.E., 2008, *The multi-element probabilistic collocation method (ME-PCM): Error analysis and applications*, Journal of Computational Physics 227 (2008) 9572-9595

Fonseca C.M., Fleming P.J., 1993, *Genetic algorithms for multi-objective optimization: formulation, discussion and generalization*, Genetic Algorithms: Proceedings of the 5th international conference, 1993

Flores R., Ortega E., 2007, *PUMI: an explicit 3D unstructured finite element solver for the Euler equations*. CIMNE 2007.

GiD. The pre and post processor tool. CIMNE (www.gid.cimne.com)

Goett H.J., Bullivant W.K., 1938; *Tests of N.A.C.A. 0009, 0012, and 0018 airfoils in the full-scale tunnel*, Report 647 N.A.C.A., July 1938

Goldberg D.E., 1988; *Genetic algorithms in search, optimization, and machine learning*, Ed. Reading Mass. Addison-Wesley, 1988, ISBN 0201157675

Goldberg D.E., 1994; *Genetic and Evolutionary algorithms Come of age* , Communications of the ACM, 1994

Hamalainen J.P., Makinen R.A.E., Tarvainen P., Toivanen J., 2000, *Evolutionary shape optimization in CFD with industrial applications*, ECOMASS, Barcelona, 2000

Helton J.C., Davis F.J., 2003, *Latin hypercube sampling and the propagation of uncertainty in analysis of complex systems*, Reliability Engineering and System Safety 81 (2003) 23-69, Elsevier 2003

Hiroyasu T., Nakayama S., Miki M., 2005, *Comparison study of SPEA2+, SPEA2, and NSGA-II in diesel engine emissions and fuel economy problem*, IEEE 2005 conference,

Hurtado J.E., 2004, *Structural Reliability – Statistical learning perspectives*, Ed Springer, 2004

Hurtado J.E., Barbat A.H., 1998, *Monte Carlo techniques in computational stochastics mechanics,* Archives in Computational Methods in Engineering, Springer, Vol 5 num 1 , 1998, pg 3-29

Huyse L., Lewis R.M., 2001, *Aerodynamic shape optimization of two-dimensional airfoils under uncertain operating conditions*, ICASE Report 2001-1, January 2001.

Hua J., Kong F.M., Jay Liu P., Zingg D.W., 2003, *Optimization of long-endurance airfoils,* AIAA-2003-3500, 21a AIAA Applied Aerodynamics Conference, 2003

Idelsohn S., Oñate E., 2004, *Mesh or Meshless methods? Is this the right question?,* Proocedings of 6th World Congress on Computational mechanics, 2004.

Idelsohn S., Oñate E., Calvo N., Del Pin F., 2002, *The meshless finite element method,* 2002

Iman, R.L.; Helton, J.C.; and Campbell, J.E., 1981. *An approach to sensitivity analysis of computer models, Part 1. Introduction, input variable selection and preliminary variable assessment*. Journal of Quality Technology 13 (3): 174–183.

Jameson A., 1991, *Time-dependent calculations using multigrid with applications to unsteady flows past airfoils and wings. AIAA paper 91-1596*, 1991

Jakeman J.D., Roberts S.G., 2009, *Stochastic galerkin and collocation methods for quantifying uncertainty in differential equations: a review*, ANZIAM Journal 50 (CTAC2008), pp815-830, ISSN 1446-8735, 2009

Jeong S., Murayama M., Yamamoto K., 2004, *Efficient optimization design method using Kriging Model*, AIAA 2004-118.

Kirkpatrick S, Gelatt C.D., and Vecchi M.P. 1983. *Optimization by Simulated Annealing*. Science, vol 220, No. 4598, pp671-680.

Kouhi M., Oñate E., Bugeda G., 2008, *Robust Design Methods In Aerospace Engineering*. CIMNE Report 328, November 2008

Kushner H., George Yin G., 1997, *Stochastic Approximation Algorithms and applications*, Ed. Springer, 1997

Lagarias J.C., Reeds J.A., Wright M.H., Wright P.E., 1998, *Convergence properties of the Nelder-Meead simplex method in low dimensons,* SIAM J. Optim. V19, N1, 112-147 (1998)

Lee D.S.C., Gonzalez L.F., Periaux J., Srinivas K., 2009, *Hybrid Game Strategies for Multi-objective and Multi-Disciplinary Design Optimisation in Aerospace Design,* Preprint 2009

Lee D.S.C., Srinivas K., Gonzalez L.F., Periaux J. and Obayashi S., 2010, *Robust Multidisciplinary Design Optimisation Using CFD & Advanced Evolutionary Algorithms*. Computation Fluid Dynamics Review 2010, World Scientific, ISBN 978-981-4313-36-0. June 2010.

Lee D.S.C., Gonzalez L.F., Periaux J. and Srinivas K., 2009, *Evolutionary Optimisation Methods with Uncertainty for Modern Multidisciplinary Design in Aeronautical Engineering*, Notes on Numerical Fluid Mechanics and Multidisciplinary Design (NNFM 100), 100 Volumes NNFM and 40 Years Numerical Fluid Mechanics. Pages 271-284, Ch. 3., Heidelberg: Springer-Berlin, ISBN 978-3-540-70804-9, 2009.

Lee D.S.C., Srinivas K., Gonzalez L.F., Periaux J.,2009, *Uncertainty Based MDO of UAS Using HAPMOEA*. Computational Fluid Dynamics 2008. Pages 649-654, Part 34: Optimization 2, Heidelberg: Springer-Berlin, ISBN 978-3-642-01272-3, 2009.

Lee D.S.C., Gonzalez L.F., Srinivas K. and Periaux J., 2008. *Robust Evolutionary Algorithms for UAV/UCAV Aerodynamic and RCS Design Optimisation*, Special Issue: Computers and Fluids. Vol 37. Issue 5, pages 547-564, ISSN 0045-7930, 2008

Lee D.S.C., Gonzalez L.F., Srinivas K. and Periaux J., 2008. *Robust Design Optimisation using Multi-Objective Evolutionary Algorithms*, Special Issue: Computers and Fluids. Vol 37. Issue 5, pages 565-583, ISSN 0045-7930, 2008

Lee D.S.C., Gonzalez L.F., Periaux J., 2010, *UAS Mission Path Planning System (MPPS) Using Hybrid-Game Coupled to Multi-Objective Design Optimizer.* Journal of Dynamic System, Measurement and Control ASME, DS-09-1135, Vol. 132, Iss. 4. 041005-1 -11, 2010

Lee D.S., Gonzalez L.F., Walker R., Periaux J., and Onate E., 2010, Reduction Environmental Effect Of Civil Aviation Through Multi-Objective Flight Plan Optimisation. The 9th World Congress on Computational Mechanics and 4th Asian Pacific Congress on Computation Mechanics (WCCM/APCOM 2010), IOP Conf. Series: Materials Science and Engineering 10, doi: 10.1088/1757-899X/10/1/012197. 2010.

Lee D.S.C., Gonzalez L.F., Periaux J., 2010, *UAS Mission Path Planning System (MPPS) Using Hybrid-Game Coupled to Multi-Objective Design Optimizer*. Journal of Dynamic System, Measurement and Control ASME, DS-09-1135, Vol. 132, Iss. 4. 041005-1 -11, 2010.

Lee D.S.C., Gonzalez L.F., Walker R., Periaux J., and Onate E., 2010, *Reduction Environmental Effect Of Civil Aviation Through Multi-Objective Flight Plan Optimisation*. The 9th World Congress on Computational Mechanics and 4th Asian Pacific Congress on Computation Mechanics (WCCM/APCOM 2010), IOP Conf. Series: Materials Science and Engineering 10, doi: 10.1088/1757-899X/10/1/012197. 2010.

Ledesma M., Baleriola G., 1989, *Meteorología aplicada a la aviación*, Ed Paraninfo, 1989

Li W., Padula S., 2003, *Robust Airfoil optimization in High Resolution Design Space,* NASA 2003

Li W., Huyse L., Padula S., 2002, *Robust airfoil optimization to achieve drag reduction over a range of Mach numbers,* Struct Multidisc Optim 24, pp38-50. Springer-Verlag, 2002

Loeven G.J.A., Bijl H., 2008, *Airfoil analysis with uncertain geometry using the Probabilistic Collocation method*, Proceedings of 49th AIAA/ASME/ASCE/AHS/ASC Structures, Structural Dynamics, and Materials conference 2008, AIAA2008-2070

Loeven G.J.A., Bijl H., 2009, *An efficient framework for uncertainty quantification in CFD using Probabilistic Collocation*, Proceedings of 50th AIAA/ASME/ASCE/AHS/ASC Structures, Structural Dynamics, and Materials conference 2009, AIAA2009-2275

Loeven G.J.A., Witteveen, Bijl H., 2007, *Probabilistic Collocation: an efficient non-intrusive approach for arbitrarily distributed parametric uncertainties*, Proceedings of 45th AIAA Aerospace Sciences Meeting and Exhibit, AIAA2007-317, January 2007

Löhner R., Sacco C., Oñate E., & Idelsohn S., 2002, *A finite point method for compressible flow*. *Int. J. Num. Meth. Eng.*, 2002

López R., 2007, *Flood A1. An open source Neural Networks C++ Library User Guide*, CIMNE, 2007.

López R., 2008, *Neural Networks for Variational Problems in Engineering,* PhD Thesis, 2008

López R., Oñate E., 2006, *A variational formulation for the Multilayer Perceptron, Artificial Neural Networks*, ICANN 2006, Lecture Notes in Computer Science 4132(I) pp159-168, 2006.

López R., Balsa-Canto E., Oñate E., 2008, *Neural networks for variational problems in engineering*, International Journal for Numerical Methods in Engineering, Early View, 2008. Computer Software

Marco N., Desideri J.A., Lanteri S., 1999, *Multi-objective optimization in CFD by Genetic Algorithms*, INRIA Report nº 3686, 1999.

Mathelin L., Hussaini M.Y., 2003, *A stochastic collocation algorithms for uncertainty analysis*, NASA/CR – 2003 – 212153, 2003

Mathelin L., Hussaini M.Y., Zang T.A.. 2008, *Stochastic approaches to uncertainty quantification in CFD simulations*, Numercial Algorithms, pp209-236, Springer 2008

McKay, M.D.; Conover, W.J.; and Beckman, R.J., 1979. *A Comparison of Three Methods for Selecting Values of Input Variables in the Analysis of Output from a Computer Code*. Technometrics 21: 239–245.

Nelder, J.A., Mead R., 1965, *A simplex method for function minimisation*, The Computer Journal 7 308–313. (1965)

Mengistu T., Whaly G., 2000, *Global Optimization Methods for the Aerodynamic Shape Design of transonic cascades*. 2000

Messac A., Ismail-Yahaya A., 2002, *Multiobjective robust design using physical programming*, Struct Multidisc Optim 23, pp357-371, Springer-Verlag, 2002

Metropolis N., Rosenbluth A.W., Rosenbluth M.N., Teller A.H., and Teller E., 1953. *Equation of State Calculation by Fast Computing Machines*, J. of Chem. Phys., 21, 1087-1091.

Mitra A., 2007, *Design of transonic airfoil using genetic algorithms*. Preprint

Monge F., Tobio B., 1988, *Aerodynamic design by means of the control Theory,* Computationals Mechanics, New trends and Applications, 1988

Nagarathinam S., González L.F., Whitney E.J., Srinivas K., Périaux J., 2006; *Aerodynamic shape optimization using a robust evolutionary algorithm and grid-free flowsolve,* 44th AIAA Aerospace Sciences Meeting and Exhibit, 9 - 12 January 2006, Reno, Nevada

Nash S.G., Sofer A., 1996, *Linear and non-linear programming*. McGraw-Hill, 1996.

Nemhauser G.L., Rinnoy Kan A.H.G., Todd M.J., 1994, *Optimization Vol 1*, Ed North Holland Elsevier, 1994

Nobile F., Tempone R. Webster C.G., 2007, *A sparse grid stochastic collocation method for partial differential equations with random input data*, ISIAM J. Numer. Anal. **45** (2007), pp. 1005–1034

Obayashi S.,JeongiSD.,Chiba K., 2005, *Multi-Objective DesignExplorationfor Aerodynamics Configurations*,AIAA-2005-4666, 35th AIAA Fluid Dynamics Conference and Exhibit. 6 - 9 June 2005.

Obayashi S., Sasaki D., Takeguchi Y., 1998, *Design optimization of supersonic wings using evolutionary algorihms*, ECOMASS 1998.

Obayashi S., Sasaki D., Takeguchi Y., 2000, *Evolutionary computation of supersonic wing shape optimization*. 2000

Obayashi S., Sasaki D., 2003, *Visualization and Data Mining of Pareto Solutions Using Self-Organizing Map*, Second International Conference on Evolutionary Multi-Criterion Optimization, Faro, Portugal, LNCS 2632, Springer-Verlag Berlin Heidelberg 2003, pp. 796-809, April 2003

Oñate E., Idelsohn S., Celigueta M.A., Rossi R., 2008, *Advances in the particle finite element method for the analysis of fluid–multibody interaction and bed erosion in free surface flows*. Comput. Methods Appl. Mech. Engrg. 197 (2008) 1777–1800

Ortega E., Oñate E. & Idelsohn S. 2007, *An improved finite point method for three-dimensional potential flows*. Comp. Mech., 2007

Ortega E., Oñate E. & Idelsohn S., 2009, *A finite point method for adaptive three-dimensional compressible flow calculations. Int. J. Num. Meth. Fluids*, 2009

Papadrakakis M., Lagaros N.D., Tsompanakis Y., 2008, *Structural optimization using evolution strategies and neural networks,* Comput. Methods Appl. Mech. Engrg 156 pp309-333, 1998.

Parashar, S., Pediroda, V., Poloni, C., *Self organizing maps (SOM) for design selection in robust multi-objective design of aerofoil*. In 46th AIAA aerospace sciences meeting and exhibit, Reno, Nevada, AIAA 2008-914, 2008

Park G-J., Lee T-H, Lee K-H, Hwang K-H., 2006, *Robust Design: An Overview*. AIAA Journal Vol. 44, No. 1, January 2006.

Parussini L., Pediroda V., 2007, *Fictitious Domain with Least-Squares Spectral Element Method to Explore Geometric Uncertainties by Non-Intrusive Polynomial Chaos Method,* Computer Modeling in Engineering & Sciences, Vol. 22, No. 1, pp. 41-64, 2007

Parussini L., Pediroda V., 2008, *Investigation of Multi Geometric Uncertainties by Different Polynomial Chaos Methodologies Using a Fictitious Domain Solver*, Computer Modeling in Engineering & Sciences, Vol. 23, No. 1, pp. 29-52, 2008

Pediroda V., Clarich A., 2004, *The use of Robust Design and Game Theory in PSO*, FENET Report and Presentation, Glasgow, 2004.

Pediroda V., Poloni C., 2006, *Robust Design, Approximation Methods and Self Organising MapsTechniques for MDO problems,* Introduction to Optimization and Multidisciplinary Design, VKI Lectures 2006-03, March 2006

PDAS, Public Domain Aeronautical Software, http://www.pdas.com/avd.html

Plateeuw, P.D.A., 2008, *Application of the Probabilistic Collocation method to uncertainty in turbulence models*, Master of Science Thesis, Delft University of Technology, May 2008

Plevris V., Lagaros N. D., Papadrakakis M., 2005; *Robust design optimization of steel structures*; 5th GRACM International Congress on Computational Mechanics Limassol, 29 June – 1 July, 2005

Press W.H., Teukolsky S.A., Vetterling W.T., Flanner B.P., 2002, *Numerical Recipes in C:The art of scientific computing*, Cambridge University Press, Electronic Edition from Cornell University 2002

Quagliarella D., Vicini A., 1999, *Designing high-lift airfoils using Genetic Algorithms*. Procedings of EUROGEN 1999

Rogalsky, T., Kocabiyik, S. and Derksen, R., 2000: *Differential evolution in aerodynamic optimization*, Canadian Aeronautics and Space Journal, **46**(4) (2000), 183–190.

Rutenber R.A., 1989, *Simulated Annealing Algorithms: An Overview*, IEEE Circuits and Devices, Jan. 1989, pp19-26.

Sasaki D., Morikawa M., Obayashi S., Nakahashi K., 2001, *Aerodynamic shape optimization of supersonic wings by adaptative range multiobjective genetic algorithms,* Lecture Notes in Computer Sciences, Springer, Vol 1993/2001, pg 639-652, 2001

Schaffer J.D., 1985, *Multi-objective Optimization with Vector Evaluated Genetic Algorithms*. Proceedings of the 1st International Conference on Genetic Algorithms, 1985

Schaffer J.D., Grefenstette J.J., 1985, *Multi-objective learning via Genetic Algorithms*. Proceedings on the Ninth International Joint Conference on Artificial Intelligence, 1985

Sorensen D.C., 1982, *Newton's method with a model trust region modification*. SIAM J. Numer. Anal. V19, 2, April 1982

STAC. 2006. A software platform for stochastic analysis using Monte Carlo method. CIMNE, Barcelona, 2006. (http://www.cimne.com/stac/)

Stull R.B., 2000, *Meteorology for scientists and engineers*, Ed Brooks and Cole, 2000

Taguchi, G., Chowdhury, S., 2000, *Robust Engineering*, McGrawHill, New York, 2000.

Tang Z., Periaux J., Oñate E., Bugeda G., 2005, *Lift maximization with uncertainties on angle of attack for high lift devices optimization,* CIMNE Report, 2005

Taylor R.L., Zienkiewicz O.C., 1994, *El método de los elementos finitos. Formulación Básica y problemas lineales. Vol 1*, Ed. McGraw Hill, Barcelona 1994

Taylor R.L., Zienkiewicz O.C., 1994, *El método de los elementos finitos. Mecánica de sólidos, dinámica y no linealidad. Vol 2*, Ed. McGraw Hill, Barcelona 1994

Tdyn. 2007, A finite element code for multiphysics fluid dynamics problems. COMPASS (www.compassis.com), 2007.

Thamotheram C.P., 2002; *Aerodynamic shape optimisation using probabilistic-stochastic search methodologies*, June 2002

Theodorsen T., 1940, *Theory of wing sections of arbitrary shape,* NACA Report 411, 1940

Theodorsen T., Garrick I.E., 1949, *General Potential Theory of arbitrary wing sections,* NACA Report 452, 1949

UIUC Airfoil Data Site http://www.ae.illinois.edu/m-selig/ads.html, Department of Aerospace Engineering, University of Illinois at Urbana-Champaign

Xiu D., Karniadakis G.E., 2003, *Modeling uncertainty in flow simulations via generalized polynomial chaos,* Journal of Computational Physics 187, 137–167 (2003)

Xiu D., Karniadakis G.E., 2002, *Modeling uncertainty in steady state diffusion problems via generalized polynomial chaos,* Comput. Methods Appl. Mech. Engrg. 191, 4927–4948 (2002)

Xiu D., Lucor D., Su s-H., Karniadakis G.E., 2002, *Stochastic Modeling of Flow-Structure Interactions Using Generalized Polynomial Chaos,* Journal of Fluids Engineering Vol. 124, 51-59 (2002)

Wang X., Damodaran M., 2001, *Aerodynamic shape optimization using computational fluid dynamics and parallel simulated annealing algorithms*, AIAA Journal, vol 39 n8, pag 1500-1508, 2001

Webster M., Tatang M.A., McRae G.J., 1996, *Application of the probabilistic collocation method for an uncertainty analysis of a simple ocean model*, MIT, Joint Program Report Series, January 1996

Witteveen J.A.S, Bijl H., 2008, *Efficient quantification of the effect of uncertainties in advection-diffusion problems using polynomial chaos*, Numerical Heat Transfer, Part B, 53, pp437-465, 2008

Whitley D., 2001, *An overview of Evolutionary Algorithms: Practical Issues and Pitfalls,* Information and software technology, Elsevier 2001